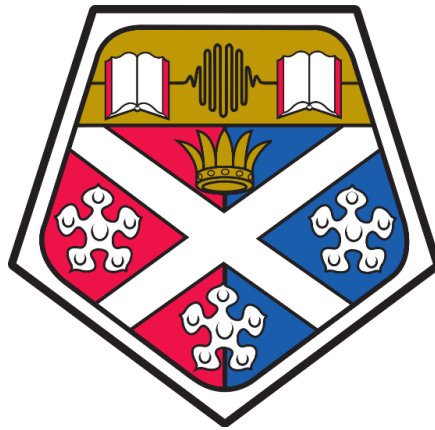


**EXPERIMENTAL AND MODELLING STUDY  
ON THE RELEASE OF POTASSIUM DURING  
BIOMASS COMBUSTION**



**WENHAN CAO**

Department of Chemical & Process Engineering

University of Strathclyde

A Thesis Submitted to the University of Strathclyde for the  
Degree of Doctor of Philosophy

2019

Wenhan Cao

*Experimental and Modelling Study on the Release of Potassium during Biomass  
Combustion*

Department of Chemical and Process Engineering

University of Strathclyde

PhD Thesis

© November 2019

## Declaration

This thesis is the results of the author's original research. It has been composed by the author and has not been previously submitted for examination, which has led to the award of a degree.

The copyright of this thesis belongs to the author under the terms of the United Kingdom Copyright Acts as qualified by University of Strathclyde Regulation 3.50. Due acknowledgement must always be made of the use of any material contained in, or derived from, this thesis.

Signed:

Date:

Dedicated to the loving memory of my grandfather, Zengfu Li.

谨以此献给我亲爱的姥爷

1930-2017

## ACKNOWLEDGEMENTS

---

Firstly, I would like to thank both my supervisors Dr. Jun Li and Dr. Leo Lue for giving me the opportunity to undertake this research project and for all their help, guidance and insightful discussion through every stage of the research.

I would like to thank my mum, dad, grandparents and my families for all the supports, encouragement and love they have sent and for sticking with me throughout this long and all-consuming ordeal, without them, this work would not have been possible.

A big thank you goes to all my friends and colleagues at Strathclyde for making my time at Glasgow so enjoyable and memorable. I have also received significant assistance from many of the Chemical and Process Engineering support staff at the University of Strathclyde without whom, the completion of my work would not have been possible.

Best wishes to you all,

Wenhan Cao

November 2019

## PREVIOUSLY PUBLISHED WORK

---

- Cao W, Martí-Rosselló T, Li J, Lue L. Prediction of potassium compounds released from biomass during combustion. *Applied Energy*. 2019 Sep 15; 250:1696-705.
- Cao W, Li J, Martí-Rosselló T, Zhang X. Experimental study on the ignition characteristics of cellulose, hemicellulose, lignin and their mixtures. *Journal of the Energy Institute*. 2019 Oct; 92(5): 1303-1312.
- Cao W, Peshkur T, Lue L, Li J. Experimental study on the influences of operating parameters on the retention of potassium during the biomass combustion. *Energy Procedia*. 2019 Feb 1; 158:1033-8.
- Cao W, Li J, Lue L. Study on the ignition behaviour and kinetics of combustion of biomass. *Energy Procedia*. 2017 Dec 1; 142:136-41.
- Cao W, Li J, Lue L, Zhang X. Release of alkali metals during biomass thermal conversion. *Archives of Industrial Biotechnology*. 2016 Nov 29; 1(1):1-3.

## ABSTRACT

---

Understanding the release mechanism of potassium (K) is crucial in tackling alkali metal-induced ash problems during the combustion process of biomass. This thesis focuses on enhancing the knowledge on the release mechanism of potassium experimentally and developing a model to predict the release profiles of potassium compounds from biomass.

In the beginning, the thesis investigated the thermal characteristics of biomass and its major chemical components in a thermogravimetric analyser (TGA). According to the tests, the thermal conversion process of natural biomass can be predicted through the analyses of artificial biomass, which is the mixture of major chemical components. The results illustrate the feasibility to use major chemical components as initial inputs in the biomass combustion model. Biomass combustion experiments were then performed in a high-temperature furnace-balance system (FBS). The results revealed that the final temperature affects the K transition the most. Over 60% of the initial K was lost as the final temperature increased from 30°C to 1000°C. The heating rate affects the K transition during combustion by influencing the devolatilisation of volatile matter related K and the structural changes of particles. The higher the heating rate, the more release of K. The developed kinetically controlled model was validated and used to estimate the release of different K compounds under different scenarios. The results indicate that KCl is the major compound released at the early stage of combustion, followed by KOH and K<sub>2</sub>SO<sub>4</sub>. Analysing the reaction path of K reveals that KO and KO<sub>2</sub> are the most critical intermediate species during combustion. The initial concentration of Cl significantly affects the release of major species: KCl, KOH, HCl and K<sub>2</sub>SO<sub>4</sub>; while the initial concentration of S can affect the release of KOH and K<sub>2</sub>SO<sub>4</sub> at high temperatures. The existence of O<sub>2</sub> in the system favours the formation of KO and KO<sub>2</sub>, and thus to control the release of major K species.

# TABLE OF CONTENTS

---

<b>ACKNOWLEDGEMENTS</b> .....	<b>3</b>
<b>PREVIOUSLY PUBLISHED WORK</b> .....	<b>4</b>
<b>ABSTRACT</b> .....	<b>5</b>
<b>TABLE OF CONTENTS</b> .....	<b>6</b>
<b>LIST OF FIGURES</b> .....	<b>10</b>
<b>LIST OF TABLES</b> .....	<b>13</b>
<b>ABBREVIATIONS</b> .....	<b>15</b>
<b>NOMENCLATURE LIST</b> .....	<b>19</b>
<b>CHAPTER 1 INTRODUCTION</b> .....	<b>21</b>
1.1 Background.....	21
1.2 Biomass energy .....	22
1.3 Project aims and objectives .....	25
1.4 Summary of thesis outline.....	25
Bibliography.....	27
<b>CHAPTER 2 LITERATURE REVIEW</b> .....	<b>31</b>
2.1 Lignocellulosic biomass .....	31
2.2 Combustion of lignocellulosic biomass and ash-related challenges.....	32
2.3 Experimental study on the release of K.....	36
2.3.1 Release of K during the combustion process.....	36
2.3.2 Release of K during the pyrolysis process .....	39
2.4 Modelling study on the release of K.....	42
2.5 Summary and research gap.....	45
Bibliography.....	48
<b>CHAPTER 3 MATERIALS AND METHODOLOGY</b> .....	<b>57</b>
3.1 Experimental methods and materials .....	57

3.1.1	Raw materials .....	57
3.1.2	Reactors.....	58
3.1.3	Solid residues characterisation.....	61
3.2	Model development.....	62
3.2.1	Initial values.....	63
3.2.2	Biomass devolatilisation model.....	64
3.2.3	Release kinetics of inorganic elements .....	66
3.2.4	Gas species combustion model.....	67
3.3	Summary of the chapter .....	70
	Bibliography.....	71
<b>CHAPTER 4 THERMAL CHARACTERISTICS OF BIOMASS AND ITS CHEMICAL COMPONENTS.....</b>		<b>73</b>
4.1	Background.....	73
4.2	Experiment.....	73
4.3	Thermal characteristics of cellulose, xylan and lignin .....	74
4.4	Thermal characteristics of artificial and natural biomass.....	76
4.5	Summary of the chapter .....	79
	Bibliography.....	80
<b>CHAPTER 5 POTASSIUM TRANSITION PERFORMANCE DURING BIOMASS COMBUSTION .....</b>		<b>82</b>
5.1	Background.....	82
5.2	Experiment.....	82
5.2.1	Experiment procedure.....	82
5.2.2	Quantity of K content .....	83
5.3	Influence of final temperature on K transition .....	84
5.3.1	Test results.....	84
5.3.2	Analysis and discussion .....	86

5.3.3	Summary of findings .....	91
5.4	Influence of heating rate on K transition.....	93
5.4.1	Test results.....	93
5.4.2	Analysis and discussion .....	96
5.4.3	Summary of findings .....	99
5.5	Summary of the chapter .....	100
	Bibliography.....	102
<b>CHAPTER 6 PREDICTION OF THE RELEASE OF POTASSIUM COMPOUNDS DURING BIOMASS COMBUSTION .....</b>		<b>106</b>
6.1	Background.....	106
6.2	Model setup .....	106
6.3	Validation of the model .....	107
6.4	Predicted results of the release of K compounds .....	109
6.4.1	The release profiles of K species.....	109
6.4.2	The reaction paths of K species .....	115
6.5	Summary of the chapter .....	125
	Bibliography.....	127
<b>CHAPTER 7 EFFECTS OF CHLORINE AND SULPHUR CONCENTRATIONS ON THE RELEASE OF POTASSIUM COMPOUNDS.....</b>		<b>129</b>
7.1	Background.....	129
7.2	Model setup .....	131
7.3	Effect of Cl concentration on the release of K compounds.....	131
7.3.1	Release profiles of major species.....	131
7.3.2	Changes of major transition cycles of K.....	137
7.4	Effect of S concentration on the release of K compounds.....	141
7.4.1	Release profiles of major species.....	141

7.4.2	Changes of major transition cycle of K.....	146
7.5	Summary of the chapter .....	152
	Bibliography.....	154
<b>CHAPTER 8 EFFECTS OF OXYGEN CONCENTRATION ON THE RELEASE OF POTASSIUM COMPOUNDS .....</b>		<b>157</b>
8.1	Background.....	157
8.2	Model setup .....	158
8.3	Results and discussion.....	158
8.3.1	Release profiles of K compounds.....	158
8.3.2	Change of major transition cycles of K.....	161
8.4	Summary of the chapter .....	163
	Bibliography.....	165
<b>CHAPTER 9 CONCLUSIONS AND FUTURE WORK .....</b>		<b>166</b>
9.1	Final conclusions .....	166
9.2	Suggestions for the future work .....	169
<b>APPENDIX.....</b>		<b>171</b>
	<b>Appendix I.....</b>	<b>171</b>
	<b>Appendix II.....</b>	<b>173</b>
	<b>Appendix III.....</b>	<b>176</b>
	<b>Appendix IV.....</b>	<b>178</b>
	<b>Appendix V.....</b>	<b>180</b>

## LIST OF FIGURES

---

Figure 1.1 Different fuels contribution to the overall renewable energy consumption (adapted from [8]).....	21
Figure 1.2 Schematic of fluidized bed biomass firing system and the ash-related problems (pictures are taken from [24, 26-28]).....	23
Figure 2.1 Condensation of K during biomass combustion.....	34
Figure 2.2 K and Na contents in different kinds of biomass ash (adapted from [50]).....	35
Figure 3.1 TGA device.....	59
Figure 3.2 Furnace-balance system (left); schematic diagram (right).....	59
Figure 3.3 Mass loss (left) and derivative mass loss (DTG) curves obtained from TGA and FBS.....	60
Figure 3.4 Analysis devices.....	61
Figure 3.5 Schematic of the network.....	63
Figure 3.6 Kinetic mechanisms of cellulose, hemicellulose and lignin during the pyrolysis (adapted from [3, 8, 9]).....	64-65
Figure 3.7 Fitting results of the release of K (a), S (b) and Cl (c).....	67
Figure 4.1 Thermal characteristics of individual chemical components in the air (combustion) and nitrogen (pyrolysis) atmospheres.....	75
Figure 4.2 Thermal characteristics of biomass samples in the air and nitrogen atmospheres: (a) wheat straw; (b) softwood; (c) artificial wheat straw (AWS); (d) artificial softwood (ASW).....	77
Figure 5.1 Mass loss curve (red, left axis) and the percentage of K mass retained in residues (dry basis, black, right axis).....	85
Figure 5.2 Temperature-dependent transition route of K during combustion (Integrated with the conclusions from [2,4,13,18]).....	92

Figure 5.3 The change of K concentration (dry basis) with the change of heating rate.....	94
Figure 5.4 The change of the conversion ratio of the samples with the change of heating rate.....	97
Figure 6.1 Distribution of yielded products after devolatilisation.....	107
Figure 6.2 Comparison of results between this study (solid lines) and the Ref. [3] (dashed-dotted lines).....	108
Figure 6.3 Release profiles of the major species.....	110
Figure 6.4 Release profiles of intermediate species.....	112
Figure 6.5 Generalized reaction path of K.....	115
Figure 6.6 Reaction path diagrams of K in the low temperature range (the value on the arrows in represents the rates at which species are formed from other species, kmol/m <sup>3</sup> s).....	116-117
Figure 6.7 Reaction path diagrams of K in the medium temperature range (the value on the arrows in represents the rates at which species are formed from other species, kmol/m <sup>3</sup> s).....	119-120
Figure 6.8 Reaction path diagrams of K in the high temperature range (the value on the arrows in represents the rates at which species are formed from other species, kmol/m <sup>3</sup> s).....	122-123
Figure 6.9 Major transition cycles of K in different temperature ranges.....	124
Figure 7.1 The changes of release profiles of the major species with the change of initial input of Cl.....	132
Figure 7.2 Changes of major transition cycle of K with the change of initial input of Cl in the low temperature range (the value on the arrows in represents the rates at which species are formed from other species, kmol/m <sup>3</sup> s).....	138
Figure 7.3 Changes of major transition cycle of K with the change of initial input of Cl in the medium temperature range (the value on the arrows in represents the rates at which species are formed from other species, kmol/m <sup>3</sup> s).....	140

Figure 7.4 Changes of major transition cycle of K with the change of initial input of Cl in the high temperature range (the value on the arrows in represents the rates at which species are formed from other species, kmol/m<sup>3</sup> s).....141

Figure 7.5 The changes of release profiles of major species with the change of initial input of S.....142

Figure 7.6. The changes of release profiles of S-related species with the change of initial input of S.....145

Figure 7.7 Changes of major transition cycles of K with the change of initial input of S in the low temperature range (the value on the arrows in represents the rates at which species are formed from other species, kmol/m<sup>3</sup> s).....147

Figure 7.8 Changes of major transition cycles of K with the change of initial input of S in the medium temperature range (the value on the arrows in represents the rates at which species are formed from other species, kmol/m<sup>3</sup> s).....148

Figure 7.9 Changes of major transition cycles of K with the change of initial input of S in the high temperature range (the value on the arrows in represents the rates at which species are formed from other species, kmol/m<sup>3</sup> s).....149

Figure 7.10 Release route of K<sub>2</sub>SO<sub>4</sub> during the combustion process.....150

Figure 8.1 The changes of release profiles of major K compounds with the change of O<sub>2</sub> concentration.....159

Figure 8.2 The changes of release profiles of intermediate K compounds with the change of O<sub>2</sub> concentration.....160

## LIST OF TABLES

---

Table 2.1 Thermal characteristics of cellulose, hemicellulose and lignin.....	32
Table 2.2 Reaction rate coefficients for the K/O/H/Cl system*.....	44
Table 3.1 Proximate, ultimate and ash analysis of samples.....	58
Table 3.2 Summary of the kinetic parameters.....	67
Table 4.1 Sample list.....	74
Table 5.1 Summary of testing conditions.....	83
Table 5.2 Calculated uncertainty of the K concentration measurements at different final temperatures.....	84
Table 5.3 Summary of the SEM-EDX results at different temperatures.....	86
Table 5.4 Calculated uncertainty of the K concentration measurements at different heating rates.....	93
Table 5.5 Summary of the SEM-EDX results at different heating rates.....	95
Table 5.6 BDEs of K related bonds.....	98
Table 6.1 Characteristics of wheat straw and initial input values.....	107
Table 6.2 Initial Input of K and Cl (mol/ g biomass).....	109
Table 7.1 Initial input values of Cl and S.....	131
Table 8.1 Initial input values of O <sub>2</sub> .....	158
Table 8.2 Major transition cycles of K in the different temperature ranges.....	162
Table I Kinetic scheme of cellulose, hemicellulose and lignin pyrolysis.....	171-172
Table II Kinetic Scheme of K/S/Cl reactions.....	173-175
Table III Detailed reaction paths of K species under different conditions of initial input of Cl.....	176-177

Table IV Detailed reaction paths of K species under different conditions of initial input of S content.....	178-179
Table V Detailed reaction paths of K species under different conditions of combustion and pyrolysis.....	180-182

## ABBREVIATIONS

---

Al	Aluminium
Al <sub>2</sub> O <sub>3</sub>	Aluminium Oxide
ar	As Received
ASW	Artificial Softwood
AWS	Artificial Wheat Straw
BDEs	Bond Dissociation Energies
C	Carbon
Ca	Calcium
CaO	Calcium Oxide
CFD	Computational Fluid Dynamics
CH <sub>3</sub> OCH <sub>3</sub>	Dimethyl Ether
CH <sub>3</sub> OH	Methanol
Cl/Cl <sub>2</sub>	Chlorine
ClO	Chlorine-Oxygen
CO	Carbon Monoxide
CO <sub>2</sub>	Carbon Dioxide
CPFAAS	Collinear Photofragmentation and Atomic Absorption Spectroscopy
C <sub>2</sub> H <sub>5</sub> COOH	Propionic Acid
C <sub>6</sub> H <sub>5</sub> OH	Phenol
db	Dry Basis
DTG	Derivative Thermogravimetric

EDX	Energy Dispersive X-ray Spectroscopy
FAAS	Flame Atomic Absorption Spectrometry
FBS	High-temperature Furnace-Balance system
FC	Fixed Carbon
FES	Flame Emission Spectroscopy
Fe <sub>2</sub> O <sub>3</sub>	Iron (III) Oxide
GHG	Greenhouse Gas
H/H <sub>2</sub>	Hydrogen
HCl	Hydrochloric
HO <sub>2</sub>	Hydroperoxyl
H <sub>2</sub> O	Water
H <sub>2</sub> O <sub>2</sub>	Hydrogen Peroxide
IC	Ion Chromatography
ICCD	Intensified Charge Couple Device
ICP-MS	Inductively Coupled Plasma Mass Spectroscopy
ICP-OES	Inductively Coupled Plasma Optical Emission Spectroscopy
K	Potassium
KAlSiO <sub>4</sub>	Potassium Aluminium Silicate
KAlSiO <sub>6</sub>	Potassium Aluminium Silicate
KAlSi <sub>2</sub> O <sub>6</sub>	Potassium Aluminium Silicate
KAlSi <sub>3</sub> O <sub>8</sub>	Potassium Aluminium Silicate
KCl	Potassium Chlorine
KHSO <sub>4</sub>	Potassium Bisulphate

KO	Potassium-Oxygen
KO <sub>2</sub>	Potassium Superoxide
KOH	Potassium Hydroxide
KPO <sub>3</sub>	Potassium Metaphosphate
KSO <sub>2</sub> /KSO <sub>3</sub>	Potassium Sulphite
KSO <sub>3</sub> Cl	Potassium Chloride Sulphite
K <sub>2</sub> CaSiO <sub>4</sub>	Potassium Calcium Silicate
K <sub>2</sub> CO <sub>3</sub>	Potassium Carbonate
K <sub>2</sub> CrO <sub>4</sub>	Potassium Chromate
K <sub>2</sub> Cr <sub>2</sub> O <sub>7</sub>	Potassium Dichromate
K <sub>2</sub> O	Potassium Oxide
K <sub>2</sub> P <sub>2</sub> O <sub>7</sub>	Potassium Pyrophosphate
K <sub>2</sub> SO <sub>4</sub>	Potassium Sulphate
K <sub>2</sub> SiO <sub>3</sub>	Potassium Silicate
K <sub>2</sub> Si <sub>4</sub> O <sub>9</sub>	Potassium Silicate
K <sub>3</sub> PO <sub>4</sub>	Tripotassium Phosphate
LIG	Lignin
LIG-C/H/O	Lignin-C/H/O
LIBS	Laser-Induced Breakdown Spectroscopy
Mg	Magnesium
MgO	Magnesium Oxide
MSA	Mass Spectrometer Analysis
N/N <sub>2</sub>	Nitrogen

Na	Sodium
Na <sub>2</sub> O	Sodium Oxide
NH <sub>3</sub>	Ammonia
NIST	National Institute of Standards and Technology
O/O <sub>2</sub>	Oxygen
OH	Hydroxide
P <sub>2</sub> O <sub>5</sub>	Phosphorus Pentoxide
S	Sulphur
SH	Sulphur-Hydrogen
SEM	Scanning Electron Microscopy
Si	Silicon
SiO <sub>2</sub>	Silicon Dioxide
SO <sub>2</sub>	Sulphur Dioxide
SO <sub>3</sub>	Sulphur Trioxide
TDLAS	Tunable Diode Laser Absorption Spectroscopy
TG	Thermogravimetry
TGA	Thermogravimetric Analyzer
Ti	Titanium
TiO	Titanium (II) Oxide
VM	Volatile Matter
XRF	X-ray Fluorescence Spectrometer

## NOMENCLATURE LIST

---

A	Pre-Exponential Factor (First Order: 1/s)
b	Empirical Parameter
$C_p$	Heat Capacity (J/K)
E	Activation Energy (kJ/mol)
$f(\alpha)$	Reaction Model
H	Total Enthalpy (J)
i	Generated/Consumed Species
k	Reaction Rate Constant
m	Mass (g)
n	Fitting Times
Q	Rate of Heat Transfer through Walls (W)
R	Universal Gas Constant (J/mol·K)
r	All the Reactions that Related to Species i
T	Reaction Temperature (K)
t	Time (s)
W	Molecular Weight
Y	Mass Fraction

---

### Subscript

exp	Result of the Release of Element from the Experiment
i	Species
i <sub>gen</sub>	Generation of the Species i
in	Flow Rate of the Content in the Reactor
i <sub>0</sub>	Initial of the Species i

ir	Remaining of the Species i
it	Species i at Time t
out	Flow Rate of the Content Out of the Reactor
sim	Result of the Release of Element from the Simulation

---

### **Greek Symbols**

$\alpha$	Fractional Conversion of the Species
$\beta$	Heating Rate (K/min)
$\nu$	Stoichiometric Coefficient

# CHAPTER 1

## INTRODUCTION

---

### 1.1 Background

Global rapid development has increased the energy consumption by approximately 165% since 1970; various kinds of sources are used to generate energy, yet the way in which energy is generated from traditional fossil fuels remains predominantly unchanged [1]. Because they are cheap, efficient and reliable source of energy, conventional fossil fuels supply more than 70% of the world energy demand [2]. However, the high demand for energy has resulted in a rapid depletion of energy sources, which has led to a worldwide energy crisis. It is anticipated that these fossil fuel sources will deplete within the next 40 years for oil and gas, and within 100 years for coal [3]. The energy crisis has become increasingly severe because of the massive consumption of non-renewable fuels. Besides, the large consumption of traditional fossil fuels has caused a 125% rise in energy-related CO<sub>2</sub> emissions during the same period with emissions reaching a historic high of 32.5 gigatonnes in 2017-2018 [4]. The enormous CO<sub>2</sub> emission as greenhouse gas (GHG) is one of the main reasons that cause the current global warming [5]. Under these circumstances, it is imperative to find alternative renewable energy sources to ease the dependence on traditional fossil fuels and to reduce the net-CO<sub>2</sub> emission. Currently, renewable energy provides over 10% of world energy supply [6], and the renewable energy resources that are used worldwide are wind energy, solar energy, hydro energy, geothermal energy and biomass energy [7]. Their contribution to the total world renewable energy consumption is summarised in Figure 1.1.

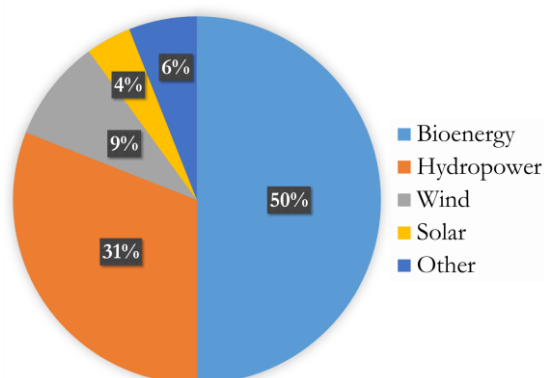


Figure 1.1 Different fuels' contributions to the overall renewable energy consumption. (adapted from [8])

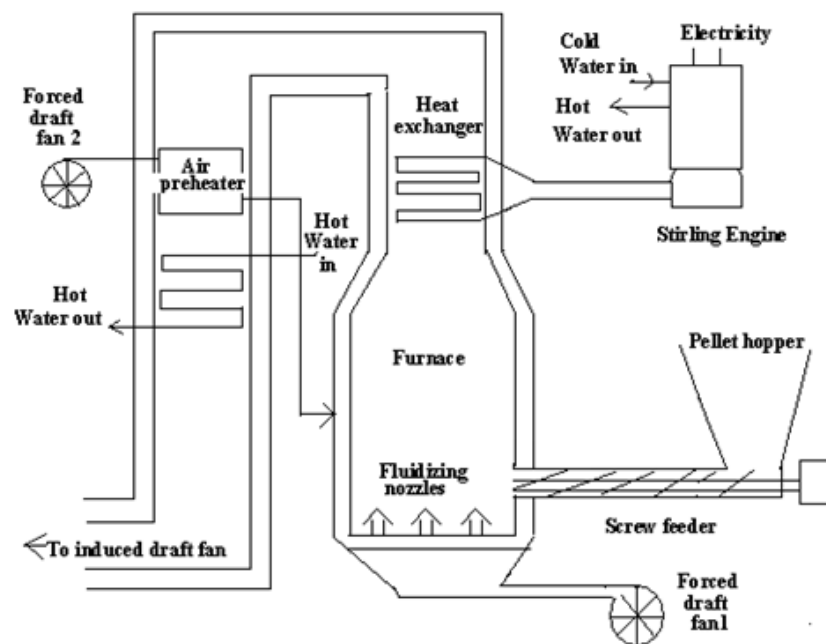
## 1.2 Biomass energy

As shown in Figure 1.1, bioenergy contributes half of the current renewable energy consumption among the renewable energy sources, and it is predicted to be the largest source of growth in renewable consumption over the period 2018-2023 [8]. Bioenergy is the energy stored in biomass resources. As reported by Shafiee et al.[3], the world bioenergy potential is approximately 1700EJ/y from wood and 1200EJ/y from herbaceous plants [9], which made the forest by-products (i.e. branches, bark, sawdust and shell) and agricultural crop residues (i.e. straw, stalks, cobs and husks) are among the most used resources for bioenergy today and supply the most of the biomass consumption.

Biomass is defined as any organic matter which is derived from plants, animal materials, organic industrial and human and animal wastes [10, 11]. According to its definition, there are various kinds of biomass resources such as products, by-products and residues from agriculture, forestry etc. [12]. Biomass is a sustainable and clean energy source, due to its unlimited supply, as people can always grow agricultural products and trees, wastes will always exist, and these make biomass an easily accessible and affordable energy source for most parts of the world [13]. Also, the thermal treatment of biomass will add no extra CO<sub>2</sub> to the atmosphere compared to the use of traditional fossil fuels (e.g. coal, natural gas and petroleum) when neglecting the transportation and processing steps, as the CO<sub>2</sub> produced from fully combusted biomass is equal to the amount which was taken from the atmosphere during the growing stage of plants and trees [2, 14]. In fact, biomass source has great potential to replace the traditional fossil fuel, as it shares many characteristics with fossil fuels, which means that the existing combustion apparatus for solid fossil fuels can also be used for biomass feedstock, and this could save a great deal of time and money in not having to redesign the boilers. Furthermore, the most used lignocellulosic biomass is not part of the human food chain; therefore, its use for energy does not threaten the world's food supply [15].

Biomass can be converted to fuel energy by numerous methods such as pyrolysis, gasification and combustion, among which, direct combustion and co-combustion with coal for electricity and heating production from biomass materials have been found to be a promising way for the near future [16]. Despite its renowned advantages such as high-energy-generation potential and CO<sub>2</sub> neutral character, thermal conversion of biomass for

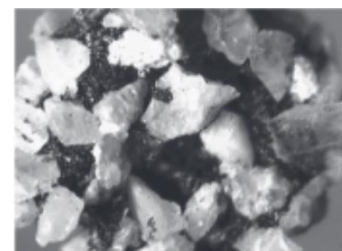
energy production remains challenging for several reasons. The challenges include its low energy density, collection, transportation and storage costs [17], pelleting and milling, firing and co-firing technologies and ash-related problems that occur both during and after the thermal conversion process [18]. Among these issues, ash-related problems during the thermal conversion process remain the most challenging problem for the general use of biomass [19]. As shown in Figure 1.2, in a typical industrial plant, the ash-related issues that happened in the firing system include alkali-induced slagging, which can limit the heat transfer and thus reduce the boiler efficiency [20, 21]; corrosion on the boiler surfaces which is caused by the accumulated ash underneath the slagging deposit [22, 23]; and ash agglomeration and fusion phenomena inside the boiler [24, 25].



Slagging



Corrosion



Agglomeration

Figure 1.2 Schematic of fluidized bed biomass firing system and the ash-related problems (pictures are taken from [24, 26-28])

The severity of ash-related problems depends mostly on the fractions of alkali metals and other inorganic elements, such as Cl and S in the virgin biomass that are transferred to the vapour, and the fraction that remains in the solid products [29]. These issues become particularly extreme when utilising herbaceous and agricultural residues (straw), fast-growing non-food crops and wood species, which contain high concentrations of alkali metals, Cl and S [30].

Previous studies [31-39] are mainly focused on the release behaviour of alkali metals during the thermal conversion process of biomass in a preheated reactor at temperatures around 1000°C. Only a few studies have attempted to investigate the release behaviour of alkali metals from biomass that thermally treated with different operating conditions [40, 41]. Still, these research were not designed to study the influences of operating factors on the release of K. There is a lacking of study regarding how the change of operating conditions affect the release behaviour of alkali metals, as they can significantly affect the compositions and properties of thermal conversion of biomass and thus manipulate the release behaviour of alkali metals [42]. Besides, the transformation of particle structural during the thermal conversion could also affect the release fate of alkali metal, but this kind of information is seldom reported either. Moreover, only several attempts [43-46] have been carried out to develop a model to predict the released amount of elemental alkali metals from biomass; however, they are equilibrium based and mainly focus on the prediction of the total amount of released elemental or atomic alkali metals. There is an urgent need to develop a kinetically controlled model, which can provide dynamic information on the release behaviour of K and to predict the release of different alkali metal compounds temperature/time-dependently.

As the thermal conversion of biomass is a promising energy supply method, better understanding the release mechanisms of alkali metals can provide useful information to control the release of ash compounds. Moreover, the prediction of their release profiles using modelling tools can help us to make a quick judgment as to what extent different alkali metals species would be released to the gas phase, and thus will provide crucial information to enhance apparatus design and to control and mitigate the ash-related problems. It is anticipated to offer insights of knowledge for guiding the development of ash-problem-free biomass combustion technologies as well as prolonging the service life

of biomass boilers, with interests of making the biomass energy more economically competitive and environmentally friendly.

### 1.3 Project aims and objectives

This work aims to improve and extend the investigation on the release mechanism of K during combustion of biomass via experimental methods and the development of a kinetically controlled model that can be used to predict the release profiles of different K compounds under different circumstances. Several vital objectives are defined to address the aim of this research:

- Investigate the mutual interactions among cellulose, hemicellulose and lignin during the combustion process in controlled lab-scale experiments.
- Quantify the K content in the solid residues obtained under different combustion conditions experimentally, and characterise the ash residues using morphology method.
- Develop a kinetically controlled model to predict the release of different K compounds during biomass combustion.
- Use the developed model to determine the influence of combustion conditions on the release profiles of different K compounds during the thermal conversion process of biomass.

### 1.4 Summary of thesis outline

The outline of this thesis, including a brief description of each chapter, is provided below:

Chapter 2. This chapter presents a critical literature review undertaken on biomass sources, combustion of biomass and the associated ash-related challenge. The existing knowledge available on the experimental and modelling study on the release mechanisms of ash-related elements is then reviewed, followed by the details of gaps in the research.

Chapter 3. This chapter first describes the raw materials, experimental devices and analysis methods used in this study. Secondly, a detailed explanation of the development of the kinetically controlled model is provided.

Chapter 4. This chapter demonstrates the experimental study on the combustion characteristics of major chemical compositions of biomass and then compares the thermal behaviour of artificial and natural biomass. The experimental data are used to investigate the influence of interactions among major compositions on the combustion behaviour of

biomass. An evaluation is made of the feasibility to use the major chemical compositions as initial input in the model study.

Chapter 5. This chapter provides the results of experimental tests of the release behaviour of K and ash characterisation from the combustion of wheat straw via a custom-designed reactor. The tests are carried out with different operating factors (final temperature and heating rate), in order to assess the influence of operating factors on the K transition performance during the combustion process.

Chapter 6. This chapter provides the model prediction of the release of K compounds under different final temperatures via the developed two-step kinetic model. It then discusses the transition routes among the different K compounds at different final temperatures.

Chapter 7. In this chapter, the model predicted results of the release of different K compounds with the different initial Cl and S contents are presented, along with the change of transition routes. The influence of changing of initial Cl and S contents on the release behaviour of K compounds during the combustion process is then discussed.

Chapter 8. This chapter illustrates the prediction of the release of K compounds under the condition of combustion and pyrolysis, as well as comparing the transition route within different temperature ranges. The discussion about how the existence of O<sub>2</sub> affects the release behaviour of K compounds during the thermal conversion process is carried out afterwards.

Chapter 9. This final chapter displays the main conclusions for the experimental and modelling outcomes of this PhD work. Then it gives suggestion and recommendations for future research.

## Bibliography

1. Global, B.P., BP statistical review of world energy June 2017. Relatório. Disponível em: <http://www.bp.com/en/global/corporate/energy-economics/statistical-review-of-world-energy.html>, 2017.
2. Saidur, R., et al., A review on biomass as a fuel for boilers. *Renewable and Sustainable Energy Reviews*, 2011. 15(5): p. 2262-2289.
3. Shafiee, S. and E. Topal, When will fossil fuel reserves be diminished? *Energy Policy*, 2009. 37(1): p. 181-189.
4. Iea.org. (2019). Global Energy & CO<sub>2</sub> Status Report. [online]. Available at: <https://www.iea.org/geco/> [Accessed 6 Mar. 2019].
5. Karl, T.R., et al., Global climate change impacts in the United States. 2009: Cambridge University Press.
6. IEA, S., International Energy Agency, 2016. 2017.
7. Ellabban, O., H. Abu-Rub, and F. Blaabjerg, Renewable energy resources: Current status, future prospects and their enabling technology. *Renewable and Sustainable Energy Reviews*, 2014. 39: p. 748-764.
8. Iea.org. (2019). Renewables 2018: Key Findings. [online]. Available at: <https://www.iea.org/renewables2018/> [Accessed 28 Feb. 2019].
9. Tao, G., et al., Biomass properties in association with plant species and assortments I: a synthesis based on literature data of energy properties. *Renewable and Sustainable Energy Reviews*, 2012. 16(5): p. 3481-3506.
10. Lim, C.H. and H.L. Lam, Biomass supply chain optimisation via novel biomass element life cycle analysis (BELCA). *Applied Energy*, 2016. 161: p. 733-745.
11. Chiew, Y.L., T. Iwata, and S. Shimada, System analysis for effective use of palm oil waste as energy resources. *Biomass and Bioenergy*, 2011. 35(7): p. 2925-2935.
12. Long, H., et al., Biomass resources and their bioenergy potential estimation: A review. *Renewable and Sustainable Energy Reviews*, 2013. 26: p. 344-352.
13. Demirbas, A., Combustion characteristics of different biomass fuels. *Progress in Energy and Combustion Science*, 2004. 30(2): p. 219-230.
14. Field, C.B., J.E. Campbell, and D.B. Lobell, Biomass energy: the scale of the potential resource. *Trends in Ecology & Evolution*, 2008. 23(2): p. 65-72.

15. Marriott, P.E., L.D. Gómez, and S.J. McQueen-Mason, Unlocking the potential of lignocellulosic biomass through plant science. *New Phytologist*, 2016. 209(4): p. 1366-1381.
16. Demirbas, A., Potential applications of renewable energy sources, biomass combustion problems in boiler power systems and combustion related environmental issues. *Progress in Energy and Combustion Science*, 2005. 31(2): p. 171-192.
17. Vassilev, S.V., et al., An overview of the chemical composition of biomass. *Fuel*, 2010. 89(5): p. 913-933.
18. Rycroft, M., *Co-firing biomass with coal for power generation*. 2015, EE Publishers.
19. Cao, W., et al., Release of alkali metals during biomass thermal conversion. *Archives of Industrial Biotechnology*, 2016. 1(1).
20. Xu, W., et al., A new agro/forestry residues co-firing model in a large pulverized coal furnace: Technical and economic assessments. *Energies*, 2013. 6(9): p. 4377-4393.
21. Livingston, W. Biomass ash deposition, erosion and corrosion processes. in *Workshop on ash related issues in biomass combustion*. Glasgow: IEA Task. 2006.
22. Melissari, B., Ash related problems with high alkali biomass and its mitigation experimental evaluation. *Memoria Investigaciones en Ingeniería*, 2014. 12: p. 31-44.
23. Nielsen, H., et al., The implications of chlorine-associated corrosion on the operation of biomass-fired boilers. *Progress in Energy and Combustion Science*, 2000. 26(3): p. 283-298.
24. Yu, C., et al., Experimental determination of agglomeration tendency in fluidized bed combustion of biomass by measuring slip resistance. *Fuel*, 2014. 128: p. 14-20.
25. Pääspanen, M.H., et al., Prediction of bed agglomeration propensity directly from solid biofuels: a look behind fuel indicators. *Energy & Fuels*, 2012. 26(4): p. 2427-2433.
26. Focus on Biomass Ash. <http://biomassproject.blogspot.com/2014/01/focus-on-biomass-ash.html>, 2014. Accessed 1 Sep. 2019.

27. Combating corrosion, fouling and emissions in biomass fired heat and power plants. <http://www.besustainablemagazine.com/cms2/chlorout-combating-corrosion-fouling-and-emissions-in-biomass-fired-heat-and-power-plants/>, 2013. Accessed 1 Sep, 2019.
28. Swaminathan, R., Cost effective, low capacity, biomass fired power plant. *Energy and Power*, 2013. 3(1): p. 1-6.
29. Tchoffor, P.A., K.O. Davidsson, and H. Thunman, Transformation and release of potassium, chlorine, and sulfur from wheat straw under conditions relevant to dual fluidized bed gasification. *Energy & Fuels*, 2013. 27(12): p. 7510-7520.
30. Sommersacher, P., et al., Application of novel and advanced fuel characterization tools for the combustion related characterization of different wood/kaolin and straw/kaolin mixtures. *Energy & Fuels*, 2013. 27(9): p. 5192-5206.
31. Meng, X., et al., Release of Alkalis and Chlorine from Combustion of Waste Pinewood in a Fixed Bed. *Energy & Fuels*, 2019. 33(2): p. 1256-1266.
32. Fagerström, J., et al., Alkali transformation during single pellet combustion of soft wood and wheat straw. *Fuel Processing Technology*, 2016. 143: p. 204-212.
33. Johansen, J.M., et al., Release of K, Cl, and S during combustion and co-combustion with wood of high-chlorine biomass in bench and pilot scale fuel beds. *Proceedings of the Combustion Institute*, 2013. 34(2): p. 2363-2372.
34. Mason, P.E., et al., Observations on the release of gas-phase potassium during the combustion of single particles of biomass. *Fuel*, 2016. 182: p. 110-117.
35. Liu, Y., et al., Characteristics of alkali species release from a burning coal/biomass blend. *Applied Energy*, 2018. 215: p. 523-531.
36. Sommersacher, P., et al., Simultaneous Online Determination of S, Cl, K, Na, Zn, and Pb Release from a Single Particle during Biomass Combustion. Part 1: Experimental Setup—Implementation and Evaluation. *Energy & Fuels*, 2015. 29(10): p. 6734-6746.
37. Sommersacher, P., et al., Simultaneous online determination of S, Cl, K, Na, Zn, and Pb release from a single particle during biomass combustion. Part 2: results from test runs with spruce and straw pellets. *Energy & Fuels*, 2016. 30(4): p. 3428-3440.

38. Fatehi, H., et al., LIBS measurements and numerical studies of potassium release during biomass gasification. *Proceedings of the Combustion Institute*, 2015. 35(2): p. 2389-2396.
39. Striūgas, N., M. Sadeckas, and R. Paulauskas, Investigation of K\*, Na\* and Ca\* flame emission during single biomass particle combustion. *Combustion Science and Technology*, 2019. 191(1): p. 151-162.
40. Van Lith, S.C., et al., Release to the gas phase of inorganic elements during wood combustion. Part 1: development and evaluation of quantification methods. *Energy & Fuels*, 2006. 20(3): p. 964-978.
41. Wu, D., et al., Release of alkali metals during co-firing biomass and coal. *Renewable Energy*, 2016. 96: p. 91-97.
42. Cao, W., et al., Experimental study on the influences of operating parameters on the retention of potassium during the biomass combustion. *Energy Procedia*, 2019. 158: p. 1033-1038.
43. Zhang, Z., et al., Experiments and modelling of potassium release behavior from tablet biomass ash for better recycling of ash as eco-friendly fertilizer. *Journal of Cleaner Production*, 2018. 170: p. 379-387.
44. Akbar, S., U. Schnell, and G. Scheffknecht, Modelling potassium release and the effect of potassium chloride on deposition mechanisms for coal and biomass-fired boilers. *Combustion Theory and Modelling*, 2010. 14(3): p. 315-329.
45. Fatehi, H., et al., Modeling of alkali metal release during biomass pyrolysis. *Proceedings of the Combustion Institute*, 2017. 36(2): p. 2243-2251.
46. Liu, Y., et al., Measurement and kinetics of elemental and atomic potassium release from a burning biomass pellet. *Proceedings of the Combustion Institute*, 2019. 37(3): p. 2681-2688.

## CHAPTER 2

### LITERATURE REVIEW

---

This literature review chapter firstly describes lignocellulosic biomass, its composition and chemical structure. Secondly, it introduces the most used technology to utilize biomass resources. It discusses the ash-related problems that are caused by the usage of biomass materials, and the importance to study the release mechanisms of ash-related elements is provided. Then, this chapter critically reviews the existing knowledge available on the experimental and modelling study on the release mechanisms of ash-related elements. The final part will illustrate the research gap and the areas needing attention.

#### 2.1 Lignocellulosic biomass

Biomass is defined as any organic matter, which is derived from plant and animal materials such as crops, wood, material left over from agricultural and forestry processes, organic industrial, and human and animal wastes [1]. Biomass contains varying amounts of organic materials, like cellulose, hemicellulose, lignin and small amounts of lipids, proteins, simple sugars and starches. It also contains inorganic constituents, which represents ash-forming components, like alkali and alkaline earth metals (K, Na, Ca and Mg) [2], Cl, S and Si, as well as moisture. Among the organic compounds, cellulose, hemicellulose and lignin are the three main constituents in biomass; they are strongly intermeshed and bonded inside the biomass materials [1]. The combination of cellulose, hemicellulose and lignin are called “lignocellulose”, lignocellulosic biomass (which includes woody, herbaceous biomass, and et al.) is the most abundant carbohydrate on Earth [3]. Thus making it one of the most promising biomass sources to use as fuel and has been studied in detail.

Cellulose is generally the largest component of lignocellulosic biomass, which presents 40-50 wt% of the biomass. It is a long-chain polymer with a high degree of polymerization and massive molecular weight. It is followed by hemicellulose, which is a macromolecule constructed from different sugars and normally occupies 20-40 wt% of the biomass. Lignin usually presents about 20-35 wt% of the biomass; it is an aromatic polymer synthesized from phenylpropanoid precursors and acts as a cementing agent for cellulose fibres holding adjacent cells together [1, 4-6]. As cellulose, hemicellulose and lignin account for most of the biomass mass, their thermal properties directly influence the

thermal behaviour of lignocellulosic biomass. In addition, their thermal characteristics [5, 7-10] are summarised in Table 2.1. As indicated, cellulose and hemicellulose mainly contribute to the release of volatile matter during thermal conversion, while lignin controls the formation of char.

Table 2.1 Thermal characteristics of cellulose, hemicellulose and lignin

	Cellulose	Hemicellulose	Lignin
Initiation of pyrolysis	277-357°C	152-352°C	252-502°C
Major products	Liquid tar	Gas + relatively less tar	Char

## 2.2 Combustion of lignocellulosic biomass and ash-related challenges

Biomass can be converted to energy by means of conversion technologies, i.e., pyrolysis, combustion, co-combustion and gasification, among which, direct combustion of biomass is the most mature method and the only proven technology to utilize biomass for heat and power production in the near future [1, 11, 12]. Besides, biomass shares many similar characteristics to those of solid fossil fuels like coal; therefore, the current solid fossil fuel-treatment facilities can be slightly modified or directly used to treat biomass; this could save lots of time and costs to redesign and rebuild the devices. Currently, combustion of biomass is responsible for over 97% of the world's bioenergy production [13]. However, several challenges restrict its comprehensive usage when burning the lignocellulosic biomass, i.e., pre-preparation of biofuel (collection, transportation, leaching, pelleting and milling), energy efficiency, firing and co-firing technologies (injection co-firing, co-milling, pre-gasification co-firing, etc.), and ash-related problems that happen during and after the combustion [14, 15].

Among the discussed challenges when utilizing biomass sources, ash-related issues (i.e. slagging, agglomeration and corrosion) remain as the most intractable problem [14] and restrict the comprehensive usage of biomass. Within the combustion stage, the slagging phenomenon on the heating surfaces inhibit heat transfer by increasing thermal resistance and decreasing its absorption of radiation [16] and would thus reduce the boiler efficiency [17, 18]. Moreover, the accumulated ash on the tube surfaces can result in the corrosion underneath the deposit [19-21], which could further damage the boiler and cost more to fix the device. Alongside slagging and corrosion, the agglomeration phenomenon also remains a significant challenge in biomass combustion, as it can lead to the unscheduled

shutdown of the entire power plant [21-24]. The agglomeration is usually caused by the accumulation of low melting point ashes, as well as its reaction with Si and Ca to generate more low-melting K-Si-Ca salt and adhere together via molten phase [21, 25, 26]. Besides, the condensed ash can increase the fine solid fraction, which accumulates in the grate and then causes sintering, affecting the conversion in the bed, restricting the effectiveness of the boiler and negatively affect the appropriate control of gaseous emission [27-31]. Additionally, partial of the fine ash particles can end up being released as aerosols to the atmosphere, leading to the respiratory diseases [32, 33].

During the combustion process, the aforementioned ash related problems are mainly caused by the release of inherent alkali metal content from biomass. Alkali metals undergo a series of complex chemical reactions and transformation and then released as gaseous products. After release, the flue gas starts to cool down, leading to part of the alkali metal aerosols to grow and form submicron ash particles via the routes of nucleation, adsorption, condensation, and chemical reaction. The submicron ash particles could then condense on the surfaces of the heating area and form the first layer of sticky slagging through thermophoresis and turbulent diffusion. The initial sticky layer can act like an adhesive that captures the subsequent fly ash and adherent to the heating surfaces [34, 35]. Moreover, partial of the alkali metal aerosols could also condense on the surface of the fly ash in the boiler and either form a sticky layer to the fly ash or form low-melting species through the reaction with  $\text{SiO}_2$  [14] and  $\text{Fe}_2\text{O}_3$  [35], which are contained in the fly ash. Furthermore, partial of the alkali metal aerosols can form low-temperature eutectic mixtures, like  $\text{KCl} + \text{K}_2\text{SO}_4$  that can melt at  $550^\circ\text{C}$  [36] and become part of the sticky layer. Afterwards, the formed coarse fly ash, with or without the aforementioned sticky layer, will be deposited on the surface of the existing initial layer of sticky slagging via inertial impaction [37, 38]. Once the initial slagging layer is no longer adhesive enough to capture and hold further fly ash, a new sticky slagging layer reforms, which mainly contains submicron ash particles that are enriched in alkali metals [14]. Subsequently, the accumulated submicron ash particles and the captured coarse ash particles lead to the formation of an overlapping multi-layered structure [38]. Alongside acting as a supporting role in the formation of multi-layered slagging, the alkali metals can also play a role to cause agglomeration when combined with  $\text{SiO}_2$  during the combustion process. Aside from inducing the slagging, there is also partial of the alkali metals could react with  $\text{SiO}_2$  in the fly ash and generate molten silicates. As a result, these low melting temperature

K-Si species can be formed on the surfaces of bed particles via the reactions with gaseous, aerosols or even liquid K compounds. Besides, the occurrence of agglomeration during combustion is also related to the direct adhesion of bed particles through the partial molten ash-derived K-Si particle/droplet [39, 40]. According to the above mechanisms, a schematic of the condensation of alkali metal (K) during the combustion of biomass is illustrated in Figure 2.1.

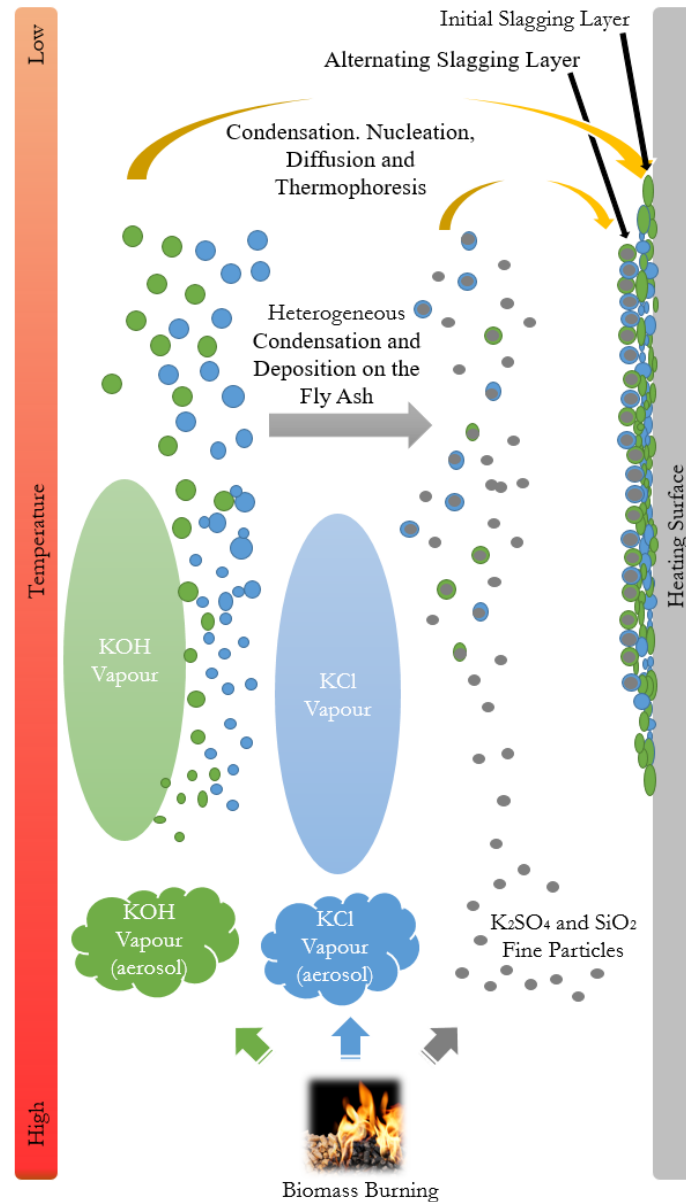


Figure 2.1 Condensation of K during biomass combustion

In conclusion, the release of alkali metals is the main reason that causes the series of ash-related problems during the combustion process of biomass, accompanied by the release

of Cl and S content and the inherent Si content. Therefore, the release mechanisms of alkali metals have been studied intensively, with the aim to better understand and control the ash-related problems. Among the release of alkali metals, scholars are more focused on the investigation of the release of K and Na content from biomass samples, especially the release of K content as there is a much higher concentration of K in the biomass than that of Na. Figure 2.2 summarises the K and Na content in the different kinds of biomass sources. As we can see, K content is higher than that of Na content in the ash analysis, and this could result in more severely K-induced ash problems. Normally, K is a crucial macro-nutrient for growing plants [41], especially in the woody and herbaceous biomass, which consists of 0.4 wt% and 1.3 wt% of initial K content, respectively [42]. More than 60-90% of the inherent K content in woody biomass and over 50% of the inherent K content in herbaceous biomass could be released after complete combustion at a final temperature over 900°C [43-45]. By contrast, Na is not an essential stimulant for the growth of plants and can be toxic with higher concentrations [41]. Besides, the concentration of K is around one to two orders-of-magnitude large than that of Na [46, 47] inherent the lignocellulosic biomass, leading to the more common studies in the release of K than those of Na [48]. Additionally, due to the abundant consumption of lignocellulosic biomass materials nowadays, the loss of large amounts of nutrients like K in the soil could affect the sustainability of the ecosystem negatively [49]. Since K is a key nutrient to grow plants, the loss of K in the soil would result in the deterioration of the soil.

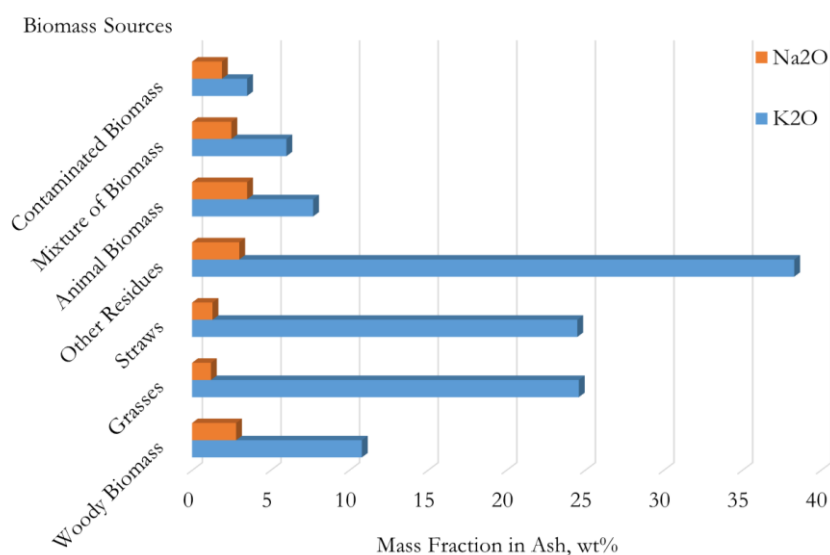


Figure 2.2 K and Na contents in different kinds of biomass ash (adapted from [50])

In order to better understand the release behaviour of K during the thermal conversion process of biomass, so to mitigate the K-induced ash-related problems, the study that focus on the release mechanisms and kinetics of K has been carried out experimentally for decades, as well as the attempt on predicting the release profiles of K via the simulation method.

### 2.3 Experimental study on the release of K

As stated before, combustion is a widely used technology to treat biomass source; therefore, the study of release behaviour of K is more commonly focused on the combustion process of biomass. Alongside the combustion, pyrolysis is another thermal treatment that used to treat biomass materials, but not as mature as combustion technology; however, suffering the K-induced ash problems as well. In this way, this part will firstly review the study that focuses on the release behaviour of K during the combustion process and then review the research that focuses on the release behaviour of K during the pyrolysis process.

#### 2.3.1 Release of K during the combustion process

During the thermal conversion process, the release behaviour of K from biomass samples can be studied by tracking its composition either in the gaseous products or in the remaining solid residues. This study involves various kinds of detective technologies, i.e., Inductively Coupled Plasma Optical Emission Spectroscopy (ICP-OES)/Mass Spectroscopy (ICP-MS) [51], Flame Emission Spectroscopy (FES) [52], Laser-Induced Breakdown Spectroscopy (LIBS) [53], Flame Atomic Absorption Spectrometry (FAAS) [54] and et al.

##### 2.3.1.1 Quantify the loss of K content from solid residues

ICP-MS/OES is the most used technique to quantify the left K content in the digested solution of solid residues from the combustion of biomass. Then the results are used to investigate the release behaviour of K. The study carried out by Meng et al. [55] on the K release from the combustion of woody material in a fixed-bed reactor reveals that large fraction (around 80%) of K in the woody biomass is in the form of inorganic salts, i.e. KCl and  $K_2CO_3$ . Besides, moderately high primary airflow rates could lead to an enhanced release of K content from biomass during the combustion process. Fagerstrom et al. [56] also reported the alkali transformation during the combustion process of wood and wheat straw pellet, and according to their study, wood and wheat straw has a similar release

behaviour of K content when the combustion temperature below 700°C. The release of K happens mainly during the char combustion phase, and the total release of K content is around 30% and 20% for wood and wheat straw, respectively. Moreover, the ash analysis concluded that K could be captured by glassy silicates and remains as molten ash in the solid residues eventually.

In van Lith et al.'s series research [45, 46] on the release of gas-phase K during the wood combustion, they concluded that the release of K strongly relies on both the combustion temperature and the fuel composition. The release of K in noticeable amount starts at around 500°C, and the released amount is relatively low (approximately 20%) up to 800°C, which is mainly caused by the release of char-K (originating from organically associated K and/or KCl that reacted with char during the pyrolysis phase). When the temperature is higher than 850°C, the release of K strongly relies on the inorganic composition of the biomass material and could happen the decomposition of  $K_2CO_3$ . Moreover, Knudsen et al. [44] and Johansen et al. [43] presents the similar release mechanism of K content via the observation of combustion of annual biomass through a controlled lab-scale experiment, which is, at a temperature below 700°C, Cl is the primary facilitator for the release of K content through the sublimation of KCl. However, K released to the gas phase in a significant amount at temperatures above 700°C, and at 1150°C, about 50-90% of the total initial K is released to the gas phase. In addition, Johansen et al [57] also observed a liner raise of the release of K from 50% at 900°C to 80% at 1200°C during the combustion of corn stover.

Besides, the X-ray Fluorescence Spectrometer (XRF) technique is also used to detect the K concentration in the solid residues. As reported by Jin et al. [58], high reactivity K compounds would be released to the gas phase during the combustion of biomass, which then undergoes complex reactions. KCl is the most stable K containing species in the system, and when the temperature is lower than 700°C, KCl presents mainly in the form of fine particles, while at temperatures higher than 800°C, it is mostly in the form of vapour.

Apart from been released in the main form of KCl, KOH and  $K_2CO_3$ , K could also exist in the ash as  $K_2SO_4$  and evaporated at temperatures above 1000°C [59]. Besides, according to the study [43], Si/Al chemistry plays a crucial role in the retention of K in the residues.

As stated by Oris et al. [60] and Yang et al. [61], after the combustion, the left K in the residue matrix mainly exists in the form of  $\text{KAlSi}_2\text{O}_6$ ,  $\text{KAlSiO}_4$ ,  $\text{KAlSi}_3\text{O}_8$  and  $\text{KAlSiO}_6$ . This result indicates that the Si and Al contents in biomass fuel could inhibit the release of K during the combustion process.

#### 2.3.1.2 Directly observation on the release of gas-phase K

Alongside the study of release behaviour of K from the solid residues, direct observation on the release of gas-phase K during the biomass combustion is another effective way to study the release behaviour of K, and many different techniques have been used to approach this goal.

In He et al. [62] study, the release of gas-phase K from the combustion of biomass in a Hencker Burner was detected in-situ by FES, through the investigation, it is feasible to use FES for on-line monitoring the release of gas-phase K content during the combustion. In addition, three stages (devolatilisation, char and ash) can be distinguished by the changing points of K concentration. The study also proposed that the volatile content in the biomass influences the release behaviour of K; the change of water content can significantly affect the ratio of the release of K from low-volatile-contained biomass. Same detective technique also used by Mason et al. to observe a time-dependent release of K during the biomass combustion. General release behaviours of K are made through the online observation: (1) The release of K content during the devolatilisation stage of combustion is small compared to the subsequent release during the char oxidation stage. (2) The peak rate of release during char oxidation correlates to the initial K content in the biomass. (3) During the combustion, the proportion of K released to that retained correlates to the initial K content.

Besides, LIBS is another online detective device that commonly used to observe the release of gas-phase K during the combustion process, as studies reported by Fatehi et al. [63], Liu et al. [64, 65] and Zhang et al. [66]. According to their observation, there is only a minor fraction of K released during the devolatilisation stage (4-5%). While at the char oxidation stage, the release rate of K slowly increased at first, then becomes more steeply, the peak of the release rate of K occurs at the char oxidation stage. During char oxidation, K mainly exists in the form of inorganic salts and char-K. Thermal decomposition and sublimation are the main ways to loss inorganic K content, while the release of char-K is mainly through its conversion to inorganic K and to be released when burnt the char.

Apart from the detective methods of FES and LIBS, other detective techniques are also used to directly observe the release behaviour of gas-phase K during the combustion of biomass time/temperature-dependently. Striūgas et al. [67] carried out the observation on the combustion of single biomass particle by analysing the flame via Intensified Charge Couple Device (ICCD) camera. The study observed the intense emission of ions K during the period from the ignition to the char oxidation. Kim et al. [68] and Dayton et al. [69] used Mass Spectrometer Analysis (MSA) to observe the release of K from the combustion of biomass. According to Kim, an increase in the combustion temperature results in a rise in the emission of KCl. Moreover, Dayton observed that initial feedstock composition has a significant influence on the amount and species of K that released during the combustion process. The predominant K containing species released during the biomass combustion is KCl, while adding excess steam to the combustion tends to shift the release form of K from KCl to KOH.

In addition, Sorvajärvi et al. [70] attempted to detect the gas phase K, KCl and KOH during the combustion of biomass by using Collinear Photofragmentation and Atomic Absorption Spectroscopy (CPFAAS). Weng et al. [71] measured the quantity information of the release of atomic K during the combustion using a Tunable Diode Laser Absorption Spectroscopy (TDLAS). Moreover, Sommersacher et al. [72, 73] coupled ICP-MS with a single particle reactor, with the aim to detect the release of gas-phase K from the combustion of biomass time-dependently. Through the above attempts and observations, the feasibility and accuracy of the mentioned online detective methods are tested, and the existing release mechanisms of K during the combustion of biomass that proposed in the literature are verified.

### 2.3.2 Release of K during the pyrolysis process

Pyrolysis is a thermal conversion process that occurs in the inert atmosphere, with the aim to produce liquids, high heating values gases and char. Pyrolysis is an effective conversion method and regarded as a promising technology that can make biomass fuels compete with and replace the traditional fossil fuels [74], which has brought more attention in the recent decade. Normally, the primary stage of combustion is regarded as the pyrolysis; thus, the study on the release behaviour of K during biomass pyrolysis is meaningful to help to understand the initial behaviour of ash deposition [75]. As indicated

above, the study of the release behaviour of K during the pyrolysis process is usually carried out by either analyse the solid residues or directly observe the released gas products.

Several attempts have been reported to investigate the release of K via the analysis of solid residues from the pyrolysis process. ICP-OES/MS is still the most used technique to study the release mechanism of K from biomass during the pyrolysis process. According to the pyrolysis experiments carried out by Deng et al. [75], different biomass materials are pyrolysed in a fixed-bed reactor. The study reveals that the ratio of the released K is far less than the ratio of the distribution of water-soluble K inherent the biomass. At 400°C, a sudden raise happens to the fraction of ion-exchangeable K, whereas a significant increase occurs to the fraction of insoluble K at temperatures higher than 800°C. Moreover, the study indicates that wheat straw only loses 5% of the initial K when the pyrolysis temperature below 500°C, then this value abruptly increases to about 40% when the temperature reaches 1000°C. At the same time, corn stalk has the lowest release of K during 400°C-800°C. Meanwhile, the transformation and release of inherent K during the pyrolysis of straw is also investigated by Zhao et al. [76] and Jensen et al. [77] by using the same detective method, and similar conclusions can be obtained from the experimental studies. During the pyrolysis, most K is released from the original binding sites. Organic-K dominates the release of K content at low temperatures, while inorganic-K affects the release of K at high temperatures. The original inorganic-K in the biomass is mainly in the form of KCl, and it dominates the release of K content at the temperature of 700°C-900°C. Then, the release of the significant amount of char-K, K<sub>2</sub>CO<sub>3</sub> and K<sub>2</sub>SO<sub>4</sub> that are mainly generated after devolatilisation take place at 1000°C. They also reported that the formation of insoluble K silicates is found at 900°C-1000°C.

Researchers also used Ion Chromatography (IC) technique [78] to detect the concentration of K in the dissolved solution of solid residue. Okuno et al. [79] used IC detector to study the primary release of alkali metals during the pyrolysis of pulverized pine and sugarcane bagasse in a wire-mesh reactor. Through the investigation, about 15-20% of the initial alkali metals are released during the tar evolution stage, while further isothermal heating could cause the nearly complete release of the alkali metals. They also suggested that the secondary reactions (adsorption and desorption) between the char matrix and alkali species prevents the release of alkali species and allow them to transform into thermally stable char-K and/or non-volatiles species, i.e. K-silicates. Also, in Keown

et al.'s study [80], the same detective device is used to quantify the volatilised K content from the pyrolysis of different biomass samples in fluidized and fixed-bed reactors. The researchers have investigated the effect of heating rate on the release of K content and draw the conclusion. When pyrolyse cane bagasse and can trash at 1000°C, a slow heating rate (10°C/s) can result in a minimal release of K content (normally <20%), while a high heating rate (1000°C/s) can cause the release of K content up to 80%. Moreover, Chen et al. [81] used FAAS to investigate the release and transformation characteristics of K and Cl during the pyrolysis process of straw. According to their study, sample weight, particle size and heating rate affect the release of Cl, which is mainly caused by the secondary reactions of recaptured Cl. However, the influence of secondary reactions on the release of K is not significant. They also observed that the reaction intensities of K compounds (i.e. KCl) and major chemical compounds (cellulose, xylan and lignin) are different, due to the different contents of carboxyl groups in the raw chemical compounds and the free radicals formed during the pyrolysis process.

Apart from the above study on the solid phase K, attempts have been carried out to directly observe the release of gas phase K during the pyrolysis process as well. By far, surface ionization (SI) [82, 83] detector is the most reported method that used to directly observe the release of gas phase K during the pyrolysis process of biomass. In Olsson et al.'s study [84], wheat straw samples are pyrolysed in a laboratory reactor under the atmosphere of N<sub>2</sub>, then the online detection of K is performed via the SI method. According to the investigation, only a small fraction of the K content is released in the low temperature range (130°C-520°C). It is mainly caused by the decomposition of the organically associated K. While the significant release of K happens at high temperatures (>520°C). Moreover, high Cl content could only enhance the emission of K at high temperatures. They also proposed a first-order rate behaviour of the release of K during the pyrolysis process, and the activation energies during the low temperature release are found in the range of 156-186 kJ/mol, while it is within the range of 168-238 kJ/mol for the high temperature release. The same technique is also used by Kowalski et al. [85] to qualitative evaluate the release of alkali metal during the pyrolysis of different kinds of biomass samples on a thermogravimetric analyser. A similar release mechanism is reported: there are two peaks of the release of K can be observed during the pyrolysis process, the first happens at temperatures below 430°C, while the second occurs at

temperatures exceed 520°C. Besides, they proposed that the low temperature peak of release is caused by the decomposition of organic K species, which believed is acetates K through the analysis.

#### 2.4 Modelling study on the release of K

Through the above review, we can see that the release behaviour of K is similar in different thermal conversion conditions. The release mechanisms have been investigated thoroughly. However, the detective methods are limited and mainly used the digestion of solid residues and tested by the ICP-OES/MS device, in order to determine the release of K content. Several methods are used to observe and determine the release of atomic K during the thermal conversion process time/temperature-dependently.

The lack of detective methods results in the absence of the quantity information on the release profile of different K compounds during the thermal conversion process of biomass. Under this circumstance, modelling is a useful tool to obtain such valuable information, several models have been developed in an attempt to study the release mechanism and to predict the release profile of K during the thermal conversion of biomass materials.

A chemical kinetic model is present by Glarborg et al. [86] for the gaseous sulfation study of alkali hydroxide and alkali chloride. The study proposed a detailed reaction mechanism for sulfation and stated that the alkali transformation during the combustion process is processed by several molecule-molecule reactions. Turn et al. [87] used chemical equilibrium calculation to predict the K concentration in the gas from the thermal conversion of biomass. The equilibrium model not only includes the fuel and oxidizer inputs but also add a fraction of the bed material, and the modelling results show the same trends as their experiment data. Moreover, a better agreement can be observed in greater abundance in the fuel.

In Fatehi et al.'s series research [63, 88], a biomass thermochemical conversion and K release model is developed and employed to simulate the various stages of K release during the biomass thermal conversion process. The model is validated by the experiments via the direct detection of gas-phase K using a LIBS device. Two stages of release of K regarding devolatilisation and char reaction and ash-cooking are proposed according to the study, the rate of release of K during char reaction and ash-cooking stage

follows a first-order Arrhenius expression with  $A = 2.5 \times 10^5 \text{ 1/s}$ ,  $E = 266 \text{ kJ/mol}$ , and the activation energy of the release of K during the pyrolysis process is stated within the range of 168-198 kJ/mol. The same detective method also used by Liu et al. [64] to acquire the experimental data, and then developed a two-step (devolatilisation and char and ash oxidation) kinetic model for the release of K during the combustion of biomass pellet. According to their results, in the devolatilisation step, the kinetic parameters for straw and poplar are  $A = 2.24 \text{ 1/s}$ ,  $E = 64.8 \text{ kJ/mol}$  and  $A = 4.64 \text{ 1/s}$ ,  $E = 84.6 \text{ kJ/mol}$ , respectively; while in the char and ash oxidation step, the kinetic parameters for straw and poplar are  $A = 15.3 \text{ 1/s}$ ,  $E = 62.8 \text{ kJ/mol}$  and  $A = 20.5 \text{ 1/s}$ ,  $E = 55.4 \text{ kJ/mol}$ , respectively.

Other attempts are also reported regarding the kinetic model of the release rate of K during the thermal conversion of biomass. Based on the experimental time-dependent data for the combustion of switch grass, Peters et al. [89] proposed the kinetic parameters of emission formation of  $\text{KCl (s)} \rightarrow \text{KCl (g)}$ , with  $A = 1.85 \times 10^2 \text{ 1/s}$ ,  $E = 74.3 \text{ kJ/mol}$ , and a good agreement can be obtained between the kinetic data determined yield and the experiment data.

A prediction model on the release of K compounds during the combustion been developed and implemented into the 3D CFD program AIOLOS by Akbar et al. [90]. The model based on the assumption that the conversion of K in biomass involves vaporization of K via heterogeneous reactions and transformation of K compounds in the gas phase via homogeneous reactions. In the study, the authors proposed a first-order rate expression on the release and bonding of K during the combustion process, with  $A_{\text{release}} = 1.6 \times 10^{11} \text{ 1/min}$ ,  $E_{\text{release}} = 256 \text{ kJ/mol}$  and  $A_{\text{bonding}} = 2.4 \times 10^7 \text{ 1/min}$ ,  $E_{\text{bonding}} = 155 \text{ kJ/mol}$ , respectively. Moreover, the study also presented the reaction rate coefficients for the K/O/H/Cl system, as summarised in Table 2.2.

In recent, the prediction of gas-phase K release from the combustion of a single particle of biomass has been reported by Mason et al. [91] The model integrates a single particle combustion model with K release model that consists the three-stage of release (devolatilisation, char combustion and ash decomposition), which follows a first-order Arrhenius expression. The model takes the release of KOH and KCl into account, which is modelled as functions of temperature and vaporization enthalpy, with 164 kJ/mol and 147 kJ/mol, respectively [92]. A good agreement then acquired by comparing the modelled release patterns of K with the experimentally measured release of K using flame

emission spectroscopy. Besides, Zhang et al. [93] established a Matlab code for the estimation of the release of K from biomass ash based on the experiments data. The results evidenced that the model can be generalized to describe the release behaviour of any nutrient elements and can be used to optimize the production of controlled-release fertilizer.

Table 2.2 Reaction rate coefficients for the K/O/H/Cl system\*

No.	Reaction	$A, 1/s$	$n$	$E/R, 1000K$
1	$KOH + H \leftrightarrow K + H_2O$	5.0E13	0.00	0
2	$K + O_2 + M \leftrightarrow KO_2 + M$	3.6E14	0.00	0
3	$KO_2 + H \rightarrow KO + OH$	5.0E13	0.00	0
4	$KO + H_2O \leftrightarrow KOH + OH$	1.3E14	0.00	0
5	$KOH + HCl \leftrightarrow KCl + H_2O$	1.7E14	0.00	0
6	$K + HCl \leftrightarrow KCl + H$	9.1E12	0.00	594
7	$K + Cl + M \leftrightarrow KCl + M$	1.8E20	-1.00	0
8	$KO + HCl \leftrightarrow KCl + OH$	1.7E14	0.00	0
9	$H + HCl \leftrightarrow H_2 + Cl$	4.9E12	0.00	1599.90
10	$H + Cl_2 \leftrightarrow Cl + HCl$	8.4E13	0.00	579.77
11	$Cl + Cl + M \leftrightarrow Cl_2 + M$	7.2E14	0.00	-905.89
12	$O + HCl \leftrightarrow Cl + OH$	6.9E12	0.00	3371.92
13	$OH + HCl \leftrightarrow Cl + H_2O$	7.8E12	0.00	0

\*Table 2.2 is adapted from [90]

Nevertheless, as reviewed above, there is barely any reports regarding the prediction on the detailed information about the release of K compounds quantitatively and qualitatively during the thermal conversion process of biomass. To date, Wei et al. [94] carried out the chemical equilibrium calculation in FactSage to predict the release behaviour of gaseous K species during thermal utilization of various kinds of biomass. The prediction shows that the main K containing species are KCl, KOH and  $K_2Si_4O_9$  in straw combustion, while they are KCl, KOH and  $K_2SO_4$  in wood combustion. Also, according to the study, air excess coefficient has an insignificant effect on the release of gaseous K and Cl during the straw combustion, while increasing the pressure facilitates the release of HCl and reduce the amount of KCl at high temperatures.

## 2.5 Summary and research gap

Through the above literature review, it can be seen that the study on the release behaviour of K has been conducted thoroughly, experimental study especially. The general release mechanism of K during the thermal conversion process can be concluded as: K exists inherent the biomass in the form of organic and inorganic species. At low temperatures, the organically associated and loosely bonded K are released first, which however are less (normally <10% of the initial amount present in the biomass), and depending on the different contents of moisture and Cl in the biomass, the K released in this phase is mainly in the form of KOH and/or KCl. At high temperatures, a significant fraction of K is released, mainly caused by the decomposition of char-K and sublimation of inorganic K, and the mainly released form of K is KOH, K<sub>2</sub>O and K<sub>2</sub>SO<sub>4</sub>. After char combustion, K minerals and K-Al-Si-Ti compounds remained as the solids in the ash residues as insoluble K species.

However, due to the limitation of lack of detective technologies, more detailed and accurate information of time/temperature-dependent release profile of K is still unclear, i.e. the release amount of different K compounds (KCl, KOH, K<sub>2</sub>SO<sub>4</sub>, etc.) at different time/temperatures. Besides, the reported studies are mostly carried out in TGA device or a small size reactor, which requires minor amounts of the samples, and the reactions are always tested in high final temperatures with rapid heating up program. Information about how the external factors (low-high temperature range and heating rate) affect the release of K is rarely reported. Moreover, a more precise and comprehensive kinetic model is needed to predict the release profile of K from various kinds of biomass fuels under different thermal conversion conditions. In conclusion, these can be summarised as the below research gaps need to be solved and have been attempted and presented in this thesis.

- Lack of information about the influence of external factors on the release of K during biomass combustion

During the combustion, apart from the compositions of biomass, external operating parameters affect the release of ash content as well [31]. Since operating parameters play a significant role to affect the composition and properties of products from the thermal conversion of biomass [95], and crucial to the emission from the thermal conversion process [96]. In addition, the combustion conditions and operation mode can further

affect the ash behaviour, which is related to the rig design [97-101]. During the reactions, many external operating factors influence the extent and rate of the thermal fragmentations of the productions, such as final temperature, heating rate and biomass feed et al. [95]. Among the above external factors, the final temperature has greatly affect the composition of the products [102], while the reactivity in reactions is affected by the heating rate during the thermal conversion of biomass [103]. This implies that all these factors could significantly influence the release of K content during the combustion process of biomass. However, there is a lack of such comprehensive study that investigates the influences of operating factors (final temperature and heating rate) on the transition of potassium during the biomass combustion, since the transformation reactions of potassium can be greatly influenced by the temperature and heating rate [14]. Besides, as mentioned before, most of the studies are carried out in small size reactors, which are difficult to acquire enough solid samples, also hard to mimic the real-to-life combustion situation when there are more samples burned in the boiler with a large chamber.

In this way, a study on the release of K that carried out in a large size boiler is needed and investigate the influence of operating factors on the release behaviour of K during the combustion process. A better understanding of how the operating factors affect the release behaviour of K could help us to optimize the reaction process, and to control the ash problems. Therefore, it will have great implications for developing clean and efficient utilization technologies for biomass, prolonging the service life of biomass burning plants, which will make the biomass fuel economically competitive [104].

- Lack of a kinetic model to quantitatively and qualitatively predict the release of K from biomass under different conditions.

As reviewed above, many on-line and off-line detective methods have been used to detect the release of K; however, the obtained information is mainly on the release of atomic K during the thermal conversion process. Due to the limitation of detective methods, it is difficult to directly observe and acquire the released amount of different K compounds at various stages time/temperature-dependently. Although several models have been reported regarding the release fate of K during the thermal conversion process, but the models are focus on the prediction of the total amount of the released K at a specific condition, and the simulated biomass is based on the elemental components, i.e., C, H, O

et al. There is still a lack of a model that more close to the real biomass material, which using the major chemical components (cellulose, hemicellulose and lignin) to simulate the different kinds of biomass, as well as obtaining the release amount of different K compounds at different stages. Moreover, the transition path between different K compounds during the combustion process is also unclear. Besides, most of the currently reported models are based on the chemical equilibrium calculation. The estimations are acquired with the assumptions of a high-enough reacting temperature, and a long-enough reacting time to approach the equilibrium, the dynamic information of release of K compounds with the change of reaction conditions are thus not provided. Under this circumstance, a kinetic controlled model is needed to estimate the release of different K compounds.

Knowing the dynamic release performance of K compounds at different stages can offer an insight into the transition mechanism of K with other significant ash-forming elements temperature/time-dependently. The yields of released K compounds under various conditions from different biomass materials can be useful in making a quick and accurate judgement as to what extent those species would be released and the seriousness of the slagging and fouling issues initiated by K [12]. In this way, the prediction model is useful to provide such valuable information that can be used to advise the biomass boiler design and thus to mitigate the ash-related problems that caused by the release of K, Cl and S [105, 106] during the combustion of biomass sources. Moreover, the simulation tool is also helpful to predict the release of different K compounds from different kinds of raw materials, which is crucial to the sample preparation, selection, pre-treatment and the optimization of the reaction process.

## Bibliography

1. Saidur, R., et al., A review on biomass as a fuel for boilers. *Renewable and Sustainable Energy Reviews*, 2011. 15(5): p. 2262-2289.
2. Long, J., et al., Release characteristics of alkali and alkaline earth metallic species during biomass pyrolysis and steam gasification process. *Bioresource Technology*, 2012. 116: p. 278-284.
3. Alzate, C.C. and O.S. Toro, Energy consumption analysis of integrated flowsheets for production of fuel ethanol from lignocellulosic biomass. *Energy*, 2006. 31(13): p. 2447-2459.
4. Lu, H., Experimental and modeling investigations of biomass particle combustion. 2006.
5. Klass, D.L., *Biomass for renewable energy, fuels, and chemicals*. 1998: Elsevier.
6. Kumar, J.V. and B.C. Pratt, Compositional analysis of some renewable biofuels. *American Laboratory*, 1996. 28(8): p. 15-20.
7. Hudo, K. and E. Yoshida, The decomposition process of wood constituents in the course of carbonization I. The decomposition of carbohydrate and lignin in Mizunara. *J. Japan Wood Research Soc*, 1957. 3(4): p. 125-127.
8. Diebold, J. and A. Bridgwater, Overview of fast pyrolysis of biomass for the production of liquid fuels, in *developments in thermochemical biomass conversion*. 1997, Springer. p. 5-23.
9. Mohan, D., C.U. Pittman Jr, and P.H. Steele, Pyrolysis of wood/biomass for bio-oil: a critical review. *Energy & Fuels*, 2006. 20(3): p. 848-889.
10. Naik, S., et al., Characterization of Canadian biomass for alternative renewable biofuel. *Renewable Energy*, 2010. 35(8): p. 1624-1631.
11. Nussbaumer, T., Combustion and co-combustion of biomass: fundamentals, technologies, and primary measures for emission reduction. *Energy & Fuels*, 2003. 17(6): p. 1510-1521.
12. Cao, W., et al., Prediction of potassium compounds released from biomass during combustion. *Applied Energy*, 2019. 250: p. 1696-1705.
13. Demirbas, A., Combustion characteristics of different biomass fuels. *Progress in Energy and Combustion Science*, 2004. 30(2): p. 219-230.
14. Niu, Y., H. Tan, and S.e. Hui, Ash-related issues during biomass combustion: Alkali-induced slagging, silicate melt-induced slagging (ash fusion), agglomeration,

- corrosion, ash utilization, and related countermeasures. *Progress in Energy and Combustion Science*, 2016. 52: p. 1-61.
15. Rycroft, M., Co-firing biomass with coal for power generation. 2015, EE Publishers.
  16. Zhang, Y., Q. Li, and H. Zhou, Theory and calculation of heat transfer in furnaces. 2016: Elsevier.
  17. Xu, W., et al., A new agro/forestry residues co-firing model in a large pulverized coal furnace: Technical and economic assessments. *Energies*, 2013. 6(9): p. 4377-4393.
  18. Livingston, W. Biomass ash deposition, erosion and corrosion processes. in Workshop on ash related issues in biomass combustion. Glasgow: IEA Task. 2006.
  19. Livingston, W. Biomass ash characteristics and behavior in combustion systems. in IEA Task 32 Workshop on Ash Related Issues in Biomass Combustion. 2006.
  20. Nielsen, H., et al., The implications of chlorine-associated corrosion on the operation of biomass-fired boilers. *Progress in Energy and Combustion Science*, 2000. 26(3): p. 283-298.
  21. Melissari, B., Ash related problems with high alkali biomass and its mitigation experimental evaluation. *Memoria Investigaciones en Ingeniería*, 2014. 12: p. 31-44.
  22. Yu, C., et al., Experimental determination of agglomeration tendency in fluidized bed combustion of biomass by measuring slip resistance. *Fuel*, 2014. 128: p. 14-20.
  23. De Geyter, S., et al., Effects of non-quartz minerals in natural bed sand on agglomeration characteristics during fluidized bed combustion of biomass fuels. *Energy & Fuels*, 2007. 21(5): p. 2663-2668.
  24. Piispanen, M.H., et al., Prediction of bed agglomeration propensity directly from solid biofuels: a look behind fuel indicators. *Energy & Fuels*, 2012. 26(4): p. 2427-2433.
  25. Grimm, A., et al., Bed agglomeration characteristics in fluidized-bed combustion of biomass fuels using olivine as bed material. *Energy & Fuels*, 2012. 26(7): p. 4550-4559.

26. Visser, H., S.C. van Lith, and J. Kiel, Biomass ash-bed material interactions leading to agglomeration in FBC. *Journal of Energy Resources Technology*, 2008. 130(1): p. 011801.
27. Carvalho, L., et al., Performance of a pellet boiler fired with agricultural fuels. *Applied Energy*, 2013. 104: p. 286-296.
28. Sippula, O., et al., Effect of wood fuel on the emissions from a top-feed pellet stove. *Energy & Fuels*, 2007. 21(2): p. 1151-1160.
29. Houshfar, E., T. Løvås, and Ø. Skreiberg, Experimental investigation on NOx reduction by primary measures in biomass combustion: straw, peat, sewage sludge, forest residues and wood pellets. *Energies*, 2012. 5(2): p. 270-290.
30. Díaz-Ramírez, M., et al., Influencing factors on NOX emission level during grate conversion of three pelletized energy crops. *Applied Energy*, 2014. 115: p. 360-373.
31. Royo, J., et al., Experimental study on the ash behaviour in combustion of pelletized residual agricultural biomass. *Fuel*, 2019. 239: p. 991-1000.
32. Juneman, A. and G. Legarreta, Inhalación de humo de leña: una causa relevante pero poco reconocida de Enfermedad Pulmonar Obstructiva Crónica. *Revista Americana de Medicina Respiratoria*, 2007. 7(2): p. 21-57.
33. Tian, D., et al., Assessment of biomass burning emissions and their impacts on urban and regional PM<sub>2.5</sub>: A Georgia case study. *Environmental Science & Technology*, 2008. 43(2): p. 299-305.
34. Niu, Y., et al., Study on deposits on the surface, upstream, and downstream of bag filters in a 12 MW biomass-fired boiler. *Energy & Fuels*, 2010. 24(3): p. 2127-2132.
35. Mu, L., et al., Elemental distribution and mineralogical composition of ash deposits in a large-scale wastewater incineration plant: a case study. *Industrial & Engineering Chemistry Research*, 2012. 51(25): p. 8684-8694.
36. Lindberg, D., et al., Towards a comprehensive thermodynamic database for ash-forming elements in biomass and waste combustion—Current situation and future developments. *Fuel Processing Technology*, 2013. 105: p. 129-141.
37. Garba, M., et al., Prediction of potassium chloride sulfation and its effect on deposition in biomass-fired boilers. *Energy & Fuels*, 2012. 26(11): p. 6501-6508.

38. Niu, Y., et al., Slagging characteristics on the superheaters of a 12 MW biomass-fired boiler. *Energy & Fuels*, 2010. 24(9): p. 5222-5227.
39. Brus, E., M. Öhman, and A. Nordin, Mechanisms of bed agglomeration during fluidized-bed combustion of biomass fuels. *Energy & Fuels*, 2005. 19(3): p. 825-832.
40. Grimm, A., et al., Bed agglomeration characteristics in fluidized quartz bed combustion of phosphorus-rich biomass fuels. *Energy & Fuels*, 2011. 25(3): p. 937-947.
41. Cao, W., et al., Release of alkali metals during biomass thermal conversion. *Archives of Industrial Biotechnology*, 2016. 1(1): p. 1-3.
42. Mason, P.E., et al., Observations on the release of gas-phase potassium during the combustion of single particles of biomass. *Fuel*, 2016. 182: p. 110-117.
43. Johansen, J.M., et al., Release of K, Cl, and S during pyrolysis and combustion of high-chlorine biomass. *Energy & Fuels*, 2011. 25(11): p. 4961-4971.
44. Knudsen, J.N., P.A. Jensen, and K. Dam-Johansen, Transformation and release to the gas phase of Cl, K, and S during combustion of annual biomass. *Energy & Fuels*, 2004. 18(5): p. 1385-1399.
45. Van Lith, S.C., et al., Release to the gas phase of inorganic elements during wood combustion. Part 1: development and evaluation of quantification methods. *Energy & Fuels*, 2006. 20(3): p. 964-978.
46. Van Lith, S.C., et al., Release to the gas phase of inorganic elements during wood combustion. Part 2: influence of fuel composition. *Energy & Fuels*, 2008. 22(3): p. 1598-1609.
47. Werkelin, J., et al., Ash-forming elements in four Scandinavian wood species part 3: Combustion of five spruce samples. *Biomass and Bioenergy*, 2011. 35(1): p. 725-733.
48. Saddawi, A., J. Jones, and A. Williams, Influence of alkali metals on the kinetics of the thermal decomposition of biomass. *Fuel Processing Technology*, 2012. 104: p. 189-197.
49. Freire, M., H. Lopes, and L.A. Tarelho, Critical aspects of biomass ashes utilization in soils: Composition, leachability, PAH and PCDD/F. *Waste Management*, 2015. 46: p. 304-315.

50. Vassilev, S.V., et al., An overview of the composition and application of biomass ash. Part 1. Phase–mineral and chemical composition and classification. *Fuel*, 2013. 105: p. 40-76.
51. Lindon, J.C., G.E. Tranter, and D. Koppenaal, *Encyclopedia of spectroscopy and spectrometry*. 2016: Academic Press.
52. Winefordner, J., J. Fitzgerald, and N. Omenetto, Review of multielement atomic spectroscopic methods. *Applied Spectroscopy*, 1975. 29(5): p. 369-383.
53. Hahn, D.W. and N. Omenetto, Laser-induced breakdown spectroscopy (LIBS), part I: review of basic diagnostics and plasma–particle interactions: still-challenging issues within the analytical plasma community. *Applied Spectroscopy*, 2010. 64(12): p. 335A-366A.
54. Fernández, B., L. Lobo, and R. Pereiro, *Atomic Absorption Spectrometry: Fundamentals, Instrumentation and Capabilities*. 2018.
55. Meng, X., et al., Release of Alkalis and Chlorine from Combustion of Waste Pinewood in a Fixed Bed. *Energy & Fuels*, 2019. 33(2): p. 1256-1266.
56. Fagerström, J., et al., Alkali transformation during single pellet combustion of soft wood and wheat straw. *Fuel Processing Technology*, 2016. 143: p. 204-212.
57. Johansen, J.M., et al., Release of K, Cl, and S during combustion and co-combustion with wood of high-chlorine biomass in bench and pilot scale fuel beds. *Proceedings of the Combustion Institute*, 2013. 34(2): p. 2363-2372.
58. Jin, X., et al., Condensation behaviors of potassium during biomass combustion. *Energy & Fuels*, 2017. 31(3): p. 2951-2958.
59. Wang, Y., et al., The condensation and thermodynamic characteristics of alkali compound vapors on wall during wheat straw combustion. *Fuel*, 2017. 187: p. 33-42.
60. Oris, C., et al., Forms of potassium and chlorine from oxy-fuel co-combustion of lignite coal and corn stover. *Carbon Resources Conversion*, 2019. 2(2): p. 103-110.
61. Yang, T., et al., Release and transformation of potassium during corn straw and coal co-combustion. *Energy Sources, Part A: Recovery, Utilization, and Environmental Effects*, 2018. 40(3): p. 327-334.

62. He, Z., et al., Experimental investigation on temporal release of potassium from biomass pellet combustion by flame emission spectroscopy. *Fuel*, 2019. 253: p. 1378-1384.
63. Fatehi, H., et al., LIBS measurements and numerical studies of potassium release during biomass gasification. *Proceedings of the Combustion Institute*, 2015. 35(2): p. 2389-2396.
64. Liu, Y., et al., Measurement and kinetics of elemental and atomic potassium release from a burning biomass pellet. *Proceedings of the Combustion Institute*, 2019. 37(3): p. 2681-2688.
65. Liu, Y., et al., Characteristics of alkali species release from a burning coal/biomass blend. *Applied Energy*, 2018. 215: p. 523-531.
66. Zhang, Z.-h., et al., Temporal release of potassium from pinewood particles during combustion. *Combustion and Flame*, 2015. 162(2): p. 496-505.
67. Striūgas, N., M. Sadeckas, and R. Paulauskas, Investigation of K\*, Na\* and Ca\* flame emission during single biomass particle combustion. *Combustion Science and Technology*, 2019. 191(1): p. 151-162.
68. Kim, S.S., et al., Release of potassium and sodium species during combustion of various rank coals, biomass, sludge and peats. *Journal of Industrial and Engineering Chemistry*, 2012. 18(6): p. 2199-2203.
69. Dayton, D.C., R.J. French, and T.A. Milne, Direct observation of alkali vapor release during biomass combustion and gasification. 1. Application of molecular beam/mass spectrometry to switchgrass combustion. *Energy & Fuels*, 1995. 9(5): p. 855-865.
70. Sorvajärvi, T., et al., In situ measurement technique for simultaneous detection of K, KCl, and KOH vapors released during combustion of solid biomass fuel in a single particle reactor. *Applied Spectroscopy*, 2014. 68(2): p. 179-184.
71. Weng, W., et al., Quantitative measurement of atomic potassium in plumes over burning solid fuels using infrared-diode laser spectroscopy. *Energy & Fuels*, 2017. 31(3): p. 2831-2837.
72. Sommersacher, P., et al., Simultaneous Online Determination of S, Cl, K, Na, Zn, and Pb Release from a Single Particle during Biomass Combustion. Part 1: Experimental Setup—Implementation and Evaluation. *Energy & Fuels*, 2015. 29(10): p. 6734-6746.

73. Sommersacher, P., et al., Simultaneous online determination of S, Cl, K, Na, Zn, and Pb release from a single particle during biomass combustion. Part 2: results from test runs with spruce and straw pellets. *Energy & Fuels*, 2016. 30(4): p. 3428-3440.
74. Demirbaş, A., Biomass resource facilities and biomass conversion processing for fuels and chemicals. *Energy Conversion and Management*, 2001. 42(11): p. 1357-1378.
75. Deng, L., et al., Transformation and release of potassium during fixed-bed pyrolysis of biomass. *Journal of the Energy Institute*, 2018. 91(4): p. 630-637.
76. Zhao, H.-b., et al., Study on the transformation of inherent potassium during the fast-pyrolysis process of rice straw. *Energy & Fuels*, 2015. 29(10): p. 6404-6411.
77. Jensen, P.A., et al., Experimental investigation of the transformation and release to gas phase of potassium and chlorine during straw pyrolysis. *Energy & Fuels*, 2000. 14(6): p. 1280-1285.
78. Lemmon, J., *Ion Chromatography*. 2001.
79. Okuno, T., et al., Primary release of alkali and alkaline earth metallic species during the pyrolysis of pulverized biomass. *Energy & Fuels*, 2005. 19(5): p. 2164-2171.
80. Keown, D.M., et al., Volatilisation of alkali and alkaline earth metallic species during the pyrolysis of biomass: differences between sugar cane bagasse and cane trash. *Bioresource Technology*, 2005. 96(14): p. 1570-1577.
81. Chen, H., et al., Release and transformation characteristics of K and Cl during straw torrefaction and mild pyrolysis. *Fuel*, 2016. 167: p. 31-39.
82. Jäglid, U., J.G. Olsson, and J.B. Pettersson, Detection of sodium and potassium salt particles using surface ionization at atmospheric pressure. *Journal of Aerosol Science*, 1996. 27(6): p. 967-977.
83. Davidsson, K.O., et al., A surface ionization instrument for on-line measurements of alkali metal components in combustion: Instrument description and applications. *Energy & Fuels*, 2002. 16(6): p. 1369-1377.
84. Olsson, J.G., et al., Alkali metal emission during pyrolysis of biomass. *Energy & Fuels*, 1997. 11(4): p. 779-784.
85. Kowalski, T., C. Ludwig, and A. Wokaun, Qualitative evaluation of alkali release during the pyrolysis of biomass. *Energy & Fuels*, 2007. 21(5): p. 3017-3022.

86. Glarborg, P. and P. Marshall, Mechanism and modeling of the formation of gaseous alkali sulfates. *Combustion and Flame*, 2005. 141(1-2): p. 22-39.
87. Turn, S.Q., Chemical equilibrium prediction of potassium, sodium, and chlorine concentrations in the product gas from biomass gasification. *Industrial & Engineering Chemistry Research*, 2007. 46(26): p. 8928-8937.
88. Fatehi, H., et al., Modeling of alkali metal release during biomass pyrolysis. *Proceedings of the Combustion Institute*, 2017. 36(2): p. 2243-2251.
89. Peters, B. and J. Smula-Ostaszewska, Simultaneous prediction of potassium chloride and sulphur dioxide emissions during combustion of switchgrass. *Fuel*, 2012. 96: p. 29-42.
90. Akbar, S., U. Schnell, and G. Scheffknecht, Modelling potassium release and the effect of potassium chloride on deposition mechanisms for coal and biomass-fired boilers. *Combustion Theory and Modelling*, 2010. 14(3): p. 315-329.
91. Mason, P.E., et al., Gas phase potassium release from a single particle of biomass during high temperature combustion. *Proceedings of the Combustion Institute*, 2017. 36(2): p. 2207-2215.
92. Westberg, H.M., M. Byström, and B. Leckner, Distribution of potassium, chlorine, and sulfur between solid and vapor phases during combustion of wood chips and coal. *Energy & Fuels*, 2003. 17(1): p. 18-28.
93. Zhang, Z., et al., Experiments and modelling of potassium release behavior from tablet biomass ash for better recycling of ash as eco-friendly fertilizer. *Journal of Cleaner Production*, 2018. 170: p. 379-387.
94. Wei, X., U. Schnell, and K.R. Hein, Behaviour of gaseous chlorine and alkali metals during biomass thermal utilisation. *Fuel*, 2005. 84(7-8): p. 841-848.
95. Akhtar, J. and N.S. Amin, A review on operating parameters for optimum liquid oil yield in biomass pyrolysis. *Renewable and Sustainable Energy Reviews*, 2012. 16(7): p. 5101-5109.
96. Faengmark, I., et al., Influence of combustion parameters on the formation of polychlorinated dibenzo-p-dioxins, dibenzofurans, benzenes, and biphenyls and polyaromatic hydrocarbons in a pilot incinerator. *Environmental Science & Technology*, 1993. 27(8): p. 1602-1610.
97. Díaz-Ramírez, M., et al., Partitioning of K, Cl, S and P during combustion of poplar and brassica energy crops. *Fuel*, 2014. 134: p. 209-219.

98. Rainer, B., et al., Ash Transformation Chemistry during Combustion of Biomass. *Energy & Fuels*, 2012.
99. Becidan, M.I., et al., Optimal mixtures to reduce the formation of corrosive compounds during straw combustion: A thermodynamic analysis. *Energy & Fuels*, 2011. 25(7): p. 3223-3234.
100. Khor, A., et al., Straw combustion in a fixed bed combustor. *Fuel*, 2007. 86(1-2): p. 152-160.
101. Magdziarz, A., A.K. Dalai, and J.A. Koziński, Chemical composition, character and reactivity of renewable fuel ashes. *Fuel*, 2016. 176: p. 135-145.
102. Solar, J., et al., Influence of temperature and residence time in the pyrolysis of woody biomass waste in a continuous screw reactor. *Biomass and Bioenergy*, 2016. 95: p. 416-423.
103. Fushimi, C., et al., Effect of heating rate on steam gasification of biomass. 1. Reactivity of char. *Industrial & Engineering Chemistry Research*, 2003. 42(17): p. 3922-3928.
104. Cao, W., et al., Experimental study on the influences of operating parameters on the retention of potassium during the biomass combustion. *Energy Procedia*, 2019. 158: p. 1033-1038.
105. Brunner, T., et al. Behaviour of ash forming compounds in biomass furnaces-measurement and analyses of aerosols formed during fixed-bed biomass combustion. in *Proc. of the international IEA Seminar "Aerosols in Biomass Combustion"*, Zuerich, Switzerland. 2001.
106. Clery, D.S., et al., The effects of an additive on the release of potassium in biomass combustion. *Fuel*, 2018. 214: p. 647-655.

## CHAPTER 3

### MATERIALS AND METHODOLOGY

---

This chapter describes the experimental approach and model development that are applied for the studies on the release of K during biomass combustion. The experimental section includes experiment materials and test facilities, as well as the detection methods that were used to quantify the K content and to observe the ash structure. In the modelling section, the theory applied for modelling of the devolatilisation of biomass will be illustrated first, followed by the release kinetics of inorganic elements, as well as the theory of combustion of gas species.

#### 3.1 Experimental methods and materials

##### 3.1.1 Raw materials

Two biomass materials were studied in this thesis, wheat straw and softwood, which are purchased from Agripellets Ltd. The wheat straw pellets are mainly used to study the K transition during the combustion process in the reactor. Since herbaceous biomass normally consists of more K content (around 1.3 wt%) than that in woody biomass (<0.4 wt%) [1], the combustion of herbaceous biomass could suffer more serious ash-related problems compared to that of the woody biomass, and thus, needs more investigation. The average weight of a straw pellet is 0.8 g, with a diameter of 5 mm and an average length of 40 mm. The straw pellets were air-dried until the weight became constant, with the aim of eliminating the extra moisture content; afterwards, half of the wheat straw remained as pellets, the other half was milled into fine particles.

Three chemicals were also used in this thesis to investigate the interactions among the major chemical components of biomass during the thermal conversion, which were cellulose, xylan (which has often been considered as a substitute of hemicellulose [2]) and lignin. Cellulose and xylan powder was purchased from Sigma-Aldrich, and lignin powder was purchased from Carbosynth. The analysis of the above samples is summarised in Table 3.1.

Table 3.1 Proximate, ultimate and ash analysis of samples

	Wheat straw	Softwood	Cellulose	Xylan	Lignin
					
Proximate analysis, wt%					
Moisture <sup>ar</sup>	9.00	3.50	2.70	2.90	3.20
VM <sup>db</sup>	74.80	58.36	89.70	84.80	51.30
Ash <sup>db</sup>	7.40	1.12	1.70	1.70	15.00
FC <sup>db</sup>	17.80	40.52	8.60	13.50	33.70
Ultimate analysis, wt%					
C <sup>db</sup>	45.20	58.28	42.18	38.41	62.09
H <sup>db</sup>	5.25	4.71	6.15	6.18	5.88
O <sup>db</sup>	48.90	36.51	51.66	55.40	30.52
N <sup>db</sup>	0.71	0.50	0.01	0.01	0.51
Cl <sup>db</sup>	0.05	-	-	-	-
S <sup>db</sup>	0.14	-	-	-	-
Ash analysis, wt%					
SiO <sub>2</sub>	31.88	39.00	-	-	-
Al <sub>2</sub> O <sub>3</sub>	0.86	2.52	-	-	-
CaO	5.24	32.90	-	-	-
MgO	1.61	1.55	-	-	-
Na <sub>2</sub> O	0.12	0.94	-	-	-
K <sub>2</sub> O	9.13	6.00	-	-	-
P <sub>2</sub> O <sub>5</sub>	46.74	5.27	-	-	-
Fe <sub>2</sub> O <sub>3</sub>	0.15	2.00	-	-	-
TiO <sub>2</sub>	<0.05	0.17	-	-	-
Other	2.5	9	-	-	-

\*db: dry basis; ar: as received.

### 3.1.2 Reactors

Two types of equipment at the University of Strathclyde were selected as the main reactors for the investigation on the thermal conversion of samples.

#### 3.1.2.1 Thermogravimetric analyser (TGA)

The combustion characteristics of the biomass and chemical samples were carried out by the TGA device, as shown in Figure 3.1, the device model is a Netzsch STA449F3 Jupiter. The TGA device could be operated at temperatures up to 1550°C, with the heating rate up to 50°C/min. The sample mass of 15 mg ±1 mg was selected to run each experiment.



Figure 3.1 TGA device

### 3.1.2.2 High-Temperature furnace-balance system (FBS)

Normally, a TGA is used to study the thermal behaviour of solid fuels; however, the testable quantity of sample is small, leading to the lack of solid residue to conduct the follow-up analysis and it is also difficult to simulate the real-life combustion situation. Furthermore, the samples studied in TGA are usually at fine sizes, it is not accurate to study the thermal conversion of pelletized biomass in TGA, as well as to investigate the release behaviour of K from a large number of biomass samples. Under this circumstance, the combustion of wheat straw to acquire solid residues was conducted in a custom-designed furnace-balance system (FBS), which is a combined device.

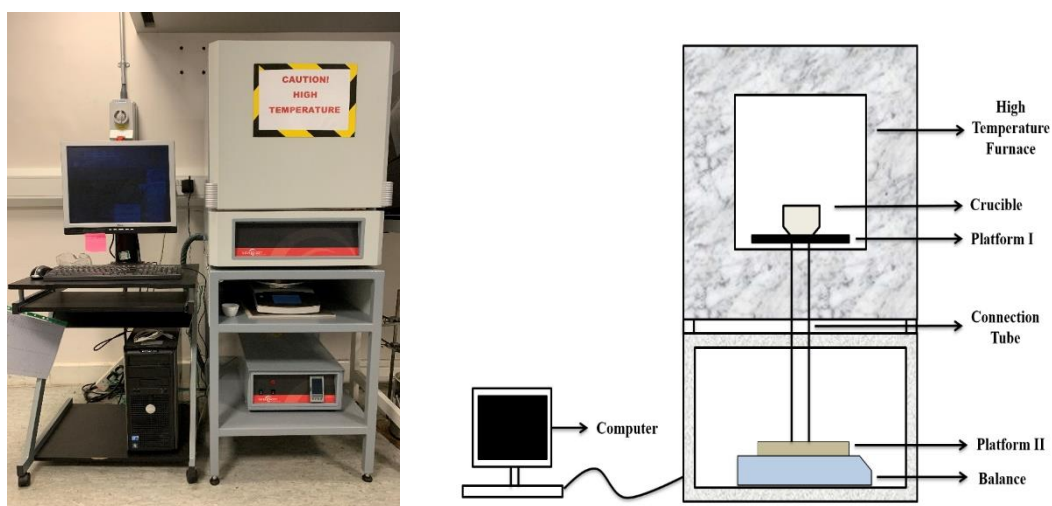


Figure 3.2 Furnace-balance system (left); schematic diagram (right)

The furnace in FBS is a ThermConcept High-Temperature furnace, which is centrally controlled through a Eurotherm 3208 controller. The highest setting temperature for the controller is 1200°C, with the heating rate up to 50°C/min. A Satorius balance is connected to a platform with a thermal insulation tube, in order to record the mass change of sample on a real-time basis. The FBS device and a sketch of the connection are presented in Figure 3.2.

### 3.1.2.3 Performance comparison between FBS and TGA

The reliability of the FBS was tested by comparing the results with that of the TGA device. The tests were carried out under the same combustion condition: the final temperature was 700°C, with the heating rate of 20°C/min. Then the obtained mass loss curves and derivative mass loss curves are shown in Figure 3.3.

As indicated in Figure 3.3, the difference between the mass loss curves obtained from the TGA and the FBS is clear. In the drying stage, there is no noticeable drop in the TGA test, but a visible drop in the FBS result. This result is due to the small amount of sample (with only 10 mg) tested in this device; besides, the sample was air-dried and milled; as a result, there was not much moisture content left. In contrast, there was a more substantial amount of the sample (with approximately 5g) tested in the FBS, and the loss of moisture content during the pre-treatment process was relatively small. Besides, the moisture loss in the FBS during the drying phase was about 9% of initial weight, which is the same as indicated in Table 3.1.

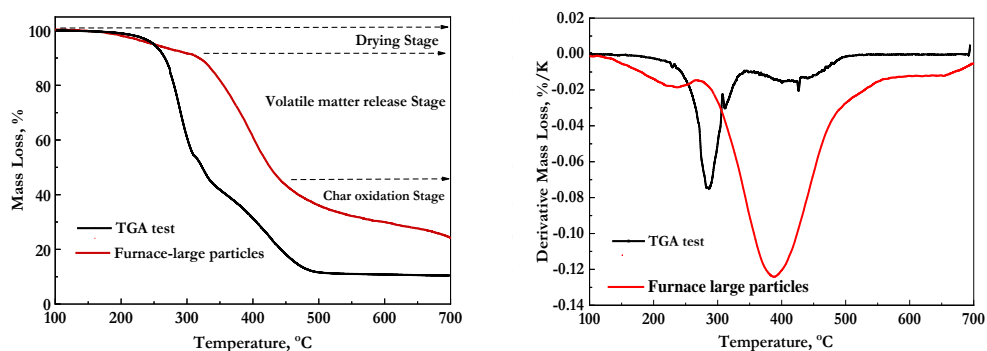


Figure 3.3. Mass loss (left) and derivative mass loss (right) curves obtained from TGA and FBS.

With the temperature increasing, in the volatile matter release stage, the steep mass loss started at around 230°C in the TGA, while there was an apparent delay in the FBS, at

about 300°C, but the sharp decrease of mass in the two tests all stopped at 480°C. The delay might be caused by the effect of heat transfer on the reaction progress for large particles (thermally thick) and the longer time that was needed to heat the large volume of the furnace chamber (which is 10 L) to reach the target temperature. Besides, the sample in the furnace was much larger, leading to the less efficiency of heat transfer compared to that of the TGA. The release of volatile matter from the sample happened gradually from its surface to the inside of the sample container in the FBS, and the total released volatile matter occupied almost the same volume like that in the TGA, which proved that the data obtained in this stage was reliable. Nevertheless, in the char oxidation stage (which occurred after 480°C), it took much longer time to burn out the remaining char in the FBS, which in turn reflected a much wider temperature range. Besides, the concentration of oxygen in the FMS not being as sufficient as that of the TGA at these temperatures since the TGA had a steady and continuous injection of O<sub>2</sub>. Due to the differences in ash concentration and distribution in raw materials, the residues left in the FBS was about 15%, a little higher than that in the TGA, which was 10%.

### 3.1.3 Solid residues characterisation

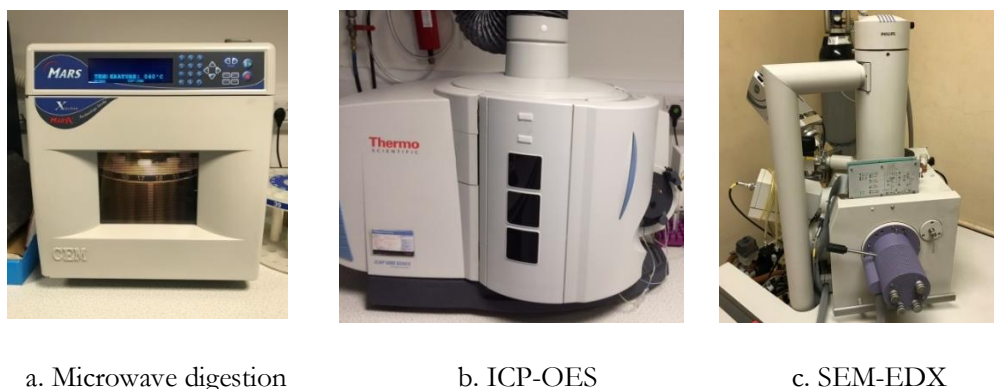


Figure 3.4 Analysis devices

#### 3.1.3.1 Microwave digestion

The collected solid residues were digested in the microwave first, in order to dissolve the remaining potassium and be ready to be tested. The microwave digestion was conducted in a CEM, MARS-5 microwave device, as shown in Figure 3.4 a. Samples were milled into fine particles first, and then 50±5 mg of each sample was digested with 9 ml concentrated nitric acid (>69%), and 1 ml deionised water in a microwave at 200°C for 120 min.

#### 3.1.3.2 Inductively Coupled Plasma Optical Emission Spectrometry (ICP-OES)

The digested solutions were analysed by ICP-OES in the Department of Civil and Environmental Engineering at the University of Strathclyde, in order to quantify the potassium in the solid residues. The ICP-OES device used in this thesis was a Thermo Scientific iCAP 6000 with the detection capability of <1 ppb. The device is shown in Figure 3.4 b.

### 3.1.3.3 Scanning Electron Microscopy – Energy Dispersive X-ray Spectroscopy (SEM-EDX)

The structural change of the solid residues and the distribution of different elements (K, S, and Si et al.) were examined by SEM-EDX in the Department of Chemistry at the University of Glasgow, aiming to investigate the effect of the changes of the biomass particles structures on the distribution and release of inorganic elements during the combustion process. The SEM-EDX device that was used in the present study was an XL30 ESEM attached by an Oxford Instruments Energy 250 energy dispersive spectrometer system, as shown in Figure 3.4 c. Prior to the analysis, solid samples were placed evenly on a carbon sticker and coated with a thin layer of gold (between 5-50 nm) to provide a conductive coating to dissipate charging artefacts.

## 3.2 Model development

Normally, devolatilisation is regarded as the initial step of the combustion, during which the gas products are primarily devolatilised [3]. Subsequently, occur the combustion of gas species and char oxidation [4]. In this way, for the design of the simulation model to predict the release profiles of K, two steps had been considered: devolatilisation of biomass and combustion of gas products. The kinetically controlled release process of elemental K, S and Cl were also integrated into the devolatilisation part of the model. After the devolatilisation, the yielded gas products, along with the released elemental K, S and Cl contents, were stored in a string and ready to be combusted.

In the combustion stage, the model is also kinetically controlled. It is assumed that all the gas products are following the ideal gas behaviour and are homogeneously distributed in the system, which states are functions of time/temperature. Moreover, in order to eliminate the influence of pressure on the gaseous species, the pressure in the system is assumed to keep constant all the time. Under this circumstance, an Ideal-Gas-Constant-Pressure reactor is used to consider all the possible reactions among the gas products.

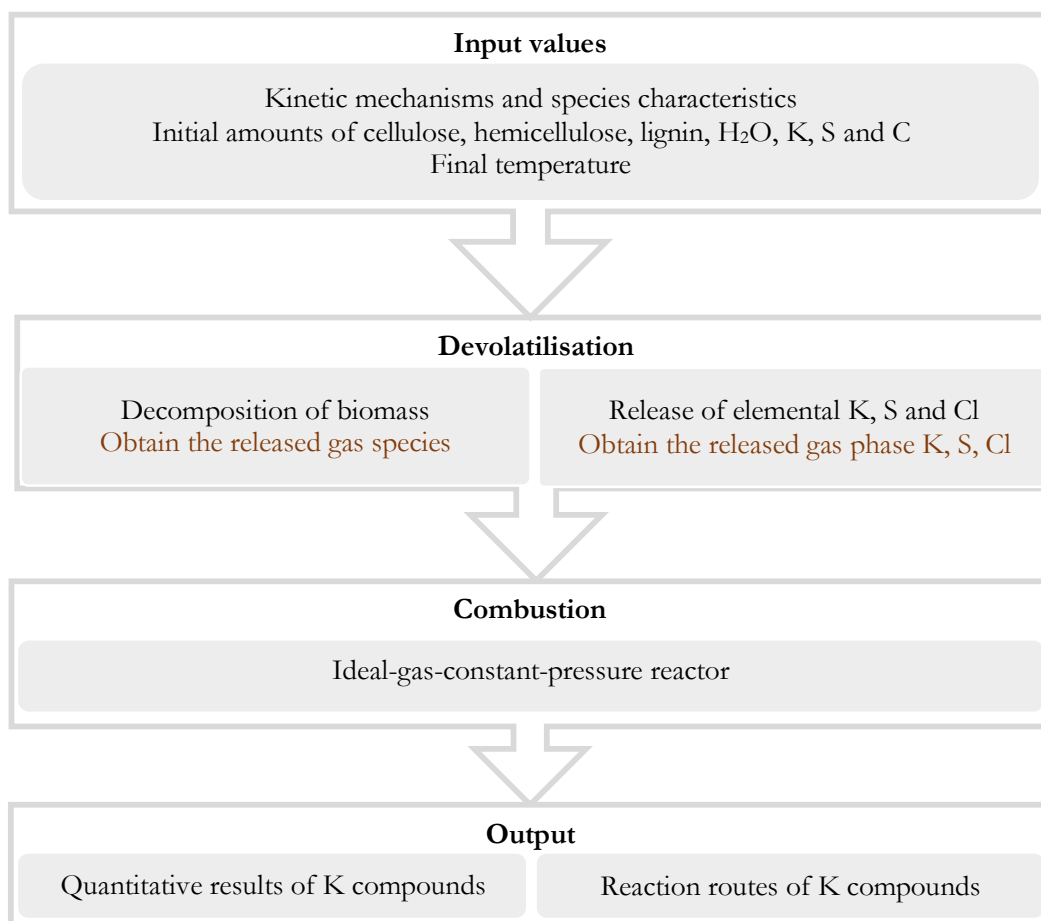


Figure 3.5 Schematic of the network

Through this two-step-reaction, a detailed quantity data of all the gas phase K compounds will be obtained, along with the reaction path of different K compounds during the combustion and their reaction rates. A schematic of the methodology of the devolatilisation and combustion network is depicted in Figure 3.5.

### 3.2.1 Initial values

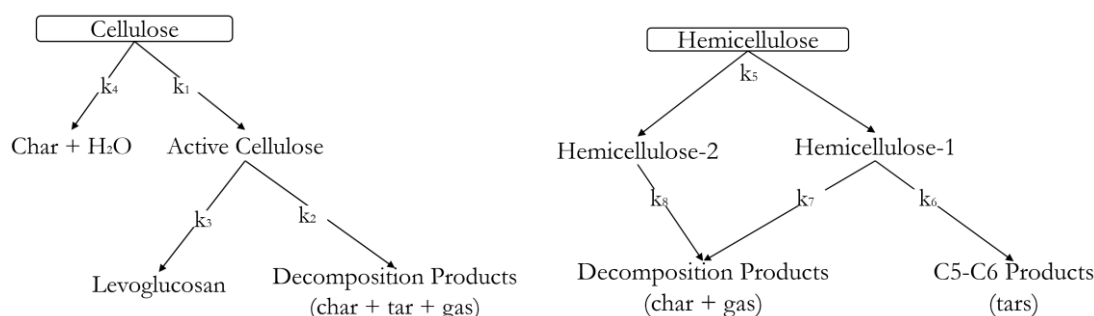
Biomass materials are varying from different sources, but commonly can be characterised by their major chemical components (including cellulose, hemicellulose and lignin), inorganic components and moisture content. The distinct thermal characteristics of chemical components strongly affect the release behaviour of K compounds. In addition, the concentration of oxygen affects the gas and char oxidation under the condition of combustion, and thus, influences the formation and release of K compounds as well. In this way, there were three parts of initial input values included in the model: major chemical components (cellulose, hemicellulose and lignin) that was used to describe the

biomass material; the initial amount of K, S, Cl and H<sub>2</sub>O contents; and the O<sub>2</sub> concentration in the atmosphere.

To calculate the mass fractions of major chemical components in the tested sample, a fitting method developed by a colleague has been employed, this method is described in general terms here and in more detail in the literature [5]. The method estimates the contributions of cellulose, hemicellulose and lignin to the volatile yield via linking the observable features of derivative thermogravimetric (DTG) curves to the parameters of chemical reaction kinetics, along with the fractions of each chemical component. While the initial amounts of K, S, Cl and H<sub>2</sub>O are calculated according to the proximate and ash analysis results of the tested biomass. The initial value of oxygen is calculated based on the test condition. In this thesis, O<sub>2</sub> concentration was calculated following its proportion in the air in the test of combustion, while it was set as zero in the test of pyrolysis.

### 3.2.2 Biomass devolatilisation model

As the major chemical components of lignocellulosic biomass, the thermal characteristics of cellulose, hemicellulose and lignin can be used to provide a generalised description of the thermal process of different biomass materials [2]. It is assumed that the decomposition of these major components is independent, and through a multistep, branched mechanism which followed first-order reactions [6, 7]. The lumped kinetic mechanisms of cellulose, hemicellulose and lignin that used in this model at the devolatilisation stage were extracted from the reference [3], as listed in Appendix I. The summaries of the kinetic mechanisms of these chemical components during the pyrolysis process are illustrated in Figure 3.6 according to the studies of Ranzi et al. [3, 8] and Blondeau et al. [9].



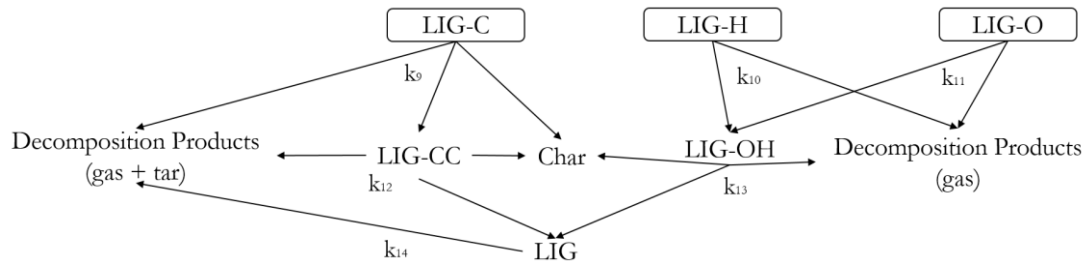


Figure 3.6 Kinetic mechanisms of cellulose, hemicellulose and lignin during the pyrolysis  
(adapted from [3, 8, 9])

In addition, from the previous studies [10-12], the main products from the tar cracking are light gases, and the amount of char is negligible during the devolatilisation process; thus, it will not significantly affect the gas yields. The generation/consumption of different species can be regarded as a function of the conversion:

$$\alpha = \frac{m_{i0} - m_{it}}{m_{i0} - m_{ir}} \quad \text{Eq. (3-1)}$$

where  $m_{i0}$ ,  $m_{it}$  and  $m_{ir}$  represent the initial weight of the species  $i$ , the weight at time  $t$ , and the remaining weight of the species, respectively, g.

For the first order reaction model in this study, the rate of reaction depends on the temperature and the amount of remaining sample, then the reaction model  $f(\alpha)$  can be calculated as:

$$f(\alpha) = 1 - \alpha \quad \text{Eq. (3-2)}$$

Normally, a constant heating rate is involved, so the temperature changes with the time can be obtained according to:

$$dT = \beta dt \quad \text{Eq. (3-3)}$$

Then the rate law of generation/consumption of species with respect to the temperature can be assumed as:

$$\frac{dm_i}{dT} = \frac{1}{\beta} \sum_r v k(T) f(\alpha) \quad \text{Eq. (3-4)}$$

where  $i$  represents the generated/consumed species;  $T$  is the reaction temperature, K;  $\beta$  is the heating rate, K/min;  $r$  represents all the reactions that related to species  $i$ ;  $v$  is the stoichiometric coefficient of the species;  $k(T)$  is the conversion rate.

In this study, the conversion rate constant  $k(T)$  is expressed as a first-order reaction Arrhenius equation as following:

$$k(T) = A \exp\left(\frac{-E_a}{R \cdot T}\right) \quad \text{Eq. (3-5)}$$

where  $R$  representing the universal gas constant, J/mol·K;  $A$  is the pre-exponential factor, 1/s;  $E_a$  is the activation energy, kJ/mol.

In conclusion, when the initial fractions of major chemical components of biomass material are certain, it is possible to simulate the devolatilisation process and to estimate the yields of gas products. The feasibilities will be tested and validated in this thesis experimentally.

### 3.2.3 Release kinetics of inorganic elements

Alongside the devolatilisation, the release kinetics of K, S and Cl are coupled into the devolatilisation model as well. It enables an estimation of the yielded amounts of elemental K, S and Cl at a given condition. The experimental results in the thesis supposed to offer the release profiles of K, S and Cl for the calculation of release kinetics, however, due to the Cl-lean character of the tested sample in this study (see Table 3.1); it cannot provide the necessary data. Nevertheless, the release of Cl is crucial and can significantly affect the release of K during the combustion process, and thus needs to be considered. Under this circumstance, the kinetically controlled release of K, S and Cl were all calculated based on the experimental data regarding their mass loss profiles, which were extracted from the test results in the literature [13], in order to keep the consistency of the input information and the data is presented in Figure 3.7 (in dots).

Assuming a first-order reaction model of the release of K, S and Cl, which follows the first-order Arrhenius behaviour, then the least-squares fitting is used to find out the suitable kinetic parameters:

$$S^2 = \frac{\sum_{i=1}^n (r_{exp} - r_{sim})^2}{n} \quad \text{Eq. (3-6)}$$

where  $r_{exp}$  is the result of the release of the element from the experiment,  $r_{sim}$  is the result of the release of the element from the simulation,  $n$  is the fitting times.

The experiment results are the final amounts of K, S and Cl acquired at different final temperatures. The temperature programme for each run consists of a constant heating

rate of 20 K/min, up to a final temperature, at where the sample is held for 10 min. The data from all the different final temperatures are fitted simultaneously; therefore, the kinetics must be suitable for all the different final temperatures, to get an overall least square, not individually. The fitting results of K, S and Cl conversion are summarised in Figure 3.7, alongside the experimental data (shown in dots), and the calculated kinetic parameters used in this study are presented in Table 3.2.

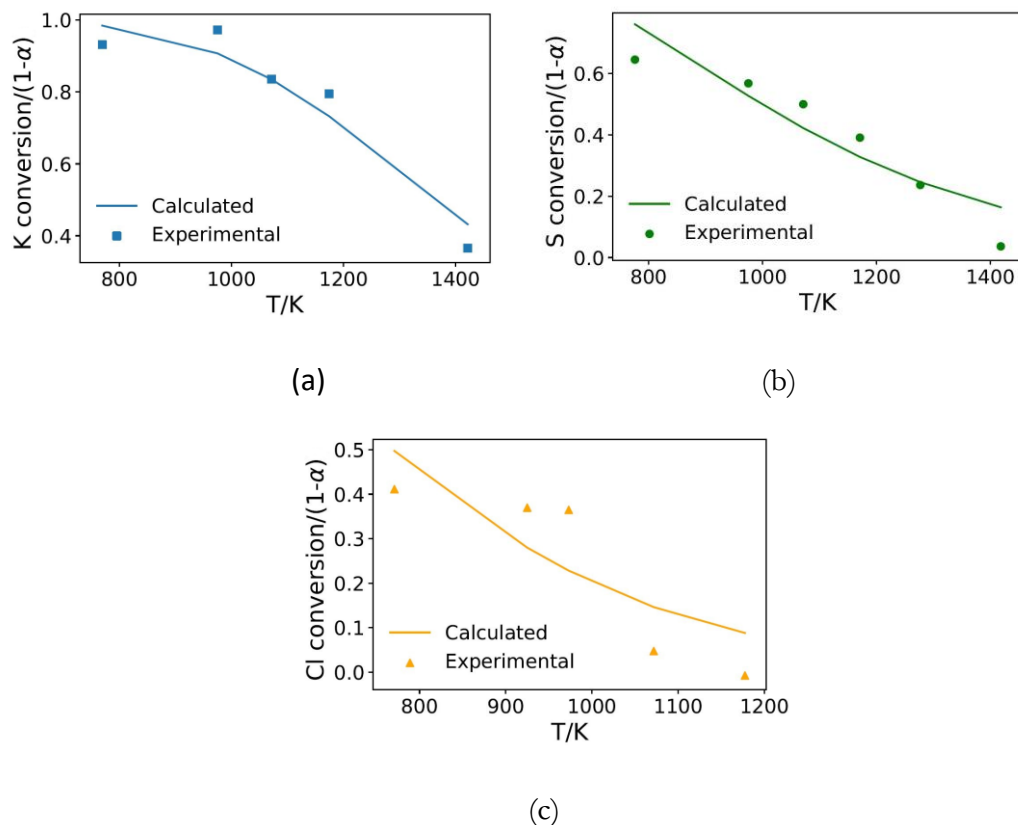


Figure 3.7 Fitting results of the release of K (a), S (b) and Cl (c)

Table 3.2. Summary of the kinetic parameters

	K	$R^2$	S	$R^2$	Cl	$R^2$
$E_a$ , kJ/mol	55.43	0.924	26.65	0.987	22.82	0.991
$A$ , 1/s	1.50E-01		2.80E-02		4.10E-02	

### 3.2.4 Gas species combustion model

During the combustion, the reaction rates and the yields of products from biomass are determined by the reaction kinetics. Combustion characteristics of biomass are driven by the reaction paths with many reactions and intermediate species. In this research, the

kinetic module was employed in this part to simulate the combustion process of all the gaseous products after the devolatilisation in Cantera 2.4.0. Normally, there are two steps to prepare a simulation of combustion in Cantera:

(1) Define solution objectives for the potential reactants to be flowing through the reactor

The solution objective used in this research was a modified reaction mechanism M-GRI30.mech, based on the GRI30.mech [14]. The M-GRI30.mech includes the oxidation of hydrocarbon, as well as the combustion of K, S and Cl species. There are 77 species and 420 reactions that are involved in this modified mechanism, including 325 reactions of hydrocarbon that are originally from GRI30.mech, which is a detailed combustion model of the hydrocarbon including their elementary reactions and is developed by the University of California at Berkeley and sponsored by the Gas Research Institute [14]. The rest of the 95 reactions are the detailed combustion mechanisms of K, S and Cl species which are extracted from literature. The reaction mechanisms of K, S and Cl in the literature are supplied by JANAF tables [15] and are listed in Appendix II. The K reaction mechanisms used in this model are the summary and calculation work done by Peter et al [16] based on other evaluations with high-level theoretical work. The summary and extension work has been done by Cerru et al. [17], which provide the S reaction mechanisms to the model in this research. Furthermore, the Cl related reaction mechanisms were assembled by Sliger et al. [18], based on the H/C/O reaction set from Warnatz et al. [19], along with the Cl related reactions from the NIST database [20].

(2) Define the reactor type that describes the system

A reactor in Cantera is a created environment for the mixture to react, which represents the form of a chemical reaction system. In this model, an Ideal-Gas-Constant-Pressure reactor was selected to simulate the combustion of gas species released from biomass devolatilisation; it is a homogeneous, constant pressure, zero-dimensional reactor. It is an instance of the class reactor where the pressure is held constant, and the volume is not a state variable but instead takes on whatever value is consistent with holding the pressure constant. The implementations of the zero-dimensional simulation are often directly or indirectly incorporated to solve complex three-dimensional problems, and the homogenous zero-dimensional reactor is well suited to validate the computation of the kinetic reactions and the thermodynamic species properties [21]. The reactor corresponds

to an extensive thermodynamic controlled volume, and all state variables are homogeneously distributed inside the reactor. The system is generally unsteady; all states are functions of temperature. In particular, chemical reactions leading to the transient state changes are possible. Meanwhile, thermodynamic equilibrium is assumed to be present throughout the reactor at all moments. In this research, it was assumed that all the gas species behave like ideal gas, and those gas species are controlled by mass, species and energy conservations during the combustion process. The governing equations for these conversions are:

- **Mass Conservation:** The total mass of the reactor's contents changes as a result of flow through the reactor's inlets and outlets, and production of homogeneous phase species on the reactor:

$$\frac{dm}{dt} = \sum_{in} m_{in} - \sum_{out} m_{out} \quad \text{Eq. (3-7)}$$

where  $m$  is the mass flow rate of the content, g/s;  $t$  is the time, s.

- **Species Conservation:** The total rate at which species  $i$  is generated through homogeneous phase reactions is:

$$m_{i,gen} = V_{w_i} W_i \quad \text{Eq. (3-8)}$$

The rate of change in the mass of each species is:

$$\frac{d(mY_n)}{dt} = \sum_{in} m_{in} Y_{i,in} - \sum_{out} m_{out} Y_i + m_{i,gen} \quad \text{Eq. (3-9)}$$

Assuming the species conservation happens when the weight of the sample is stable, which means  $dm/dt$  equals to 0,  $m$  is constant. Expanding the derivative on the left-hand side and substituting the equation of Eq (3-8), then the equation for each homogeneous phase species can be calculated as:

$$m \frac{dY_i}{dt} = \sum_{in} m_{in} (Y_{i,in} - Y_i) + m_{i,gen} \quad \text{Eq. (3-10)}$$

where  $W_i$  is the molecular weight of species  $i$ ;  $Y_i$  is the mass fractions of species  $i$  (dimensionless).

- **Energy Conservation:** The solution of the energy equation is disabled in this research so that the temperature holds at the set initial time of the system. For the ideal gas reactor, the total enthalpy as a state variable with the temperature is replaced by writing the total

enthalpy in terms of the mass fractions and temperature:

$$H = m \sum_i Y_i h_i(T) \quad \text{Eq. (3-11)}$$

$$\frac{dH}{dt} = h \frac{dm}{dt} + m c_p \frac{dT}{dt} + m \sum_i h \frac{dY_i}{dt} \quad \text{Eq. (3-12)}$$

Substituting the corresponding derivatives yields an equation for the temperature:

$$m c_p \frac{dT}{dt} = -Q - \sum_i h_i m_{i,gen} + \sum_{in} m_{in} (h_{in} - \sum_i h_i Y_{i,in}) \quad \text{Eq. (3-13)}$$

where  $H$  represents the total enthalpy of the reactor contents, J;  $Q$  is the overall rate of heat transfer through all walls, W;

- Conversion Rate: The reaction kinetic model used in the Cantera is a rate law that follows the Arrhenius expression of temperature dependence:

$$k(T) = A T^b \exp\left(\frac{-E_a}{RT}\right) \quad \text{Eq. (3-14)}$$

where  $T$  is representing the reaction temperature, K;  $R$  is representing the universal gas constant, J/mol\*K;  $b$  is an empirical parameter;  $A$  is the pre-exponential factor, 1/s;  $E_a$  is the activation energy, kJ/mol.

Through the combustion of gas species, detailed quantity information about the release of different K compounds will be acquired, as well as the transition route regarding the K during the combustion process.

### 3.3 Summary of the chapter

In this chapter, the experimental methods involved in investigating the biomass, cellulose, xylan and lignin combustion and analysis methods (Microwave digestion, ICP-OSE and SEM-EDX) of solid residues were presented in detail; a high-temperature FBS was designed and compared the thermal performance with that of the TGA. Then, the development of a two-step kinetically controlled model to simulate the thermal conversion process of biomass and to predict the release profile of K were described in detail.

## Bibliography

1. Mason, P.E., et al., Observations on the release of gas-phase potassium during the combustion of single particles of biomass. *Fuel*, 2016. 182: p. 110-117.
2. Cao, W., et al., Experimental study on the ignition characteristics of cellulose, hemicellulose, lignin and their mixtures. *Journal of the Energy Institute*, 2018.
3. Ranzi, E., P.E.A. Debiagi, and A. Frassoldati, Mathematical modeling of fast biomass pyrolysis and bio-oil formation. Note I: kinetic mechanism of biomass pyrolysis. *ACS Sustainable Chemistry & Engineering*, 2017. 5(4): p. 2867-2881.
4. Nussbaumer, T., Combustion and co-combustion of biomass: fundamentals, technologies, and primary measures for emission reduction. *Energy & Fuels*, 2003. 17(6): p. 1510-1521.
5. Martí-Rosselló, T., J. Li, and L. Lue, Quantitatively modelling kinetics through a visual analysis of the derivative thermogravimetric curves: Application to biomass pyrolysis. *Energy Conversion and Management*, 2018. 172: p. 296-305.
6. Ranzi, E., et al., Chemical kinetics of biomass pyrolysis. *Energy & Fuels*, 2008. 22(6): p. 4292-4300.
7. Lewis, A.D. and T.H. Fletcher, Prediction of sawdust pyrolysis yields from a flat-flame burner using the CPD model. *Energy & Fuels*, 2013. 27(2): p. 942-953.
8. Ranzi, E., P.E.A. Debiagi, and A. Frassoldati, Mathematical modeling of fast biomass pyrolysis and bio-oil formation. Note II: secondary gas-phase reactions and bio-oil formation. *ACS Sustainable Chemistry & Engineering*, 2017. 5(4): p. 2882-2896.
9. Blondeau, J. and H. Jeanmart, Biomass pyrolysis at high temperatures: Prediction of gaseous species yields from an anisotropic particle. *Biomass and Bioenergy*, 2012. 41: p. 107-121.
10. Liden, A., F. Berruti, and D. Scott, A kinetic model for the production of liquids from the flash pyrolysis of biomass. *Chemical Engineering Communications*, 1988. 65(1): p. 207-221.
11. Diebold, J.P., The cracking kinetics of depolymerized biomass vapors in a continuous, tubular reactor. 1985, Colorado School of Mines. Arthur Lakes Library.
12. Boroson, M.L., et al., Product yields and kinetics from the vapor phase cracking of wood pyrolysis tars. *AIChE Journal*, 1989. 35(1): p. 120-128.

13. Knudsen, J.N., P.A. Jensen, and K. Dam-Johansen, Transformation and release to the gas phase of Cl, K, and S during combustion of annual biomass. *Energy & Fuels*, 2004. 18(5): p. 1385-1399.
14. Gregory P. Smith, e.a. [http://www.me.berkeley.edu/gri\\_mech/](http://www.me.berkeley.edu/gri_mech/).
15. Chase Jr, M.W. and N.-J.T. Tables, Data reported in NIST standard reference database 69, June 2005 release: NIST Chemistry WebBook. *J. Phys. Chem. Ref. Data, Monograph*, 1998. 9: p. 1-1951.
16. Glarborg, P. and P. Marshall, Mechanism and modeling of the formation of gaseous alkali sulfates. *Combustion and Flame*, 2005. 141(1-2): p. 22-39.
17. Cerru, F., A. Kronenburg, and R. Lindstedt, Systematically reduced chemical mechanisms for sulfur oxidation and pyrolysis. *Combustion and Flame*, 2006. 146(3): p. 437-455.
18. Sliger, R.N., J.C. Kramlich, and N.M. Marinov, Towards the development of a chemical kinetic model for the homogeneous oxidation of mercury by chlorine species. *Fuel Processing Technology*, 2000. 65: p. 423-438.
19. Warnatz, J., U. Maas und RW Dibble: *Combustion*. 1996, Springer, Heidelberg.
20. J. A. Manion, R.E.H., R. D. Levin, D. R. Burgess Jr., V. L. Orkin, W. Tsang, W. S. McGivern, J. W. Hudgens, V. D. Knyazev, D. B. Atkinson, E. Chai, A. M. Tereza, C.-Y. Lin, T. C. Allison, W. G. Mallard, F. Westley, J. T. Herron, R. F. Hampson, and D. H. Frizzell, NIST Chemical Kinetics Database, NIST Standard Reference Database 17, Version 7.0 (Web Version). National Institute of Standards and Technology, Gaithersburg, Maryland, 20899-8320. Web address: <http://kinetics.nist.gov/>, 2015.09.
21. Langer, R., et al. A comparison of numerical frameworks for modelling homogenous reactors and Laminar flames. In *Joint Meeting: The German and Italian Sections of the Combustion Institute-41st Meeting ASICI*. 2018. ITA.

## CHAPTER 4

# THERMAL CHARACTERISTICS OF BIOMASS AND ITS CHEMICAL COMPONENTS

---

In this chapter, the thermal characteristics of biomass and its major chemical components (cellulose, xylan and lignin) are studied in the TGA device. Firstly, the combustion characteristics of individual chemical components were investigated. Secondly, the combustion of mixtures of chemical components was conducted and compared against the combustion of natural biomass (wheat straw and softwood), with the aim of identifying the effects of interactions among them on the overall combustion behaviours.

### 4.1 Background

Lignocellulosic biomass is primarily made of three most abundant organic substances: cellulose, hemicellulose and lignin [1]. The distinct thermal characteristics of the major chemical components are often applied as an effective method to provide a comprehensive understanding and to study the thermal behaviour of biomass materials, as well as to distinguish their mutual interactions along with the thermal conversion processes [2-6]. Understanding these characteristics will allow us to design the biomass devolatilisation model based on the input of major chemical components.

### 4.2 Experiment

A total of five materials are used in this study: wheat straw, softwood, cellulose, xylan and lignin. The chemical components were also mixed according to the different ratios, with the aim of simulating the different natural biomass. In total, seven samples were prepared and tested, as listed in Table 4.1. The prepared samples were combusted in the TGA device at a heating rate of 20°C/min up to 900°C. Then the acquired thermogravimetry (TG) and derivative thermogravimetry (DTG) results were used to discuss the thermal characteristics of different samples.

The Coning and Quartering Method [7] was applied to prepare the mixtures in this study, because of its advantages for the preparation of samples with poor flowability (i.e. xylan and lignin), which can reduce the sampling size of the powder sample without generating a systematic bias. Individual samples are mixed in a container according to the predetermined mixing ratio as detailed in Table 4.1, following the mix procedures: 1) pour

a cone of the mixture into a plate; 2) divide the cone into halves; 3) divide the cone into quarters; 4) discard the two opposite quarters of the sample; 5) recombine the remaining sample. The procedure is repeated three times to prepare each mixture sample.

Table 4.1. Sample list

	Sample	Mixing rate, wt.%
Individual samples	Cellulose	-
	Xylan	-
	Lignin	-
	Wheat straw	-
	Softwood	-
Artificial samples*	Wheat straw	Cellulose / Xylan / Lignin: 61.3/19.3/19.4
	Soft wood	Cellulose / Xylan / Lignin: 43.1/24.1/32.8

\* The ratio is calculated according to the method described in the literature [8]

#### 4.3 Thermal characteristics of cellulose, xylan and lignin

The mass loss profiles of cellulose, xylan and lignin during the thermal conversion process in air and nitrogen atmospheres are summarized in Figure 4.1 (a-c). Due to the different chemical structures of the individual components, substantial differences in the thermal behaviours among them could be expected [9].

Figure 4.1 (a) shows the decomposition of cellulose starts at a temperature of 325°C and quickly lost over 80% of its mass before 410°C, which is close to the content of its volatile matter, as shown in Table 3.1 in Chapter 3. When the temperature exceeds 410°C, the mass loss curves of its pyrolysis and combustion processes start to diverge, where the pyrolysis curve is tending to flatten, indicating no further decomposition of the cellulose sample. By the end of the pyrolysis process, approximately 8% of its initial mass remains as solid residues. Figure 4.1 (a) also shows that in the case of combustion, mass loss of cellulose takes place continuously up to 600°C, with less than 1% of its initial mass left as solid residue. The yield difference between the amount of the solid residue after pyrolysis and combustion is equal to the fixed carbon content in cellulose, and the solid residue after combustion is equivalent to the ash content in cellulose.

The thermal characteristics of xylan are shown in Figure 4.1 (b). As shown, its decomposition starts at 190°C, and the pyrolysis and combustion curves start to diverge at 370°C. At this point, the pyrolysis rate stabilises, while the second drop of mass

happens in the combustion process due to char oxidation. After thermal conversions, the solid residue left after pyrolysis and combustion processes is 18% and 1.5% of the initial mass of xylan, respectively, which are similar to its fixed carbon and ash contents.

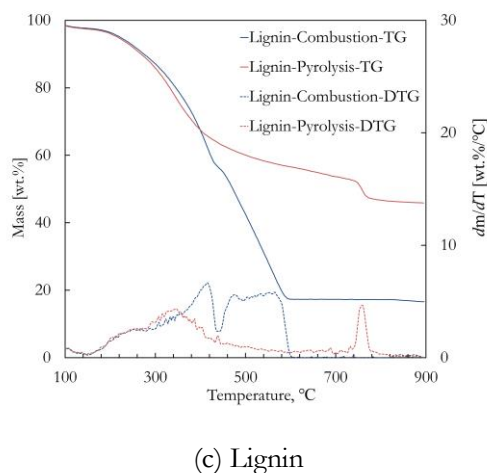
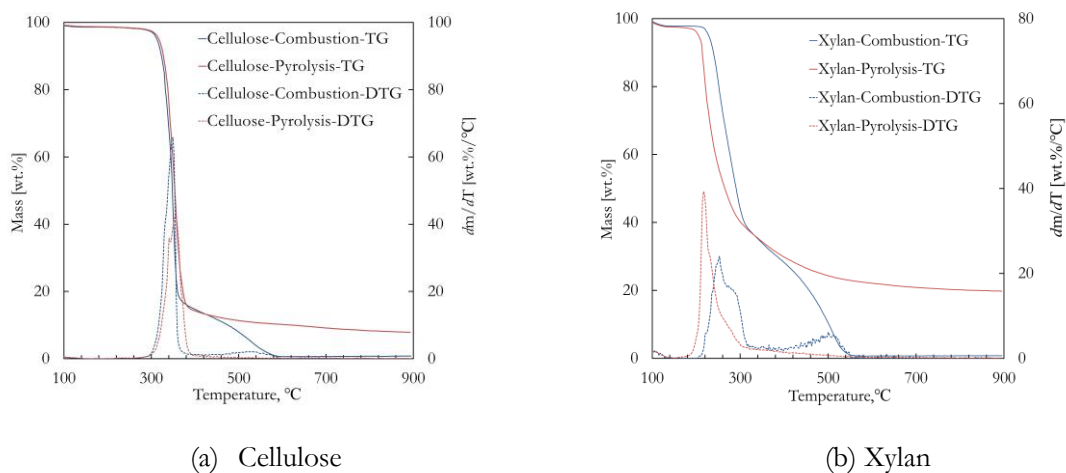


Figure 4.1. Thermal characteristics of individual chemical components in the air (combustion) and nitrogen (pyrolysis) atmospheres

The results in Figure 4.1 (c) shows that lignin starts to decompose at 210°C, and the divergence of its pyrolysis and combustion curves occurs at 405°C. During pyrolysis, after divergence, lignin is observed to decompose slowly in the temperature range of 405°C to 750. The remaining solid after total pyrolysis accounts for approximately 45% of its initial mass, which is equal to the sum of its fixed carbon and ash contents. While during combustion, the lignin sample lost more than half of its mass between 405°C and 600°C, and left 15% of its initial mass in the end, which is equal to its ash content.

By comparing the TGA results of cellulose, xylan and lignin presented in Figure 4.1, it can be observed that nearly all the mass loss curves for the pyrolysis and combustion processes overlapped until the divergence occurs; the slight deviation between them might be caused by the differences in the thermal conductivity of air and nitrogen [10]. It implies that at the early stage of thermal conversion, the temperature is the dominant factor of the reactions, rather than the existence of oxygen. Moreover, among the three components, cellulose has the narrowest decomposition temperature range and lost the most of its mass during the decomposition process. Xylan requires the lowest temperature to initiate the sharp loss of mass. Lignin has the widest decomposition temperature range and generates the most of the solid residues.

#### 4.4 Thermal characteristics of artificial and natural biomass

To identify the effect of the interaction of chemical components upon the thermal properties of biomass, natural and artificial biomass samples (artificial wheat straw (AWS) and artificial softwood (ASW)) were tested. The TG and DTG results of artificial biomass were compared to those obtained from natural biomass samples, with the aim to investigate the accuracy of the prediction on the thermal characteristics of biomass using the mixture of major chemical components. The summarised TG and DTG results are presented in Figure 4.2.

Figure 4.2 (a) and (b) shows the decomposition of wheat straw and softwood starts at 250°C and 255°C, respectively. Then, due to the release of abundant volatile and moisture contents, wheat straw loses 60% of its initial mass when the temperature reaches 350°C, while softwood loses nearly 70% when the temperature approaches 405°C. Following this, the pyrolysis and combustion curves start to diverge. The pyrolysis curve flattens out until the end, at which point, there are 25% and 20% of the initial mass left as the solid residue for wheat straw and softwood, respectively, which consists of the fixed carbon and ash content. In contrast, the combustion curve shows the second drop in mass, the endpoint for wheat straw and softwood is 510°C and 500°C, respectively; this leads to a further mass loss that ends at 18% and 39% of the initial mass of wheat straw and softwood, respectively. The lost mass values correspond to the fixed carbon content, as listed in Table 3.1 in Chapter 3. In the results of the DTG curves for both samples, two obvious peaks appear before the temperature at which behaviours diverge. The first one is at 100°C, due to the evaporation of moisture content. The second occurs at 300°C for wheat

straw and 330°C for softwood, which is caused by the release of volatile matter. Then the pyrolysis curve becomes stable, while for combustion, a third peak appears in the curve at 460°C for wheat straw, and 500°C for softwood, which is caused by the char oxidation.

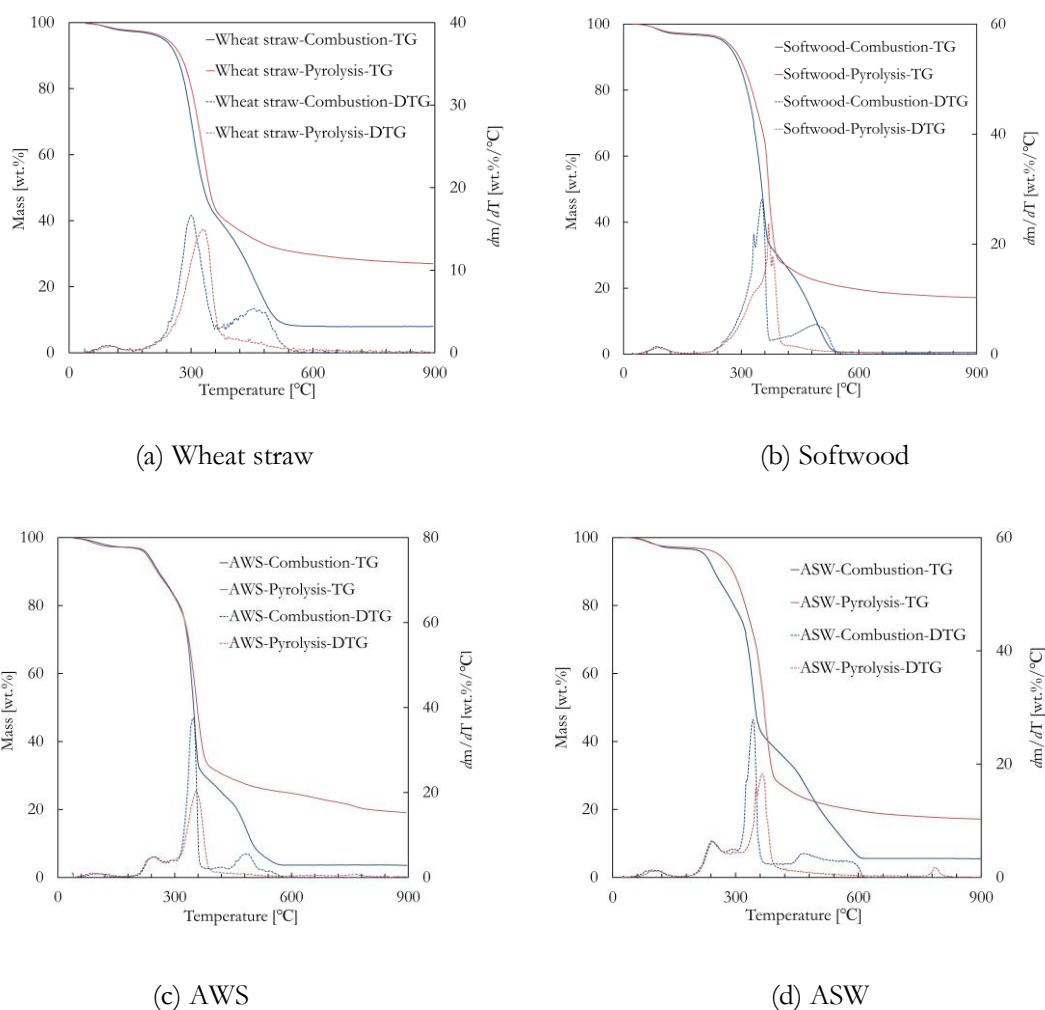


Figure 4.2. Thermal characteristics of biomass samples in the air and nitrogen atmospheres: (a) wheat straw; (b) softwood; (c) AWS; (d) ASW

Figure 4.2 (c) shows the test result of AWS. Its first phase decomposition starts at 220°C and continues to 365°C. The pyrolysis and combustion curves show two steep decreases of mass during this phase, the first of which occurs from 220°C to 340°C in TG curves; it reaches its peak at 260°C in DTG curves. It is mainly caused by the decomposition of xylan, the least thermally stable component in biomass [11], due to the breakdown of its C-O-C and pyranose C-C bonds [12]. According to the individual components test results, xylan has the lowest temperature to decompose, which is at 180°C, and sharply lost 65% of its mass before 300°C. However, at this temperature range, cellulose and lignin are

partially decomposed, implying the existence of cellulose and lignin does not affect the thermal behaviour of xylan significantly. The second drop in the TG curve occurs in the temperature range of 340°C-380°C, and as can be seen in the DTG curve, it reaches its peak at 355°C. As illustrated in Figure 4.1, at this temperature range, cellulose lost nearly 90% of its initial mass, while lignin lost 15%, and xylan only lost 4%, indicating that cellulose and lignin are the main components that attribute to the mass loss during this stage. The pyrolysis and combustion curves of AWS start to diverge at 375°C. Beyond this, AWS continues to lose its mass slowly, with 20% of its initial mass remaining at the end of the pyrolysis test; this is the same as the sum of partial contributions of the fixed carbon and ash contents of each component. While under the combustion scenario, char oxidation occurred; most of the mass loss at the char oxidation stage is attributed to lignin and xylan. Both of these have much higher fixed carbon contents, with 33.7 wt.% in lignin and 13.5 wt.% in xylan compared to that of cellulose (8.6 wt.%).

The test results of ASW are illustrated in Figure 4.2 (d). A similar conclusion can be drawn; the decomposition of each component is distinguishable. The TGA curves show the first stage decomposition starts at 240°C, until to 490°C for pyrolysis and it is 210°C-460°C for combustion, and there are two drops of mass happened during this stage. The first drop starts at 240°C to 350°C in pyrolysis curve, while it is 210°C-330°C for combustion curve, and both reached their peaks at 240°C in DTG curves. As shown in Table 4.1, the content of xylan in ASW is similar to that of AWS, which leads to the semblable temperature range of the first drop. Then, due to the decomposition of cellulose and lignin, the second drop occurred within 350°C-390°C in pyrolysis result and within 330°C-360°C in combustion result and reaching their peaks at 344°C and 367°C in DTG results, respectively. Beyond 390°C, the pyrolysis curve becomes flat and with 20% of its initial mass remains at the end. While the combustion occurred the char oxidation phase, and the remaining residues were equal to the sum of the partial contributions of ash contents of each component.

The thermal decomposition results of artificial biomass show a similar trend to that of natural biomass samples. For wheat straw, the devolatilisation happened within the temperature range of 250°C-350°C in the natural sample, while a similar temperature range (220°C-365°C) can be observed for the artificial sample. Moreover, for both natural and artificial samples, the char oxidation stage ceases at around 520°C. Also, a similar

conclusion can be drawn for the results of artificial and natural softwood as well. Both samples occurred the devolatilisation stage at a similar temperature range (255°C-400°C and 240°C-390°C for natural and artificial softwood, respectively). However, a prolonged oxidation of char is observed in the result of artificial softwood. This phenomenon might be caused by the melting and formation of agglomerated lignin particles, which could wrap the nearby cellulose and xylan particles [6], lowering the heat transfer efficiency of the particles. Furthermore, the lignin structure consists of phenylpropane, which coupled with C-C and/or C-O-C bonds that covers an extremely wide range of decomposition temperature (152°C- 700°C) [13]. Accordingly, the above reasons may lead to a higher temperature to burn out the samples.

Through the investigation, the test results of artificial biomass can be used to estimate the temperature range of different stage of combustion of natural biomass. Besides, a high similarity of mass loss can be observed at different stage between the results of natural and artificial biomass. Moreover, the contribution to the mass loss at different stage is reflected by the thermal characteristics of each chemical component. This implies that it is feasible to predict the thermal behaviour of different biomass materials via the thermal behaviour of the mixture of major chemical components: cellulose, hemicellulose and lignin.

#### 4.5 Summary of the chapter

This chapter has investigated the thermal characteristics of cellulose, xylan, lignin, artificial and natural biomass samples using a TGA device. According to the tests, cellulose has the narrowest decomposition temperature range and lost most of its mass during the decomposition process. Xylan requires the lowest temperature to initiate the loss of mass, while lignin has the widest decomposition temperature range and generates the most of the solid residues. Moreover, by comparing the TG and DTG results of artificial and natural biomass, the occurring temperature range and mass loss of different stages of thermal conversions are predictable. In particular, the thermal conversion results of wheat straw can be predicted with high accuracy, and this illustrates the potential to use the major chemical components to predict the thermal characteristics of different biomass types.

## Bibliography

1. Zhang, L., C.C. Xu, and P. Champagne, Overview of recent advances in thermochemical conversion of biomass. *Energy Conversion and Management*, 2010. 51(5): p. 969-982.
2. Raveendran, K., A. Ganesh, and K.C. Khilar, Pyrolysis characteristics of biomass and biomass components. *Fuel*, 1996. 75(8): p. 987-998.
3. Worasuwannarak, N., T. Sonobe, and W. Tanthapanichakoon, Pyrolysis behaviors of rice straw, rice husk, and corncob by TG-MS technique. *Journal of Analytical and Applied Pyrolysis*, 2007. 78(2): p. 265-271.
4. Wang, G., et al., TG study on pyrolysis of biomass and its three components under syngas. *Fuel*, 2008. 87(4-5): p. 552-558.
5. Wang, S., et al., Influence of the interaction of components on the pyrolysis behavior of biomass. *Journal of Analytical and Applied Pyrolysis*, 2011. 91(1): p. 183-189.
6. Cao, W., et al., Experimental study on the ignition characteristics of cellulose, hemicellulose, lignin and their mixtures. *Journal of the Energy Institute*, 2018.
7. Campos-M, M. and R. Campos-C, Applications of quartering method in soils and foods. Vol. 7. 2017. 35-39.
8. Martí-Rosselló, T., J. Li, and L. Lue, Quantitatively modelling kinetics through a visual analysis of the derivative thermogravimetric curves: Application to biomass pyrolysis. *Energy Conversion and Management*, 2018. 172: p. 296-305.
9. Kai, X., et al. The effect of biomass components on the co-combustion characteristics of biomass with coal. In 2011 Second International Conference on Digital Manufacturing & Automation. 2011. IEEE.
10. Li, J., M.C. Paul, and K.M. Czajka, Studies of ignition behavior of biomass particles in a down-fire reactor for improving co-firing performance. *Energy & Fuels*, 2016. 30(7): p. 5870-5877.
11. López-González, D., et al., Thermogravimetric-mass spectrometric analysis on combustion of lignocellulosic biomass. *Bioresource Technology*, 2013. 143: p. 562-574.
12. Cheng, K., W.T. Winter, and A.J. Stipanovic, A modulated-TGA approach to the kinetics of lignocellulosic biomass pyrolysis/combustion. *Polymer Degradation and Stability*, 2012. 97(9): p. 1606-1615.

13. Stefanidis, S.D., et al., A study of lignocellulosic biomass pyrolysis via the pyrolysis of cellulose, hemicellulose and lignin. *Journal of Analytical and Applied Pyrolysis*, 2014. 105: p. 143-150.

## CHAPTER 5

# POTASSIUM TRANSITION PERFORMANCE DURING BIOMASS COMBUSTION

---

In this chapter, the transition performance of K inherent in biomass is studied experimentally at different combustion operations. The effects of final temperature and heating rate on the transition of K during biomass combustion process associated with the structural changes of the biomass particles are discussed.

### 5.1 Background

During the combustion process, both internal and external factors can affect the release process of K content. The internal factors include the inherent organic, inorganic and ash components of selected biomass samples, while the external factors contain the combustion operations. As stated in Chapter 2, the operating parameters (final temperature and heating rate) have significant influences on the thermal conversion of biomass materials and thus could affect the release behaviour of K. In consequence, the study of the influence of operating parameters on the K transition performance during the biomass combustion process can provide an insight of the transition behaviour of K. The resulting data is anticipated to guide the reactor design and optimize the combustion process, aiming to mitigate the K-related ash problems.

### 5.2 Experiment

#### 5.2.1 Experiment procedure

Due to the high concentrations of K, S and Cl in the wheat straw compared to that of softwood (see Chapter 3, Table 3.1), the study of K transition performance has been focused on the tests of wheat straw in this thesis. The combustion tests were carried out in FBS, as the device allows the combustion of a large number of wheat straw pellets and the generation of sufficient solid residues for the follow-up analysis. The final temperature was ranged from 300°C to 1000°C. The heating rate was set as 8°C/min, 17°C/min and 25°C/min according to the reference [1]. The tests conditions are summarised in Table 5.1.

Before each test,  $5 \pm 0.1$ g of uniformly selected pellets were evenly distributed in the crucible, and overlapping was avoided. Place the crucible in the FBS; after the balance

becomes stable, start the heating up programme that is set according to Table 5.1. After the combustion, the crucible was transferred to an oven for cooling down before solid residues were collected. The reproducibility of the measured results of each test has been ensured by performing the repeat experiments. The collected solid residue samples were then digested and analysed using a Microwave Digestion System, ICP-OES and SEM-EDX, aiming to obtain the retention amount of K and the structural changes of biomass particles.

Table 5.1. Summary of testing conditions

		Final temperatures, °C								Holding time, min
		300	400	500	600	700	800	900	1000	
Heating	8	√	√	-	√	-	-	√	√	10
rates,	17	√	√	√	√	√	√	√	√	
°C/min	25	√	√	-	√	-	-	√	√	

### 5.2.2 Quantity of K content

Biomass samples would undergo the loss of moisture content, volatile matters, and fixed carbon during the reactions, the K content in the solid residues are concentrated and varying according to the collection stage. Thus, the test results from ICP-OES cannot be directly used to study the release behaviour of K under different conditions. In order to compare the K contents in the solid residues, a calculation is developed to convert the K content from mg/kg in measured samples to mg/kg in raw material (normalized for the amount of K in the fuel), as  $R_k$  (dry basis), following the calculation:

$$R_k = \frac{m_k C_r}{m_0} 100\% = \frac{m_{kt} m_{ash0} m_{out}}{m_{kot} m_{ash} m_{in}} 100\% \quad \text{Eq. (5-1)}$$

Where  $m_k$  donates the K content in the solid residue (mg/kg),  $C_r$  refers to the residue ratio, which is the amount of solid left after combustion divided by the amount of initial input sample (%), and  $m_0$  is the measured K content in the wheat straw (mg/kg).

All these parameters are calculated from the measurements, as presented in Eq. (5-1), where  $m_{kt}$  and  $m_{kot}$  represent the K contents of digested samples and wheat straw, respectively, ( $\pm 0.001$ ppm);  $m_{ash}$  and  $m_{ash0}$  refer to the weighted solid residues and wheat straw before digestion, respectively, ( $\pm 0.001$ g);  $m_{in}$  and  $m_{out}$  represent the weighted samples before and after combustion, respectively, ( $\pm 0.001$ g). The K concentrations  $R_k$  calculated from Eq. (5-1) that depends on the measured quantities, and the uncertainty of each

measurement influences the results of  $R_k$ . Since the errors in the measured quantities are independent of each other, the uncertainty of  $R_k$  can be calculated by using:

$$(\delta R_k)^2 = \sum_i \left( \frac{\partial R_k}{\partial m_i} \right)^2 (\delta m_i)^2 \quad \text{Eq. (5-2)}$$

Where  $m_i$  represents the different variables, and in this study, there are six of them, as indicated in Eq. (5-1).

### 5.3 Influence of final temperature on K transition

#### 5.3.1 Test results

The uncertainty of each sample is summarized in Table 5.2. As we can see, the calculated uncertainties of all the results are under 0.3%, indicating that the results of the experiments are reliable and varied within a small range.

Table 5.2. Calculated uncertainties of the K concentration measurements at different final temperatures

Temperature, °C	30	200	300	400	500	600	700	800	900	1000
$\delta R_k, \%$	0.24	0.27	0.26	0.24	0.23	0.24	0.23	0.22	0.21	0.13

The retention of K in different solid residues and the mass loss of wheat straw pellets are presented in a temperature basis in Figure 5.1. The results indicate that nearly 80% of K retained in the residues before 500°C and more than 75% of K left in the residues when the temperature reached 700°C. This result is in good agreement with the results of Johansen et al. [2], who observed that only about 10-20% of K was released below 700°C. However, a sharp decrease in K concentration is observed when the temperature is higher than 800°C, and there is only 42% of K left when the final temperature reaches 1000°C. As for the mass loss of wheat straw, a steep loss of the sample weight starts from 200°C and continues to 500°C, during which more than 70% of its weight is lost because of the abundant release of moisture and volatile matter contents. In addition, when the final temperature exceeds 500°C, the sample loses its weight more gradually until 1000°C, which is caused by the oxidization of fixed carbon. The final remains are the ash residues, which represent less than 10% of the original wheat straw mass.

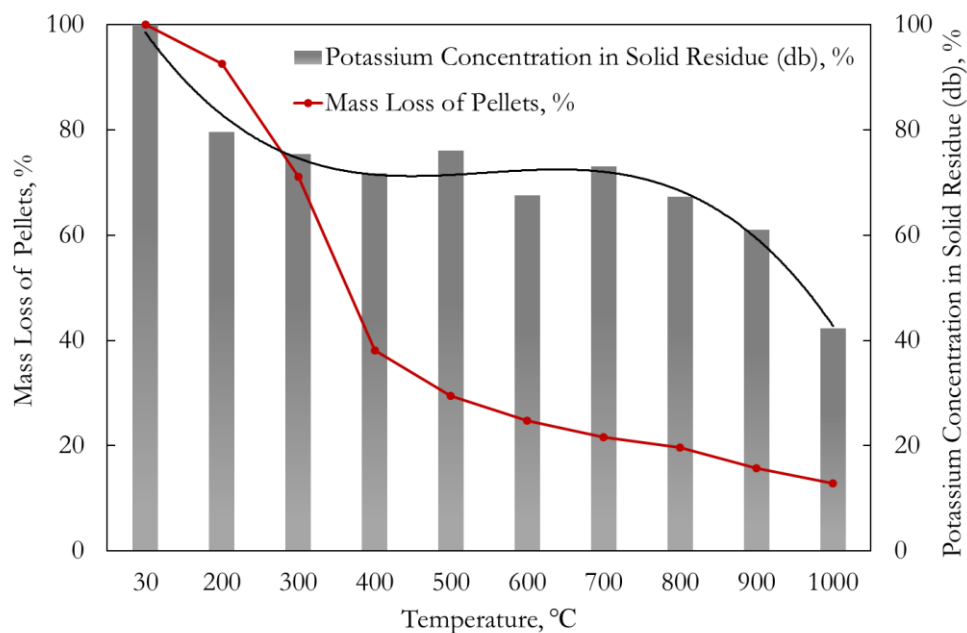


Figure 5.1. Mass loss curve (red, left axis) and the percentage of K mass retained in residues (dry basis, black, right axis).

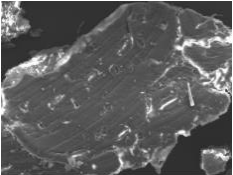
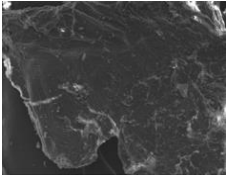
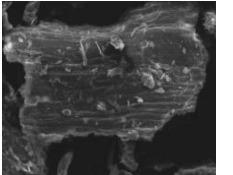
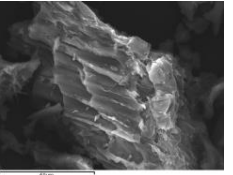
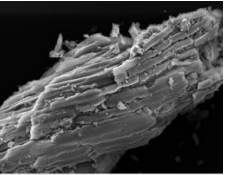
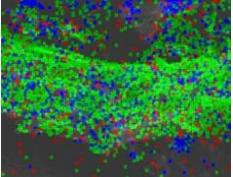
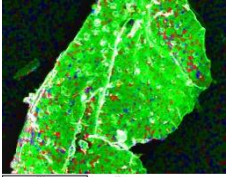
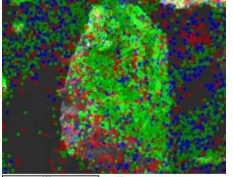
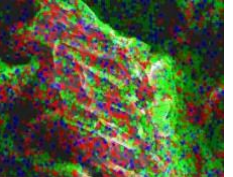
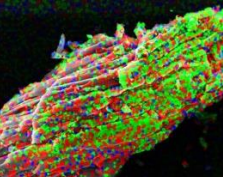
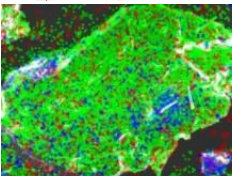
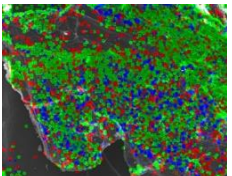
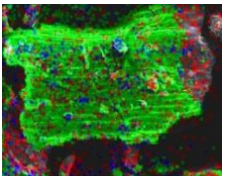
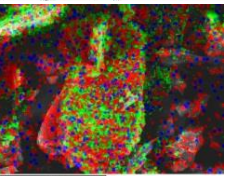
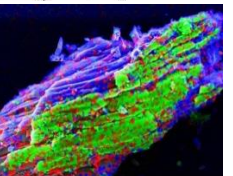
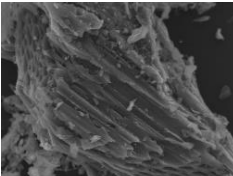
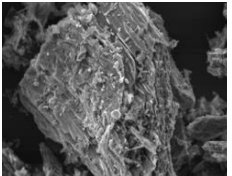
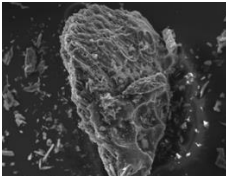
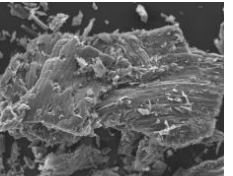
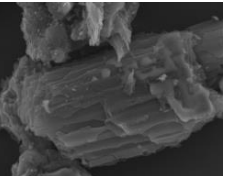
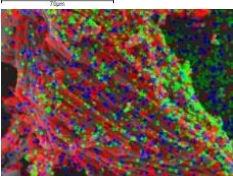
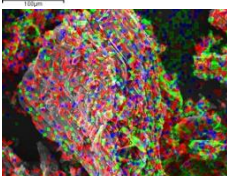
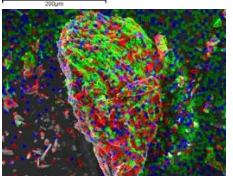
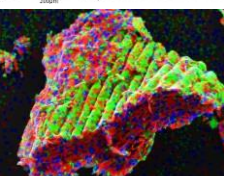
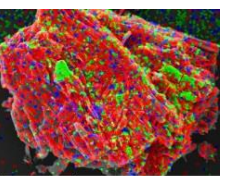
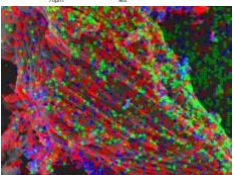
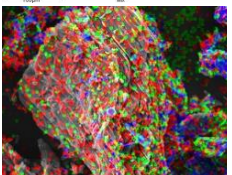
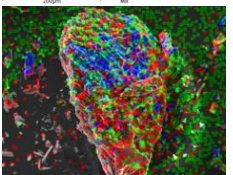
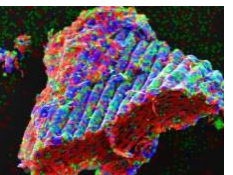
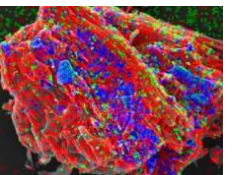
The structural changes of the wheat straw residues and the distribution of inorganic elements (K, O, Si and S) were investigated by SEM-EDX, and the results are summarized in Table 5.3.

Table 5.3 shows that, with increasing the final temperature, the solid residues undergo significant structural changes. There are noticeably broke down of straw particles and the collapsing of pore structure, yet the overall fibrous structure was still maintained. The stem-like structure is easily recognizable with clearly defined channels at all the tested temperatures. It is evident that fusing is insignificant when the final temperature is below 800°C. As the final temperature reaches 900°C, the particles get partially fused; further at 1000°C, large fused surfaces appear on the particles, homogeneous external area covered with minor ash particles. Similar results are also observed in other studies [3-5]. The large ash particles are the remains of the outer skeleton of the samples, with no fusing when the temperature is below 700°C; while at 1000°C, the ash structure is flaky with a molten appearance, which is mainly composed of K and Si.

The results of EDX test revealed that a trace amount of K exists on the surface of the wheat straw particles; however, more K is distributed inside the particles. With increasing the combustion temperature, collapse of particle structure leads to the exposure of more

interiorly located K, which could potentially accelerate the release of K. Meanwhile, Si can be detected throughout the particles at all the tested temperatures, and mainly co-exists with O and K. When the final temperature reaches 900°C and 1000°C, more Si and K clusters are detectable

Table 5.3 Summary of the SEM-EDX results at different temperatures

		Temperature, °C				
		30	200	300	400	500
SEM	SEM					
	EDX (Red: K Green: O Blue: S)					
	EDX (Red: K Green: O Blue: Si)					
		600	700	800	900	1000
SEM	SEM					
	EDX (Red: K Green: O Blue: S)					
	EDX (Red: K Green: O Blue: Si)					

### 5.3.2 Analysis and discussion

According to the results presented in Figure 5.1, there are two apparent drops of K concentration happened as the combustion temperature increased. As a result, the change

of K concentration can be divided into three stages: first drop (<500°C), holding phase (500°C-700°C), and second drop (>700°C).

a) Stage 1: First drop (<500°C)

Figure 5.1 shows that nearly 75% of K is left within this stage. The loss of K starts at 200°C, which is the same temperature point that straw pellets start to decompose. Then there continues the slow loss of K as the final temperature increases to 500°C; in the meantime, the straw pellets suffered a steep loss of its total mass with nearly 70%.

According to the investigation, the loosely-bonded K is more likely to attach to hydroxyl or carboxyl groups or other oxygen-containing groups [6, 7]. It is released from the surface of the particles at temperatures below 300°C [8, 9] in the form of  $K^+(g)$ , then the  $K^+(g)$  can react with  $H_2O$  and/or Cl to generate  $KOH(g)$  and/or  $KCl(g)$  depending on the concentrations of moisture and Cl content [6, 10]. Primarily,  $KOH$  is the main form of K that is released at temperatures below 400°C. However, when biomass sample has a high Cl content, the release of Cl in the form of  $HCl(g)$  will react with  $KOH(g)$  to generate  $KCl(g)$  and will be substantially released as the final temperature increased. Nevertheless, the released K compounds are all in small amounts, as indicated in Figure 5.1, there is only 3% of K content lost. Meanwhile, the inorganic-K and partial organic-K remain stable at these temperatures.

When the final temperature reaches 500°C, the straw samples released an abundant amount of volatile matter [11], and most of the organic carbon compounds are evolved and oxidized to  $CO_2(g)$  [12]. Organic-K is partially decomposed to generate char-K and continuing to release as  $K^+(g)$ . At the same time, inorganic-K remains stable as the temperature is too low to trigger the evaporation and decomposition reactions of inorganic-K compounds. The wheat straw pellets used in the tests are Cl-lean materials, indicating  $KOH$  is the main released form of K. Due to the presence of large amounts of  $CO_2(g)$  at this temperature in the combustion atmosphere and the lack of Cl in the gas phase, the released  $KOH(g)$  is partially condensed through carbonation reactions and may stay on the surface of the particles in the stable form as  $K_2CO_3(s)$ , via the R5-1. This reaction may lead to more retention of K content in the solid products, as the generated  $K_2CO_3$  will not be decomposed until the temperature reaches its evaporation and decomposition limits.

In Table 5.3, the SEM tests reveal that the sample particles can hold most of its structure when the final temperature is below 300°C. Combined with the EDX results, the major parts of the particle surface areas are covered with O and detectable Si and K, while more K and S can be detected in the internal structure of the solid sample. When increasing the final temperature up to 500°C, the volatile matter is further released, and more organic-K is converted to char-K, so that the structure of biomass becomes fragile, starting to collapse and fall apart. However, the most of the stem-like structure remains intact, and it can be observed that K and S are hidden inside the channel structures, while Si and O consist most of the external structure of particles. Nevertheless, the small amount of detectable S indicates that  $K_2SO_4$  (s) is not one of the main existing forms of K in the wheat straw,  $K_2SO_4$  could be generated as the temperature increased. With the combustion temperature increasing from 300°C to 500°C, there is only 2% more of K lost according to the results in Figure 5.1, mainly because of the release of inherent KOH(s) at a temperature below 500°C and the partial decomposition of char-K that generated from organic-K at temperature exceed 300°C through the R5-2 and R5-3.

As the final temperature increases up to 500°C, with the breakdown of particles, more inside located K exposed, however, the mass loss of K is insignificant, indicating that the major part of the K exists in the internal structure of biomass is thermally stable. The reaction between the Si-rich layers and the exposed K to form stable K silicates is negligible at low temperatures [3], meaning that the occurrence mode of inside located K is inorganic salts and high stability char-K [13]. In fact, highly mobile K in living biomass is mostly presented as free  $K^+$  ions in solution within the xylem cells [14]. During the air-drying process, these ions precipitate as inorganic potassium salts [15], which can make up to more than 90% of the total potassium in raw biomass and are thermally stable at lower temperatures.

#### b) Stage 2: Holding phase (500°C-700°C)

The results in Figure 5.1 show that about only 5% more of K is lost in this stage, which is mainly attributed by the decomposition of char-K compounds (such as R-benzene-O-K, which can be decomposed at the temperature range of 400°C-600°C) since char oxidation and decomposition normally occurs after the devolatilisation [16]. The minor released K might in the form of KOH (g) via the reaction with the moisture that decomposed from carbonates [17]. Besides, since the sample that employed in this study

is Cl-lean, and it is widely acknowledged that most of the Cl content could be released below 500°C [9, 18-20], indicating that under this circumstance, there are minor Cl compounds exist in the reactor that could consume KOH. While the remaining char-K is oxidized to produce  $K_2CO_3(s)$  via the reaction of R5-4 under the condition with sufficient oxygen content, and it could also react with S to form  $K_2SO_4(s)$ . After the release of organic-K and the oxidization of char-K at the end of this stage, the remaining K content in the solid residues mainly exists in the form of thermally stable inorganic salts.

The morphology results in Table 5.3 indicate that there are less significant changes in particle structure when increasing the final temperature from 500°C to 700°C. The particles are not fully collapsed; however, the channels become more fragile since more char has been oxidized with oxygen. The pores continue to collapse but are still visibly detectable; the surfaces of the particles are getting rougher and covered with fine ash particles. When the final temperature reaches 700°C, there is only 20% of the original sample remained as solid residue, which mainly consists of ash and unoxidized char. Previous studies indicate that the main volatile components have already been mostly devolatilized and decarbonized at this temperature [21]. The high Si content in the raw material in this study is the key to preserve the pore structure since it is mainly present as a silicate skeleton on the external surface of the straw, which provides structural strength and protection to against the breakdown of particles [3].

More K and S can be observed in the EDX images as the particle structure breaks down. The substantial amount of K exists inside the pores is exposed and likely to react with S in the presence of oxygen to form  $K_2SO_4(s)$  via the R5-5. In addition, the observed K-Si clusters in Table 5.3 suggests the co-existence of K and Si in this stage, but not as a compound, since the reaction between them to form stable species is still insignificant at these temperatures [13]. This observation indicates that the K is likely to be captured by the Si matrix during the combustion process; it is well documented that alkali metal oxides can be incorporated into silicate networks and become less volatile [9, 22, 23], and the captured K can then react with Si when the temperature is sufficiently high.

In conclusion, during this stage, the transition of the existing form of K is very likely to take place, such as the conversion of char-K and organic-K into thermal-stable inorganic-K species. The release of K in this stage is insignificant compared to the loss of organically associated K during stage 1.

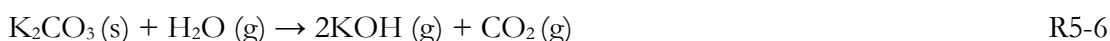
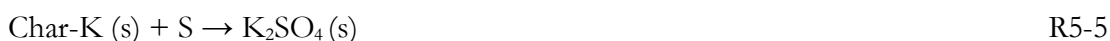
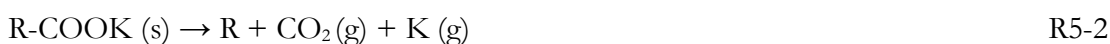
c) Stage 3: Second drop ( $>700^{\circ}\text{C}$ )

As the final temperature increased, high temperature facilitates the further oxidation of the remaining char and the dissociation and release of mineral salts, resulting in the sample continues to lose its mass, but with only 8%. In the meantime, K however, continues to significantly lose over 30% of its mass.

After been released at low-medium temperatures, there is nearly no organic-K, and partial inorganic-K could be left, and the remaining K exists mainly in forms as  $\text{K}_2\text{CO}_3$ ,  $\text{K}_2\text{SO}_4$  and  $\text{K}_2\text{SiO}_3$ . When the final temperature exceeds  $800^{\circ}\text{C}$ , some of the  $\text{K}_2\text{CO}_3$  (s) could be released, while partial of the  $\text{K}_2\text{CO}_3$  (s) could react with  $\text{H}_2\text{O}$  to generate  $\text{KOH}$  (g) via the R5-6. Moreover, at temperatures above  $900^{\circ}\text{C}$ ,  $\text{K}_2\text{CO}_3$  (s) could primarily dissociate to form  $\text{K}_2\text{O}$  (g) and  $\text{K}$  (g), following the R5-7 and R5-8 [3], and released, leading to the further loss of K content. However, the released K can be partially captured by the Si matrix. Previous studies [3, 24] stated that the formation of K-Si species is significant at combustion temperature above  $900^{\circ}\text{C}$ , following the R5-9, and the K-Si species can remain stable. As the final temperature increased to  $1000^{\circ}\text{C}$ ,  $\text{K}_2\text{SO}_4$  (s) could be evaporated [4], resulting in an additional loss of K content from solids. After complete combustion of biomass samples and release of inorganic-K compounds at high temperature, the remaining K is presented in the thermal stable forms in the solid residues, such as  $\text{K}_2\text{SiO}_3$  (s) and  $\text{K}_2\text{O}$  (s), as well as the possible forms like  $\text{K}_2\text{CaSiO}_4$  (s) and  $\text{KAlSi}_3\text{O}_8$  (s) [25].

According to Table 5.3, the structure and surface of the particles have changed significantly during this stage compared with that of other stages. At  $800^{\circ}\text{C}$ , the pore structure continues to break down, and fine particles coat the surface of larger residue particles; fusing area is more detectable on the particles in the SEM images as well. The EDX results show that the collapse of the pore structure continues to expose more inside located K and S. Meanwhile, Si still covers most of the surface area, but the breakdown of the particle results in the more peeling of Si-rich structures, which also exposes more inside located K and leads to its transformation of existing forms. At  $900^{\circ}\text{C}$ , the external surfaces of the larger particles are partially fused, and the fused areas are rich in Si and K; while the pore structure continues to shrink and close. Small Si-rich particles and small  $\text{K}_2\text{SO}_4$  particles adhere to the external surface of the larger residue particles, which is similar to the result observed by Knudsen et al. [3].

When the final temperature reaches 1000°C, pore structure becomes difficult to detect. Larger fused external areas can be observed, and the particles start to agglomerate into large structures with smooth surfaces. Due to the continuing evaporation of K<sub>2</sub>SO<sub>4</sub> (s), the detectable K and S clusters are decreased. Still, more K and Si clusters are detectable, as well as isolated K and K-O clusters. The result suggests that the Si matrix can capture the K (s) and K<sub>2</sub>O (s) after they are released. As reported in the studies [9, 26], when the final temperature exceeds 1200°C, K<sub>2</sub>SiO<sub>3</sub> (s) can be partially released as well, causing the further loss of K, while the trapped K (s) and K<sub>2</sub>O (s) can further react with Ca to form K-Ca-silicate, which remains stable in the molten residue ash.



### 5.3.3 Summary of findings

The release and transformation behaviour of K were studied during the wheat straw combustion. Through the investigation, the final temperature has greatly affected the release of K during the combustion of biomass, with the increasing of final temperature, the left K in the solid residues declined, and there is over 60% of the initial K released when the final temperature reaches 1000°C.

Based on the above-described results and the discussions with the results of the release of gas-phase K that extracted from references [2, 4, 13, 18], a comprehensive K transition pathway during the combustion process corresponding to the final temperature is proposed for a better understanding of the transition behaviour of K at different temperatures, as shown in Figure 5.2.

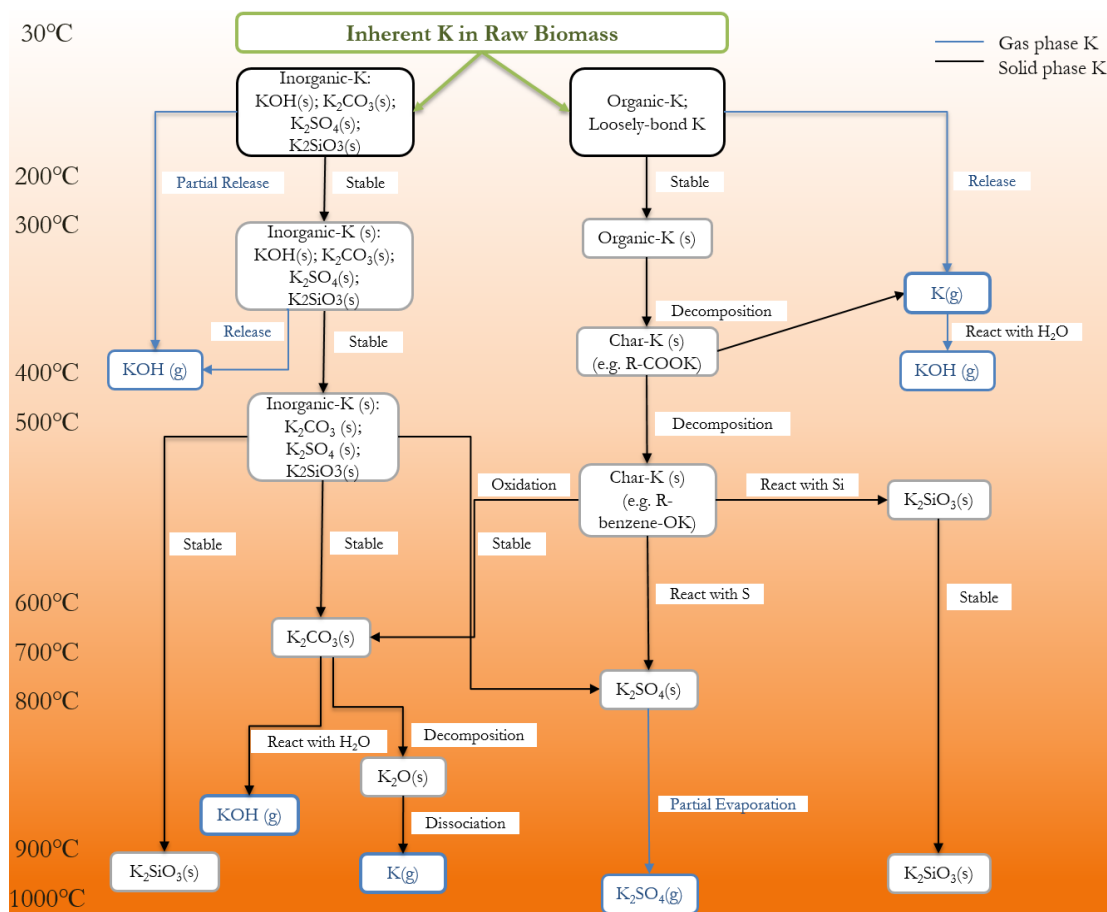


Figure 5.2. Temperature-dependent transition route of K during combustion  
(Integrated with the conclusions from [2, 4, 13, 18])

As indicated in the figure, when the final temperature is below 800°C, the release of loosely bounded K and organic-K mainly in the form of KOH, and this dominates the loss of K from the wheat straw. However, the minor loss of the total K indicates that at low-medium temperatures, the dominating behaviour is the transformation of the occurrence modes of K: (1) capture of released K compounds by Si-matrix, which caused by the change of particle structures and further exposure of inside located K; (2) the transformation from organic-K to char-K inside the solid residues; (3) the oxidization and sulfation of char-K to form the thermally stable salts like  $K_2CO_3$  and  $K_2SO_4$ . The transformation of particles from a rigid and porous structure to collapsed and small rough particles significantly affect the transition pathway of K within this period. When the final temperature is higher than 800°C, the abundant decomposition and evaporation of K compounds (like  $K_2CO_3$  and  $K_2SO_4$ ) dominate the release of K, while the reactions between Si and the captured K to form thermally stable K silicate [3, 24] prevent the

further loss of K. Moreover, the further breakdown and collapse of the ash structure and its fusion phenomenon demonstrate the significant influence that Si has on the retention of K during the combustion process since the fusion area is rich in K and Si.

#### 5.4 Influence of heating rate on K transition

As reviewed in Chapter 2, the heating rate has been known as a key factor that affects the biomass thermal conversion and could thus influence the transition behaviour of K. In addition, according to the discussion in 5.3, the final temperature has significantly affected the transition of K during the combustion process. So in this part, five typical final temperatures (300°C, 400°C, 600°C, 900°C and 1000°C) representing the different temperature ranges are selected to investigate the influence of heating rate on the transition performance of K during the combustion process.

##### 5.4.1 Test results

The uncertainties of the results are summarized in Table 5.4. As indicated in the results, the acquired uncertainties are all under 0.5%, indicating the results of the experiments in this part are in low variation and highly reliable.

Table 5.4. Calculated uncertainties of the K concentration measurements at different heating rates

Temperature, °C	Heating Rate, °C/min	$\delta R_k$ , %	Temperature, °C	Heating Rate, °C/min	$\delta R_k$ , %
300	8	0.41	400	8	0.39
	17	0.26		17	0.24
	25	0.35		25	0.39
600	8	0.39	900	8	0.33
	17	0.24		17	0.21
	25	0.38		25	0.33
1000	8	0.15			
	17	0.13			
	25	0.13			

The change of K concentrations in the residues according to the change of heating rate at different temperatures are summarized in Figure 5.3. The results show the similar trends of the results under the three different heating rates, the K concentration in the solid residues, however, are different. For the heating rate of 8°C/min and 17°C/min, the K concentration in the residues under the same final temperature is close to each other. At 300°C, there is 78% of the initial K left in the solid residues when the heating rate is 8°C/min, while it is 75% when the heating rate is 17°C/min, and as the temperature

increased, K concentration decreased mildly for both heating rates. When the temperature reaches 1000°C, K concentration in the solid residue drops to 46% and 42% of its initial mass for the heating rate of 8°C/min and 17°C/min, respectively. The difference of K concentration between these two heating rates is small (<5%) for all the tested temperatures.

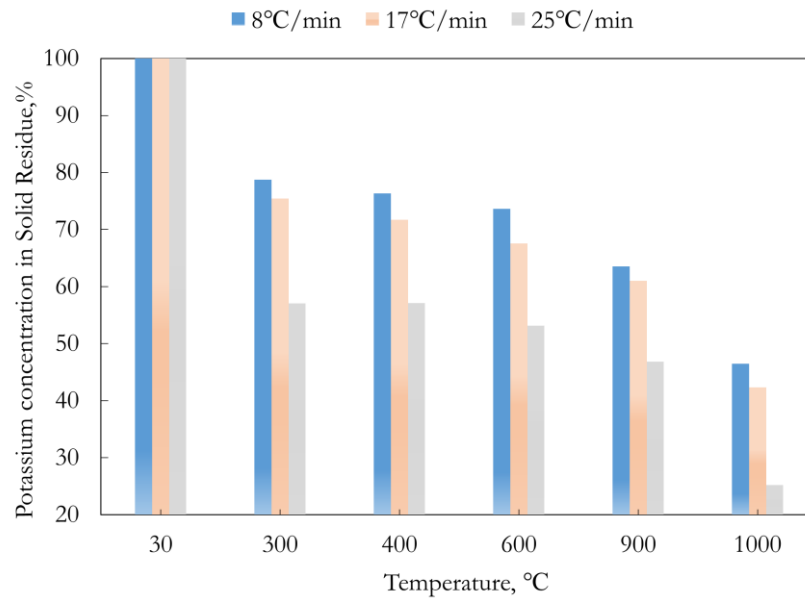
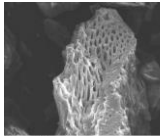
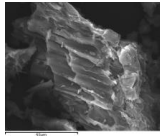
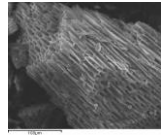
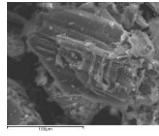
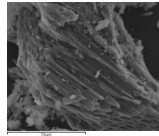
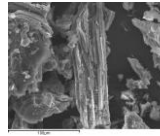
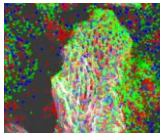
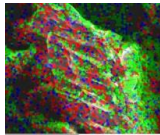
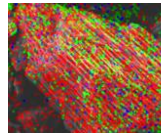
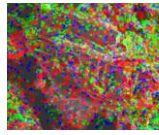
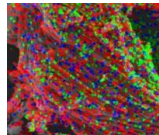
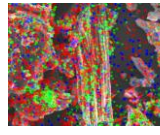
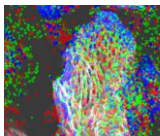
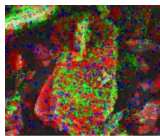
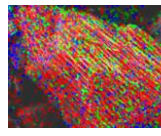
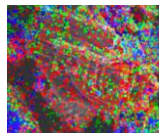
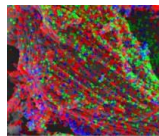
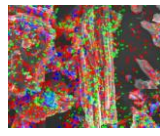
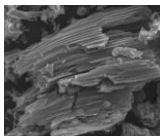
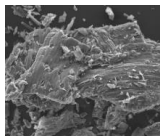
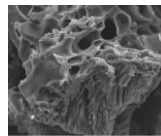
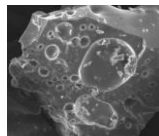
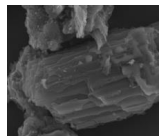
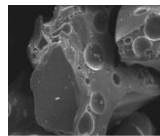
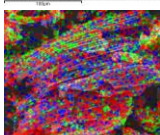
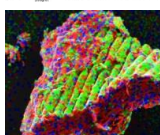
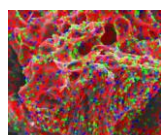
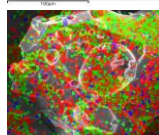
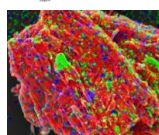
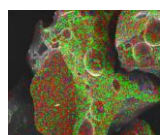
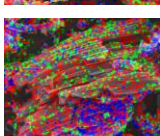
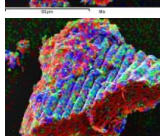
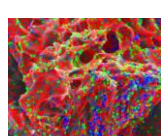
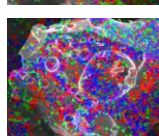
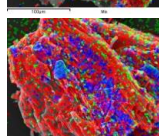
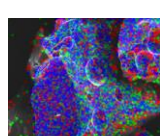


Figure 5.3 The change of K concentration (dry basis) with the change of heating rate

Nevertheless, when the heating rate increases to 25°C/min, the obtained K concentration in the solid residues is much less than that of 8°C/min and 17°C/min at the same temperature. At 300°C, there is only 57% of the initial K left in the solid residues, while this value steeply decreased to 25% at 1000°C. It also can be observed in Figure 5.3 that under the same final temperature, the differences between the K concentration in the solid residues under these three heating rates are consistent, with a 5% difference between the results of the heating rate of 8°C/min and 17°C/min, and the difference between the results of the heating rate of 17°C/min and 25°C/min is 20%.

Table 5.5. Summary of the SEM-EDX results at different heating rates

Temperature, °C	400			600		
Heating rate, °C/min	8	17	25	8	17	25
SEM						
EDX (Red: K; Green: O; Blue: S)						
EDX (Red: K; Green: O; Blue: Si)						
Temperature, °C	900			1000		
Heating rate, °C/min	8	17	25	8	17	25
SEM						
EDX (Red: K; Green: O; Blue: S)						
EDX (Red: K; Green: O; Blue: Si)						

The morphology and EDX (K, O, S and Si) distribution results under the different heating rates are summarised in Table 5.5. As illustrated in the SEM results, at low temperature (400°C), the increasing of heating rate has insignificant influence on the particle structures, the stem-like structure is easily identified but with minor slits, and the particle shape is mainly maintained with slightly break down. When the final temperature reaches 600°C, with the raising of heating rate, the channel structure still can be easily identified; however, the breakdown of particles becomes more detectible, and more fragments can be observed. At higher temperature like 900°C, the influence of heating rate on the change of particle structures becomes significant. As we can see, at the heating rate of 8°C/min, the overall fibrous structure is maintained, and the pore structure is recognizable. While at the heating rate of 17°C/min, apart from the further breakdown and collapse of the

pore structure, the particle was partially fused; whereas at the high heating rate ( $25^{\circ}\text{C}/\text{min}$ ), the natural porosity becomes less visible, instead, large cavities appear, and more melted surfaces can be observed. At  $1000^{\circ}\text{C}$ , the morphology results of solid residues of the three heating rates show the similar trends: there is no visible stem-like structure, the particles covered with large fused surfaces; the high heating rate resulting in the more plastic deformation of particles (i.e. melting), leading to the smooth surfaces and large cavities. Same morphology results of biomass combustion are observed by Cetin et al. [27] and Guerrero et al. [28] as well.

The EDX results show that, at lower temperatures like  $400^{\circ}\text{C}$  and  $600^{\circ}\text{C}$ , the higher the heating rate, the more K can be detected, and K is more likely to locate inside the pore structures as well. S is less detectable at low heating rates but can be observed when heating rate increase to  $25^{\circ}\text{C}/\text{min}$ . Si can be detected at the outer surface of the particles. For the observed results under three heating rates, when the final temperature reaches  $900^{\circ}\text{C}$ , K is the most detectable element on the particle surfaces in all the tests; while at  $1000^{\circ}\text{C}$ , the large melting surface on the particles is mainly constituted by the K and Si. Besides, at the high final temperature, the higher the heating rate, the less the detectable K-S clusters

#### 5.4.2 Analysis and discussion

As summarized above, the difference of the retained K concentration in solid residues is small between the heating rate of  $8^{\circ}\text{C}/\text{min}$  and  $17^{\circ}\text{C}/\text{min}$ , but at the heating rate of  $25^{\circ}\text{C}/\text{min}$ , the left K concentration in the residue is much less than that of the heating rate of  $8^{\circ}\text{C}/\text{min}$  and  $17^{\circ}\text{C}/\text{min}$ .

Devolatilisation is the initial step of the thermal conversion process, during which, thermal cut of the chemical bonds in virgin polymers causes the formation of light products and activated intermediates [29]. According to the studies [30-32], the high heating rate can enhance the probability of simultaneous bond breaking, leading to the release of volatile matters in a larger amount. The conversion rates of the tested samples under the different heating rates are summarised in Figure 5.4, as illustrated, high heating rate results in the high conversion rates of the samples during the combustion process, similar results are also observed by Fushimi et al. [33].

At a given final temperature, the high heating rate implies that the sample can be heated to the target temperature in a shorter time [34], energy could be provided more rapidly, this could accelerate the molecular motions and trigger the decomposition reactions, then affect the conversion rate of biomass samples and leads to the different kinetic parameters [35]. According to [29, 36, 37], a low heating rate can result in a high value of apparent activation energy of the biomass decomposition, but a high heating rate can lead to a low value of apparent activation energy. As aforementioned in 5.3.2, the release of K starts with the release of loosely bonded K and organic-K, they might be associated with the volatile matters, which are mainly devolatilised during the devolatilisation stage. This explains the release of more volatile matters can promote the release of K.

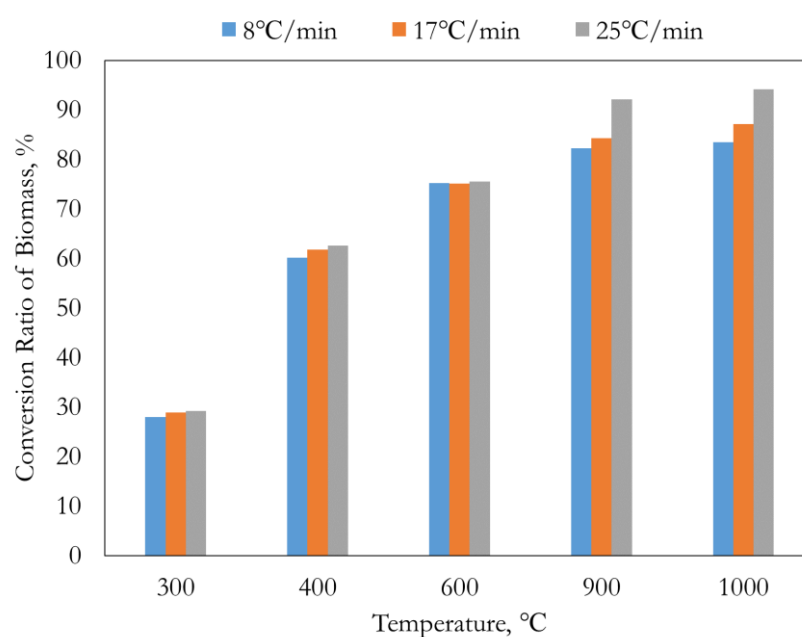


Figure 5.4 The change of the conversion ratio of the samples with the change of heating rate

However, as we can see, the high heating rate has much more influence on the release of total K content than that of volatile matters. In fact, after the devolatilisation, the volatile matter related K are almost devolatilised. The further dissociations of organically and inorganically bonded K and generating free K/K<sup>+</sup> within the particles might attribute to the more release of K. Especially the break of low bond dissociation energies (BDEs) required K bonds (i.e. organic-K and K<sup>+</sup>/K-X bonds). When the energy is sufficient, the high BDEs required K bonds would start to break as well.

Normally, the activation energies of biomass decomposition are within the range of 1-180 kJ/mol [38], which means, the BDEs of K bonds that lower than 180 kJ/mol can also be broken alongside the biomass decomposition when sufficient energy is provided. The energies required to break the bonds between K and other compounds that potentially exist inside the biomass particles are summarised Table 5.6. As indicated in the table, the BDEs of  $K^+$ -X bonds are relatively small and all below 180 kJ/mol, implying the preference of dissociation of  $K^+$ -X bonds during the decomposition process. Also, as reported in the reference [39], the BDEs of organic-K are all within 100 kJ/mol, similar to that of  $K^+$ -X bonds, which can be easily broken during the biomass decomposition process. Besides, the high heating rate can suppress the surface diffusion [40]; thus, the dissociated  $K^+$ /K from the organic-K and  $K^+$ -X can leave the particle surface more quickly. The high heating rate results in a quicker and higher degree of devolatilisation [41], which means  $H_2O$  and  $HCl$  would be released in higher concentrations and rate than that of low heating rate. Then the free gaseous  $K^+$  would be more likely to react with these gas species and to generate stable gaseous K compounds (i.e.  $KOH$  and  $KCl$ ).

Table 5.6. BDEs of K related bonds

The K bonds	BDEs, kJ/mol	The K bonds	BDEs, kJ/mol
K-H	183.4	$K^+$ -O	17.5
K-Cl	433.0	$K^+$ -KCl	172
K-O	276.1	$K^+$ -CO	19
K-OH	359.0	$K^+$ -CO <sub>2</sub>	35.6
(KO)-H	521.7	$K^+$ -KOH	159.0
(KOH)-KOH	190.0	$K^+$ -(KOH) <sub>2</sub>	126.0
K-H <sub>2</sub> O	24.1	$K^+$ -H <sub>2</sub> O	70.7
K-NH <sub>3</sub>	31.2	$K^+$ -K <sub>2</sub> SO <sub>4</sub>	159.0
K-K	57.0	$K^+$ -(CH <sub>3</sub> OH)-H <sub>2</sub> O	65.2
$K^+$ -K	85.7	$K^+$ -C <sub>2</sub> H <sub>5</sub> C(O)OH	87
$K^+$ -Cl	26.9	$K^+$ -C <sub>6</sub> H <sub>5</sub> OH	83.7
$K^+$ -CH <sub>3</sub> OCH <sub>3</sub>	92.9		

\*BDEs are summarized from [39]

From the observation of morphology results in Table 5.5, the influence of heating rate on the change of particle structure at low-medium temperatures (400°C and 600°C) is less significant, and the particles suffered minor breakdown and pore collapse. However, at

high temperatures (900°C and 1000°C), with the increasing of heating rate, the particle structures have suffered substantial changes. In fact, the high heating rate could cause a fast release of volatile matter and lead to a thinner wall of particles [28]; with the internal overpressure and coalescence of the small pores, the large cavities and open structure appear more frequently than that of low heating rate. The open structures could expose more inside located K, and with the decomposition and evaporation of K compounds, results in the less retention of K in the solid residues. Besides, the high heating rate could increase the char activities at higher temperatures [42], as it can lower the amount of deposit of pyrolytic carbon which retards the reactivity and generating a carbon matrix with defective microcrystallites, and this could provide a higher concentration of active site [43]. The phenomenon mentioned above would accelerate the decomposition and conversion of char-K and to form more inorganic K compounds (i.e. KOH, K<sub>2</sub>CO<sub>3</sub> and K<sub>2</sub>SO<sub>4</sub>) and could be released at high temperatures [44]. As indicated in Table 5.5, at high final temperature like 900°C and 1000°C, the higher the heating rate, the less the detectable K-S clusters also proves that more K<sub>2</sub>SO<sub>4</sub> could be released, which is one of the main K compounds that been released at high temperatures. Moreover, the declined heating rate could cause more secondary reactions as it enables an extended residence time of the volatiles in the particles [41], while the high heating rate can inhibit the secondary reactions after the devolatilisation process [45]. The shorter stay and less secondary reactions could also lead to a more escape of K content during the combustion process of biomass.

#### 5.4.3 Summary of findings

The heating rate has a great influence on the transition of K content during the combustion process. In this study, at any given temperature, increasing the heating rate from 8°C/min to 25°C/min would result in 20% more loss of the initial K concentration after combustion. During low-medium temperature range, heating rate affects the K release by decreasing the apparent activation energies of biomass decompositions and release more volatile matters related K, as well as the break of low BDEs required K bonds; the released K could react with H<sub>2</sub>O and HCl to generate more KOH and KCl. While at high temperatures, the heating rate influences the release of K by significantly changing the particle structures, like the shrink and collapse of porosity structures and generating large cavities, expose and release more inside located K. Besides, the high

heating rate can suppress the surface diffusion and secondary reactions, but enhance the activities of char. These could also result in the more release of K during the combustion process.

## 5.5 Summary of the chapter

This chapter aims to understand the effects of operating factors (final temperature and heating rate) on the transition performance of K during the combustion process of wheat straw. The experimental studies were performed in a custom-designed FBS, the collected solid residues were analysed by ICP-OES and SEM-EDX techniques, and a general conclusion can be summarised as:

- Final Temperature

Through the investigation of testing ranged from 200°C – 1000°C, the final temperature has significantly affected the transition performance of K during the biomass combustion, the higher the final temperature, the less the K that left in the solid residues. Three stages of K release can be observed as the final temperature increased: The first stage happens the release of loosely bonded K and partial organic K, which causes about 25% loss of the initial K. The second stage is likely to occur the transition of existence form of K, from thermally unstable compounds to thermally stable compounds like KOH and K<sub>2</sub>CO<sub>3</sub>, during which, only 5% more of the initial K was released. While at the third stage, the abundant release of inorganic compounds is the main reason that causes the loss of K from biomass, and during which, nearly 30% more of the initial K was lost. It can also be concluded that the majority part of K exists inside the stem-like tunnel of the biomass particles. As the temperature increased, the breakdown and collapse of particle structure could accelerate the release of K since it can expose more inside located K content. In addition, the existence of Si could help to prevent the loss of K as the Si matrix can capture the K and generate more stable K-Si compounds that can stay as solid residues.

- Heating rate

Three heating rates (8°C/min, 17°C/min and 25°C/min) were selected to perform the experiments in this chapter. As a result, the heating rate also has a great influence on the transition performance of K during the wheat straw combustion, the higher the heating rate, the less the K that left in the solid residues. The difference between the K in the solid residues under the heating rate of 8°C/min and 17°C/min is within 5%, while this

value sharply increased to 25% between the results of heating rate of 8°C/min and 25°C/min. At low-medium temperatures, high heating rate affects the K release by influencing the molecular motions and accelerating the biomass decomposition, the release of volatile matters related K, as well as the breakdown of K<sup>+</sup>/K-X bonds, leading to the more release of K. At high temperatures, heating rate affects the particle structure to accelerate the K release, the higher the heating rate, the more coalescence of small pores to generate large cavities and more open structure, which exposed more inside located K, and thus, accelerates the decomposition and sublimation of K compounds.

## Bibliography

1. McKenna, G.B. and S.L. Simon, Handbook of thermal analysis and calorimetry. V, 2002. 3: p. 49-109.
2. Johansen, J.M., et al., Release of K, Cl, and S during pyrolysis and combustion of high-chlorine biomass. *Energy & Fuels*, 2011. 25(11): p. 4961-4971.
3. Knudsen, J.N., P.A. Jensen, and K. Dam-Johansen, Transformation and release to the gas phase of Cl, K, and S during combustion of annual biomass. *Energy & Fuels*, 2004. 18(5): p. 1385-1399.
4. Van Lith, S.C., et al., Release to the gas phase of inorganic elements during wood combustion. Part 1: development and evaluation of quantification methods. *Energy & Fuels*, 2006. 20(3): p. 964-978.
5. Van Lith, S.C., et al., Release to the gas phase of inorganic elements during wood combustion. Part 2: influence of fuel composition. *Energy & Fuels*, 2008. 22(3): p. 1598-1609.
6. Clery, D.S., et al., The effects of an additive on the release of potassium in biomass combustion. *Fuel*, 2018. 214: p. 647-655.
7. Saddawi, A., J. Jones, and A. Williams, Influence of alkali metals on the kinetics of the thermal decomposition of biomass. *Fuel Processing Technology*, 2012. 104: p. 189-197.
8. Yu, C. and W. Zhang, Modeling potassium release in biomass pyrolysis. *Progress in Thermochemical Biomass Conversion*, 2001: p. 1107-1115.
9. Jensen, P.A., et al., Experimental investigation of the transformation and release to gas phase of potassium and chlorine during straw pyrolysis. *Energy & Fuels*, 2000. 14(6): p. 1280-1285.
10. Akbar, S., U. Schnell, and G. Scheffknecht, Modelling potassium release and the effect of potassium chloride on deposition mechanisms for coal and biomass-fired boilers. *Combustion Theory and Modelling*, 2010. 14(3): p. 315-329.
11. Cao, W., J. Li, and L. Lue, Study on the ignition behavior and kinetics of combustion of biomass. *Energy Procedia*, 2017. 142: p. 136-141.
12. Reid, J., et al., A review of biomass burning emissions part II: intensive physical properties of biomass burning particles. *Atmospheric Chemistry and Physics*, 2005. 5(3): p. 799-825.

13. Zhao, H.-b., et al., Study on the transformation of inherent potassium during the fast-pyrolysis process of rice straw. *Energy & Fuels*, 2015. 29(10): p. 6404-6411.
14. Koppejan, J. and S. Van Loo, *The handbook of biomass combustion and co-firing*. 2012: Routledge.
15. Tchoffor, P.A., et al., Influence of fuel ash characteristics on the release of potassium, chlorine, and sulfur from biomass fuels under steam-fluidized bed gasification conditions. *Energy & Fuels*, 2016. 30(12): p. 10435-10442.
16. Idris, S.S., N.A. Rahman, and K. Ismail, Combustion characteristics of Malaysian oil palm biomass, sub-bituminous coal and their respective blends via thermogravimetric analysis (TGA). *Bioresource Technology*, 2012. 123: p. 581-591.
17. Cao, W., et al., Prediction of potassium compounds released from biomass during combustion. *Applied Energy*, 2019. 250: p. 1696-1705.
18. Fatehi, H., et al., LIBS measurements and numerical studies of potassium release during biomass gasification. *Proceedings of the Combustion Institute*, 2015. 35(2): p. 2389-2396.
19. Dayton, D., et al., Release of inorganic constituents from leached biomass during thermal conversion. *Energy & Fuels*, 1999. 13(4): p. 860-870.
20. Olsson, J.G., et al., Alkali metal emission during pyrolysis of biomass. *Energy & Fuels*, 1997. 11(4): p. 779-784.
21. Mafu, L.D., et al., Chemical and structural characterization of char development during lignocellulosic biomass pyrolysis. *Bioresource Technology*, 2017. 243: p. 941-948.
22. Sander, B., et al. Emissions, corrosion and alkali chemistry in straw-fired combined heat and power plants. in *1st World Conference and Exhibition on Biomass for Energy and Industry*. 2000.
23. Baxter, L.L., et al., The behavior of inorganic material in biomass-fired power boilers: field and laboratory experiences. *Fuel Processing Technology*, 1998. 54(1-3): p. 47-78.
24. Zhang, Z.-H., et al., Influence of the atmosphere on the transformation of alkali and alkaline earth metallic species during rice straw thermal conversion. *Energy & Fuels*, 2012. 26(3): p. 1892-1899.

25. Vassilev, S.V., D. Baxter, and C.G. Vassileva, An overview of the behaviour of biomass during combustion: Part II. Ash fusion and ash formation mechanisms of biomass types. *Fuel*, 2014. 117: p. 152-183.
26. Bostrom, D., et al., Ash transformation chemistry during combustion of biomass. *Energy & Fuels*, 2011. 26(1): p. 85-93.
27. Cetin, E., R. Gupta, and B. Moghtaderi, Effect of pyrolysis pressure and heating rate on radiata pine char structure and apparent gasification reactivity. *Fuel*, 2005. 84(10): p. 1328-1334.
28. Guerrero, M., et al., Pyrolysis of eucalyptus at different heating rates: studies of char characterization and oxidative reactivity. *Journal of Analytical and Applied Pyrolysis*, 2005. 74(1-2): p. 307-314.
29. Biagini, E., A. Fantei, and L. Tognotti, Effect of the heating rate on the devolatilization of biomass residues. *Thermochimica Acta*, 2008. 472(1-2): p. 55-63.
30. Li, C.-Z. and P.F. Nelson, Fate of aromatic ring systems during thermal cracking of tars in a fluidized-bed reactor. *Energy & Fuels*, 1996. 10(5): p. 1083-1090.
31. Sathe, C., Y. Pang, and C.-Z. Li, Effects of heating rate and ion-exchangeable cations on the pyrolysis yields from a Victorian brown coal. *Energy & Fuels*, 1999. 13(3): p. 748-755.
32. Kershaw, J.R., et al., Fluorescence spectroscopic analysis of tars from the pyrolysis of a Victorian brown coal in a wire-mesh reactor. *Energy & Fuels*, 2000. 14(2): p. 476-482.
33. Fushimi, C., et al., Effect of heating rate on steam gasification of biomass. 1. Reactivity of char. *Industrial & Engineering Chemistry Research*, 2003. 42(17): p. 3922-3928.
34. Vamvuka, D. and S. Sfakiotakis, Combustion behaviour of biomass fuels and their blends with lignite. *Thermochimica Acta*, 2011. 526(1-2): p. 192-199.
35. Mehrabian, R., R. Scharler, and I. Obernberger, Effects of pyrolysis conditions on the heating rate in biomass particles and applicability of TGA kinetic parameters in particle thermal conversion modelling. *Fuel*, 2012. 93: p. 567-575.
36. Milosavljevic, I. and E.M. Suuberg, Cellulose thermal decomposition kinetics: global mass loss kinetics. *Industrial & Engineering Chemistry Research*, 1995. 34(4): p. 1081-1091.

37. Grønli, M., M.J. Antal, and G. Varhegyi, A round-robin study of cellulose pyrolysis kinetics by thermogravimetry. *Industrial & Engineering Chemistry Research*, 1999. 38(6): p. 2238-2244.
38. Garcia-Maraver, A., et al., Determination and comparison of combustion kinetics parameters of agricultural biomass from olive trees. *Renewable Energy*, 2015. 83: p. 897-904.
39. Luo, Y.-R., *Comprehensive handbook of chemical bond energies*. 2007: CRC Press.
40. German, R., *Sintering: from empirical observations to scientific principles*. 2014: Butterworth-Heinemann.
41. Mermoud, F., et al., Influence of the pyrolysis heating rate on the steam gasification rate of large wood char particles. *Fuel*, 2006. 85(10-11): p. 1473-1482.
42. Zygourakis, K., Effects of pyrolysis conditions on the macropore structure of coal chars. *Prepr. Pap., Am. Chem. Soc., Div. Fuel Chem.;*(United States), 1988. 33(CONF-8809228-).
43. Kumar, M. and R.C. Gupta, Influence of carbonization conditions on the gasification of acacia and eucalyptus wood chars by carbon dioxide. *Fuel*, 1994. 73(12): p. 1922-1925.
44. Cao, W., et al., Experimental study on the influences of operating parameters on the retention of potassium during the biomass combustion. *Energy Procedia*, 2019. 158: p. 1033-1038.
45. Basu, P., *Biomass gasification and pyrolysis: practical design and theory*. 2010: Academic Press.

## CHAPTER 6

# PREDICTION OF THE RELEASE OF POTASSIUM COMPOUNDS DURING BIOMASS COMBUSTION

---

This chapter describes the results produced using a two-step kinetic model. In the beginning, the chapter describes the model setup, validation. Then the estimated results are presented in two parts: the predicted results of release profiles of K compounds and the reaction paths among different K compounds.

### 6.1 Background

As indicated in the results of the experimental study in Chapter 5, the final temperature has greatly affected the transition performance of K, with the final temperature increased from 200°C to 1000°C, over 60% of the total K has been released. However, the existing experimental methods can only allow the determination of the overall released amount of K during the combustion process; they are unable to determine the release profiles of different K compounds. To obtain such information, a two-step kinetic model has been developed in this study, which consists of the biomass devolatilisation process and the reaction of gas species in the combustion environment. Therefore, the change of reaction temperature on the change of release profiles of K compounds during the combustion process will be investigated, in order to acquire the detailed information on the release of different K compounds, as well as a better understanding of the reaction mechanism of K compounds at different temperatures.

### 6.2 Model setup

Wheat straw has been selected as the biomass material due to its high concentration of K content [1]. The major chemical compositions of wheat straw and the calculated initial input values are summarised in Table 6.1.

At the devolatilisation stage, biomass was heated at a heating rate of 20°C/min until reached a designed final temperature that is ranged from 327°C-1127°C, with a 100°C interval. Once the devolatilisation stage was completed, the homogeneous combustion in the gas phase will take place at each final temperature with a residence time of 10 min. Then the release profiles and the reaction path of different K compounds will be obtained.

Table 6.1 Characteristics of wheat straw and initial input values

	Biomass							Oxidizer
	Cellulose <sup>db</sup>	Hemicellulose <sup>db</sup>	Lignin <sup>db</sup>	H <sub>2</sub> O <sup>ar</sup>	K <sup>db</sup>	S <sup>db</sup>	Cl <sup>db</sup>	O <sub>2</sub>
Fraction, wt%	48.27	31.60	20.12	9.00	1.20	0.17	0.27	-
Initial inputs, mol/g biomass	$2.8 \times 10^{-3}$	$2.3 \times 10^{-3}$	$9.2 \times 10^{-4}$	$5.0 \times 10^{-3}$	$3.1 \times 10^{-4}$	$5.3 \times 10^{-5}$	$7.6 \times 10^{-5}$	$3.58 \times 10^{-2}$

\* *db* = dry basis; *ar* = as received

### 6.3 Validation of the model

The model has been validated in two parts: firstly, the validation of the yielded products from the devolatilisation part; secondly, the validation of the yielded K compounds from the combustion part.

Figure 6.1 compares the devolatilisation results between the experiment and modelling. As we can see, with the increasing of final temperature, the yields of gas products are increased, the solid products, however, are decreased. This trend agrees well with our experimental data illustrating that the mixtures of cellulose, hemicellulose and lignin could be used to represent the thermal decomposition properties of biomass materials [2], and the results from the test are summarised in Figure 6.1 as well.

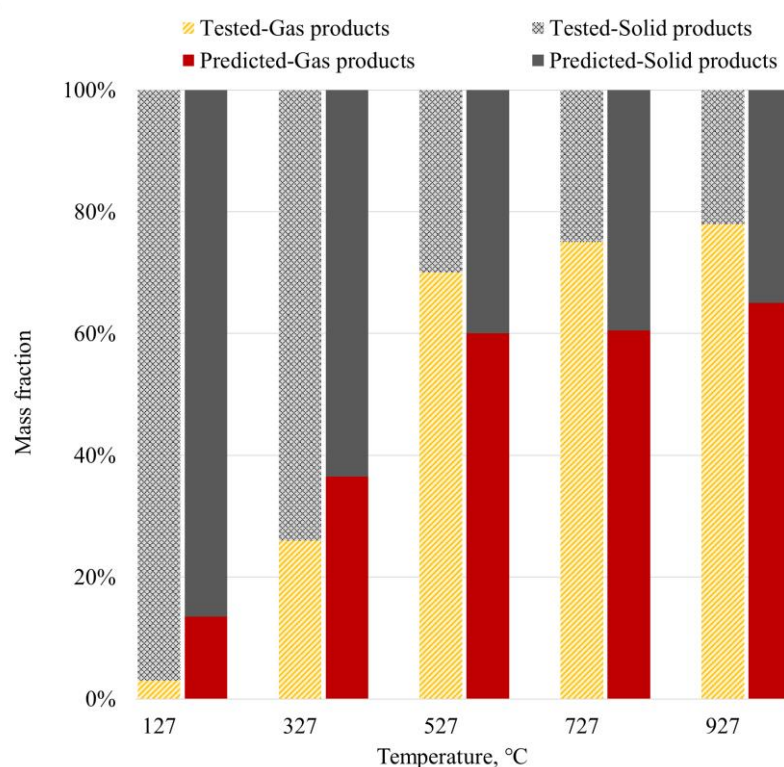


Figure 6.1 Distribution of yielded products after devolatilisation

Also as illustrated in Figure 6.1, at 127°C, the predicted yield of gas products is less than 20% of the initial amount of biomass, while this value raises to 30% and 60% at a temperature of 327°C and 527°C, respectively. With the temperature further increases, the predicted yield of the gas products remains nearly constant, and a similar trend can be observed from the test results too. When the temperature is lower than 527°C, the predicted amount of weight loss is higher than that of the measured results. At low temperature like 127°C, the evaporation of moisture content from the biomass dominates the weight loss; the moisture content of the biomass studied in the model is set as 9% as the received basis (see Table 3.1); however, the samples that used in the experiment are almost dried powder, resulting in the less loss of weight at low temperature. When the temperature is higher than 327°C, the model under-predicts the yield of gas products (mainly volatile matter), this is because of the tested samples are the mixture of high-purity compounds which contains negligible ash and mineral contents, but the model considered wheat straw with 5% of ash content and a certain amount of mineral species.

The prediction of the yielded major compounds (KCl and HCl) after the combustion is shown in Figure 6.2, and the yields are presented in the unit of mole/g biomass and compared with the work of Wei et al. [3]; in their study, FactSage is used to perform thermodynamic equilibrium analysis to determine the release of K compounds during biomass combustion.

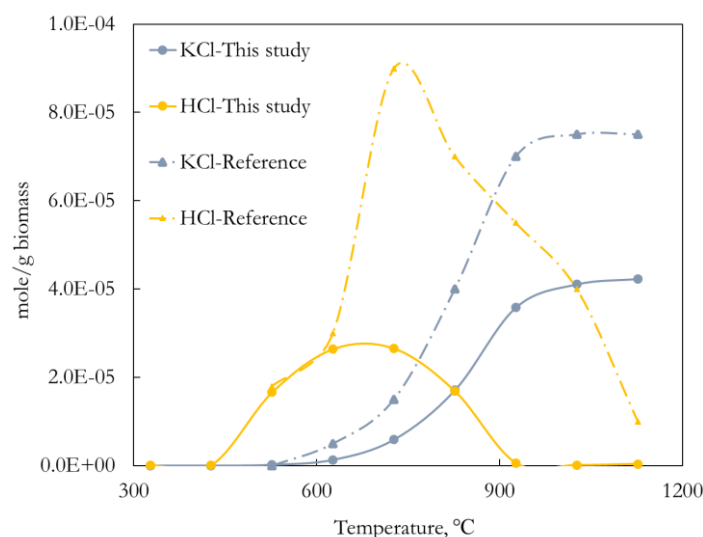


Figure 6.2 Comparison of results between this study (solid lines) and the Ref. [3] (dashed-dotted lines)

Notably, Figure 6.2 shows that the predicted amounts of the selected gas species from the reference are higher than the predicted results in this work. Firstly, the initial input values of K and Cl in the reference are higher than that in this study, as indicated in Table 6.2; a high chlorine content could contribute to the high yields of chloride, especially KCl and HCl. Secondly, Wei's method assumed a sufficient residence time to reach the equilibrium state, simplifying the importance of residence time. Thirdly, as mentioned before, major chemical components are used to represent biomass material in this model instead of the commonly used elemental composition, the different devolatilisation reaction mechanisms that used in the model could affect the products in the gas phase and the relevant reactions. Despite the above differences, the predicted results in this work show a good agreement with the referenced results: the release peaks of KCl and HCl all appear at 927°C and 727°C, respectively; the released amount of KCl becomes flat when the final temperature exceeds 927°C. It is worth to mention that no experimental data are existing with such detailed yields of various kinds of K compounds, while the similar trends against equilibrium modelling results illustrate that the predicted results from this model are reasonable.

Table 6.2 Initial Input of K and Cl (mol/ kg biomass)

	This work	Ref. [3]
K	307	329
Cl	76	132

## 6.4 Predicted results of the release of K compounds

### 6.4.1 The release profiles of K species

This model includes 13 possible K compounds that could be released as gas products during the combustion process: K, KO, KO<sub>2</sub>, KSO<sub>2</sub>, KSO<sub>3</sub>, KOH, KCl, KH, KSO<sub>3</sub>Cl, (KOH)<sub>2</sub>, (KCl)<sub>2</sub>, KHSO<sub>4</sub>, and K<sub>2</sub>SO<sub>4</sub>. However, not all of the mentioned K compounds are released or yielded in large fractions; instead, some of those may play significant roles as intermediate species during the reactions, either facilitating or inhibiting the conversion of K content into the major species and thus affect the release of K compounds [4]. Under this circumstance, the predicted results from the model are divided into two parts: the release profiles of major species and the release profiles of intermediate species.

### 6.4.1.1 Major species

According to the previous study [5-7], during the combustion process of biomass, K mainly released in the form of KCl, KOH and  $K_2SO_4$ . Besides, the existence of Cl species, like HCl, would promote the release of K content [8, 9]. The release profile of HCl is thus crucial to the release study of K. The released mole fractions of these major species with the increase of final temperature are shown in Figure 6.3.

As shown in Figure 6.3, the notable release of HCl starts first, at 427°C, and the fraction quickly reaches its peak at 727°C, with  $8.0 \times 10^{-4}$  %, and then the fraction starts to decline. When the final temperature exceeds 927°C, the release of HCl becomes negligible compared to the rest of the major species. The notable release of KCl starts at 527°C, and its release in large fraction begins at 627°C, followed by a steep increase to  $1.1 \times 10^{-3}$  % at 927°C. Then the increases of fraction slow down, and finally reach  $1.3 \times 10^{-3}$  % at 1127°C. While the release of KOH becomes notable when the final temperature exceeds 927°C, then the fraction sharply increased, and reaches its peak at 1027°C, with  $7.5 \times 10^{-4}$  %, and then starts to decline. However, the fraction of  $K_2SO_4$  is negligible compared to the rest of the major species when the temperature below 1027°C, but jumped to  $5.4 \times 10^{-4}$  % at 1127°C, yet still lower than that of KCl, with  $1.3 \times 10^{-4}$  %, but almost the same as that of KOH, with  $5.7 \times 10^{-4}$  %.

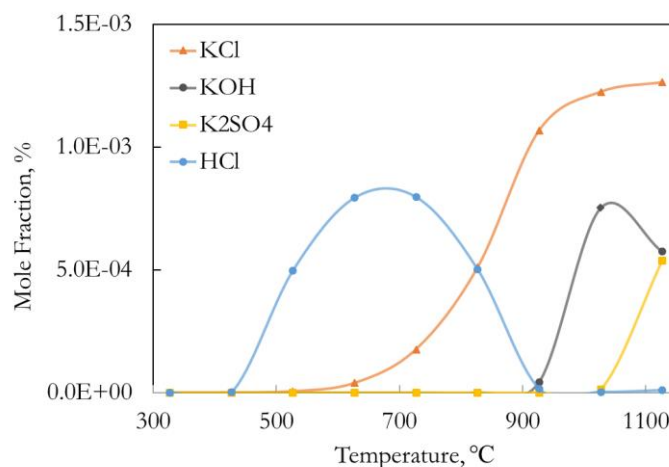


Figure 6.3 Release profiles of the major species

During the combustion process, Cl is usually released at low temperatures in the form of HCl [10], mainly from the ion-exchange reactions with suitable functional groups in the

organic matrix [11], which occupies 20-50% of the initial Cl content [11]. Nevertheless, the dominant Cl compounds found in biomass is in the form of KCl, which remains stable in the solid state until temperature reaches about 627°C-727°C [10, 12-15]. When the temperature exceeds this range, the sublimation of KCl becomes of a dominant path to the release of both K and Cl and remains as one of the major K compounds that released the most. The yield of KOH is negligible compared to the amount of KCl and HCl at temperatures below 927°C, due to the large amount of HCl, KOH is mainly converted to KCl via R6-1. This is also reflected by the large fraction of the released KCl, which means, apart from its sublimation, the major contributor of KCl in the gas phase is the consumption of KOH by HCl. When the temperature exceeds 927°C, the release of HCl is in small fraction compared to the rest of the major species and continuing to decline; KOH, however, starts to release abundantly without the consumption of HCl. Meanwhile, the fraction of released KCl becomes constant, due to the lack of HCl retards the R6-1. As for K<sub>2</sub>SO<sub>4</sub>, it is thermally stable at low-medium temperatures, and as final temperature increases to 1127°C, K<sub>2</sub>SO<sub>4</sub> will be evaporated and released gradually [16] from the biomass and becoming one of the major released species of K at high temperatures.

In summary, during the combustion, HCl would be released abundantly at low temperature. The dominate K compounds found in the gas phase is KCl, which represents more than half of the released K contents, and the release of KCl is mainly from its sublimation and through the R6-1. The release of KOH starts after the complete dechlorination, due to the reaction between K and water vapour which is governed by the thermal decomposition of carbonates [17]. K<sub>2</sub>SO<sub>4</sub> will not be released until a sufficiently high temperature is reached, and its release is dominated by evaporation [15, 16]. The predicted formation and release performance of these major species agreed well with that concluded from the experimental studies [15, 18-20].

#### 6.4.1.2 Intermediate species

During the devolatilisation process, loosely bonded K will be firstly released in the form of K<sup>+</sup>, which could react with other presenting organic and inorganic species [10, 21-23]; in addition, the inherent inorganic K could also interact with other components during the thermal conversion process. These could involve important intermediate products, which affect the release rate and type of K compounds. As the intermediate species might be thermally unstable and the reactions can take place within a very short time, it is,

therefore, difficult to get a detailed release profile and the yields of intermediate products. Thus, it makes this part valuable since it can provide information regarding the release of intermediate species. The amounts of selected important intermediate species as reported in the literature [24] and are summarised in Figure 6.4 (a-c), in which the changes of the total amounts of these species with the change of final temperature are demonstrated.

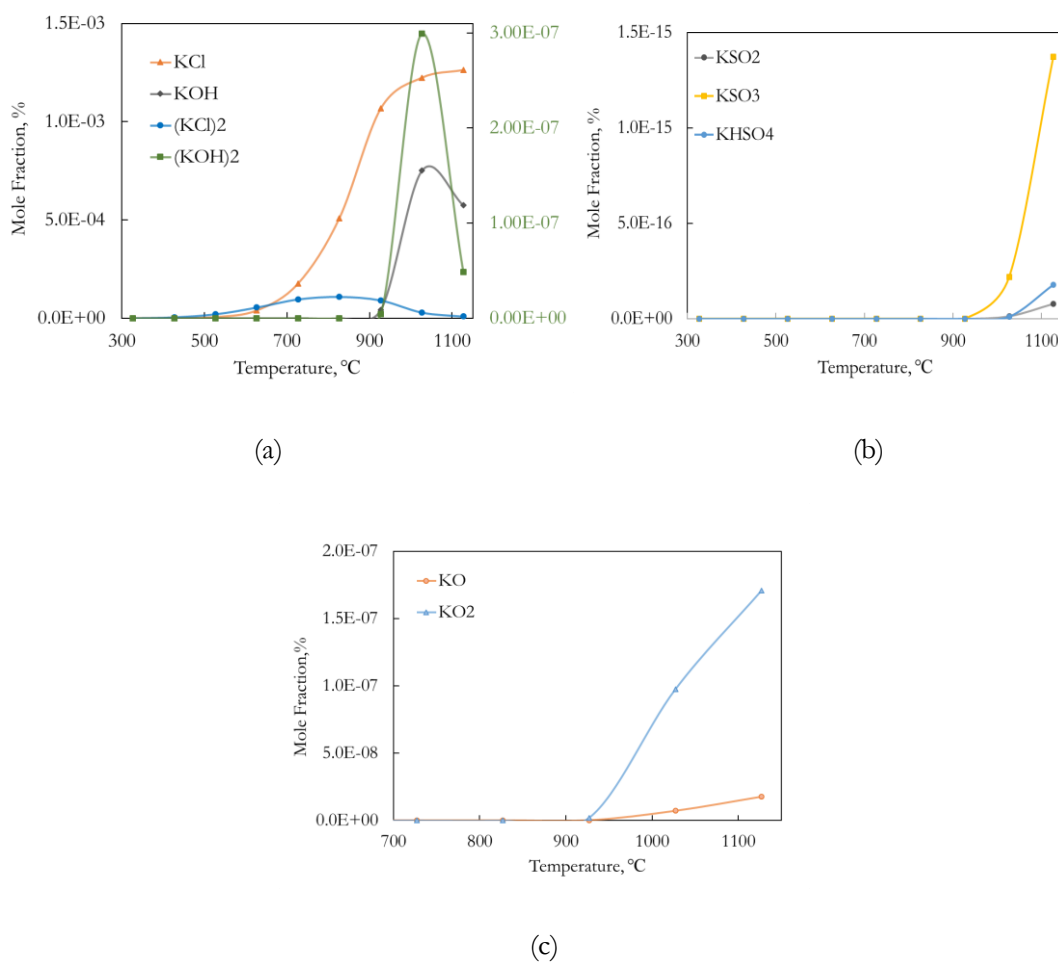


Figure 6.4 Release profiles of intermediate species

As indicated in Figure 6.4 (a), there are two intermediate K compounds released in large fractions during the combustion: (KCl)<sub>2</sub> and (KOH)<sub>2</sub>. At the final temperature below 627 °C, (KCl)<sub>2</sub> has a larger fraction than that of KCl. The result indicates that, when the temperature is relatively low, KCl is more likely to be bonded with each other to form (KCl)<sub>2</sub>, resulting in the release of K mainly in the form of (KCl)<sub>2</sub> at these temperatures. Then the fraction of (KCl)<sub>2</sub> reaches its peak at 827 °C with  $1.1 \times 10^{-4}$  %. With the final temperature further increases, the generated (KCl)<sub>2</sub> starts to dissociate to form KCl, and

along with the R6-1, boosts the fraction of KCl when the final temperature exceeds 827°C. As the final temperature exceeds 927°C, the fraction of (KCl)<sub>2</sub> starts to decline; meanwhile, the fraction of KCl becomes consistent.

During this period, the fraction of (KOH)<sub>2</sub> is negligible compared to the rest of the major and intermediate K compounds, as indicated in Figure 6.4 (a) (right Y-axis). However, the release of (KOH)<sub>2</sub> in noticeable fraction appears at the same time as the fraction of KOH becomes obvious; this reveals that KOH undergoes the same route as KCl does. At the initial stage of release, KOH tends to associate with each other to form (KOH)<sub>2</sub>; however, unlike (KCl)<sub>2</sub>, the formed (KOH)<sub>2</sub> is in a small amount and might be thermally stable at these temperatures. Nevertheless, due to the low concentration of KOH, the association rate of KOH to form (KOH)<sub>2</sub> might be much lower than the release rate of KOH, leading to the small fraction of (KOH)<sub>2</sub> in the gas products, which reaches its peak at the same temperature as KOH at 1027°C but with only  $3.0 \times 10^{-7}$  %.

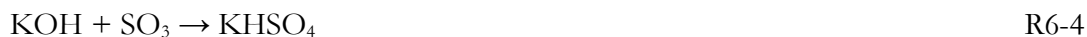
As discussed above, the formation of large fractions of (KCl)<sub>2</sub> and (KOH)<sub>2</sub> illustrate that the homogeneous reactions of the K compounds could occur during the devolatilisation and combustion process. Therefore, the release path of K chloride and hydrate species should follow the summarised reaction sequences:



The estimated result in Figure 6.4 (b) indicates that nearly no K-S compounds released at low temperatures, which however, starts to release when the final temperature exceeds 927°C. KSO<sub>3</sub> released in significant fraction after 927°C, and then sharply increases to  $1.4 \times 10^{-15}$  % at 1127°C, while the release of KSO<sub>2</sub> in noticeable amount appears after 1027°C, and the fraction reaches its peak at 1127°C, with only  $7.6 \times 10^{-17}$  %. As we can see, during the combustion process, both KSO<sub>2</sub> and KSO<sub>3</sub> are released in small fractions compared to the release of major species like KOH, KCl and K<sub>2</sub>SO<sub>4</sub>. This result indicates that KSO<sub>2</sub> and KSO<sub>3</sub> are more likely to react with other species to form stable species (e.g., K<sub>2</sub>SO<sub>4</sub>) through the reactions R6-2 and R6-3. KHSO<sub>4</sub> starts to release in noticeable fraction at 1027°C and reaches to its peak at 1127°C with  $1.8 \times 10^{-16}$  %. Apart from the direct release of KHSO<sub>4</sub> at high temperature, the reaction that follows the R6-4 might be another reason that causes the sharp increase of the release of KHSO<sub>4</sub>. This is also

reflected by the results in Figure 6.3 when the final temperature exceeds 1027°C, the fraction of KOH starts to decline.

The release profiles of KO and KO<sub>2</sub> are illustrated in Figure 6.4 (c), which fractions are negligible when the final temperature is lower than 927°C. Nevertheless, the fraction of KO<sub>2</sub> is always higher than that of KO, especially when the final temperature beyond 927°C, the difference of the fraction between KO and KO<sub>2</sub> becomes enormous. Both KO and KO<sub>2</sub> reach their peaks at 1127°C, with 1.8×10<sup>-8</sup> % and 1.7×10<sup>-7</sup> %, respectively. During the combustion process, when the concentration of oxygen is sufficient, K likely to convert to KO<sub>2</sub> firstly via the R6-5 and further react with excess oxygen to generate KO via the R6-6. At low temperature, KO could also react with SO<sub>2</sub>, H<sub>2</sub>O and HCl to generate KSO<sub>3</sub>, KOH and KCl, following the R6-7-R6-9. However, as the final temperature increases, the decreasing of the fraction of SO<sub>2</sub>, H<sub>2</sub>O and HCl could slow the depletion of KO, which in turn, results in the release of KO in a relatively higher fraction.



### 6.4.1.3 Summary of the release profiles of K

Through the above discussion, a generalized reaction path of K during combustion is summarised in Figure 6.5 to indicate the potential routes of K after being released. Indeed, the reaction path is varying with the change of final temperature. Figure 6.5 shows that the intermediate species (as presented in blue colour) are thoroughly involved in the K transition and play a crucial role to generate the major K compounds: KOH, KCl and  $K_2SO_4$  (as presented in black colour), however, the intermediate species are all released in minor fractions as presented and discussed in the previous part. This suggests that the generation of detrimental K compounds (e.g. KCl, KOH and  $K_2SO_4$ ) might be mitigated if a suitable method could be developed to alter the formation of intermediate species. As the intermediate products have not been detected experimentally [24], it is of great interest to obtain the information regarding the intermediate species from this model to guide the design of future experiments.

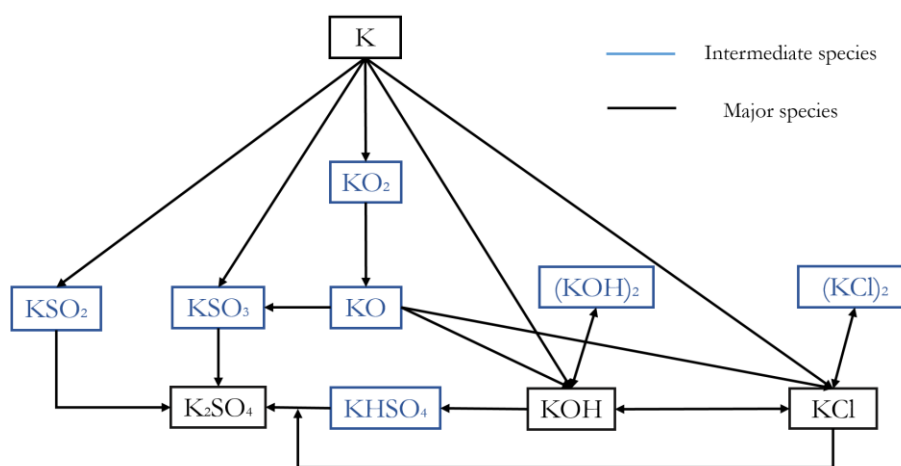


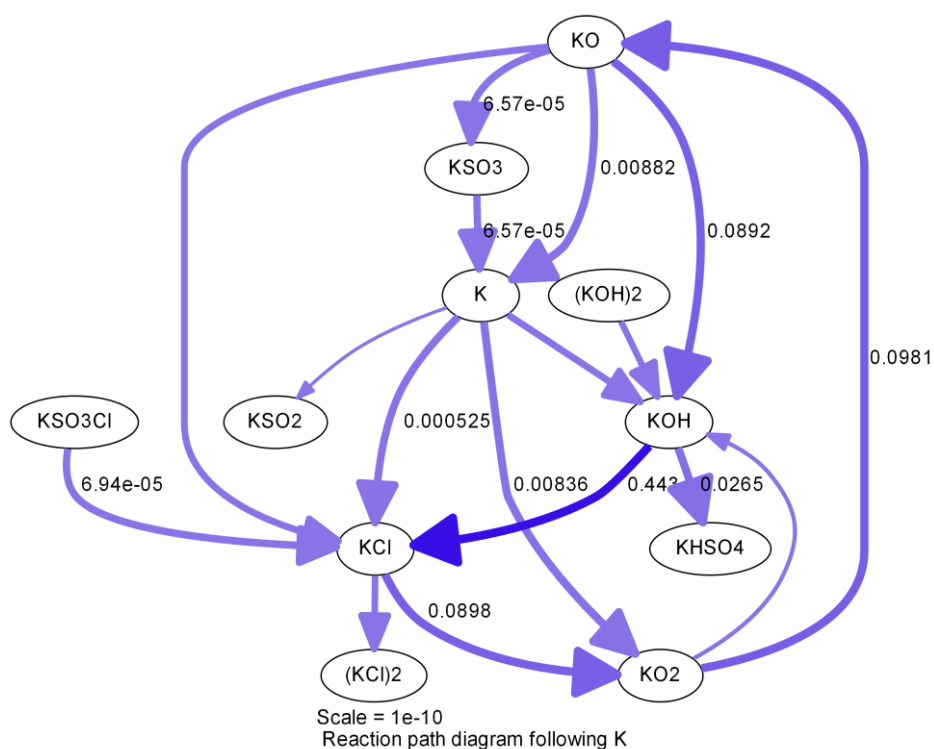
Figure 6.5 Generalized reaction path of K

### 6.4.2 The reaction paths of K species

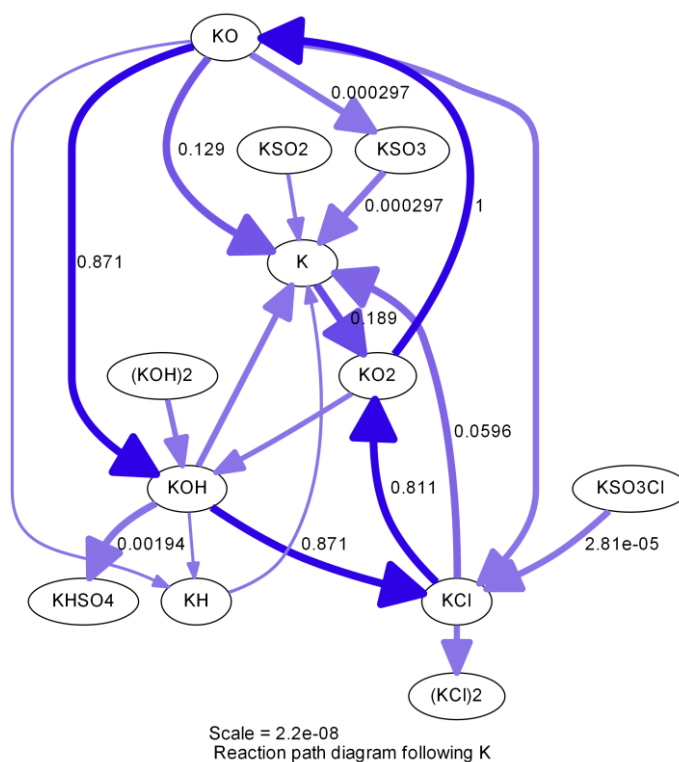
According to the different final temperatures, the results of detailed reaction path followed by K are presented according to low ( $327^{\circ}\text{C}$ - $527^{\circ}\text{C}$ ), medium ( $627^{\circ}\text{C}$ - $827^{\circ}\text{C}$ ) and high ( $927^{\circ}\text{C}$ - $1127^{\circ}\text{C}$ ) temperature ranges. Figure 6.6-6.8 illustrate the transition of K among different compounds during the combustion process at different ranges of temperature. It is worth noting that the values on the arrows in the graphs are the rates at which species are formed from other species,  $\text{kmol}/\text{m}^3\text{ s}$ , the larger the value, the higher the formation rate of the targeted species. While the shade of the arrow represents the occupation of the reaction among the overall reaction rate.

### 6.4.2.1 Low temperature range (327°C-527°C)

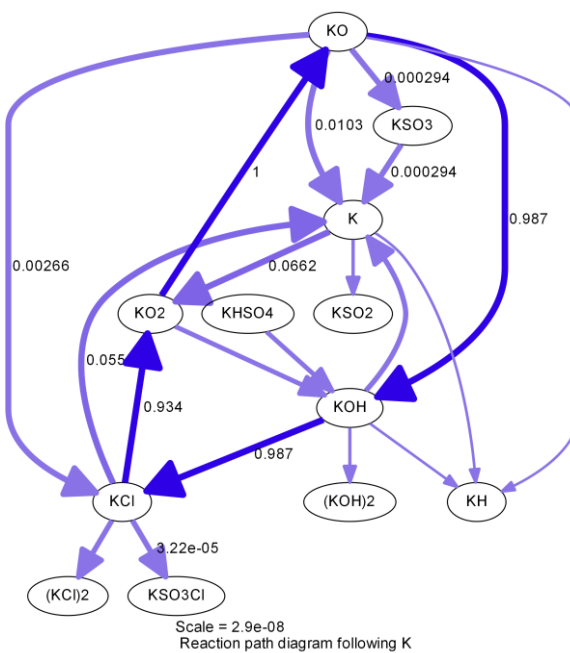
As been discussed before, at low temperatures, there is only a limited amount of K been released, which mainly comes from the loosely-bonded and organically-associated K. As illustrated in Figure 6.6, at 327°C, the reaction between KCl and KOH is the only major transition, while the transitions of the other K compounds all occurred at low rates. At 427°C, apart from the major transition route from KOH to KCl, the intermediates species KO and KO<sub>2</sub> and their transitions to KOH and KCl start to become more significant. The same result can also be observed at 527°C but with even higher reaction rates; since the increasing of temperature results in the more release of gas species and K that involved in the reactions.



327°C



427°C



527°C

Figure 6.6 Reaction path diagrams of K in the low temperature range (the value on the arrows in represents the rates at which species are formed from other species,  $\text{kmol/m}^3 \text{s}$ )

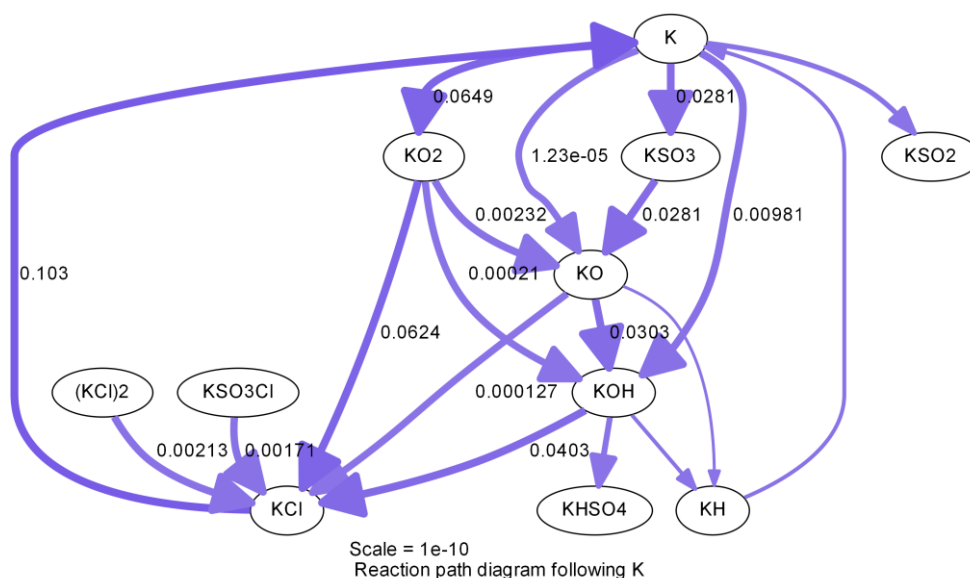
Figure 6.6 also shows that, as the final temperature raised, the rest of the K compounds and their transition rates are negligible compared to the transition among KOH, KCl, KO and KO<sub>2</sub>. As aforementioned, HCl starts to release at low temperatures (around 427°C), which causes the depletion of KOH to form KCl following the R6-1. Moreover, as the final temperature increased, more loosely bonded K and organically associated K are dissociated and then released, which can be either oxidized or reacted with other hydroxide compounds and to form intermediate species, such as KO and KO<sub>2</sub>. Then, these phenomena could accelerate the transition among KOH, KCl, KO and KO<sub>2</sub>, which are all reflected by the high rates on the arrows. Besides, as shown in Figure 6.6, the release of (KCl)<sub>2</sub> start to appear with high rate at 527°C and gradually become one of the major released K compounds. This agrees well with the results presented in Figure 6.4 (a), (KCl)<sub>2</sub> is the main released K compounds when the temperature below 527°C, followed by the KCl. However, (KOH)<sub>2</sub> only has a negligible reaction rate within this temperature range. Moreover, no K<sub>2</sub>SO<sub>4</sub> can be observed in the reaction paths in Figure 6.6, instead, the transition routes from other K compounds to KHSO<sub>4</sub>, KSO<sub>2</sub> and KSO<sub>3</sub> are noticeable, but all in low reaction rates. This reveals that the formation of K-S species may start at the early stage of the combustion, but the transition and release of stable K-S compounds (i.e. K<sub>2</sub>SO<sub>4</sub>) are favoured by the high final temperatures. As discussed before, at this temperature range, there almost no inorganic K is released; therefore, the reaction path in Figure 6.6 mainly reveals the potential transition routes of K after it dissociates from the loosely connected bond and organic matrix.

#### 6.4.2.2 Medium temperature range (627°C-827°C)

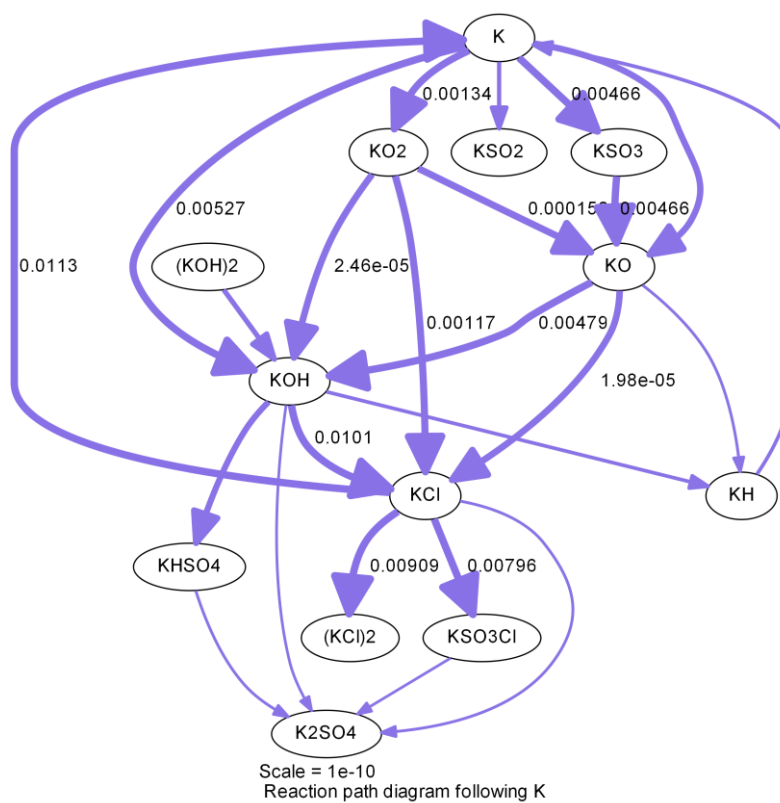
Figure 6.7 shows the reaction paths of K in the medium temperature range. The transition routes become more complicated with the increasing of the final temperature. Additional transfer paths are involved during the combustion process compare to the results of the low temperature range. Among all the transition routes, KCl and KOH are still the final products of most of the reactions within the pathways. Within this temperature range, the depletion of KOH to form KCl is still one of the major reactions, due to the existence of a large amount of HCl during this temperature range, this is also reflected by its high reaction rate.

As the final temperature further increases, conversions of other K compounds to KCl are increased, such as from KO and KO<sub>2</sub> to KCl through the reaction with HCl. Besides, the

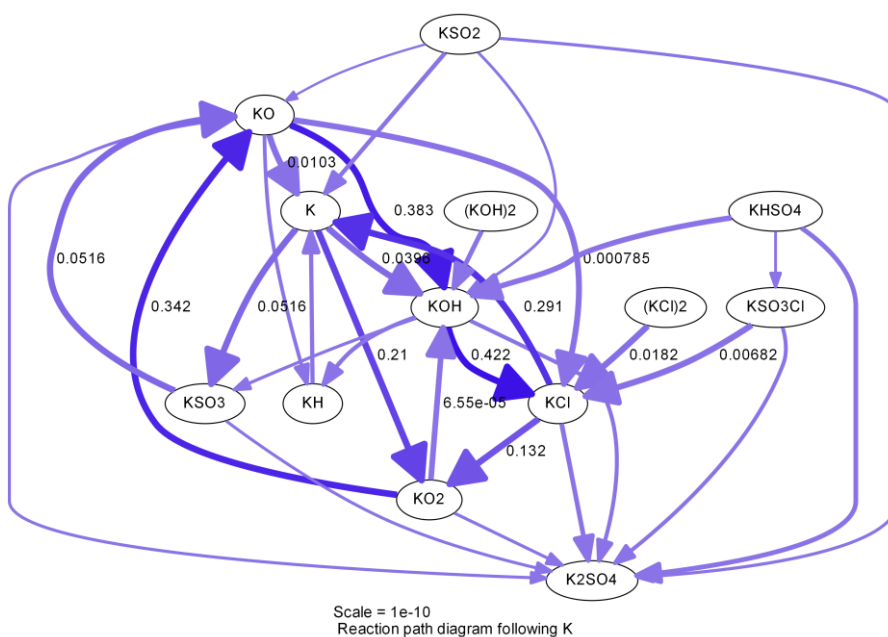
formation of KOH would also involve more species, e.g., KO, KO<sub>2</sub> and KHSO<sub>4</sub> that could react with H<sub>2</sub>O, which is generated from the decomposition of carbonates at high temperatures. However, due to the abundant existence of HCl within this temperature range, the KOH related reactions are all in low rates. When the final temperature reaches 827°C, the rates of all the transition reactions are accelerated quickly, among which the transition sequence KO → KOH → KCl is the major reaction route of K, leading to the release of KCl in large fraction, this can also be observed in the results presented in Figure 6.3. Although the release of HCl starts to decrease at temperatures beyond 727°C, as illustrated in the results summarised in Figure 6.3, however, still in large fraction. This causes the high reaction rate of KOH → KCl and allows it to be one of the main reaction routes at the medium temperature range. Meanwhile, (KCl)<sub>2</sub> gets more involved in the reaction of KCl within the medium temperature range, while the reaction rate of (KOH)<sub>2</sub> is still negligible compared to the rest of the K compounds.



627°C



727°C



827°C

Figure 6.7 Reaction path diagrams of K in the medium temperature range (the value on the arrows in represents the rates at which species are formed from other species, kmol/m<sup>3</sup> s)

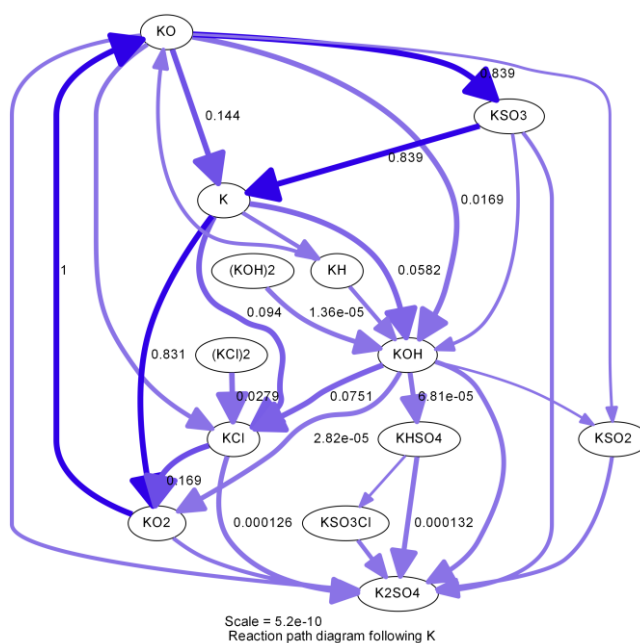
As shown in Figure 6.7, within the medium temperature range, more K-S compounds start to involve in the reactions with other K compounds. At 727°C, the transitions of other K compounds to  $K_2SO_4$  start to occur, and  $K_2SO_4$  becomes the terminal of most of the transition routes at 827°C. However, all the reactions towards  $K_2SO_4$  are in very low reaction rates, indicating the contributions of other K compounds to  $K_2SO_4$  content are small during the combustion at this temperature range. Since  $K_2SO_4$  is thermally stable at these temperatures, most of the released K is still in the form of KCl.

#### 6.4.2.3 High temperature range (927°C-1127°C)

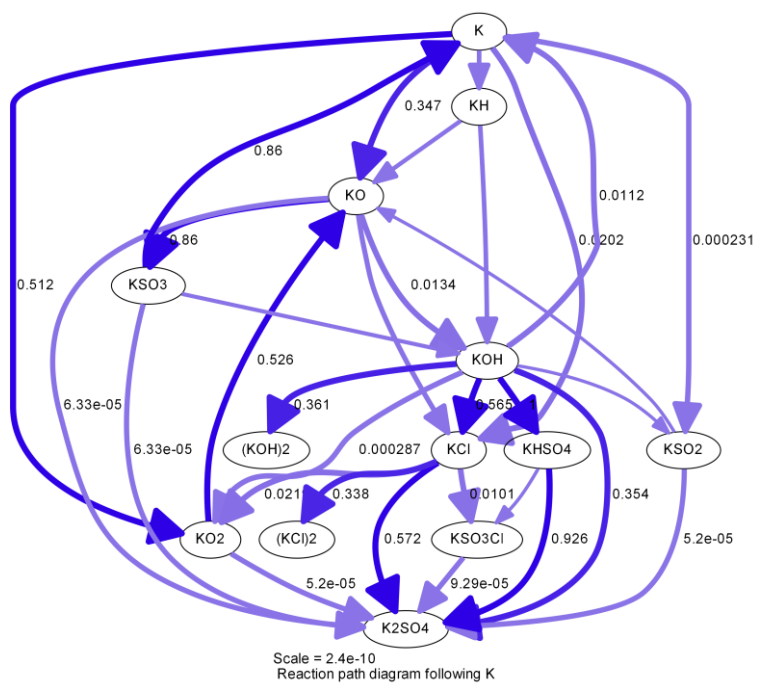
The reaction paths of K at the high temperature range are illustrated in Figure 6.8. The rate of formation of KCl is slowing down, and meanwhile, due to the depletion of HCl, more KOH starts to form as well as the conversion between KOH and  $(KOH)_2$ . Within this temperature range,  $KSO_3Cl$  becomes more involved in the reaction with KCl, while  $KHSO_4$  is the major species involved in the reaction with KOH. However, the formation rate of KO from  $KO_2$  sharply decreased from 1.0 kmol/m<sup>3</sup>s at 927°C to  $2.2 \times 10^{-4}$  kmol/m<sup>3</sup>s at 1127°C. As indicated in Figure 6.5, the decrease of  $KO_2$  content would directly affect the formation of KO, and thus reduce the formation of KCl, KOH and  $KSO_3$ , which could decrease the formation of  $K_2SO_4$ . Nevertheless, at high temperatures, nearly all Cl and H<sub>2</sub>O contents are released [8], meaning the reaction paths of  $K + Cl/Cl_2 \rightarrow KCl$  and  $K + H_2O \rightarrow KOH$  are no longer critical at high temperatures, this indicates that the formation of KCl and KOH are mainly via the intermediate species, like KO,  $(KCl)_2$ ,  $(KOH)_2$ ,  $KHSO_4$  and  $KSO_3Cl$ . This reveals that the decline of the formation of KO is one of the crucial factors that triggers the decrease of the release of KCl and KOH as temperature increased, alongside the consumption of  $(KCl)_2$  and  $(KOH)_2$  contents. Nevertheless, as presented in Figure 6.8, the total consumption rates of KCl and KOH are slower than their formation rates, which means KCl and KOH are still the major K compounds that released at the high temperature range.

Within high temperature range,  $K_2SO_4$  is the final product of most of the reaction pathways, including the transition from KCl and KOH to  $K_2SO_4$  via the possible reactions of R6-10 and R6-11.  $KSO_3$ ,  $KSO_3Cl$  and  $KHSO_4$  are the most important intermediate species that are involved in the transitions, and they are chemically stable in the gas phase at this temperature range [18], which makes them detectable as gas species. As discussed before, there is a steep increase of the release of  $K_2SO_4$  at 1027°C; however, as shown in

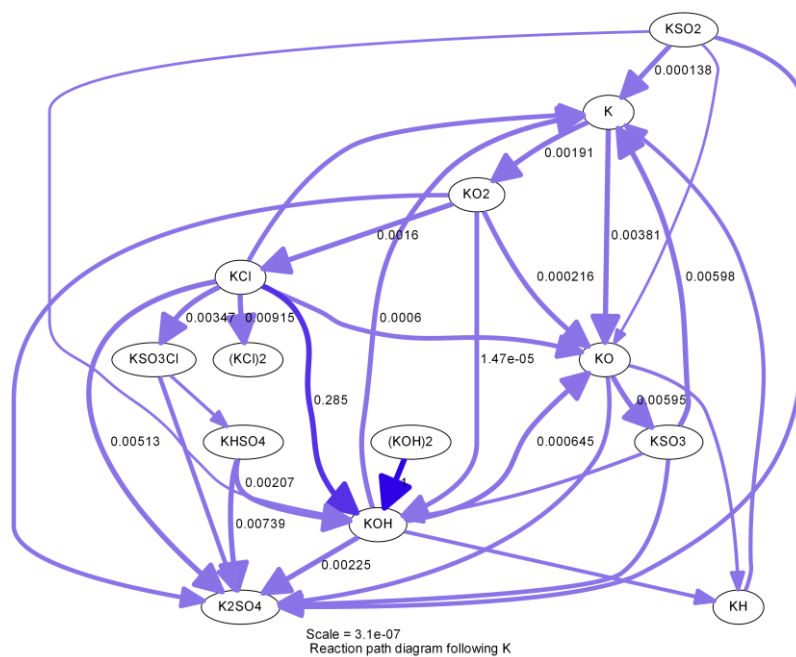
Figure 6.8, the reaction rates that toward  $K_2SO_4$  are all negligible compared to those of  $KCl$  and  $KOH$ , even though  $K_2SO_4$  is the final product of most of the potassium species. This illustrates that the release of  $K_2SO_4$  at high temperature is mainly contributed by the inherent  $K_2SO_4$  content in biomass and the ones that generated at the early stage of the combustion which in the solid form. While the transitions of other gaseous K compounds to  $K_2SO_4$  are too small to trigger the leap of the release of  $K_2SO_4$  content at high temperature range. The result also reveals that the release of  $K_2SO_4$  is less dependent on intermediate potassium species during the combustion process. It is reported that there is a two-step release mechanism of S determined during the combustion process of biomass [15]. The first step happens during the devolatilisation stage, when the organically-associated S content is released, which makes up about 50 wt% of the total S in the biomass; the second step occurs at the char-burnout stage, during which, the inorganic S content is mainly released, including the evaporation of  $K_2SO_4$  content [15]. The released S content at the devolatilisation stage is mainly in the form of oxide, like  $SO_2$  and  $SO_3$  [7] and then could be recaptured and happen the secondary reactions with char matrix. This process could facilitate the formation of  $K_2SO_4$  in the solid residues, which remains stable until the temperature is high enough for its evaporation. This again proves the previous discussion that partial of the released  $K_2SO_4$  content at high temperature comes from the reactions of sulphide at the early stage of the combustion.



927°C



1027°C



1127°C

Figure 6.8 Reaction path diagrams of K in the high temperature range (the value on the arrows in represents the rates at which species are formed from other species,  $\text{kmol/m}^3 \text{ s}$ )

#### 6.4.2.4 Summary of the reaction path

As indicated in Figure 6.6-6.8,  $(\text{KCl})_2$  and  $(\text{KOH})_2$  can only be formed from and disassociated to KCl and KOH, respectively. This reveals that during the combustion process, the way to generate and deplete  $(\text{KCl})_2$  and  $(\text{KOH})_2$  contents is only via the homogenous reaction. Also, from the reaction pathways that demonstrated above, one major transition cycle can be identified from each temperature range according to the reaction rates. These cycles represent the transition routes that happened the most frequently at different ranges of temperature, which indicates the consumption and formation of each species that included in the cycles are with high reaction rates. The transition cycles of different temperature ranges are presented in Figure 6.9.

The result indicates that, with the increase of final temperature, KCl and KOH are gradually replaced by K and  $\text{KSO}_3$  in the major transition cycles. As demonstrated in results in Figure 6.3, the release of KOH and KCl contents become constant when the final temperature exceeds  $927^\circ\text{C}$ , meaning the transition rates of KOH and KCl are low, their depletion and formation are not changed a lot. The involvement of  $\text{KSO}_3$  as a major species in the cycle in Figure 6.9 (c) indicates that it has a high reaction rate at high temperature, which could facilities the formation of  $\text{K}_2\text{SO}_4$ . This suggests that the formation of  $\text{K}_2\text{SO}_4$  is favoured by the reaction of  $\text{KSO}_3$  content. However, since more  $\text{KSO}_3$  is involved in the major transition cycle, its contribution to the formation of  $\text{K}_2\text{SO}_4$  is less important. This means the quick release of  $\text{K}_2\text{SO}_4$  at high temperatures is not mainly contributed by the reaction of other K compounds, instead, relies more on its original concentration in biomass and the formation of intermediate K compounds at the early stage of combustion, as discussed before.

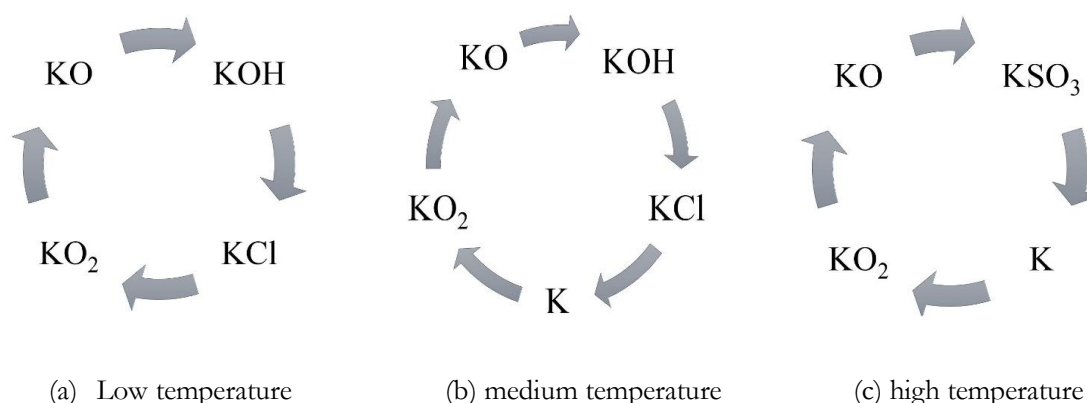


Figure 6.9 Major transition cycles of K in different temperature ranges

As we can see in Figure 6.9, KO and  $\text{KO}_2$  are the only two species that involved in the transition cycles in all temperature ranges, which are the main contributors to form the major K compounds (i.e. KOH, KCl and  $\text{K}_2\text{SO}_4$ ) in the gas phase during the combustion process as discussed in the previous part. As presented in the results in Figure 6.4, the release amount of KO and  $\text{KO}_2$  contents are all negligible compared to the major K compounds when the temperature is lower than  $927^\circ\text{C}$ . However, the large reaction rates of KO and  $\text{KO}_2$  related transitions in Figure 6.6-6.8 reveals that KO and  $\text{KO}_2$  are existed in large amounts, meaning that the initial released K content mainly exists in oxidised forms, and they are more likely to react with other components to generate chemically stable K compounds and been released afterwards. As a result, appropriate control of the reactions of KO and  $\text{KO}_2$  during the combustion process could be helpful to prevent the generation of the major K compounds.

### 6.5 Summary of the chapter

This chapter presented the prediction of the release profiles of K compounds and their reaction paths at different final temperatures using the developed two-step kinetically controlled model.

The results showed that by giving the initial compositions, it is possible to use the model to predict the release profiles of K compounds during the combustion process of biomass. The modelling results demonstrate that KOH, KCl and  $\text{K}_2\text{SO}_4$  are the major K compounds to be released during the combustion. KOH is more likely to be generated during the K release process, which involves the reactions of intermediate K compounds. KOH and KCl are the main forms of released K compounds throughout the whole temperature range, while the released amount of  $\text{K}_2\text{SO}_4$  is negligible if the temperature is below  $1027^\circ\text{C}$ , but its release sharply increases to the same level of KOH at  $1127^\circ\text{C}$ . The reaction path diagrams show that when the final temperature below  $827^\circ\text{C}$ , KOH and KCl are the two final products of most of the transitions.  $\text{K}_2\text{SO}_4$  is the final product of the majority of the transitions when the final temperature is in the range of  $827^\circ\text{C}$ - $1127^\circ\text{C}$ , but all in low transition rates. The reactions that involve the intermediate K compounds are more important to the release of KOH in addition to the release of initial concentrations of KCl and KOH while the release of  $\text{K}_2\text{SO}_4$  is highly dependent on its initial concentration in the biomass and the reactions in the solid phase at the early stage of the combustion.

The higher the final temperature, the more complex the reaction paths of K can be acquired from the model. The intermediate K compounds are released in minor amounts as gas products when compared to those of KOH, KCl and  $K_2SO_4$ , and this illustrates that during the combustion process, the intermediate species are shortly existed in the reaction system and then quickly converted to other major species. Only several of them are thermally stable and detectable in the reaction system.  $(KCl)_2$  is a key intermediate species; it represents most of the gas phase K when the final temperature is below  $727^\circ\text{C}$ . KO and  $KO_2$  are two most important intermediate species during the transition of K throughout the whole temperature range and significantly affect the conversions of KOH and KCl.  $KSO_3Cl$  and  $KHSO_4$  could participate in the transitions during the combustion process and finally converted to  $K_2SO_4$ .

## Bibliography

1. Sommersacher, P., et al., Application of novel and advanced fuel characterization tools for the combustion related characterization of different wood/kaolin and straw/kaolin mixtures. *Energy & Fuels*, 2013. 27(9): p. 5192-5206.
2. Cao, W., et al., Experimental study on the ignition characteristics of cellulose, hemicellulose, lignin and their mixtures. *Journal of the Energy Institute*, 2018.
3. Wei, X., U. Schnell, and K.R. Hein, Behaviour of gaseous chlorine and alkali metals during biomass thermal utilisation. *Fuel*, 2005. 84(7-8): p. 841-848.
4. Cao, W., et al., Prediction of potassium compounds released from biomass during combustion. *Applied Energy*, 2019. 250: p. 1696-1705.
5. Mason, P.E., et al., Observations on the release of gas-phase potassium during the combustion of single particles of biomass. *Fuel*, 2016. 182: p. 110-117.
6. Sommersacher, P., et al., Simultaneous Online Determination of S, Cl, K, Na, Zn, and Pb Release from a Single Particle during Biomass Combustion. Part 1: Experimental Setup–Implementation and Evaluation. *Energy & Fuels*, 2015. 29(10): p. 6734-6746.
7. Tchoffor, P.A., K.O. Davidsson, and H. Thunman, Transformation and release of potassium, chlorine, and sulfur from wheat straw under conditions relevant to dual fluidized bed gasification. *Energy & Fuels*, 2013. 27(12): p. 7510-7520.
8. Zhao, H.-b., et al., Study on the transformation of inherent potassium during the fast-pyrolysis process of rice straw. *Energy & Fuels*, 2015. 29(10): p. 6404-6411.
9. Zhang, Z.-H., et al., Influence of the atmosphere on the transformation of alkali and alkaline earth metallic species during rice straw thermal conversion. *Energy & Fuels*, 2012. 26(3): p. 1892-1899.
10. Jensen, P.A., et al., Experimental investigation of the transformation and release to gas phase of potassium and chlorine during straw pyrolysis. *Energy & Fuels*, 2000. 14(6): p. 1280-1285.
11. Björkman, E. and B. Strömberg, Release of chlorine from biomass at pyrolysis and gasification conditions<sup>1</sup>. *Energy & Fuels*, 1997. 11(5): p. 1026-1032.
12. Knudsen, J.N., Volatilization of inorganic matter during combustion of annual biomass. PhD thesis, Technical University of Denmark, Lyngby, Denmark, 2004. ISBN:87-91435-11-0.

13. Van Lith, S.C., Release of inorganic elements during wood-firing on a grate. 2005: Technical University of Denmark Lyngby, Denmark.
14. Knudsen, J.N., et al., Secondary capture of chlorine and sulfur during thermal conversion of biomass. *Energy & Fuels*, 2005. 19(2): p. 606-617.
15. Johansen, J.M., et al., Release of K, Cl, and S during pyrolysis and combustion of high-chlorine biomass. *Energy & Fuels*, 2011. 25(11): p. 4961-4971.
16. Van Lith, S.C., et al., Release to the gas phase of inorganic elements during wood combustion. Part 1: development and evaluation of quantification methods. *Energy & Fuels*, 2006. 20(3): p. 964-978.
17. Knudsen, J.N., P.A. Jensen, and K. Dam-Johansen, Transformation and release to the gas phase of Cl, K, and S during combustion of annual biomass. *Energy & Fuels*, 2004. 18(5): p. 1385-1399.
18. Van Lith, S.C., et al., Release to the gas phase of inorganic elements during wood combustion. Part 2: influence of fuel composition. *Energy & Fuels*, 2008. 22(3): p. 1598-1609.
19. Fatehi, H., et al., LIBS measurements and numerical studies of potassium release during biomass gasification. *Proceedings of the Combustion Institute*, 2015. 35(2): p. 2389-2396.
20. Sorvajärvi, T., et al., In situ measurement technique for simultaneous detection of K, KCl, and KOH vapors released during combustion of solid biomass fuel in a single particle reactor. *Applied Spectroscopy*, 2014. 68(2): p. 179-184.
21. Clery, D.S., et al., The effects of an additive on the release of potassium in biomass combustion. *Fuel*, 2018. 214: p. 647-655.
22. Saddawi, A., J. Jones, and A. Williams, Influence of alkali metals on the kinetics of the thermal decomposition of biomass. *Fuel Processing Technology*, 2012. 104: p. 189-197.
23. Akbar, S., U. Schnell, and G. Scheffknecht, Modelling potassium release and the effect of potassium chloride on deposition mechanisms for coal and biomass-fired boilers. *Combustion Theory and Modelling*, 2010. 14(3): p. 315-329.
24. Glarborg, P. and P. Marshall, Mechanism and modeling of the formation of gaseous alkali sulfates. *Combustion and Flame*, 2005. 141(1-2): p. 22-39.

## CHAPTER 7

# EFFECTS OF CHLORINE AND SULPHUR CONCENTRATIONS ON THE RELEASE OF POTASSIUM COMPOUNDS

---

This chapter presents and discusses the estimated results of the release of K compounds via the developed model, aiming to investigate the release profiles of K compounds with the change of concentrations of Cl and S. For each part, the work is presented according to two aspects, which are the change of release profiles of major species and the major transition cycle of K.

### 7.1 Background

In biomass, Cl is regarded as a crucial micronutrient for the growth of plants [1]; it is absorbed from the soil and present mainly as  $\text{Cl}^-$  in the plant. Cl normally exists in high concentration in biomass as its primary function is to maintain the pH level, regulate the osmotic pressure and stimulate enzyme activities [1-3]. Meanwhile, S is an essential macronutrient as its related proteins can also affect the growth of plants. It is also absorbed from the soil and present both in organic and inorganic forms in plants [4]. The absorbed S is typically in the form of sulphates and then transported upon reaching the leaves of the plant, during which, a gradual reduction takes place, leading to the incorporation of S into the organic structure of the plant [5]. The long migration of S results in a wide variety of S compounds in different oxidation states in plant [6]. Moreover, high growth rate biomass, like annual crops, need high production rates of proteins, and thereby require a high S concentration in the biomass [5].

During the combustion of biomass, elemental Cl and S are partially released to the gas phase, where they experience several chemical reactions and form aerosols [7]. The released Cl and S are also related to the formation of deposits in biomass boilers [8, 9] and are the leading cause of induced active corrosion during the combustion of biomass [10-12]. Apart from the alkali metals, Cl and S are the most critical aerosol-forming elements [13, 14]. Different research groups have studied the release mechanisms of Cl and S during the thermal conversion of biomass fuels intensively. The general release mechanisms are summarised below:

**The release mechanism of Cl.** According to Johansen et al. [15], HCl and KCl are the most abundant Cl-containing species released during the combustion of biomass. Normally, a two-step release of Cl can be observed: the release of organically associated Cl at low temperatures, and the sublimation of inorganic Cl at high temperatures [7, 16, 17]. At low temperatures ( $<300^{\circ}\text{C}$ ), about 20-50% of the initial Cl content is released [17]. Organically associated Cl content [18, 19] is usually released independently of K [15], and mainly in the form of  $\text{CH}_3\text{Cl}$  and HCl [20]. At temperatures of  $300^{\circ}\text{C}$ -  $700^{\circ}\text{C}$ , Cl is mainly released in the form of HCl and may be partially recaptured in the char via secondary reactions with available alkali metals to form KCl, then sublimated in abundant at temperatures above  $700^{\circ}\text{C}$  [21]. This recapture and re-release process could reduce the net release of HCl but facilitates the net release of KCl. The complete release of Cl content happens in combustion conditions where the final temperature exceeded  $800^{\circ}\text{C}$ . Clery et al. [22] reported that a high Cl content in the biomass could facilitate the release of KCl to the gas phase during the combustion process.

**The release mechanism of S.** Similar to the release of Cl, there is a two-step process for the release of S during combustion as well, which is the initial volatilisation of S that originates from organically bounded S, while inorganically bound S is released at high temperatures [15]. About 60-75% of the S contained in biomass is organically bound [23]. The major release of S happens during the devolatilisation of the biomass, mainly in the form of  $\text{SO}_2$ . The release of S at low temperatures ( $<500^{\circ}\text{C}$ ) composes up to 50% of the initial S content in the biomass. After release,  $\text{SO}_2$  can be partially recaptured and react with char matrix and other inorganic elements. Also, as stated by Glarborg et al. [24], the oxidation of  $\text{SO}_2$  to  $\text{SO}_3$  is the initial step of the KCl sulfation process, which controls the generation of  $\text{K}_2\text{SO}_4$ . Alongside the remaining inorganically bonded S that is retained in the solid, they are sublimated or/and dissociated at temperatures  $>900^{\circ}\text{C}$  [7, 16, 25], as well as the re-release of the recaptured S content at the early stage. Through the investigation, the complete release of S content is achieved at about  $1300^{\circ}\text{C}$  [15].

As shown in the above mechanisms, the release of Cl and S is normally associated with the release of K compounds during the biomass combustion process. However, due to the lack of direct detection methods of K compounds, the effects of the initial concentrations of Cl and S on the release profiles of different K compounds are still unclear. Knowing to what extent the different K compounds are released corresponding

to the initial concentrations of Cl and S can help us to better understand the release mechanisms of ash-forming elements. Also, this kind of knowledge is crucial to the selection and preparation of the biomass materials for the combustion and the optimization of the reaction process.

## 7.2 Model setup

The model setup was based on Chapter 6, the investigation on the influence of concentrations of Cl and S on the release of K compounds is achieved by adjusting the initial input value of Cl and S contents. In this study, six cases were considered, which refers to the scenarios of Cl-lean (case 1), Cl-normal (case 2), Cl-rich (case 3), S-lean (case 4), S-normal (case 5) and S-rich (case 6). The changes in Cl and S concentrations were the calculation based on the information in Table 6.1. The Cl and S concentrations that listed in Table 6.1 were regarded as their regular concentrations, while the concentration in Cl/S-lean situation was calculated as half of the normal Cl/S concentration and the concentration in Cl/S-rich scenario was calculated as double of the normal Cl/S concentration. The summarised initial inputs of Cl and S contents are presented in Table 7.1.

Table 7.1 Initial input values of Cl and S

Case	Cl			S		
	1	2	3	4	5	6
Initial inputs, mol/ g biomass	$3.8 \times 10^{-5}$	$7.6 \times 10^{-5}$	$1.5 \times 10^{-4}$	$2.7 \times 10^{-5}$	$5.3 \times 10^{-5}$	$1.1 \times 10^{-4}$

## 7.3 Effect of Cl concentration on the release of K compounds

### 7.3.1 Release profiles of major species

As investigated in Chapter 6, KCl, HCl, KOH and  $K_2SO_4$  are the major released species during the combustion process, while  $(KCl)_2$  and  $(KOH)_2$  are the important intermediate species and represent a majority part of gas-phase K at low-medium temperature range. In this section, the change of mole fractions of the above six species with the change of different initial inputs of Cl content according to the final temperature is summarised in Figure 7.1. As presented in Figure 7.1, the change of initial Cl content has a significant influence on the release mole fractions of the major species during the combustion process.

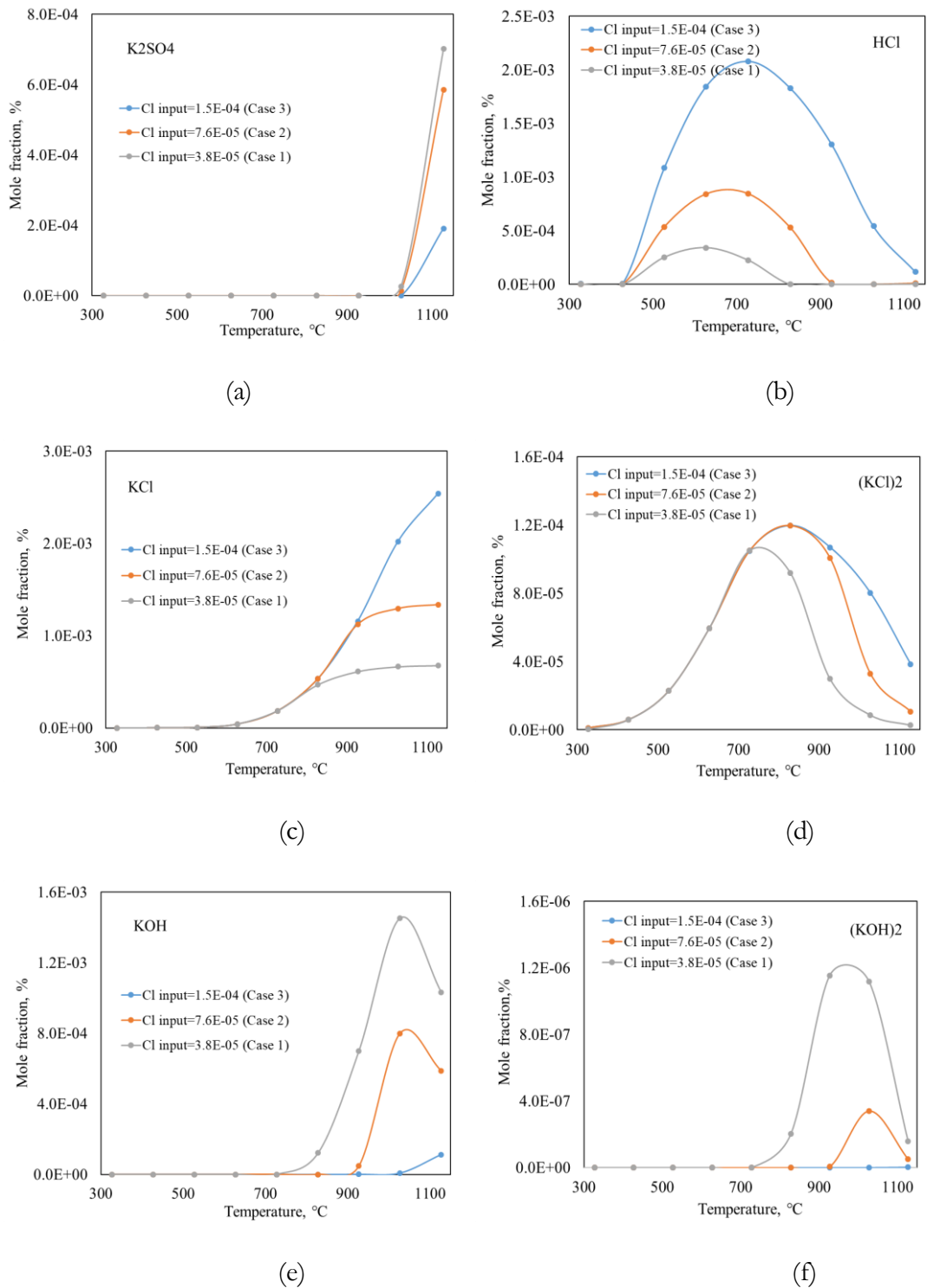


Figure 7.1. The changes of release profiles of the major species with the change of initial input of Cl

Figure 7.1 (a) illustrates the release profile of K<sub>2</sub>SO<sub>4</sub> under different conditions. As we can see, there is almost no release of K<sub>2</sub>SO<sub>4</sub> content before 1027 °C; thus, the influence of initial input of Cl content becomes negligible. However, when the final temperature

surpasses 1027°C, there is a sharp release of K<sub>2</sub>SO<sub>4</sub> content, and the lower the initial input of Cl content, the higher the release fraction of K<sub>2</sub>SO<sub>4</sub>. In case 1 and case 2, the release profile of K<sub>2</sub>SO<sub>4</sub> are similar to each other; they reached their highest released fraction at 1127°C, with 5.9×10<sup>-4</sup>% and 7.0×10<sup>-4</sup>%, respectively. The release of K<sub>2</sub>SO<sub>4</sub> also reached its highest fraction at 1127°C in case 3, but with only 1.9×10<sup>-4</sup>%. The release profile of K<sub>2</sub>SO<sub>4</sub> reveals that the high initial Cl content can inhibit the release of K<sub>2</sub>SO<sub>4</sub>, and the effect is more evident at high final temperatures. According to the reaction mechanism, KHSO<sub>4</sub> is an essential intermediate species to form K<sub>2</sub>SO<sub>4</sub> during the combustion process, and KHSO<sub>4</sub> can be generated from the reaction of SO<sub>3</sub> with KOH via R6-4 [24]. As illustrated in Figure 7.1 (e), the higher the initial Cl content, the lower the release fraction of KOH, especially in case 3, the release fraction of KOH is much less. This could lead to less formation of KHSO<sub>4</sub> and then causing the less formation of K<sub>2</sub>SO<sub>4</sub>, which is generated through the reaction R7-1 [24]. In addition, as the Cl content increases, more KCl will escape as gaseous products, which could also lead to a decrease in the generation of K<sub>2</sub>SO<sub>4</sub> species through the reaction R7-2 [24]. With the increase of initial Cl content, more K could be released in the form of KCl and (KCl)<sub>2</sub> at the early stage of combustion, as shown in Figure 7.1 (c) and (d). According to the study, the release of K<sub>2</sub>SO<sub>4</sub> is favoured by high temperature [7, 16, 26]; this means, at lower temperatures, the inherent K<sub>2</sub>SO<sub>4</sub> will stay stable, and the transition of K to K<sub>2</sub>SO<sub>4</sub> is more likely to occur during the combustion process, which will stay stable until the temperature is high enough to evaporate. Nevertheless, since more K is released in the form of KCl and (KCl)<sub>2</sub> under the scenario of high initial Cl input, there is less K left to transfer to K<sub>2</sub>SO<sub>4</sub>.

The release profile of HCl is indicated in Figure 7.1 (b). It starts to be released in a significant fraction at 427°C and reaches its peak before 727°C. Within the examined temperature range (327°C-1127°C), the higher the initial Cl content, the more release fraction of HCl, and the difference between the different scenarios is perceptible. In case 1, the fraction of released HCl reaches its peak at 627°C, with 3.4×10<sup>-4</sup>%, while it is 677°C for the condition of case 2 and 727°C for case 3, with the highest fraction of 8.5×10<sup>-4</sup>% and 2.1×10<sup>-3</sup>%, respectively. Then the release of HCl starts to decline; however, the higher the initial input of Cl content, the higher the final temperature that needed to completely release the HCl content. When the final temperature exceeds 827°C, the released HCl is negligible in case 1, while this temperature point is 927°C and 1127°C in

case 2 and case 3, respectively. During the combustion process, Cl start to release from biomass at low temperature (427°C-527°C) [17], mainly in the form of HCl [15], while the other dominant Cl species in the biomass is KCl, which remains stable in the solid phase until the final temperature passes 727°C [11, 27]. This indicates that, when the final temperature is below 727°C, the more the initial input of Cl content, the more the Cl content will be released in the form of HCl. The results in Figure 7.1 (b) and (c) show that the initial input of Cl has a more significant influence on the release of HCl than KCl, the peak of release fraction of HCl is more than doubled when double the initial input of Cl content. This reveals that, at the early stage of combustion, the release of Cl is not only via the directly evaporation of HCl, but also through other Cl-related intermediate reactions like: R7-3 and R7-4 [28], which would be facilitated by the increasing of initial input of Cl content. When the final temperature exceeds 727°C, the release fraction of HCl starts to decline and the higher the initial input of Cl, the quicker the decrease of release fraction of HCl. This again proves that Cl-related intermediate reactions play a crucial role in the release process of HCl, as the temperature increased, with the depletion of moisture content, the decline of  $O_xH_y$  species could inhibit the further formation of HCl, and with the depletion of HCl itself, the rapid decrease of the release of HCl is anticipated.

The change of release fraction of KCl is summarised in Figure 7.1 (c). As we can see, the initial Cl content has little influence on the release profile of KCl when the final temperature is lower than 727°C. However, when final temperature surpasses 727°C, the influence of initial Cl content becomes great, and the fraction of release of KCl content raises as the increase of initial Cl content. The release profiles of KCl are similar in case 1 and case 2 before they diverge at 827°C. After this temperature, the release profiles become distinguishable, they all finish the sharp increase of the release of KCl at 927°C, with the fraction of  $4.7 \times 10^{-4}$  % and  $1.1 \times 10^{-3}$  %, respectively. Then the increasing slowdown and reaches the final fraction of  $6.7 \times 10^{-4}$  % and  $1.3 \times 10^{-3}$  % at 1127°C, respectively.

Meanwhile, in case 3, the release of KCl appears a continuing increase when the final temperature exceeds 727°C. It has a similar result as that of case 2 before 927°C. Then the release of KCl becomes flat in case 2, while the release continues to rise sharply in case 3 and finally, the release of KCl reaches its highest fraction with  $2.5 \times 10^{-3}$  % at 1127°C.

Also, as we can see from the above results, at 1127°C, when the release of KCl becomes flat, the final fraction of KCl reflects the initial input of Cl content. When double the initial Cl input (as case 3), it has nearly double the release fraction of KCl compared to the results in the condition of initial input of regular Cl content (as case 2), and it is the same when comparing the results of the release of KCl under the circumstances of the case 2 and case 1. Alongside the decline of HCl, KCl starts to release in large fraction due to its sublimation when the temperature exceeds 727°C [6] and becomes the major route to release Cl and K contents at the later stage of combustion. As a result, the influence of initial input of Cl becomes more distinguishable; however, the effect is not as significant as that of HCl. According to the study, Cl is more likely to initially present as KCl [29] in the biomass, and its release behaviour and mechanisms are highly dependent on the initial amount of these two components [16]. This means, even increase the initial input of Cl content, as long as the initial input of K content remains the same, the release behaviour of KCl stays the same during its early stage of sublimation, this explains the almost identical release profiles of KCl under the different conditions before 827°C. However, the large amount of release of HCl at the early stage could react with KOH to generate more KCl and stored as a solid product, and as the final temperature increased, it occurs the rise of the release of KCl content. In addition, the more HCl that exists in the system, the more completely the reaction with KOH, indicates the more KCl could be generated and be released. Moreover, the abundant dissociation of  $(\text{KCl})_2$  at high temperature is also one of the main reasons that boosts the release of KCl, as illustrated in Figure 7.1 (c) and (d), the sharp increase of the release of KCl happens at the same time when the release of  $(\text{KCl})_2$  starts to decline.

The release profiles of  $(\text{KCl})_2$  under the different conditions are illustrated in Figure 7.1 (d), as we can see, different from the release of KCl, the release of  $(\text{KCl})_2$  starts at the early stage of combustion. Nevertheless, the results show a similar trend to that of KCl: (i) the higher the initial Cl content, the more significant the release fraction of  $(\text{KCl})_2$ ; (ii) there is no apparent effect of initial Cl content on the release of  $(\text{KCl})_2$  before 727°C; (iii) there are two diverge temperatures can be observed: 727°C between the results of case 1 and case 2, and 827°C between the results of case 2 and case 3. In these three conditions, the fraction of released  $(\text{KCl})_2$  reaches its peak at the diverge temperatures, with  $1.1 \times 10^{-4}\%$ ,  $1.2 \times 10^{-4}\%$  and  $1.2 \times 10^{-4}\%$  in case 1, case 2 and case 3, respectively. Then after the

diverge temperatures, the release of  $(\text{KCl})_2$  content starts to decline. Moreover, at  $1127^\circ\text{C}$ , the fraction of the released  $(\text{KCl})_2$  is negligible in the condition of case 1 and case 2, while the fraction decrease to  $3.9 \times 10^{-5} \%$  in case 3. At the early stage of combustion, KCl is stable and stays in the solid phase, and according to the previous study [30], it is likely to associates with each other to form  $(\text{KCl})_2$  at low temperatures, and then the formed  $(\text{KCl})_2$  will be released. As aforementioned, the release of KCl is less dependent on the Cl content at the beginning, indicates the release of  $(\text{KCl})_2$  is less affected by the initial input of Cl content as well. Thus, as illustrated in Figure 7.1 (d), the release profiles of  $(\text{KCl})_2$  are identical to each other under the different conditions of the initial input of Cl content before  $727^\circ\text{C}$ . As the final temperature exceeds  $727^\circ\text{C}$ , KCl starts to sublime, due to the release rate of KCl is faster than the homogenous association rate between each other, leading to the less formation and release of  $(\text{KCl})_2$  content. Besides, the generated thermal unstable  $(\text{KCl})_2$  starts to dissociate to generate KCl. The more the initial input of Cl content, the higher the final temperature it needed to consume the  $(\text{KCl})_2$  content completely, since more KCl and  $(\text{KCl})_2$  could be formed during the later stage of combustion.

The release profiles of KOH and  $(\text{KOH})_2$  are demonstrated in Figure 7.1 (e) and (f). Contrary to the results of KCl and  $(\text{KCl})_2$ , the released fraction of KOH and  $(\text{KOH})_2$  decreased with the increase of initial input of Cl content, and the release of KOH and  $(\text{KOH})_2$  are negligible before  $727^\circ\text{C}$  compared with that of KCl and  $(\text{KCl})_2$ . The release of KOH becomes noticeable at  $827^\circ\text{C}$  and  $927^\circ\text{C}$  in case 1 and case 2, respectively. Then the fraction of released KOH steeply increased and reached its peak at  $1027^\circ\text{C}$ , with  $1.5 \times 10^{-3} \%$  and  $8.0 \times 10^{-4} \%$  in case 1 and case 2, respectively. Subsequently, the release of KOH starts to decline, and at  $1127^\circ\text{C}$ , the final fraction of KOH is  $1.0 \times 10^{-3} \%$  in case 1, while it is  $5.9 \times 10^{-4} \%$  in case 2. As for the result of  $(\text{KOH})_2$ , it shows a similar tendency to that of KOH, its fraction reaches the peak at  $1027^\circ\text{C}$ , but with only  $1.1 \times 10^{-6} \%$  and  $3.4 \times 10^{-7} \%$  in case 1 and case 2, respectively. However, in case 3, the release fraction of KOH is unnoticeable compared to KCl and  $(\text{KCl})_2$  within the temperature range of  $327^\circ\text{C}$ - $1027^\circ\text{C}$ . There is only a minor fraction of release of KOH can be observed at  $1127^\circ\text{C}$ , with  $1.1 \times 10^{-4} \%$ ; while the release fraction of  $(\text{KOH})_2$  is negligible during the whole temperature range compared to that of KOH.

The results show that the release of KOH and  $(\text{KOH})_2$  are greatly affected by the initial input of Cl content. When increasing the initial input of Cl content, it results in a high concentration of HCl content in the system, which could consume a large amount of KOH to form KCl via the reaction R6-1. Also, KOH more likely to be formed during the combustion process other than inherent in the biomass, and as indicated in [22], the formation of KOH at the early stage of combustion relies on the K and moisture content. However, the increased Cl content in the system might facilitate the reaction between Cl and moisture to generate HCl and been released at low temperature range. This results in the less left of moisture content for K to react with, leading to the less generation and release of KOH. When decreasing the initial input of Cl content to half of its regular content (as case 1), the release fraction of KOH is much more than that of the rest of the scenarios. The release trend of  $(\text{KOH})_2$  is similar to that of KOH, since  $(\text{KOH})_2$  is formed via the homogenous reaction of KOH. The higher the initial input of Cl content, the less the KOH content, and the less the  $(\text{KOH})_2$  will be formed and released. Besides, due to the low concentration of KOH under the circumstance of high Cl system, the association rate between KOH might be much slower than the depletion and release rate of KOH [30]. Besides, the HCl could also directly react with the released  $(\text{KOH})_2$  and decrease its fraction.

### 7.3.2 Changes of major transition cycles of K

The detailed reaction path of K with the change of initial input of Cl are listed in Appendix III according to the final temperature. In this section, the influence of initial input of Cl on the major transition cycle based on the results in Chapter 6 will be summarised and discussed. The summary of the change of transition cycle at each temperature is according to the change of the formation rate of each species. The summarised major transition cycles are divided into three categories according to the final temperature, which is: low, medium and high temperature ranges. The value on the arrow presents the rate at which species are formed from other species, measured in  $\text{kmol}/\text{m}^3 \text{ s}$ .

#### 7.3.2.1 Low temperature range ( $327^\circ\text{C}$ - $527^\circ\text{C}$ )

Figure 7.2 presents the change of major transition cycle of K with the change of initial input of Cl according to the change of reaction rate. As we can see, within the low temperature range, the change of initial input of Cl has insignificant influence on the change of major transition cycle. At  $327^\circ\text{C}$ , the reaction rate among  $\text{KCl} \rightarrow \text{KO}_2 \rightarrow \text{KO}$

→ KOH increased with the increasing of initial input of Cl, while the reaction rate of  $\text{KOH} \rightarrow \text{KCl}$  decreased. When the final temperature increased to  $427^\circ\text{C}$  and  $527^\circ\text{C}$ , all the reaction rates are increased compared to that of  $327^\circ\text{C}$ , and the higher the final temperature, the higher the reaction rates within the cycle. However, at these two temperature points, the transition cycle is less affected by the change of initial Cl content. As illustrated in Figure 7.2, the rate of each reaction remains almost identical to each other when increasing the initial input of Cl content.

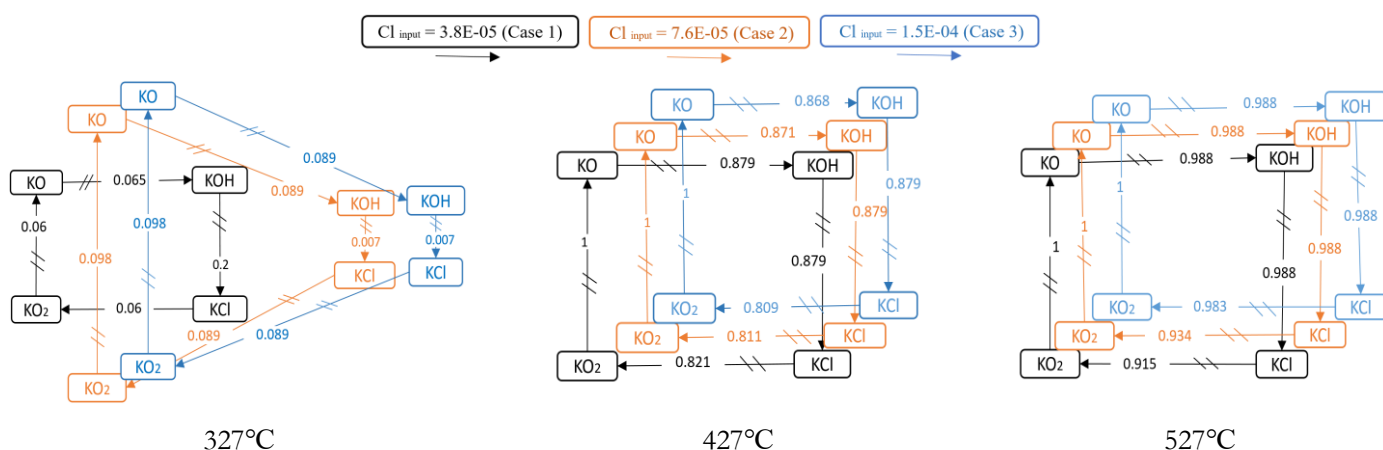


Figure 7.2 Changes of major transition cycles of K with the change of initial input of Cl in the low temperature range (the value on the arrows in represents the rates at which species are formed from other species,  $\text{kmol}/\text{m}^3 \text{ s}$ )

At  $327^\circ\text{C}$ , at the early stage of reaction, the  $\text{H}_2\text{O}$  content might still be sufficient to react with both K and Cl content. In this way, when initial input of Cl is in case 1 and case 2, there is less Cl available to react with  $\text{H}_2\text{O}$ , leading to the more available reaction between K and  $\text{H}_2\text{O}$  and to generate more KOH content. Afterwards, the formed KOH can react with Cl species to generate KCl, which makes a higher reaction rate of  $\text{KOH} \rightarrow \text{KCl}$ . While as the initial input of Cl content increased, more Cl could react with  $\text{H}_2\text{O}$  to form HCl and released directly; thus, the left  $\text{H}_2\text{O}$  might not enough for K to react and to generate abundant KOH, leading to the decline of the reaction rate of  $\text{KOH} \rightarrow \text{KCl}$ . Then as final temperature increased to  $427^\circ\text{C}$  and  $527^\circ\text{C}$ , as discussed in the previous part, at such low temperatures, only the release of HCl content has been dramatically affected by the change of initial input of Cl content. At these temperatures, the release of K compounds like KOH, KCl and  $\text{K}_2\text{SO}_4$  is negligible since most of them are thermal stable at these temperatures and remain in the solid phase. Thus, the release and transition of K compounds can be insignificantly influenced by the initial input of Cl content. In

conclusion, the major transition cycle of K is less sensitive to the initial input of Cl during the low temperature range.

### 7.3.2.2 Medium temperature range (627°C-827°C)

As the final temperature increased, the influence of the initial input of Cl content on the change of major transition cycle becomes more significant and distinguishable, the higher the initial input of Cl content, the higher the reaction rate within the major transition cycle.

As illustrated in Figure 7.3, at 627°C, the reaction rate of  $\text{KCl} \rightarrow \text{K}$  increased from 0.055 in case 1 to 0.178 in case 3. While the reaction rate of  $\text{K} \rightarrow \text{KO}_2$  increased from 0.0129 to 0.144 as the initial input of Cl content changed from case 1 to case 3. As the final temperature raised, the rates of nearly all the reactions increased with the increasing of initial input of Cl content. At 727°C, as initial input of Cl content changed from case 1 to case 3, the reaction rate of each reaction of  $\text{KO} \rightarrow \text{KOH} \rightarrow \text{KCl} \rightarrow \text{K} \rightarrow \text{KO}_2$  are increased from 0.0012 to 0.157, 0.0014 to 0.15, 0.001 to 0.5 and 0.0006 to 0.15, respectively. While at 827°C, the reaction rate of each reaction of  $\text{KO} \rightarrow \text{KOH} \rightarrow \text{KCl} \rightarrow \text{K}$  is increased from 0.01 to 0.31, 0.13 to 0.57 and 0.025 to 0.44, respectively.

As discussed in 7.3.1, during this temperature range, the initial input of Cl content has an insignificant influence on the release profiles of major K compounds like KCl,  $(\text{KCl})_2$  and KOH. However, the significant change of the major transition cycle reveals that the change of the initial input of Cl content will significantly affect the transition among major and intermediate K compounds. At 627°C, the main change occurs to the transition of  $\text{KCl} \rightarrow \text{K} \rightarrow \text{KO}_2$ , and the higher the initial input of Cl content, the higher the reaction rates. This indicates that during the combustion process, the reactions R7-5 and R6-5 [24] might be favoured by the high initial input of Cl content in the system, and thus, results in the high reaction rates among these species. As the final temperature reaches 727°C and 827°C, the major change occurs to the reaction  $\text{KO} \rightarrow \text{KOH} \rightarrow \text{KCl} \rightarrow \text{K}$ . Since the high Cl content might accelerate the reactions R7-6 and R7-7 [28, 31], which increase the rates of the reactions R7-8 and R7-9 [24], which then dominate transition of  $\text{KO} \rightarrow \text{KOH}$ . Besides, with the increasing of the initial input of Cl content, more HCl has been released during this temperature range, as illustrated in Figure 7.1 (b), the generated HCl content would consume more KOH content, leading to the high reaction rate of KOH

→ KCl. In addition, the high reaction rate of  $\text{KCl} \rightarrow \text{K}$  again proves that the reactions R7-5 and R6-5 are favoured by the high Cl content during the combustion process.

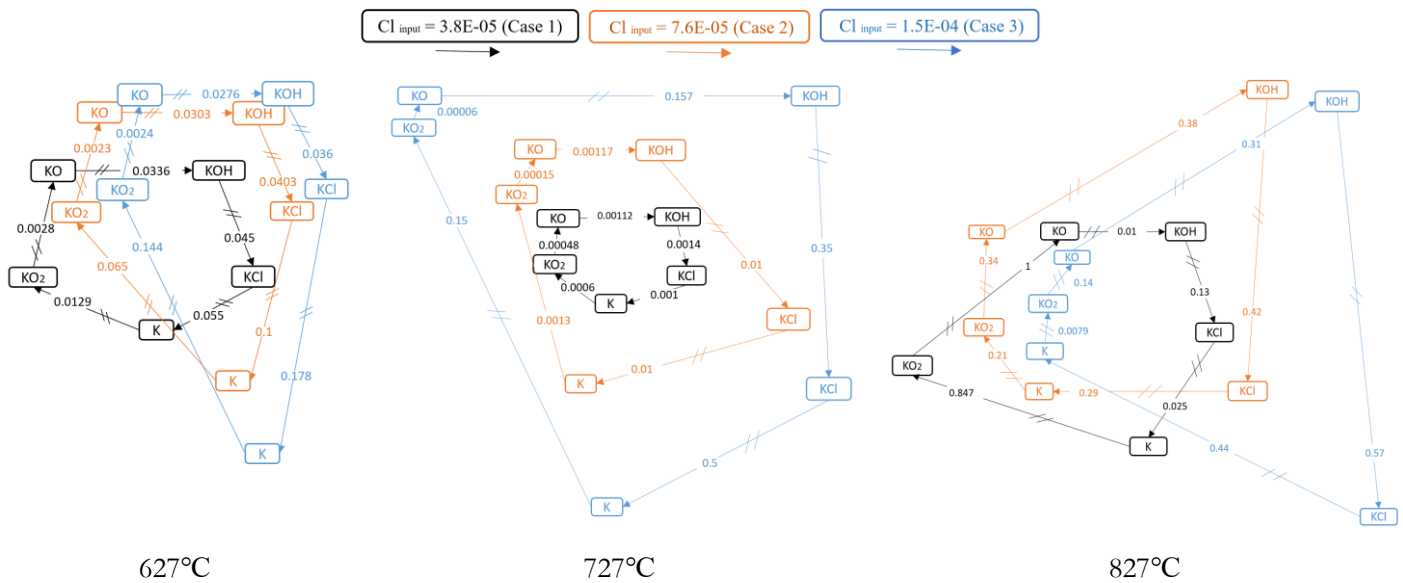


Figure 7.3 Changes of major transition cycles of K with the change of initial input of Cl in the medium temperature range (the value on the arrows in represents the rates at which species are formed from other species, kmol/m<sup>3</sup> s)

### 7.3.2.3 High temperature range (927°C-1127°C)

As presented in Figure 7.4, the change of transition cycle with the change of initial input of Cl is significant within the high temperature range, however, not as significant as that during the medium temperature range. The influence of increasing the initial input of Cl content on the transition cycle is mainly reflected in the reaction  $\text{KO} \rightarrow \text{KSO}_3 \rightarrow \text{K}$ , which increased at first and then decreased. At 927°C, the reaction rates of  $\text{KO} \rightarrow \text{KSO}_3$  and  $\text{KSO}_3 \rightarrow \text{K}$  are both increased from 0.504 in case 1 to 0.839 in case 2, and then are both decreased to 0.209 in case 3. While at 1027°C and 1127°C, as the initial input of Cl content increasing, the reaction rates are both increased from 0.066 to 0.86, then decreased to 0.57 and increased from 0.0013 to 0.0059, then decreased to 0.0021, respectively.

As shown in Figure 7.1 (b), in case 1 and case 2, the release of HCl content becomes negligible at high temperatures, indicates the possible reaction 6-9 would consume less KO content, which then could accelerate the reactions R6-7 and R7-10. This explains the increase of reaction rate of  $\text{KO} \rightarrow \text{KSO}_3$  and  $\text{KSO}_3 \rightarrow \text{K}$  at first. However, as the initial input of Cl content continues to increase to the case 3, the release fraction of HCl

becomes noticeable at these temperatures, as shown in Figure 7.1 (b). Under this circumstance, the reaction R6-9 might be favoured, which leads to the less available KO content that could be involved in the R6-7 and thus, less  $\text{KSO}_3$  for the R7-10. Besides, Figure 7.1 (a) shows that under the test condition of case 3, the release fraction of  $\text{K}_2\text{SO}_4$  is much less compared to those of the other two cases. Due to the lack of KO and  $\text{KSO}_3$  contents in the condition of high Cl content, the inhabitation of reaction R6-3 might be one of the reasons that reduce the release of  $\text{K}_2\text{SO}_4$ . This could draw the conclusion as increasing the initial Cl content could inhibit the release of  $\text{K}_2\text{SO}_4$  mainly through the control of the formation of KO and  $\text{KSO}_3$ .

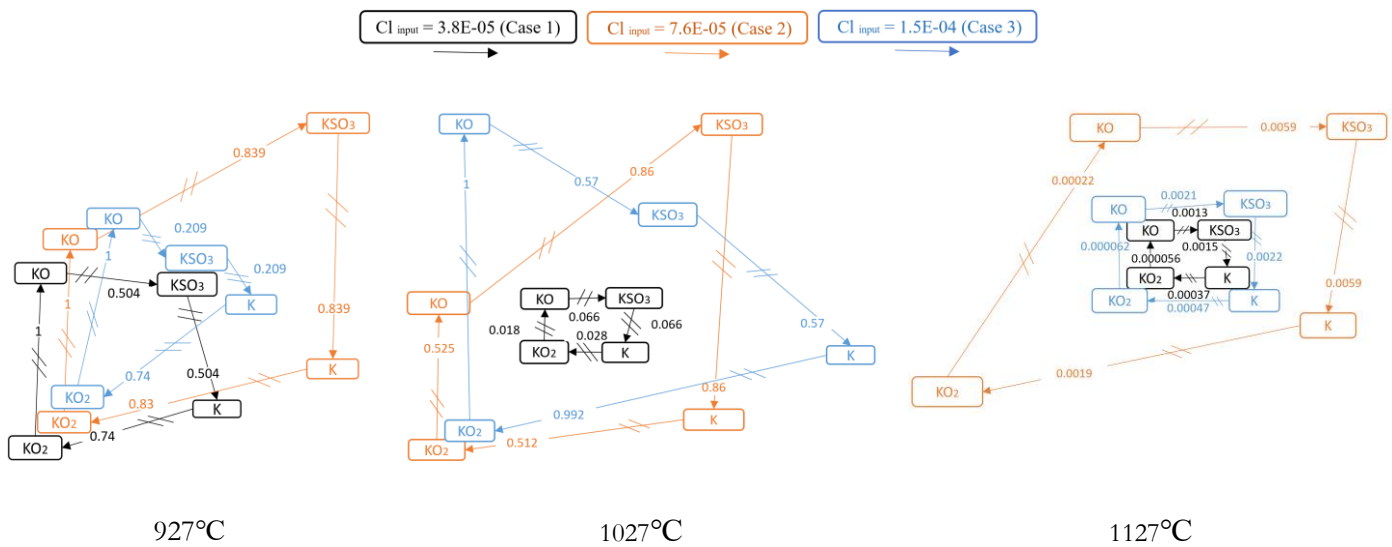
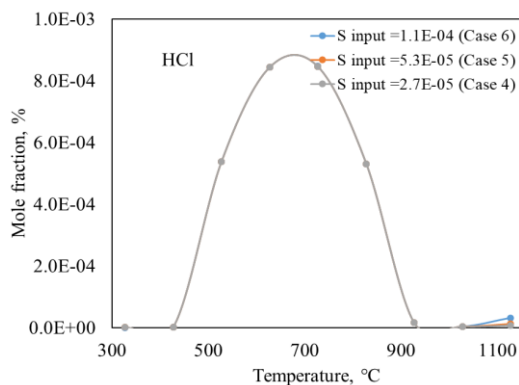


Figure 7.4 Changes of major transition cycles of K with the change of initial input of Cl in the high temperature range (the value on the arrows in represents the rates at which species are formed from other species,  $\text{kmol}/\text{m}^3 \text{ s}$ )

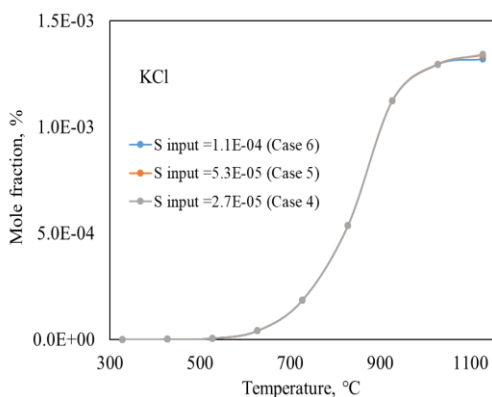
## 7.4 Effect of S concentration on the release of K compounds

### 7.4.1 Release profiles of major species

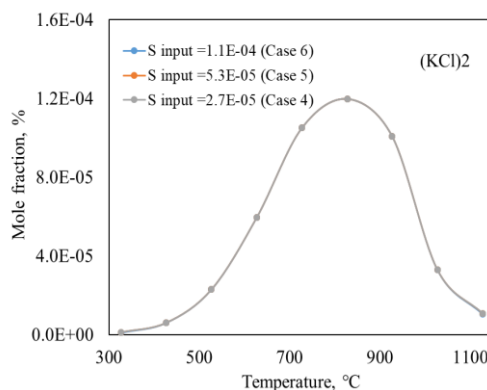
This part summarises the release profiles of different K compounds under the conditions of different initial input of S content. The results illustrated in Figure 7.5 and 7.6 are the change of release profiles of K compounds with the change of initial input of S according to the final temperature. As presented in the figures, the initial S content has insignificant influence on the release of Cl related species, but significantly affect the release of KOH and  $\text{K}_2\text{SO}_4$ , especially at high temperatures.



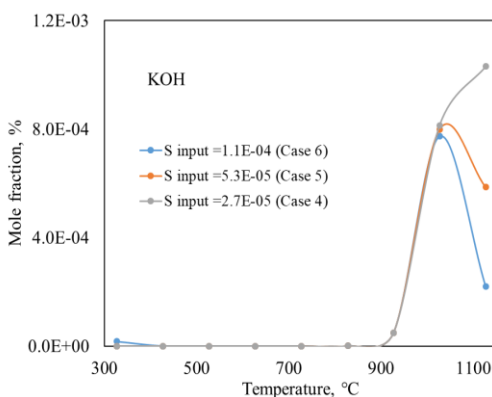
(a)



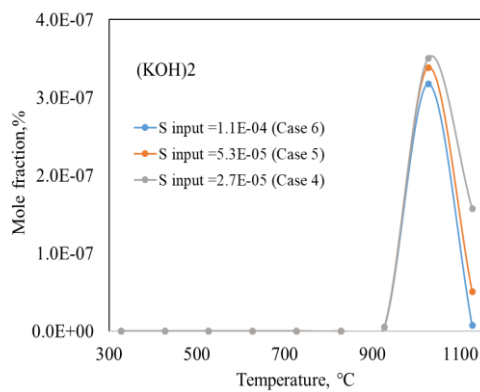
(b)



(c)



(d)



(e)

Figure 7.5 The changes of release profiles of major species with the change of initial input of S. As illustrated in Figure 7.5 (a), the change of initial input of S content has an insignificant influence on the release behaviour of HCl. The results of the three cases are all overlapped when the final temperature below 1027°C. The release of HCl in large fraction starts at

427°C and reaches its peak at 727°C, with  $8.5 \times 10^{-4}$  %. Then the release of HCl starts to decline steeply until 927°C, the release fraction of HCl becomes negligible afterwards. However, as the final temperature rises to 1127°C, the release fraction of HCl has noticeably increased from  $6.8 \times 10^{-6}$  % in case 4 to  $3.1 \times 10^{-5}$  % in case 6. Same conclusions could be drawn from the results in Figure 7.5 (b) for the release behaviour of KCl: there is no noticeable difference among the release curves of KCl under the different conditions of initial input of S content before 1027°C. The release of KCl in large fraction starts at 527°C and then sharply increase to  $1.1 \times 10^{-3}$  % at 927°C; after that, the release becomes flat. Nevertheless, as the final temperature increased to 1127°C, the release fraction of KCl decreased from  $1.3 \times 10^{-3}$  % in case 4 to  $1.4 \times 10^{-3}$  % in case 6. Meanwhile, as indicated in Figure 7.5 (c), the change of the release profile of  $(\text{KCl})_2$  is less sensitive to the change of initial input of S content. The release profiles are almost the same under the three tested conditions. The release of  $(\text{KCl})_2$  in large fraction starts at 427°C, and increased to its peak amount at 827°C, with  $1.2 \times 10^{-4}$  %, and then the release fraction starts to decline.

According to Johansen et al. [6], a two-step release mechanism of S can be concluded from the combustion of biomass: the release of organically associated S at low temperatures; and the release of inorganically associated S happens when the final temperature exceeds approximately 927°C. However, the current model excludes the reactions of the organically associated K, Cl and S species, due to the lack of related mechanisms. The majority part of the S will be released through the inorganic way, which is favoured by high temperatures [7, 16, 25]. During which, however, the Cl content has already been released abundantly in the form of HCl,  $(\text{KCl})_2$  and KCl, because of the release of Cl content is favoured by low temperatures according to the previous discussion. This reveals, when the release of HCl and KCl species started, the S related inorganic species remain stable. Besides, the main released S product at low temperatures is  $\text{SO}_2$ , which is the most stable form of S during the combustion process [32], thus unlikely to react with the released Cl species.

Increasing the initial input of S content can raise the total amount of inorganic S content, whose sublimation and evaporation are favoured by high temperatures. In this way, the change of initial S content has an insignificant influence on the transition and release of Cl species at low-medium temperatures. As final temperature surpasses 927°C, the possible explanation for the change of release of HCl and KCl at high temperatures is

increasing the S content might facilitate the reaction R7-11 at high temperatures, and the  $\text{KSO}_3\text{Cl}$  could further react with  $\text{KOH}$  via R7-12. This implies that the higher the S content in the system, the more generated  $\text{KSO}_3\text{Cl}$  content, which could then cause the release of more  $\text{HCl}$  content. In addition, as shown in Figure 7.5 (b) and 7.5 (d), as the initial input of S content increased, the decline of release fraction of  $\text{KCl}$  and  $\text{KOH}$  at high temperatures also evidence the existence and preference of R7-11 and R7-12 at high temperatures. Moreover, since the release of  $(\text{KCl})_2$  is dominated by the release of  $\text{KCl}$  content, the less sensitivity of  $\text{KCl}$  to the initial input of S content could result in the insensitivity of  $(\text{KCl})_2$  to the initial S content.

Figure 7.5 (d) presents the release profile of  $\text{KOH}$  with the change of initial input of S content according to the final temperature. The release of  $\text{KOH}$  is negligible before  $927^\circ\text{C}$  compared to the other released major species. Then sharply increased until  $1027^\circ\text{C}$ , during which, there is no significant influence of initial S content on the release of  $\text{KOH}$  can be observed. At  $1027^\circ\text{C}$ , the release fraction of  $\text{KOH}$  reaches its peak in case 6 and case 5, with  $7.8 \times 10^{-4} \%$  and  $8.0 \times 10^{-4} \%$ , respectively. After that, the released fraction of  $\text{KOH}$  start to decrease under these two conditions, and finally, the release fraction of  $\text{KOH}$  is  $2.2 \times 10^{-4} \%$  and  $5.9 \times 10^{-4} \%$ , respectively. However, in case 4, after sharply increased to  $8.1 \times 10^{-4} \%$  at  $1027^\circ\text{C}$ , the release fraction of  $\text{KOH}$  continues to increase mildly, and finally reaches  $1.0 \times 10^{-3} \%$  at  $1127^\circ\text{C}$ . Meanwhile, the release of  $(\text{KOH})_2$  shows the same trends as that of  $\text{KOH}$  before  $1027^\circ\text{C}$ , as there is no significant influence of the initial input of S content on its release behaviour. The release fraction of  $(\text{KOH})_2$  becomes noticeable when the final temperature exceeds  $927^\circ\text{C}$ , and quickly reaches its peak at  $1027^\circ\text{C}$ , with  $3.2 \times 10^{-7} \%$ ,  $3.4 \times 10^{-7} \%$  and  $3.5 \times 10^{-7} \%$  in case 6, case 5 and case 4, respectively. While as the final temperature exceeds  $1027^\circ\text{C}$ , the release of  $(\text{KOH})_2$  under the three tested conditions are all suffering a steep decline, but still, the higher the initial input of S content, the smaller the release fraction of  $(\text{KOH})_2$  eventually.

At the early stage of reaction, the moisture and the available K content dominate the formation of  $\text{KOH}$  [33]. Since the reaction between S and moisture can only take place under high pressure and the water is in the form of vapour [34]. Thus, under the circumstance of this study, the initial input of S content has less influence on the formation of  $\text{KOH}$  at the early stage of combustion. While at the temperature below  $927^\circ\text{C}$ , the release of  $\text{KOH}$  is restricted by the release of Cl species like  $\text{HCl}$ . As

aforementioned and discussed, the release of HCl is less affected by the change of initial input of S content. In this way, the release of KOH content at low-medium temperatures is insensitivity to the change of initial input of S content. While as the final temperature continues to rise to 1027°C, as the depletion of HCl, more KOH content could be released. In this way, the more S content in the system, the more consumption of KOH via the R6-4, R7-1 and R7-12, which also has been proved by the change of release profile of HCl in the previous discussion. Meanwhile, the release of (KOH)<sub>2</sub> content during the combustion process is directly related to the release behaviour of KOH. This results in the similar release profile of (KOH)<sub>2</sub> to that of KOH before 1027°C, the more the available KOH content in the system, the more chance of KOH homogenously combined to form (KOH)<sub>2</sub>. However, when the final temperature exceeds 1027°C, due to the relatively low concentration of KOH in the system, its association rate might be much slower than that of the consumption [30], which leads to the decrease of (KOH)<sub>2</sub> content under all the tested conditions at 1127°C.

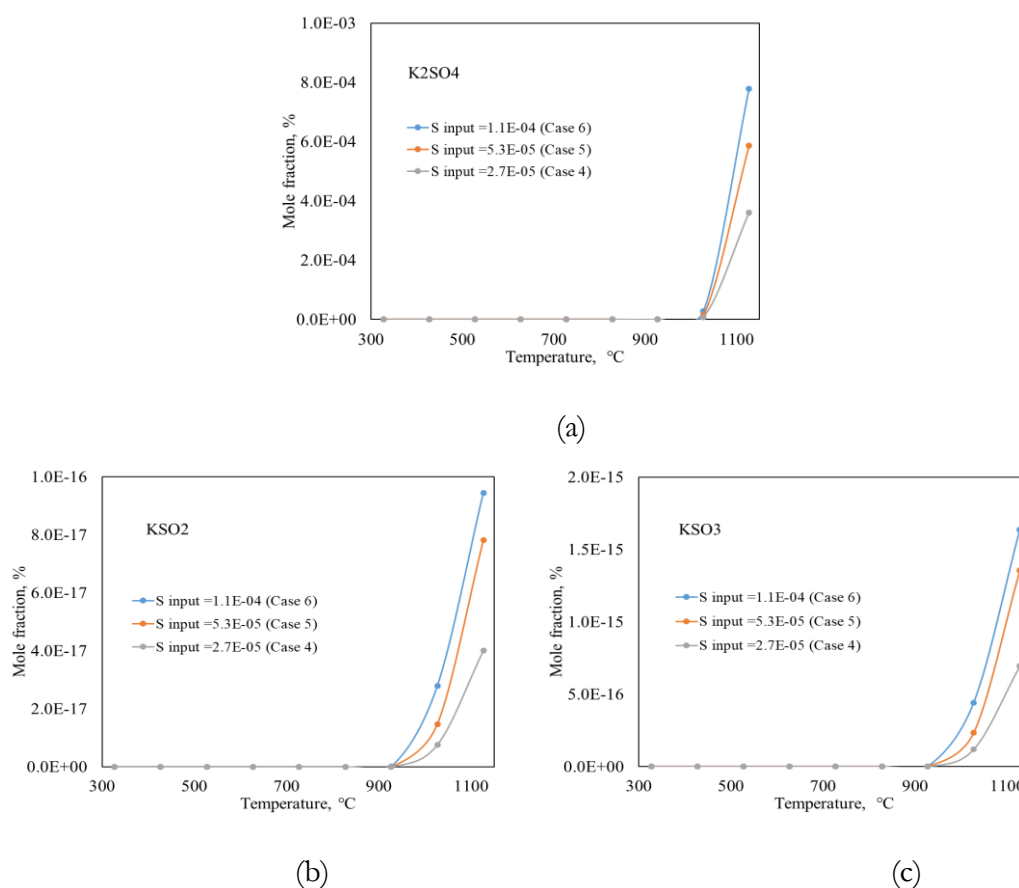


Figure 7.6. The changes of release profiles of S-related species with the change of initial input of S

The release profile of  $K_2SO_4$  with the change of initial input of S content is summarised in Figure 7.6 (a). As illustrated in the figure, the initial input of S content has dramatically affected the release of  $K_2SO_4$  at high temperature. As we can see, the release fraction of  $K_2SO_4$  is negligible before  $1027^\circ\text{C}$ , but steeply increased to  $7.8 \times 10^{-4}\%$ ,  $5.9 \times 10^{-4}\%$  and  $3.6 \times 10^{-4}\%$  at  $1127^\circ\text{C}$  in case 6, case 5 and case 4, respectively. The higher the initial input of S content, the larger the release fraction of  $K_2SO_4$  at high temperature. Similar release profiles of  $KSO_2$  and  $KSO_3$  can be observed from Figure 7.6 (b) and 7.6 (c) as well. Their releases are negligible before  $927^\circ\text{C}$ , then sharply increased when temperature surpasses  $927^\circ\text{C}$ , and the higher the initial input of S content, the larger the release fraction of  $KSO_2$  and  $KSO_3$  at  $1127^\circ\text{C}$ .

During the combustion process,  $K_2SO_4$  is the most stable forms of K and S content [32], which remains stable up to  $927^\circ\text{C}$  [16], then start to evaporate as gas product. As discussed in the previous part, the release of  $K_2SO_4$  is negligible at low temperature and less sensitivity to the change of initial input of S content, indicating the initial amount of  $K_2SO_4$  is not varying with the change of initial S content, but might be restricted by the available K content. Nevertheless, the sharply increased  $K_2SO_4$  content in the system at high temperature indicates that the initial input of S affects the release of  $K_2SO_4$  by influencing the formation and release of intermediate K-S species during the combustion process, such as  $KSO_2$  and  $KSO_3$ . Then those intermediate species would further react to generate  $K_2SO_4$  via the possible reactions R7-11 and R7-13. Investigation in the Knudsen et al. [5] study also proves that the inorganic sulphate can be transformed into other forms of solid sulphur during the thermal conversion process. Moreover, as indicated in Figure 7.6 (b) and 7.6 (c), the higher the initial input of S, the more the available  $KSO_2$  and  $KSO_3$  content, which could then accelerate the formation and release of  $K_2SO_4$ .

#### 7.4.2 Changes of major transition cycle of K

The influence of initial input of S on the summarised major transition cycle will be investigated in this part. The results are presented in three parts according to the different temperature ranges. The detailed reaction paths are listed in Appendix IV.

##### 7.4.2.1 Low temperature range ( $327^\circ\text{C}$ - $527^\circ\text{C}$ )

Figure 7.7 indicates similar results to that of the study of initial input of Cl. The change of initial input of S has insignificantly affected the reaction rates within the transition cycle.

At 327°C, the change of the transition cycle is mainly caused by the transition  $\text{KOH} \rightarrow \text{KCl}$ , and the reaction rate increased from 0.22 to 0.56 as the test condition changed from case 4 to case 6. The reaction rates of the rest reactions are almost the same under the three tested conditions. Nevertheless, as the final temperature increase to 427°C and 527°C, the transition cycle remains almost the same as increasing the initial input of S content. As we can see, the higher the final temperature, the higher the reaction rate of each reaction. However, there are no significant changes in the reaction rates can be observed as raising the initial input of S content.

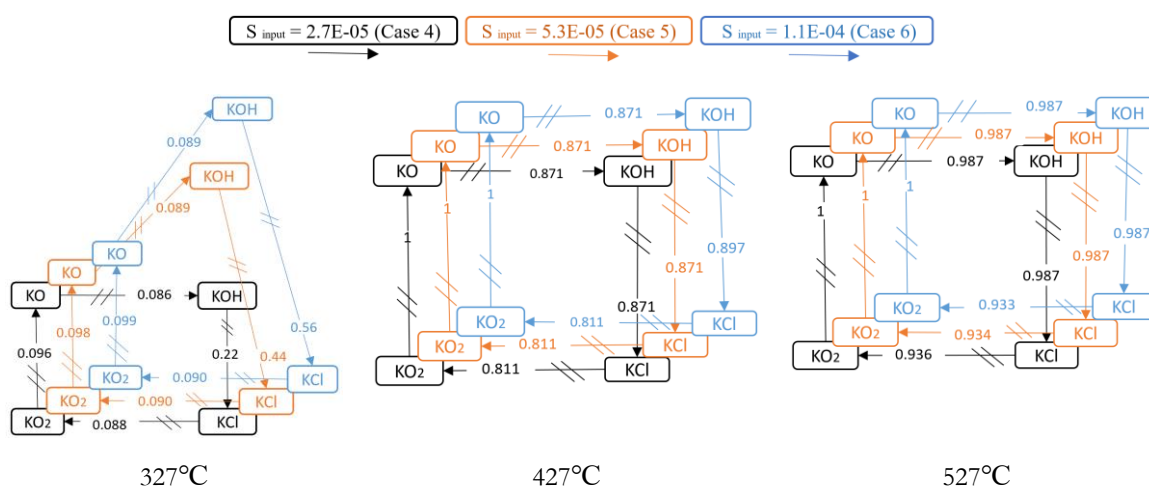


Figure 7.7 Changes of major transition cycles of K with the change of initial input of S in the low temperature range (the value on the arrows in represents the rates at which species are formed from other species,  $\text{kmol}/\text{m}^3 \text{ s}$ )

At 327°C, as illustrated before, at the early stage of combustion, the release of HCl is insensitive to the change of initial S content. As aforementioned, the initial Cl content could affect the formation of KOH content by reducing the available moisture content for K to form KOH. However, when raising the initial input of S content, the input of Cl content is fixed; thus, it will not increase the competition with K over the moisture content. Besides, S is unlikely to react with moisture directly [34], so the possible S species in the system could be SH at this temperature, which is formed via R7-14 and R7-15. Then the formed unstable SH content could facilitate the generation of  $\text{H}_2\text{O}$  and  $\text{H}_2\text{O}_2$  via R7-16 and R7-17 [35], which could then react with K via R7-18 and R7-19 to generate more KOH content. The more the initial input of S content, the more the generated  $\text{H}_2\text{O}$  and  $\text{H}_2\text{O}_2$  content, leading to the more KOH to react with HCl. In this way, the higher the initial input of S, the higher the reaction rate of  $\text{KOH} \rightarrow \text{KCl}$  at low temperatures.

As the final temperature increased, more S content could be oxidized and released as  $\text{SO}_2$  and  $\text{SO}_3$ , while the remaining SH content might be insufficient and unstable, so the formation of KOH is thus unaffected, so does the reactions that related to KOH. Moreover, as we can see in Figure 7.7, at  $427^\circ\text{C}$  and  $527^\circ\text{C}$ , the major transition species are all non-S related. As discussed before, the change of initial input of S has an insignificant influence on the release of KOH, KCl at such temperatures. Thus, the reaction rates within the transition cycle remain the same as increasing the initial input of S content.

#### 7.4.2.2 Medium temperature range ( $627^\circ\text{C}$ - $827^\circ\text{C}$ )

The changes of major transition cycle with the change of initial input of S in the medium temperature range are illustrated in Figure 7.8. As presented, the influence of different initial input of S content is less significant compared to that of different initial input of Cl content within the same temperature range. The reaction rates increased gradually with the increasing of initial input of S content.

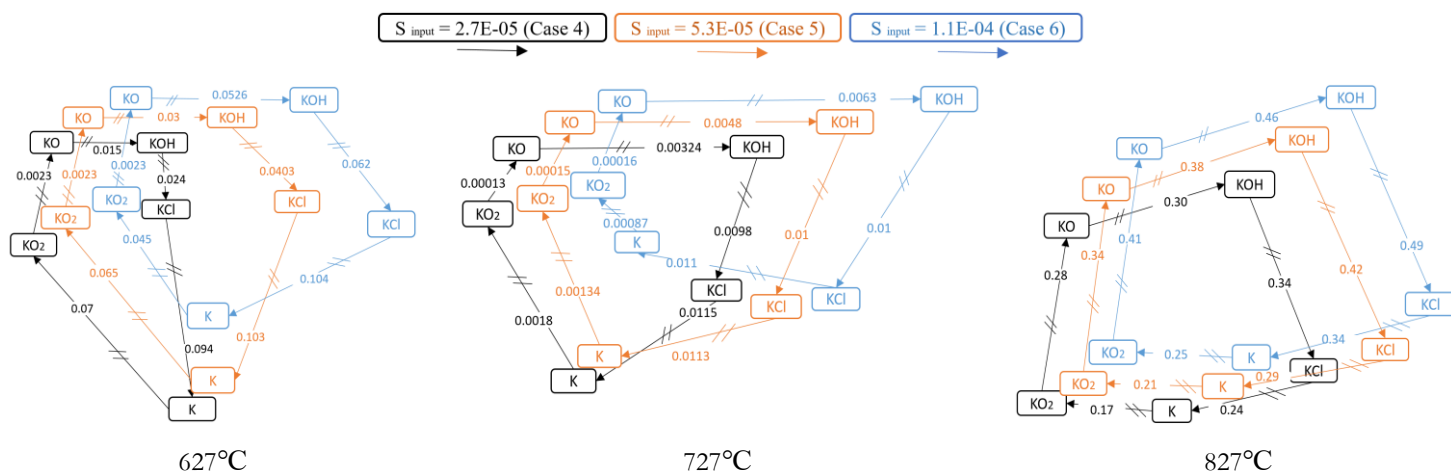


Figure 7.8 Changes of primary transition cycles of K with the change of initial input of S in the medium temperature range (the value on the arrows in represents the rates at which species are formed from other species,  $\text{kmol}/\text{m}^3 \text{ s}$ )

At  $627^\circ\text{C}$ , the reaction rate of  $\text{KO} \rightarrow \text{KOH} \rightarrow \text{KCl}$  has been dramatically increased, the rate values of  $\text{KO} \rightarrow \text{KOH}$  and  $\text{KOH} \rightarrow \text{KCl}$  are raised from 0.015 and 0.024 in case 4 to 0.053 and 0.062 in case 6, respectively. While at  $727^\circ\text{C}$ , these values are increased from 0.00324 and 0.0098 in case 4 to 0.0063 and 0.01 in case 6, and at  $827^\circ\text{C}$ , the values are increased from 0.30 and 0.46 in case 4 to 0.34 and 0.49 in case 6. As we can see, within the medium temperature range, the reaction rates of  $\text{KO} \rightarrow \text{KOH} \rightarrow \text{KCl}$  are increased

all the time as raising the initial input of S content; however, the growth rate is declined as the final temperature increased. While the change of reaction rate of the rest transitions within the cycle is less affected by the change of initial input of S content.

Combined with the investigation in Figure 7.5, the initial S content has insignificant influence on the release of major K compounds like KOH and KCl, and the release of  $K_2SO_4$  during this temperature range is still negligible. This indicates that the major transition is dominated by the K/O/H species during the medium temperature range. As discussed before, the increase of available  $H_2O$  and  $H_2O_2$  content as the increase of initial input of S content causes the increase of reaction rate of  $KO \rightarrow KOH$  at all time. While the decline of the growth rate of the reaction rate of  $KOH \rightarrow KCl$  is more likely caused by the decrease in the release of HCl content during this temperature range.

#### 7.4.2.3 High temperature range (927°C-1127°C)

Figure 7.9 presents the change of major transition cycle with the change of initial input of S in the high temperature range. As shown in Figure 7.7 and 7.8, before high temperature range, K-S species is not involved in the major transition cycle, indicating that the transition and reaction of K-S species are favoured by high temperatures. This also can be evidenced in Figure 7.9,  $KSO_3$  becomes one of the key species in the major transition cycle only within the high temperature range. When increasing the initial input of S content, nearly all of the reaction rates are increased.

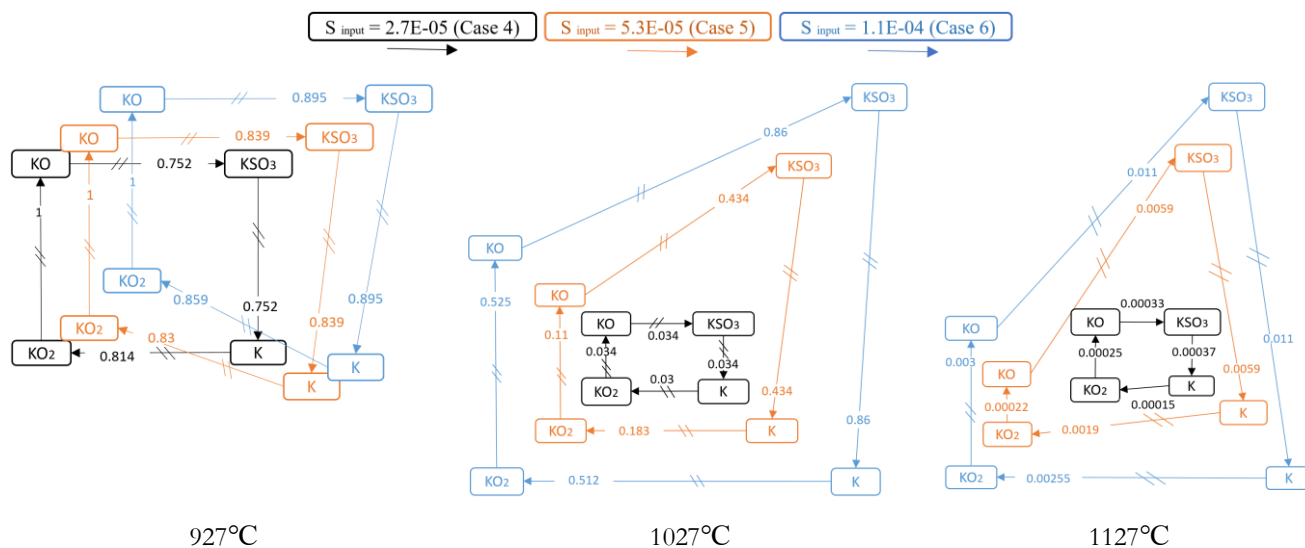


Figure 7.9 Changes of major transition cycles of K with the change of initial input of S in the high temperature range (the value on the arrows in represents the rates at which species are formed from other species,  $kmol/m^3 s$ )

At 927°C, the change of reaction rates is small and similar to that of the change during the medium temperature range. This temperature can be defined as the transitional point, where  $\text{KSO}_3$  gradually replaces  $\text{KOH}$  and  $\text{KCl}$  in the major transition cycle, but no evident influence on the release of major species, which can be proved in Figure 7.5, the changes of release profile of major K compounds occurred when the final temperature exceeds 927°C. However, at 1027°C, the growths of reaction rates are more evident within the reaction of  $\text{KO} \rightarrow \text{KSO}_3 \rightarrow \text{K}$ , the rate values of  $\text{KO} \rightarrow \text{KSO}_3$  and  $\text{KSO}_3 \rightarrow \text{K}$  are raised from 0.034 to 0.86 and 0.034 to 0.86 with the change from case 4 to case 6, respectively. While at 1127°C, their rate values are increased from 0.00033 and 0.00037 to 0.011 and 0.011, respectively.

Combined with the previous discussion, the release of  $\text{KSO}_2$  and  $\text{KSO}_3$  in noticeable amounts start at the same temperature as that of  $\text{K}_2\text{SO}_4$ , which is 1027°C. Then their release fractions are all increased dramatically. As aforementioned, the release of  $\text{K}_2\text{SO}_4$  is favoured by high temperature. This indicates that at high temperature, the release of  $\text{K}_2\text{SO}_4$  content is coming from two possible sources: the inherent and the formed  $\text{K}_2\text{SO}_4$  at the early stage during the combustion; the generated  $\text{K}_2\text{SO}_4$  from  $\text{KSO}_2$  and  $\text{KSO}_3$  at high temperature, as illustrated in Figure 7.10.

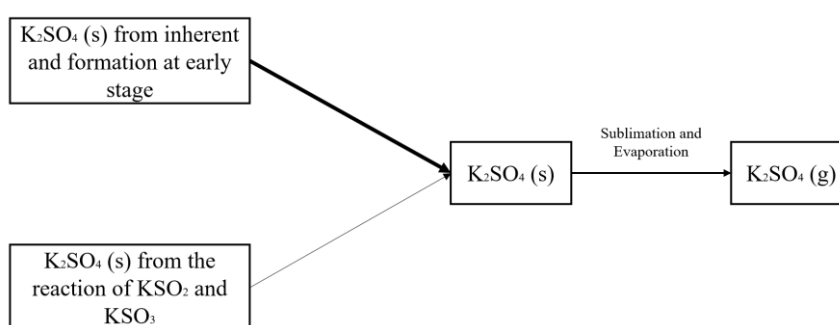
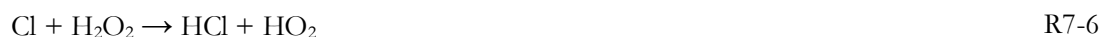
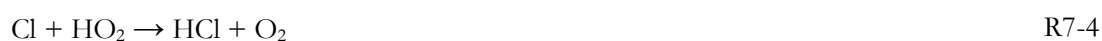
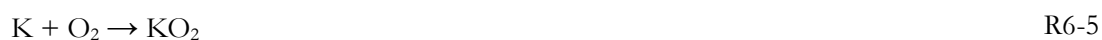


Figure 7.10 Release route of  $\text{K}_2\text{SO}_4$  during the combustion process

Since the initial S content is unlikely to react with moisture and K content directly but will be released as  $\text{SO}_2$  and  $\text{SO}_3$ . In this way, the change of initial input of S content can insignificantly affect the formation of  $\text{K}_2\text{SO}_4$  at the early stage.

Also, as presented in Figure 7.5, the higher the initial input of S, the higher the release fraction of  $\text{KSO}_2$  and  $\text{KSO}_3$  at high temperature. However, as we can see, even though the release of  $\text{KSO}_2$  and  $\text{KSO}_3$  become noticeable, their releases are still in minor fraction, and  $\text{KSO}_3$  is more likely to be involved in the reaction of  $\text{KSO}_3 \rightarrow \text{K}$  as illustrated in the

transition cycle. This means, even though increase the initial input of S would increase the release of  $\text{KSO}_2$  and  $\text{KSO}_3$ , but the formed  $\text{K}_2\text{SO}_4$  during the reaction at high temperature is insufficient to cause the dramatic increase of the release of  $\text{K}_2\text{SO}_4$  since the released amount of  $\text{KSO}_2$  and  $\text{KSO}_3$  are incomparable to that of the release of major species. In conclusion, the sublimation and evaporation of the accumulated  $\text{K}_2\text{SO}_4$  that are from the inherent and the formation at the early stage during the combustion process is the main reason that causes the abundant release of  $\text{K}_2\text{SO}_4$  content when the final temperature is high enough. The increase of initial input of S content will not affect the release of  $\text{K}_2\text{SO}_4$  dramatically at high temperature.



$\text{KO}_2 + \text{KSO}_2 \rightarrow \text{K}_2\text{SO}_4$	R7-13
$\text{S} + \text{H} \rightarrow \text{SH}$	R7-14
$\text{S} + \text{H}_2 \rightarrow \text{SH} + \text{H}$	R7-15
$\text{SH} + \text{OH} \rightarrow \text{H}_2\text{O} + \text{S}$	R7-16
$\text{SH} + \text{HO}_2 \rightarrow \text{H}_2\text{O}_2 + \text{S}$	R7-17
$2\text{K} + 2\text{H}_2\text{O} \rightarrow 2\text{KOH} + \text{H}_2$	R7-18
$\text{K} + \text{H}_2\text{O}_2 \rightarrow \text{KOH} + \text{OH}$	R7-19

## 7.5 Summary of the chapter

This chapter has investigated the influence of initial input of Cl and S on the release profiles of major species and the change of major transition cycles via the acquired estimation results.

According to the results and discussion, the influence of initial input of Cl has a significant influence on the release of major species during the combustion process. The higher the initial input of Cl content, the more the release fraction of HCl, KCl and  $(\text{KCl})_2$ , however, the less the release fraction of KOH,  $(\text{KOH})_2$  and  $\text{K}_2\text{SO}_4$ . The initial Cl content influence the release of HCl from the beginning of its release, and the higher the initial input, the higher the final temperature it needed to finish the release of HCl in large fraction. While the initial Cl content can only significantly affect the release fraction of KCl,  $(\text{KCl})_2$ , KOH and  $(\text{KOH})_2$  when the final temperature exceeds  $727^\circ\text{C}$ , and this temperature point is  $1027^\circ\text{C}$  for  $\text{K}_2\text{SO}_4$ . The results revealed that the formation and release of KCl are less depends on the Cl content than K at the early stage of combustion; the release fraction of KCl remains the same regardless the change of Cl, meaning the initial KCl content is almost the same. While during the combustion, Cl content inhibits the release of KOH via firstly affect the formation process of KOH by controlling the available moisture content that K needed to generate KOH. The release of KOH content is restricted by the released Cl content like HCl. Also, at high temperature, high initial input of Cl prevents the release of  $\text{K}_2\text{SO}_4$  through the control of the formation of KO and  $\text{KSO}_3$ .

During low temperature range, the change of initial input of Cl has less influence on the transition cycle, the reaction rates within the cycle are nearly consistent as increasing the initial input of Cl content. While in the medium and high temperature range, the initial

input of Cl dominates the change of the transition cycle, it significantly affects the intermediate reactions and thus affects the release of K compounds. The higher the initial input of Cl, the larger the change of reaction rate within the transition cycles.

The results in this chapter have indicated that the changing of the initial input of S content has less influence on the release profiles of major species, especially at low-medium temperature. The release of HCl, KCl and  $(\text{KCl})_2$  are insensitive to the change of initial input of S content, and the release profiles are nearly overlapped under the different conditions. However, as increasing the initial input of S, there is a minor increase in the release fraction of HCl at  $1127^\circ\text{C}$ , while the release of KCl is decreasing. The influence of initial S content on the release of KOH,  $(\text{KOH})_2$  and  $\text{K}_2\text{SO}_4$  are negligible when the final temperature below  $1027^\circ\text{C}$ , but becomes more distinguishable at  $1127^\circ\text{C}$ , the higher the initial input of S, the less the release fraction of KOH and  $(\text{KOH})_2$ , meanwhile, the more the release fraction of  $\text{K}_2\text{SO}_4$ . According to the investigation, the release of  $\text{K}_2\text{SO}_4$  and KOH are greatly affected by the change of initial S content. However, increasing the initial input of S content does not directly increase the existence of  $\text{K}_2\text{SO}_4$  content at the beginning, but via the increasing of formation of intermediate species:  $\text{KSO}_2$  and  $\text{KSO}_3$  during the combustion process, and then react with KOH content to generate more  $\text{K}_2\text{SO}_4$ , which then facilitates the release of  $\text{K}_2\text{SO}_4$  at high temperatures. Moreover, the sublimation and evaporation of the accumulated  $\text{K}_2\text{SO}_4$  from the inherent and the formation at the early stage is the primary source that causes the abundant release of  $\text{K}_2\text{SO}_4$  at high temperature, the increase of  $\text{KSO}_3$  content at high temperatures can only cause the minor increase of the release of  $\text{K}_2\text{SO}_4$ .

The change of initial input of S content has an insignificant influence on the transition cycle during the low and medium temperature ranges. While within the high temperature range, the initial input of S content has greatly affected the transition cycle, the higher the initial input, the higher the reaction rate, especially the  $\text{KSO}_3$  involved reactions.

## Bibliography

1. Teakle, N.L. and S.D. Tyerman, Mechanisms of Cl-transport contributing to salt tolerance. *Plant, Cell & Environment*, 2010. 33(4): p. 566-589.
2. White, P.J. and M.R. Broadley, Chloride in soils and its uptake and movement within the plant: a review. *Annals of Botany*, 2001. 88(6): p. 967-988.
3. Hindiyarti, L., Gas phase sulfur, chlorine and potassium chemistry in biomass combustion. CHEC Research Centre, DTU, Copenhagen, 2007.
4. Marschner, H., Marschner's mineral nutrition of higher plants. 2011: Academic Press.
5. Knudsen, J.N., et al., Sulfur transformations during thermal conversion of herbaceous biomass. *Energy & Fuels*, 2004. 18(3): p. 810-819.
6. Johansen, J.M., et al., Release of K, Cl, and S during pyrolysis and combustion of high-chlorine biomass. *Energy & Fuels*, 2011. 25(11): p. 4961-4971.
7. Van Lith, S.C., et al., Release to the gas phase of inorganic elements during wood combustion. Part 1: development and evaluation of quantification methods. *Energy & Fuels*, 2006. 20(3): p. 964-978.
8. Nielsen, H., et al., The implications of chlorine-associated corrosion on the operation of biomass-fired boilers. *Progress in Energy and Combustion Science*, 2000. 26(3): p. 283-298.
9. Hansen, L.A., et al., Influence of deposit formation on corrosion at a straw-fired boiler. *Fuel Processing Technology*, 2000. 64(1-3): p. 189-209.
10. Frandsen, F.J., Ash formation, deposition and corrosion when utilizing straw for heat and power production. 2010, DTU.
11. Michelsen, H.P., et al., Deposition and high temperature corrosion in a 10 MW straw fired boiler. *Fuel Processing Technology*, 1998. 54(1-3): p. 95-108.
12. Werther, J., et al., Combustion of agricultural residues. *Progress in Energy and Combustion Science*, 2000. 26(1): p. 1-27.
13. Brunner, T., et al. Behaviour of ash forming compounds in biomass furnaces-measurement and analyses of aerosols formed during fixed-bed biomass combustion. in Proc. of the international IEA Seminar "Aerosols in Biomass Combustion", Zuerich, Switzerland. 2001.
14. Dahl, J., et al. Results and evaluation of a new heavy metal fractionation technology in grate-fired biomass combustion plants as a basis for an improved

- ash utilisation. in 12th European Conference and Technology Exhibition on Biomass for Energy, Industry and Climate Protection. 2002.
15. Johansen, J.M., et al., Release of K, Cl, and S during combustion and co-combustion with wood of high-chlorine biomass in bench and pilot scale fuel beds. *Proceedings of the Combustion Institute*, 2013. 34(2): p. 2363-2372.
  16. Knudsen, J.N., P.A. Jensen, and K. Dam-Johansen, Transformation and release to the gas phase of Cl, K, and S during combustion of annual biomass. *Energy & Fuels*, 2004. 18(5): p. 1385-1399.
  17. Björkman, E. and B. Strömberg, Release of chlorine from biomass at pyrolysis and gasification conditions1. *Energy & Fuels*, 1997. 11(5): p. 1026-1032.
  18. Hamilton, J.T., et al., Chloride methylation by plant pectin: an efficient environmentally significant process. *Science*, 2003. 301(5630): p. 206-209.
  19. Egsgaard, H., J. Ahrenfeldt, and U.B. Henriksen. On the significance of methyl chloride in gasification processes. in 18th European Biomass Conference and Exhibition. 2010.
  20. Saleh, S.B., et al., Release of chlorine and sulfur during biomass torrefaction and pyrolysis. *Energy & Fuels*, 2014. 28(6): p. 3738-3746.
  21. Sommersacher, P., et al., Simultaneous online determination of S, Cl, K, Na, Zn, and Pb release from a single particle during biomass combustion. Part 2: results from test runs with spruce and straw pellets. *Energy & Fuels*, 2016. 30(4): p. 3428-3440.
  22. Clery, D.S., et al., The effects of an additive on the release of potassium in biomass combustion. *Fuel*, 2018. 214: p. 647-655.
  23. Werkelin, J., et al., Chemical forms of ash-forming elements in woody biomass fuels. *Fuel*, 2010. 89(2): p. 481-493.
  24. Glarborg, P. and P. Marshall, Mechanism and modeling of the formation of gaseous alkali sulfates. *Combustion and Flame*, 2005. 141(1-2): p. 22-39.
  25. Van Lith, S.C., et al., Release to the gas phase of inorganic elements during wood combustion. Part 2: influence of fuel composition. *Energy & Fuels*, 2008. 22(3): p. 1598-1609.
  26. Dayton, D.C. and T.A. Milne, Laboratory measurements of alkali metal containing vapors released during biomass combustion, in *Applications of advanced technology to ash-related problems in boilers*. 1996, Springer. p. 161-185.

27. Van Lith, S.C., Release of inorganic elements during wood-firing on a grate. 2005: Technical University of Denmark Lyngby, Denmark.
28. Sliger, R.N., J.C. Kramlich, and N.M. Marinov, Towards the development of a chemical kinetic model for the homogeneous oxidation of mercury by chlorine species. *Fuel Processing Technology*, 2000. 65: p. 423-438.
29. Jenkins, B., R. Bakker, and J. Wei, On the properties of washed straw. *Biomass and Bioenergy*, 1996. 10(4): p. 177-200.
30. Cao, W., et al., Prediction of potassium compounds released from biomass during combustion. *Applied Energy*, 2019. 250: p. 1696-1705.
31. NIST CHEMICAL KINETIC DATABASE.  
<http://www.cstl.nist.gov/div836/ckmech.html/1999>, 1999.
32. Miller, F., G. Young, and M. Von Seebach, Formation and techniques for control of sulfur dioxide and other sulfur compounds in Portland cement kiln systems. *R&D Serial*, 2001(2460): p. 56.
33. Fatehi, H., et al., LIBS measurements and numerical studies of potassium release during biomass gasification. *Proceedings of the Combustion Institute*, 2015. 35(2): p. 2389-2396.
34. Features of the interaction of sulfur and water. MEL Science.  
<https://melscience.com/US-en/articles/features-interaction-sulfur-and-water/>.
35. Cerru, F., A. Kronenburg, and R. Lindstedt, Systematically reduced chemical mechanisms for sulfur oxidation and pyrolysis. *Combustion and Flame*, 2006. 146(3): p. 437-455.

## CHAPTER 8

# EFFECTS OF OXYGEN CONCENTRATION ON THE RELEASE OF POTASSIUM COMPOUNDS

---

This chapter presents the investigation of the effects of oxygen concentration on the release profiles of K compounds using the developed kinetic model. The estimated results in this chapter are presented according to two aspects: changes in the release profiles of K compounds and the major transition cycles of K under different conditions.

### 8.1 Background

Biomass combustion and pyrolysis happen in the atmosphere with and without oxygen. Generally, biomass combustion takes place according to the three stages: drying, devolatilisation and char oxidation whereas in the case of pyrolysis, only the first two stages happen. The study carried out by Chouchene et al. [1] illustrated that oxygen concentration affects the degree of char oxidation. However, the emission of moisture and volatile contents from biomass are insensitive to the change of oxygen concentration, and their kinetic study also showed that the reaction order of biomass combustion and pyrolysis were not affected by the variation of the oxygen concentrations.

The insensitivity of biomass thermal conversion process to the oxygen concentration should thus lead to the less influence of oxygen concentration on the total release of K content. Since the release of organically and inorganically bonded K is associated with the degree of biomass conversion. Dayton et al. [2] reported that reducing the oxygen concentration in the atmosphere has an insignificant effect on the total release of K. The authors reported that a reduced oxygen concentration showed little influence on the combustion properties of the biomass, especially herbaceous biomass like wheat straw and corn stover, and thus, does not appear to affect the release of alkali metals significantly. However, according to Jiménez et al. [3], the oxygen concentration in the system could significantly affect the final ratio of Cl/S in the fine particles, which could react with K to generate corrosive compounds like KCl and  $K_2SO_4$ .

Previous studies revealed that the oxygen concentration in the reaction system could influence the release forms of K, but has a small effect on the release of the total amount

of K. Since different K compounds have different roles in the alkali-induced problems, for example,  $K_2SO_4$  is expected to nucleate at high temperature ( $>800^\circ C$ ); meanwhile, KCl could condense on these nuclei at lower temperatures. Knowing the effect of the oxygen concentration on the release profiles of different K compounds is thus essential, as this information can provide insightful knowledge that might help to optimize the reactor design, the reaction process and control the release of K compounds during the reactions; this will help to mitigate the ash-related problems.

However, this kind of information is rarely reported due to the limitation of detection methods. Therefore, the developed kinetic model is used in this chapter to investigate the influence of oxygen concentration on the release of K. This study will help to build a better understanding of the release mechanisms of K under different oxygen concentrations.

## 8.2 Model setup

The model setup in this chapter was based on the Chapter 6. Change in the oxygen concentration is achieved by adjusting the initial input of  $O_2$ , which is based on the conditions of combustion (the same as that in Chapter 6) and pyrolysis (without  $O_2$ ). The initial input values of  $O_2$  are presented in Table 8.1 for both conditions.

Table 8.1 Initial input values of  $O_2$

Reaction condition	$O_2$	
	Combustion	Pyrolysis
Initial input, mol/ g biomass	$3.58 \times 10^{-2}$	0.0

## 8.3 Results and discussion

### 8.3.1 Release profiles of K compounds

The changes in the release of major K compounds (KCl, KOH and  $K_2SO_4$ ) that expressed in mole fraction with the change of the reaction conditions are presented in Figure 8.1. As illustrated, there are apparent differences between the release profiles of KCl, KOH and  $K_2SO_4$  in the presence of oxygen (combustion) and without oxygen (pyrolysis).

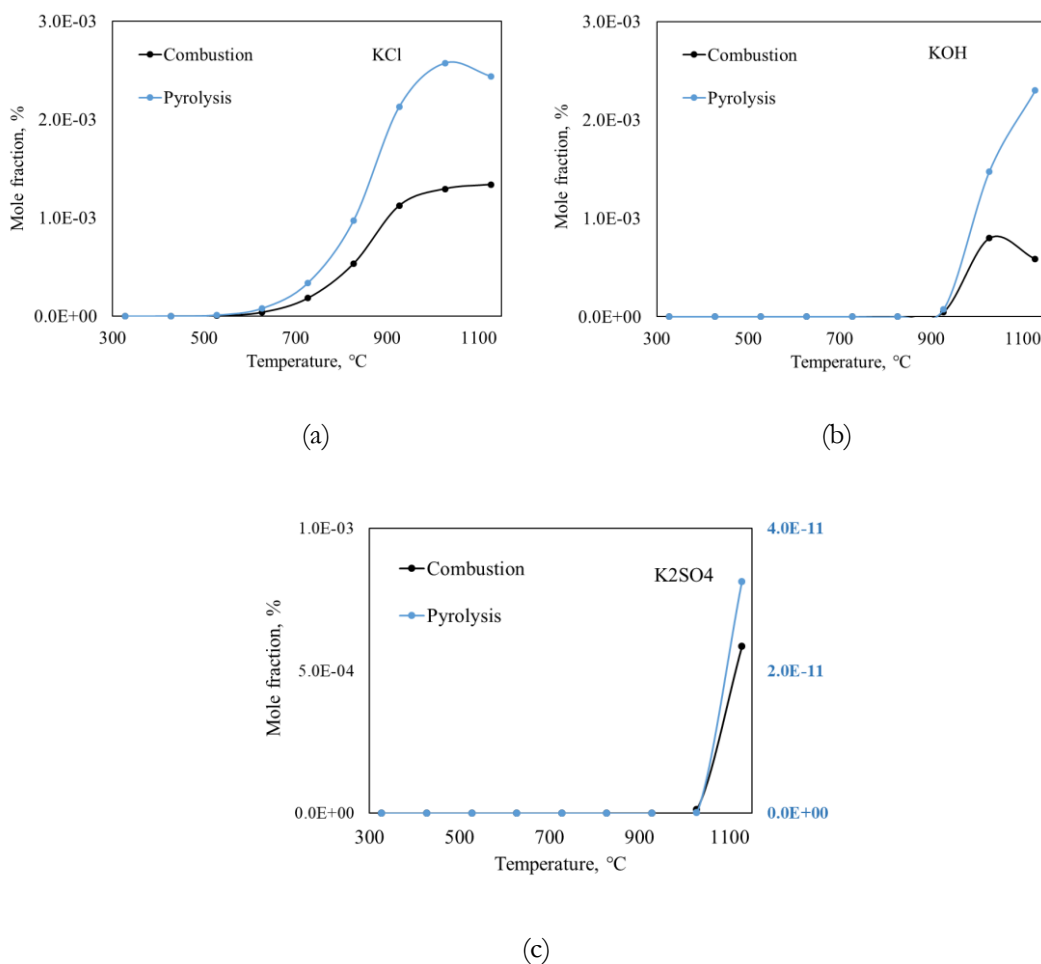


Figure 8.1 The changes of release profiles of major K compounds with the change of oxygen concentration

As shown in Figure 8.1 (a) and Figure 8.1 (b), the release fractions of KCl and KOH during the combustion process are always lower than their release fractions during the pyrolysis process. The release of KCl in large fractions started after 527°C and then increased noticeably for both conditions. During pyrolysis, the release fraction increased sharply until 1027°C, where it reaches its peak fraction corresponding to  $2.6 \times 10^{-3} \%$ . Afterwards, the release fraction starts to decline, reaching  $2.4 \times 10^{-3} \%$  at 1127°C. During combustion, the release fraction of KCl mildly increased to  $1.1 \times 10^{-3} \%$  at 927°C, and then increased slowly to  $1.3 \times 10^{-3} \%$  at a final temperature of 1127°C. While the release of KOH in large fraction starts after 927°C for both conditions, the release fraction sharply increased in the condition of pyrolysis, and finally reaches its peak at 1127°C, with  $2.3 \times 10^{-3} \%$ . In the case of combustion, the release of KOH reaches its peak fraction at 1027°C, with  $8.0 \times 10^{-4} \%$ , then starts to decline, and finally reaches  $5.9 \times 10^{-4} \%$  at 1127°C.

The same conclusion was also drawn by Dayton et al. [2]. In their report, the equilibrium calculations showed that a reduction in oxygen concentration could increase the formation of KCl and KOH. In contrast, the release fraction of  $K_2SO_4$  in the condition of combustion (left Y-axis) is several order-of-magnitude higher than that in the condition of pyrolysis (right Y-axis), as presented in Figure 8.1 (c). For both situations, the release fraction of  $K_2SO_4$  becomes obvious after  $1027^\circ\text{C}$ , and then it sharply increases to its peak fraction at  $1127^\circ\text{C}$ , with  $5.9 \times 10^{-4} \%$  in the case of combustion, while it is only  $3.3 \times 10^{-11} \%$  in the case of pyrolysis.

When there is sufficient oxygen in the system, the K content will mainly convert to KO and  $KO_2$  via R8-1 and R6-5. As indicated in Figure 8.2, the release fraction of KO and  $KO_2$  in the condition of combustion are several order-of-magnitude higher than that of pyrolysis, especially the release of  $KO_2$ . Since the existence of sufficient  $O_2$  might also facilitate the R8-2 [4], this results in a higher release of  $KO_2$  than KO under the same conditions. In addition, the existence of  $O_2$  in the system might favour the consumption of KCl and KOH via the R8-3, R8-4 and R8-5 [4]. This shows that a higher  $O_2$  concentration in the system will result in a higher released fraction of  $KO_2$  and KO, while a lower  $O_2$  concentration will result in a higher released fraction of KCl and KOH. In this way, the oxygen affects the formation of KO and  $KO_2$ , whom could then consume KCl and KOH content during the thermal conversion process, thus, causing the less release of KCl and KOH in the condition of combustion compare to the results in the condition of pyrolysis.

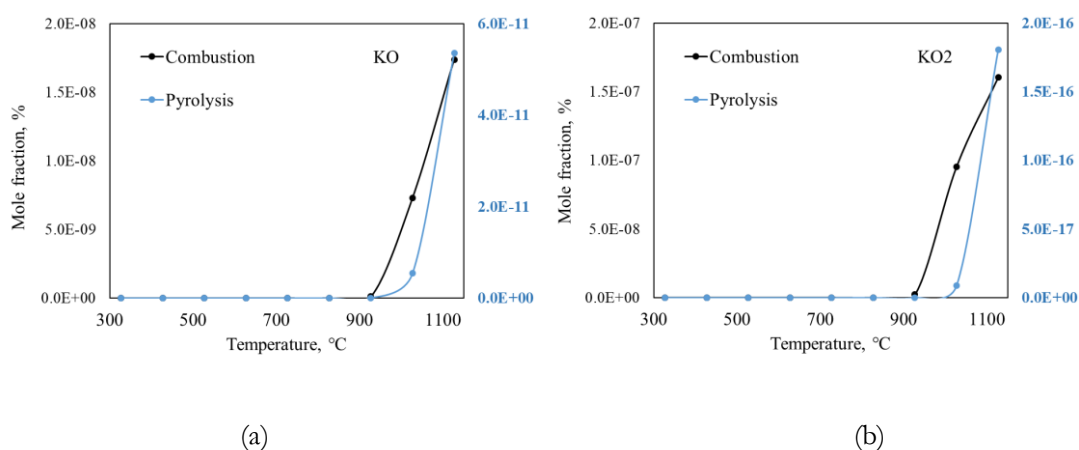


Figure 8.2 The changes of release profiles of intermediate K compounds with the change of oxygen concentration

Nevertheless, the release fraction of  $K_2SO_4$  is much less in the condition of pyrolysis compared to that of combustion. This might be caused by the lack of intermediate species like  $KSO_2$  and  $KSO_3$  and its formation in the early stage of the reactions. As discussed in the previous chapters, the release of  $K_2SO_4$  strongly relies on the S-related species (i.e.  $SO_2$ ,  $SO_3$ ,  $KSO_2$  and  $KSO_3$ ) during the thermal conversion process. Moreover, the calculation results from Dayton et al.'s report [2] also prove that when there is a higher concentration of  $SO_2$  in the system, a higher amount of  $K_2SO_4$  is released in the gas phase. Since there is no oxygen present in the pyrolysis test, less S content will convert to  $SO_2$  and  $SO_3$ , which then decrease the formation of  $KSO_2$  and  $KSO_3$ . This will lead to a lower formation and release of  $K_2SO_4$ . Besides, the predicted results of the release profiles indicate that there is a higher released fraction of  $SO_2$  and  $SO_3$  under the condition of combustion; however, a smaller released fraction of  $KSO_2$  and  $KSO_3$  can be obtained. This indicates that during the combustion, more  $KSO_2$  and  $KSO_3$  will convert to  $K_2SO_4$ , rather than been released directly.



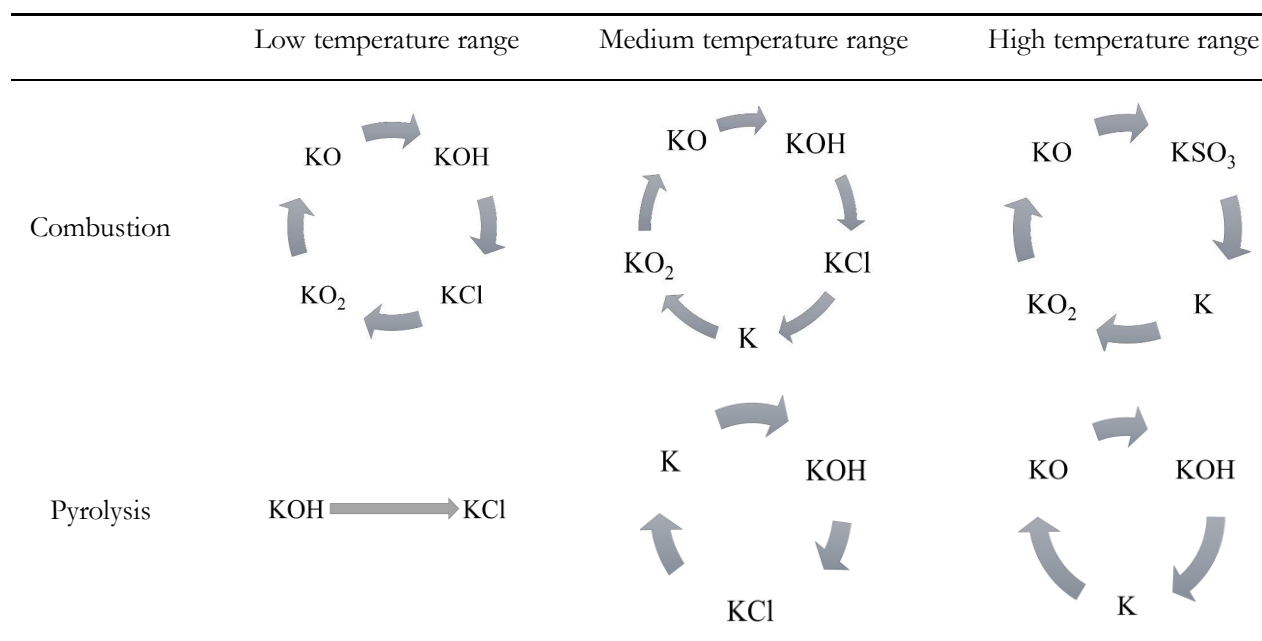
### 8.3.2 Change of major transition cycles of K

The summarised major transition cycles of K within the low ( $327^\circ\text{C}$ - $527^\circ\text{C}$ ), medium ( $627^\circ\text{C}$ -  $827^\circ\text{C}$ ) and high temperature ( $927^\circ\text{C}$  –  $1127^\circ\text{C}$ ) ranges are presented in Table 8.2. The detailed reaction paths of K under the different conditions are provided in Appendix V. As illustrated in the results, the major transition cycles are different between the tests of combustion and pyrolysis. When there exists sufficient oxygen in the system, the reaction path of K is much more complicated, leading to a more complex major transition cycle in the different temperature ranges.

During the low temperature range, there is only one major transition route of K can be concluded in the condition of pyrolysis, which is the route of  $KOH \rightarrow KCl$ . While in the test of combustion,  $KO$  and  $KO_2$  are also involved in the major transition cycle. At the beginning of the pyrolysis, there is only little available  $O_2$  in the system for K to react with,

which means, more K content could react with moisture and generate KOH. Meanwhile, the abundant release of HCl at low temperatures [5, 6] could consume a large amount of KOH and to form KCl, leading to the only one major transition route of K in low temperature range during the pyrolysis. This is also reflected in Figure 8.1, and there are higher released fractions of KOH and KCl during pyrolysis than those during combustion. However, at the initial stage of combustion, K could be oxidized when there exists sufficient oxygen content. As discussed before, KO and  $\text{KO}_2$  are the most important intermediate species during the combustion process, which mainly contribute to the formation of KOH, KCl and  $\text{K}_2\text{SO}_4$  [7]. Moreover, since partial K content is oxidized to form KO and  $\text{KO}_2$ , the direct release of KOH and KCl at the early stage could thus decrease compared to that during the pyrolysis.

Table 8.2 Major transition cycles of K in the different temperature ranges



As the final temperature increases to medium temperature range, more K content is released. During the pyrolysis process, with the depletion of Cl content, which is released as HCl, there is more available  $\text{H}_x\text{O}_y$  content for K to react with and thus facilitates the transition of  $\text{K} \rightarrow \text{KOH}$ . Meanwhile, during the combustion process, KO and  $\text{KO}_2$  still play a crucial role in the conversion process of K, as more released K content could be oxidized in the presence of  $\text{O}_2$ . As we can see from Table 8.2, at low and medium temperature ranges, the difference between the major transition cycles of combustion and pyrolysis is the involvement of KO and  $\text{KO}_2$ . This reveals that the oxidation of K at the

initial stage of the thermal conversion is a crucial step that controls the release of KCl and KOH at early stage. Besides, the formed KO and  $\text{KO}_2$  are less released at low-medium temperature range, and this can help to reserve partial K content.

At high temperatures, KCl is no longer part of the major transition cycle in both conditions. With the depletion of HCl at low temperatures, there is less reaction between HCl and KOH, and this results in the less involvement of KCl in the transition cycles. In the condition of pyrolysis, as the high final temperature triggers more decomposition reactions, there is more dissociated oxygen and  $\text{O}_x\text{H}_y$  in the system [8], which could also facilitate the reaction of  $\text{K} \rightarrow \text{KO}$ . The sufficient oxygen in the condition of combustion can still favour the oxidization of the dissociated K via the route of  $\text{K} \rightarrow \text{KO}_2 \rightarrow \text{KO}$ . This illustrates that, when there is a sufficient concentration of oxygen, K will always be involved in the oxidization reaction first, and then react and generate other stable species.

As presented in Table 8.2, apart from the oxidization route of K, KOH is still part of the major transition cycle under the circumstance of pyrolysis. At the same time, it is  $\text{KSO}_3$  in the condition of combustion. Since there is enough  $\text{O}_2$  in the system, more S content could be oxidized and reacted to form intermediate species, which are crucial to the generation of  $\text{K}_2\text{SO}_4$  at high temperatures. Moreover, the reaction of S species to form  $\text{K}_2\text{SO}_4$  might be favoured by high temperatures, which is reflected by the high reaction rate of  $\text{KSO}_3$ . This reveals that the conversion to  $\text{K}_2\text{SO}_4$  is favoured by both high temperature and the existence of  $\text{O}_2$ . However, during the pyrolysis process, due to the depletion of Cl content, and the lack of oxidized S species, K is more likely to be directly released in the stable form, like KOH, since there is enough dissociated  $\text{O}_x\text{H}_y$  content. These results also explain the higher released fraction of KOH in the result of pyrolysis when compared to that of combustion. In contrast, the release fraction of  $\text{K}_2\text{SO}_4$  is much lower in the result of pyrolysis when compared to that of combustion.

#### 8.4 Summary of the chapter

The influence of oxygen concentration on the prediction of the release of K compounds was carried out and discussed in this chapter. According to the results, when there is a sufficient oxygen content in the system, there is a lower released fraction of KCl and KOH, but a much higher released fraction of  $\text{K}_2\text{SO}_4$ . The concentration of oxygen has a significant influence on the release fraction of  $\text{K}_2\text{SO}_4$  than that of KOH and KCl. In the combustion test, KO and  $\text{KO}_2$  are the most important intermediate species involved in

the transition cycles for all the temperature ranges. While in the pyrolysis test, the major transition cycles are less complicated, and KOH is the only species involved in the transition cycles for all the temperature ranges.

These results revealed that when biomass is treated at a temperature less than 927°C, the existence of O<sub>2</sub> favours the formation of KO and KO<sub>2</sub> than any other K compounds. In this way, less K will directly react with moisture and Cl and be released in the form of KOH and KCl during the combustion process at these temperatures. When the reaction temperature is higher than 927°C, the lack of O<sub>2</sub> in the system can significantly inhibit the release of K<sub>2</sub>SO<sub>4</sub> in the order-of-magnitude level. During the combustion and pyrolysis process, there is a small difference between the release fraction of KOH and KCl. However, a big difference between the release fraction of K<sub>2</sub>SO<sub>4</sub> can be observed, and this indicates that when biomass is thermally treated, the existence of O<sub>2</sub> can influence the release behaviour of K by facilitating the release of K<sub>2</sub>SO<sub>4</sub> content at high temperatures.

## Bibliography

1. Chouchene, A., et al., Thermal degradation of olive solid waste: influence of particle size and oxygen concentration. *Resources, Conservation and Recycling*, 2010. 54(5): p. 271-277.
2. Dayton, D.C., R.J. French, and T.A. Milne, Direct observation of alkali vapor release during biomass combustion and gasification. 1. Application of molecular beam/mass spectrometry to switchgrass combustion. *Energy & Fuels*, 1995. 9(5): p. 855-865.
3. Jiménez, S. and J. Ballester, Influence of operating conditions and the role of sulfur in the formation of aerosols from biomass combustion. *Combustion and Flame*, 2005. 140(4): p. 346-358.
4. Glarborg, P. and P. Marshall, Mechanism and modeling of the formation of gaseous alkali sulfates. *Combustion and Flame*, 2005. 141(1-2): p. 22-39.
5. Björkman, E. and B. Strömberg, Release of chlorine from biomass at pyrolysis and gasification conditions<sup>1</sup>. *Energy & Fuels*, 1997. 11(5): p. 1026-1032.
6. Johansen, J.M., et al., Release of K, Cl, and S during combustion and co-combustion with wood of high-chlorine biomass in bench and pilot scale fuel beds. *Proceedings of the Combustion Institute*, 2013. 34(2): p. 2363-2372.
7. Cao, W., et al., Prediction of potassium compounds released from biomass during combustion. *Applied Energy*, 2019. 250: p. 1696-1705.
8. Debiagi, P.E.A., et al., Detailed kinetic mechanism of gas-phase reactions of volatiles released from biomass pyrolysis. *Biomass and Bioenergy*, 2016. 93: p. 60-71.

## CHAPTER 9

### CONCLUSIONS AND FUTURE WORK

---

#### 9.1 Final conclusions

This thesis experimentally and modelling investigated the release behaviour of K from biomass during its combustion process. Three objectives were defined to be accomplished in the Chapter 1 and have been carried out and evaluated in the Chapter 4 – Chapter 8 as regards the results presented. The main outcomes of this PhD work are presented below:

- **Cellulose, xylan, lignin and their mixtures were tested in the TGA device.**

The obtained thermal behaviours of different samples indicate that the different stages of combustion (devolatilisation and char oxidation) of biomass are predictable once the quantities of the major chemical components are certain. This outcome implies the feasibility to use the major chemical components as initial constitutions to estimate the thermal conversion process of biomass.

- **Wheat straw pellets were combusted in the FBS, and the results show that the final temperature affects the K transition performance the most amongst all the investigated operating factors.**

The higher the final temperature, the less the K was retained in the solid residues. Three stages can be concluded according to the release behaviour of K. The first stage occurs at low temperatures, the dissociation of loosely bonded K and partial organic K contributes to the release of K, which accounts for <25% of the initial K content. At this stage, an abundant content of K can be detected inside the porous structure, and the structural change is insignificant and has little influence on the loss of K. In the second stage, the loss of K varies by only 5%, while organic K and char K are more likely to convert to the thermal stable K compounds; whereas the particle structure starts to breakdown and collapse. The third stage occurs the abundant loss of K (up to 60%), which is mainly caused by the decomposition and evaporation of inorganic K. Moreover, biomass particle structure suffers a dramatic change, exposing the K content located within, leading to the further loss of K.

- **Heating rate also influences the transition performance of K during the combustion process.** The higher the heating rate, the more K is released as the gas product. At low-medium temperatures, the heating rate affects the release of K by influencing the molecular motions and thus controls the biomass decompositions and

release more volatile matters related K, as well as the break of low BDEs required K bonds. At high temperatures, the heating rate accelerates the K release by affecting the biomass particle structure. The higher the heating rate, the more coalescence of small pores to generate large cavities and the more open structure, exposing more of the internal K. Thereby, accelerating the decomposition and sublimation of K species.

- **A two-step kinetic controlled model was designed, which consists of the devitalisation of biomass and the oxidation of released gas products.** The model uses major chemical components as initial inputs, which is more close to the thermal characteristics of biomass than that of using the elemental as initial inputs. The model was validated by comparing the predicted volatile matter against the experimental results, as well as comparing the predicted profile of K released during combustion against the published prediction results. The validated results show a great agreement, indicating the reliability and accuracy of the developed model, and thus, could be further used to investigate the release behaviour of different K species from biomass under various conditions.

- **The developed model was used to predict the release profiles of K species and the transition route across a wide range of temperature.** The results indicate that KOH, KCl and  $K_2SO_4$  are the major K species that are released during the combustion of wheat straw. KCl is the major species of K and Cl that is released during the early stage of combustion. Followed by KOH, it is more likely to be formed during the combustion and release processes, which involves more important intermediate species.  $K_2SO_4$  becomes one of the most common K species released at temperatures exceeding  $1027^\circ C$ . Alongside the KCl and KOH. The release of  $K_2SO_4$  relies more on its initial amount in the biomass and the reactions in the solid phase during the early stages of combustion. The transition route revealed that intermediate species are briefly existed and quickly converted to other major K species during the combustion process. KO and  $KO_2$  are the most important intermediate species that could affect the generation of KCl and KOH.

- **The model was also used to predict the release profiles of K species under the scenarios of different initial values of Cl and S.** The results show that changing the initial amount of Cl has greatly affected the release behaviour of major K species at temperatures  $>727^\circ C$ . The higher the initial quantity of Cl, the greater the fraction of HCl and KCl released; however, the release of KOH and  $K_2SO_4$  is reduced. The formation and release of KCl depend less on the Cl than K in the reaction system. The content of

Cl inhibits the release of KOH via firstly affect its formation process by controlling the available water content for K to react with. Then restricts the release of KOH through the release of an abundant amount of HCl that consumes the KOH in the system. The change of the initial amount of Cl can significantly affect the major transition cycle at temperatures  $> 627^{\circ}\text{C}$ , the higher the Cl content, the bigger the change of the reaction rate within the transition cycle. Meanwhile, the initial content of Cl can also significantly influence the intermediate reactions during the combustion process and thus affect the release of K species.

The predicted results show that changing the initial amount of S can only significantly affect the release behaviour of K species at temperatures  $>1027^{\circ}\text{C}$ . The release behaviours of HCl and KCl are insensitive to the change of the initial value of S, whereas the release of KOH and  $\text{K}_2\text{SO}_4$  are greatly affected at temperatures  $>1027^{\circ}\text{C}$ , the higher the initial S content, the less the release fraction of KOH, meanwhile, the more release fraction of  $\text{K}_2\text{SO}_4$ . The S content affects the release of  $\text{K}_2\text{SO}_4$  mainly by exerting upon the formation of the intermediate species:  $\text{KSO}_2$  and  $\text{KSO}_3$  during the combustion process. Moreover, the abundant release of  $\text{K}_2\text{SO}_4$  at high temperatures under the high initial S content condition is mainly caused by the sublimation and evaporation of the accumulated  $\text{K}_2\text{SO}_4$  from the inherent sources and that formed in the early stage of the combustion. In addition, the change of initial S content can only affect the transition cycle significantly at high temperatures. The higher the S content, the higher the rates of the  $\text{KSO}_3$  involved reactions, implying the high released fraction of  $\text{K}_2\text{SO}_4$ .

- **The prediction of the release profiles of K species during the combustion and pyrolysis processes was carried out using the developed model.** The results revealed that the existence of  $\text{O}_2$  could favour the formation of KO and  $\text{KO}_2$ . This could inhibit the release of KOH and KCl when the temperature is below  $927^{\circ}\text{C}$ , while significantly facilitate the release of  $\text{K}_2\text{SO}_4$  when the temperature exceeds  $927^{\circ}\text{C}$ . However, the difference between the release fractions of KOH and KCl are small under combustion and pyrolysis conditions but huge in the case of  $\text{K}_2\text{SO}_4$ . This indicates that the presence of  $\text{O}_2$  can significantly affect the release amount of K at high temperatures, mainly by increasing the release of  $\text{K}_2\text{SO}_4$ .

## 9.2 Suggestions for the future work

The work accomplished in this PhD study has contributed to the knowledge base in the sense that proved and expanded the release mechanisms of K during the combustion of biomass in a large reactor, as well as designed a two-step kinetic model to help predict the release profiles of K from biomass under different circumstances, alongside the transition route of K. Nevertheless, as a result of the overall analysis that carried out, additional issues have been appointed and therefore should be addressed in the future work. The suggestions below describe the continued work on based on this research:

- More accurate control and record of the atmosphere inside the designed reactor (FBS) can be conducted. This will allow the experimentally study on the influence of different oxygen concentrations on the transition of K from biomass in a large reactor and provide insightful information to guide to device design.
- An investigation on the relationship between the release behaviour of K and thermal characteristics of major chemical components (cellulose, hemicellulose and lignin) could be conducted. This information is crucial for a deeper understanding of the release mechanism of K from biomass materials and to provide crucial information on the selection and preparation of raw materials.
- The experiments on the usage of an additive to prevent the loss of K during the thermal conversion process might be carried out, with the aim to find suitable additives to better control and mitigate the K release-induced problems.
- More kinds of biomass could be tested, and the experimental data can be implemented into the model, then validated the predicted results from the model. This will make the model suitable for predicting the release profiles of K from various kinds of biomass.
- The model developed in this work would benefit from adding more detailed release mechanisms of K, like the K/C/O reaction system et al. This will make the prediction more accurate and provide more information about the release of K species. In addition, liquid and solid phase reactions could be added to the model, for example, tar disassociation and char oxidation and the reaction mechanism of liquid and solid phase K species. Also, the development of the reaction mechanism of organic K species could be attempted and add it to the model. This can be achieved by testing the release behaviour of different organic-K species by combusting the pure organic-K samples and

the mixtures of organic-K samples and biomass samples. Moreover, the developed model could potentially be integrated into a single particle combustion model; in this way, a detailed prediction of three-phase-transition and released amounts of different K species from the combustion of a single particle of biomass could be obtained.

## APPENDIX

### Appendix I

Table I Kinetic scheme of cellulose, hemicellulose and lignin pyrolysis\*

Number	Reaction	A,1/s	E, kJ/mol
1	CELL → CELLA	1.5E14	196.8
2	CELLA → 0.4HAA + 0.05GLYOX + 0.15CH <sub>3</sub> CHO + 0.25HMFU + 0.15CH <sub>3</sub> OH + 0.3CH <sub>2</sub> O + 0.61CO + 0.36CO <sub>2</sub> + 0.05H <sub>2</sub> + 0.93H <sub>2</sub> O + 0.02HCOOH + 0.05C <sub>3</sub> H <sub>6</sub> O <sub>2</sub>	2.5E06	79.9
3	CELLA → LVG	3.0	41.9
4	CELL → 5H <sub>2</sub> O + 6CHAR	6.0E07	129.8
5	HCE → 0.4HCE1 + 0.7HCE2	1.0E10	129.7
6	HCE1 → 0.6XYLAN + 0.2C <sub>3</sub> H <sub>6</sub> O <sub>2</sub> + 0.12GLYOX + 0.2FURF + 0.4H <sub>2</sub> O + 0.08G {H <sub>2</sub> } <sub>s</sub> + 0.16CO	3.0	46.1
7	HCE1 → 0.4H <sub>2</sub> O + 0.79CO <sub>2</sub> + 0.05HCOOH + 0.69CO + 0.01G {CO} + 0.01G {CO <sub>2</sub> } + 0.35G {H <sub>2</sub> } + 0.30CH <sub>2</sub> O + 0.9G {COH <sub>2</sub> } + 0.625G {CH <sub>4</sub> } + 0.376G {C <sub>2</sub> H <sub>4</sub> } + 0.875CHAR	1.8E- 03	12.6
8	HCE2 → 0.2H <sub>2</sub> O + 0.275CO + 0.275CO <sub>2</sub> + 0.4CH <sub>2</sub> O + 0.1C <sub>2</sub> H <sub>5</sub> OH + 0.05HAA + 0.35ACAC + 0.025HCOOH + 0.25G {CH <sub>4</sub> } + 0.3G {CH <sub>3</sub> OH} + 0.225G {C <sub>2</sub> H <sub>4</sub> } + 0.4G {CO <sub>2</sub> } + 0.725G {COH <sub>2</sub> }	5.0E09	131.9
9	LIGC → 0.35LIGCC + 0.1COUMARYL + 0.08PHENOL + 0.41C <sub>2</sub> H <sub>4</sub> + 1.0H <sub>2</sub> O + 0.7G {COH <sub>2</sub> } + 0.3CH <sub>2</sub> O + 0.32CO + 0.495G {CH <sub>4</sub> }	1.0E11	155.7
10	LIGH → 1.0LIGOH + 0.5C <sub>2</sub> H <sub>4</sub> + 0.2HAA + 0.1CO + 0.1G {H <sub>2</sub> }	6.7E12	157.0
11	LIGO → LIGOH + CO <sub>2</sub>	3.3E08	106.8
12	LIGCC → 0.3COUMARYL + 0.2PHENOL + 0.35HAA + 0.7H <sub>2</sub> O + 0.65CH <sub>4</sub> + 0.6C <sub>2</sub> H <sub>4</sub> + 1.0H <sub>2</sub> + 1.4CO + 0.4G {CO} + 6.75CHAR	1.0E04	103.8
13	LIGOH → 0.9LIG + 1.0H <sub>2</sub> O + 0.1CH <sub>4</sub> + 0.6CH <sub>3</sub> OH + 0.05G {H <sub>2</sub> } + 0.3G {CH <sub>3</sub> OH} + 0.05CO <sub>2</sub> + 0.65CO + 0.6G {CO} + 0.05HCOOH + 0.85G {COH <sub>2</sub> } + 0.35G {CH <sub>4</sub> } + 0.2G {C <sub>2</sub> H <sub>4</sub> } + 4.25CHAR	1.0E08	125.6

14	$LIG \rightarrow 0.3ANISOLE + 0.3CO + 0.3G\{CO\} + 0.3CH_3CHO$	3.0	50.2
15	$LIG \rightarrow 0.6H_2O + 0.4CO + 0.2CH_4 + 0.4CH_2O + 0.2G\{CO\} + 0.4GG\{CH_4\} + 0.5G\{C_2H_4\} + 0.4G\{CH_3OH\} + 2.0G\{COH_2\} + 6.0CHAR$	3.0	33.5
16	$LIG \rightarrow 0.6H_2O + 2.6CO + 1.1CH_4 + 0.4CH_2O + 1.0C_2H_4 + 0.4CH_3OH$	1.0E07	101.7
17	$TGL \rightarrow 1.0ACROL + 3.0FFA$	7.0E12	191.3
18	$TANN \rightarrow 0.85FENOL + 0.15G\{PHENOL\} + 1.0G\{CO\} + 1.0H_2O + 1.0ITANN$	2.0E01	4.2
19	$ITANN \rightarrow 5.0CHAR + 2.0CO + 1.0H_2O + 1.0G\{COH_2\}$	1.0E03	104.7
20	$G\{CO_2\} \rightarrow CO_2$	1.0E06	100.5
21	$G\{CO\} \rightarrow CO$	5.0E12	209.3
22	$G\{COH_2\} \rightarrow CO + H_2$	1.5E12	297.3
23	$G\{H_2\} \rightarrow H_2$	5.0E11	314.0
24	$G\{CH_4\} \rightarrow CH_4$	5.0E12	299.4
25	$G\{CH_3OH\} \rightarrow CH_3OH$	2.0E12	209.3
26	$G\{C_2H_4\} \rightarrow C_2H_4$	5.0E12	299.4
27	$G\{PHENOL\} \rightarrow PHENOL$	1.5E12	29.7
28	$S\{H_2O\} \rightarrow H_2O$	3.0	33.5

*\*The kinetic scheme is adapted from "Ranzi, E., P.E.A. Debiagi, and A. Frassoldati, Mathematical modelling of fast biomass pyrolysis and bio-oil formation. Note I: kinetic mechanism of biomass pyrolysis. ACS Sustainable Chemistry & Engineering, 2017. 5(4): p. 2867-2881."*

## Appendix II

Table II Kinetic Schemes of K/S/Cl reactions \*

Number	Reaction	A,1/s	E, cal/mol
1	$K + O = KO$	1.5E21	0
2	$K + OH = KOH$	5.4E21	0
3	$KOH + H = K + H_2O$	5.0E13	0
4	$K + Cl + M = KCl$	1.8E20	0
5	$K + HCl = KCl + H$	9.1E12	1179.5
6	$K + Cl_2 = KCl + Cl$	4.4E14	0
7	$KOH + HCl = KCl + H_2O$	1.7E14	0
8	$K + HO_2 = KOH + O$	1.0E14	0
9	$K + HO_2 = KO + OH$	3.0E13	0
10	$K + H_2O_2 = KOH + OH$	2.5E13	0
11	$K + H_2O_2 = KO + H_2O$	1.6E13	0
12	$KO + H = K + OH$	2.0E14	0
13	$KO + O = K + O_2$	2.2E14	0
14	$KO + OH = KOH + O$	2.0E13	0
15	$KO + HO_2 = KOH + O_2$	5.0E13	0
16	$KO + H_2 = KOH + H$	1.6E13	0
17	$KO + H_2 = K + H_2O$	3.1E12	0
18	$KO + H_2O = KOH + OH$	1.3E14	0
19	$KO + CO = K + CO_2$	1.0E14	0
20	$KOH + KOH = (KOH)_2$	8.0E13	0
21	$K + ClO = KCl + O$	1.0E14	0
22	$KO + HCl = KCl + OH$	1.7E14	0
23	$KCl + KCl = (KCl)_2$	8.0E13	0
24	$K + H = KH$	3.0E17	0
25	$KH + H = K + H_2$	1.0E14	0
26	$KH + O = KO + H$	5.0E13	0
27	$KH + O = K + HO$	5.0E13	0
28	$KH + OH = K + H_2O$	1.0E14	0
29	$KH + OH = KOH + H$	1.0E13	0
30	$KH + O_2 = K + HO_2$	1.0E14	0
31	$K + O_2 = KO_2$	3.6E14	0
32	$SO_2 + O = SO_3$	3.7E11	1689.1

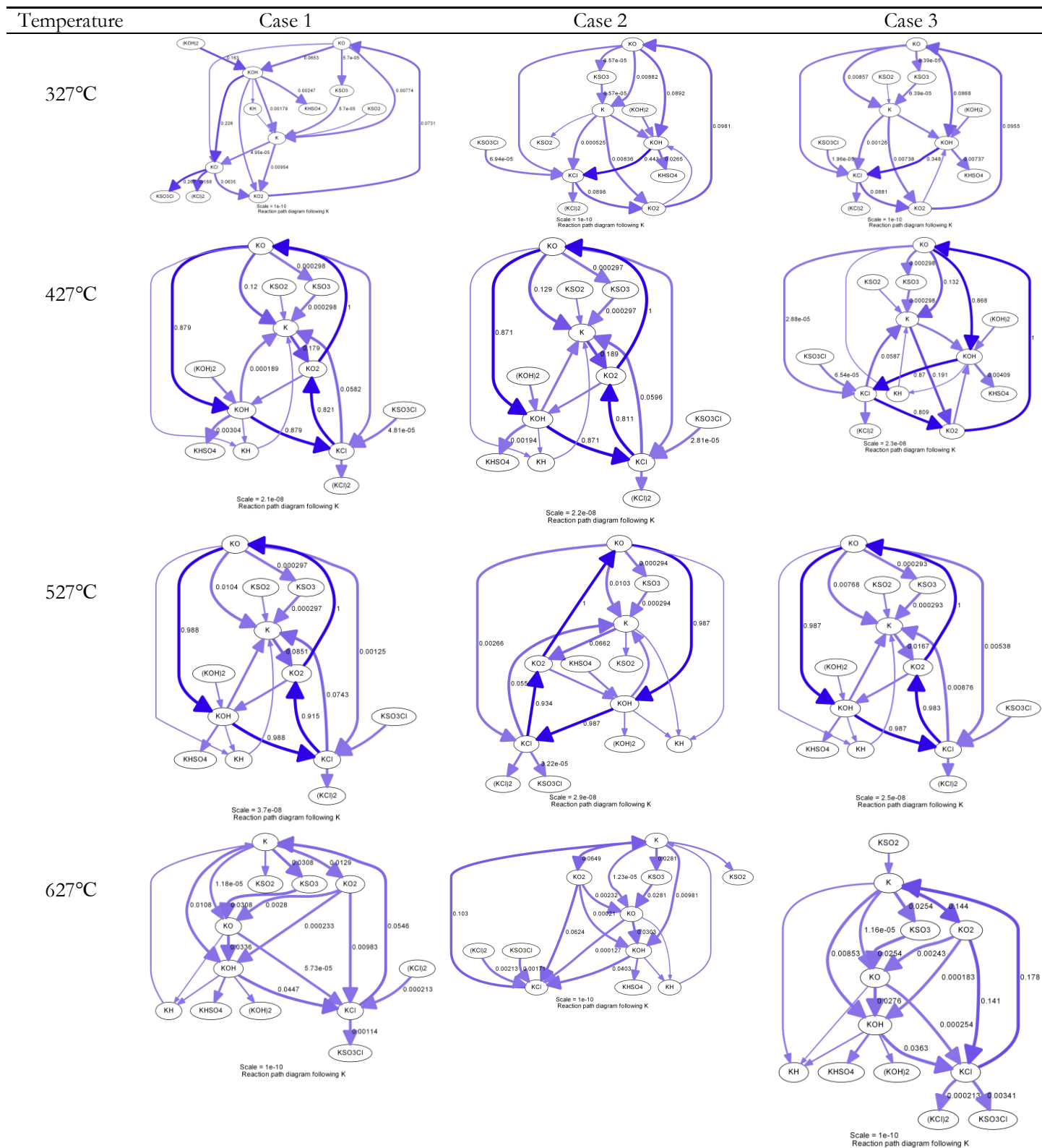
33	$\text{SO}_2 + \text{OH} = \text{SO}_3 + \text{H}$	4.9E02	23845.1
34	$\text{SO}_3 + \text{O} = \text{SO}_2 + \text{O}_2$	1.3E12	6100.4
35	$\text{SO}_3 + \text{SO} = \text{SO}_2 + \text{SO}_2$	7.6E03	2980.6
36	$\text{S} + \text{NO}_2 = \text{SO} + \text{NO}$	3.0E10	-166.7
37	$\text{S} + \text{OH} = \text{SO} + \text{H}$	2.8E09	0
38	$\text{S} + \text{O}_2 = \text{SO} + \text{O}$	1.5E10	3651.9
39	$\text{S} + \text{H}_2 = \text{SH} + \text{H}$	1.4E11	19258.2
40	$\text{S} + \text{SH} = \text{S}_2 + \text{H}$	2.7E10	0
41	$\text{S} + \text{H} = \text{SH}$	6.2E10	0
42	$\text{SO}_2 + \text{HO}_2 = \text{SO}_3 + \text{OH}$	1.2E04	0
43	$\text{SO}_2 + \text{NO}_2 = \text{SO}_3 + \text{NO}$	6.3E09	26989.6
44	$\text{SO}_2 + \text{CO} = \text{SO} + \text{CO}_2$	2.7E09	43732.7
45	$\text{SO} + \text{O}_2 = \text{SO}_2 + \text{O}$	7.6E00	2978.4
46	$\text{SO} + \text{OH} = \text{SO}_2 + \text{H}$	1.1E14	0
47	$2\text{SO} = \text{SO}_2 + \text{S}$	2.0E09	3993.5
48	$\text{SO} + \text{O} = \text{SO}_2$	1.2E05	0
49	$\text{SO}_3 + \text{N} = \text{SO}_2 + \text{NO}$	3.1E05	0
50	$\text{SH} + \text{HO}_2 = \text{H}_2\text{O}_2 + \text{S}$	1.0E08	0
51	$\text{SH} + \text{OH} = \text{H}_2\text{O} + \text{S}$	1.0E10	0
52	$\text{SH} + \text{O} = \text{SO} + \text{H}$	1.0E11	0
53	$\text{KSO}_2 + \text{KO}_2 = \text{K}_2\text{SO}_4$	1.0E14	0
54	$\text{KO}_2 + \text{H} = \text{K} + \text{HO}_2$	2.0E14	0
55	$\text{KO}_2 + \text{H} = \text{KO} + \text{OH}$	5.0E13	0
56	$\text{KO}_2 + \text{H} = \text{KOH} + \text{O}$	1.0E14	0
57	$\text{KO}_2 + \text{O} = \text{KO} + \text{O}_2$	1.3E13	0
58	$\text{KO}_2 + \text{OH} = \text{KOH} + \text{O}_2$	2.0E13	0
59	$\text{KO}_2 + \text{CO} = \text{KO} + \text{CO}_2$	1.0E14	0
60	$\text{KO}_2 + \text{Cl} = \text{KCl} + \text{O}_2$	1.0E14	0
61	$\text{KO}_2 + \text{HCl} = \text{KCl} + \text{HO}_2$	1.4E14	0
62	$\text{K} + \text{SO}_2 = \text{KSO}_2$	3.7E14	0
63	$\text{K} + \text{SO}_3 = \text{KSO}_3$	3.7E14	0
64	$\text{K} + \text{SO}_3 = \text{KO} + \text{SO}_2$	1.0E14	15568.0
65	$\text{KO} + \text{SO}_2 = \text{KSO}_3$	3.7E14	0
66	$\text{KOH} + \text{SO}_3 = \text{KHSO}_4$	1.0E14	0
67	$\text{KSO}_2 + \text{O} = \text{KO} + \text{SO}_2$	1.3E13	0
68	$\text{KSO}_2 + \text{OH} = \text{KOH} + \text{SO}_2$	2.0E13	0

69	$\text{KSO}_3 + \text{O} = \text{KO} + \text{SO}_3$	1.3E13	0
70	$\text{KSO}_3 + \text{OH} = \text{KOH} + \text{SO}_3$	2.0E13	0
71	$\text{KSO}_3 + \text{KO} = \text{K}_2\text{SO}_4$	1.0E14	0
72	$\text{KHSO}_4 + \text{KOH} = \text{K}_2\text{SO}_4 + \text{H}_2\text{O}$	1.0E14	0
73	$\text{KHSO}_4 + \text{KCl} = \text{K}_2\text{SO}_4 + \text{HCl}$	1.0E14	0
74	$\text{KCl} + \text{SO}_3 = \text{KSO}_3\text{Cl}$	1.0E14	0
75	$\text{KSO}_3\text{Cl} + \text{OH} = \text{KHSO}_4 + \text{Cl}$	1.0E14	0
76	$\text{KSO}_3\text{Cl} + \text{H}_2\text{O} = \text{KHSO}_4 + \text{HCl}$	1.0E14	0
77	$\text{KSO}_3\text{Cl} + \text{KOH} = \text{K}_2\text{SO}_4 + \text{HCl}$	1.0E14	0
78	$2\text{Cl} = \text{Cl}_2$	1.4E01	-1800
79	$\text{H} + \text{Cl} = \text{HCl}$	1.7E01	0
80	$\text{H} + \text{HCl} = \text{H}_2 + \text{Cl}$	1.3E01	3500
81	$\text{H} + \text{Cl}_2 = \text{HCl} + \text{Cl}$	1.4E01	1200
82	$\text{O} + \text{HCl} = \text{OH} + \text{Cl}$	2.8E-07	3510
83	$\text{OH} + \text{HCl} = \text{H}_2\text{O} + \text{Cl}$	6.2E-04	-223
84	$\text{O} + \text{Cl}_2 = \text{ClO} + \text{Cl}$	1.3E01	3585
85	$\text{O} + \text{ClO} = \text{Cl} + \text{O}_2$	1.3E01	-193
86	$\text{Cl} + \text{HO}_2 = \text{HCl} + \text{O}_2$	1.3E01	894
87	$\text{Cl} + \text{HO}_2 = \text{OH} + \text{ClO}$	1.3E01	-338
88	$\text{Cl} + \text{H}_2\text{O}_2 = \text{HCl} + \text{HO}_2$	1.3E01	1951
89	$\text{ClO} + \text{H}_2 = \text{HOCl} + \text{H}$	1.2E01	14100
90	$\text{H} + \text{HOCl} = \text{HCl} + \text{OH}$	1.4E01	762
91	$\text{Cl} + \text{HOCl} = \text{HCl} + \text{ClO}$	1.2E01	258
92	$\text{Cl}_2 + \text{OH} = \text{Cl} + \text{HOCl}$	1.2E01	1810
93	$\text{O} + \text{HOCl} = \text{OH} + \text{ClO}$	1.3E01	4372
94	$\text{OH} + \text{HOCl} = \text{H}_2\text{O} + \text{ClO}$	1.2E01	994
95	$\text{HOCl} = \text{OH} + \text{Cl}$	1.0E01	5672

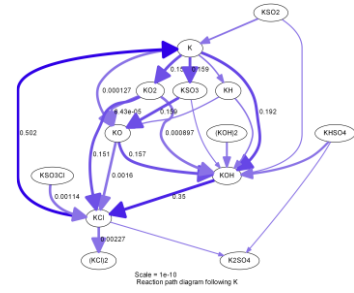
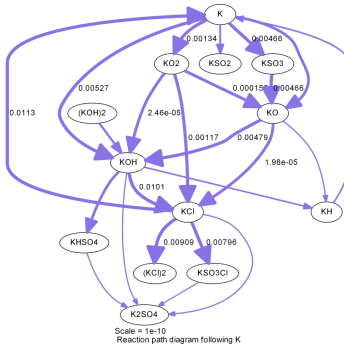
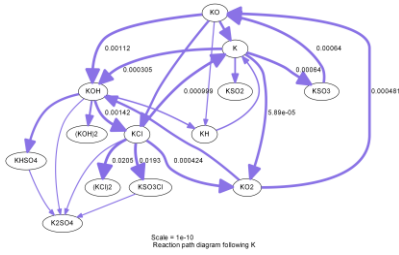
*\*The kinetic schemes are adapted from "Glarborg, P. and P. Marshall, Mechanism and modeling of the formation of gaseous alkali sulfates. Combustion and Flame, 2005. 141(1-2): p. 22-39.", "Cerru, F., A. Kronenburg, and R. Lindstedt, Systematically reduced chemical mechanisms for sulfur oxidation and pyrolysis. Combustion and Flame, 2006. 146(3): p. 437-455." and "Sliger, R.N., J.C. Kramlich, and N.M. Marinov, Towards the development of a chemical kinetic model for the homogeneous oxidation of mercury by chlorine species. Fuel Processing Technology, 2000. 65: p. 423-438."*

### Appendix III

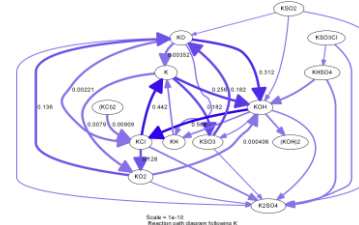
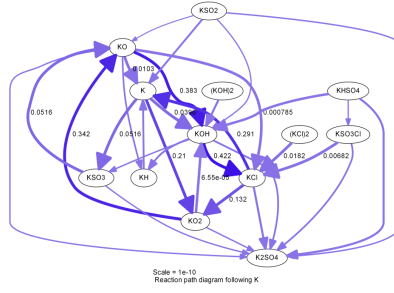
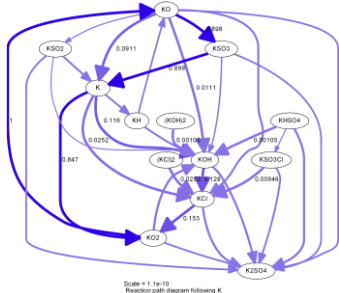
Table III Detailed reaction paths of K species under different conditions of initial input of Cl



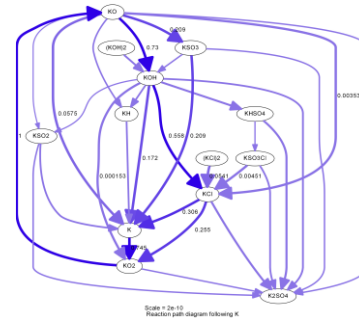
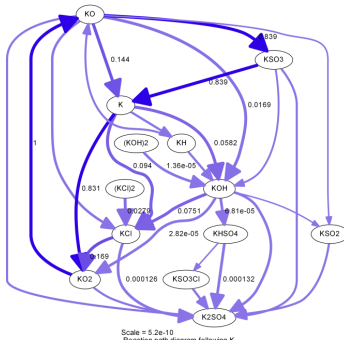
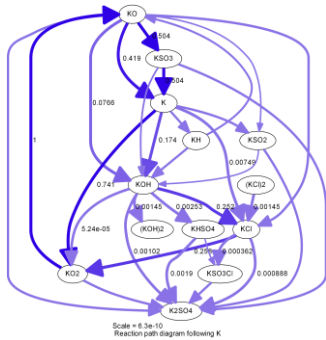
727°C



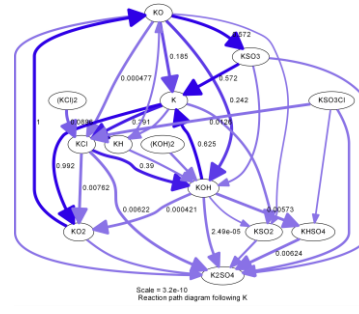
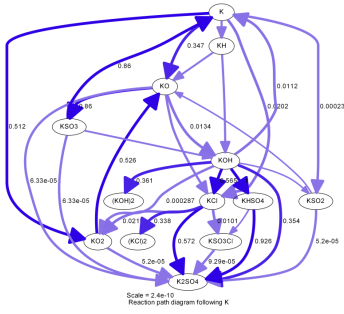
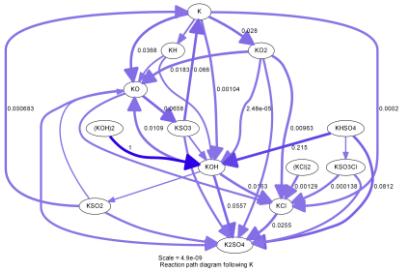
827°C



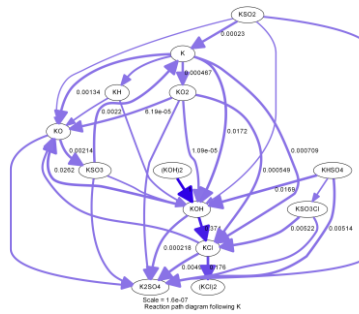
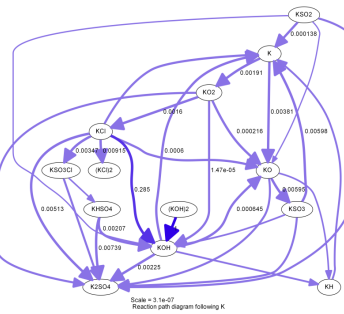
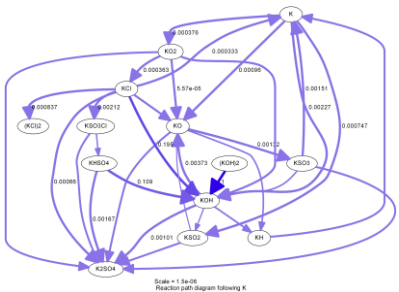
927°C



1027°C

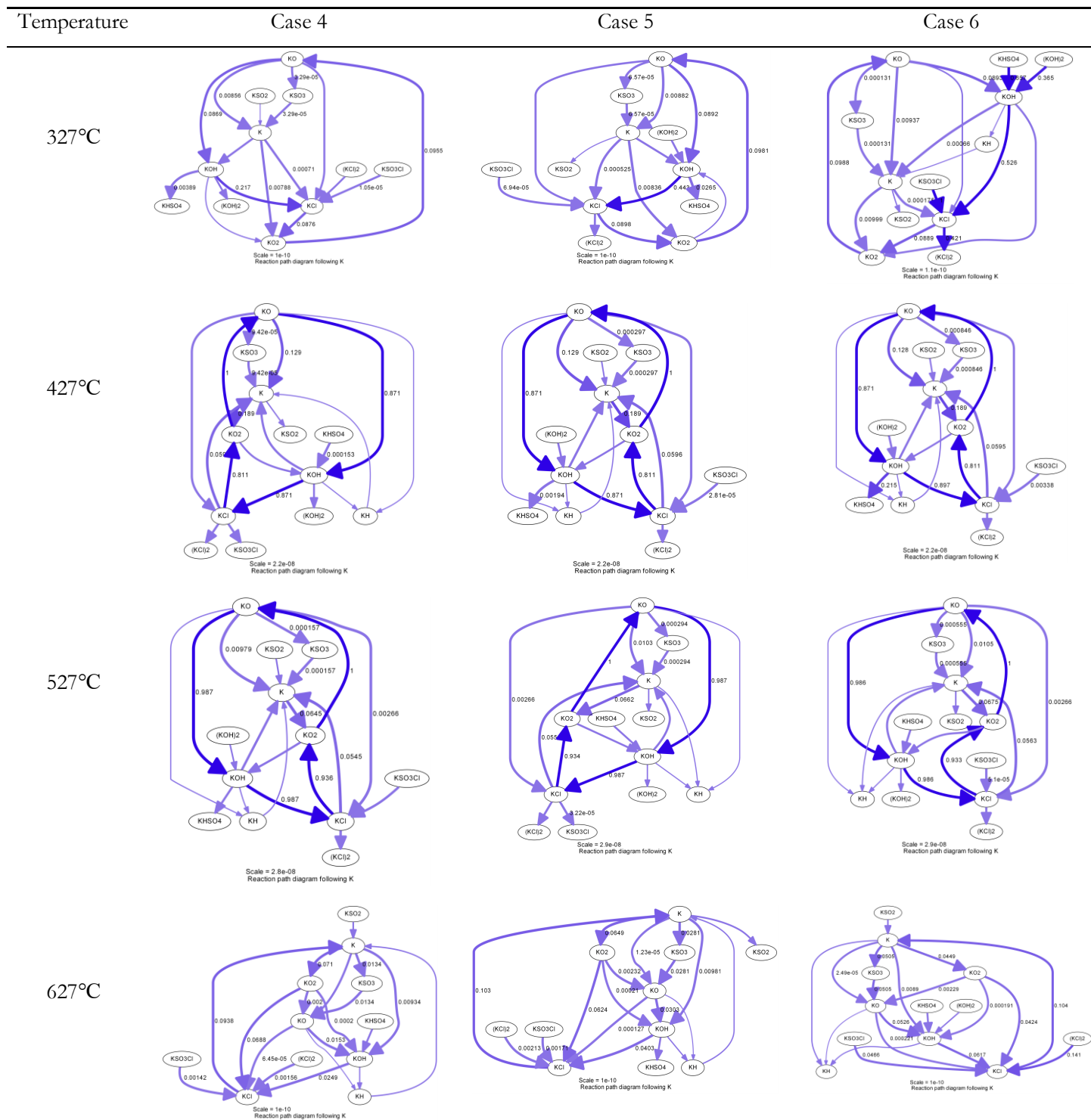


1127°C

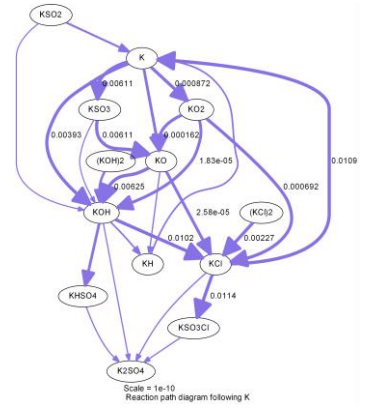
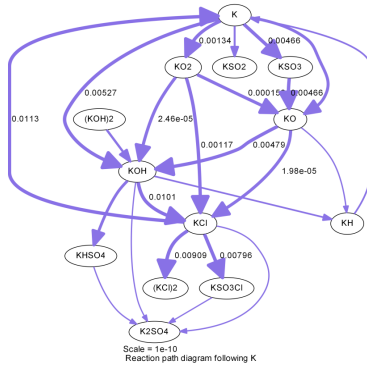
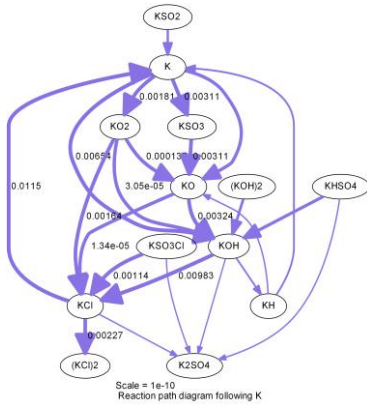


## Appendix IV

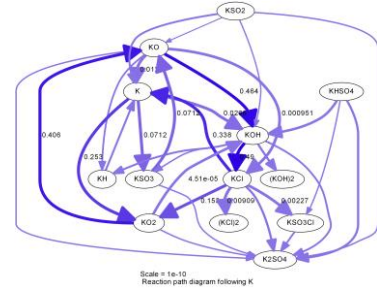
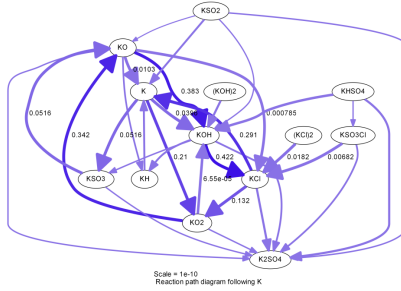
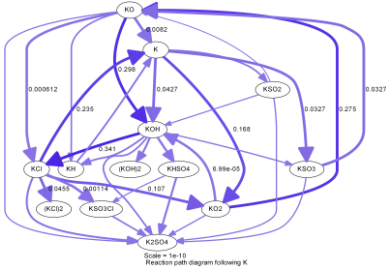
Table IV Detailed reaction paths of K species under different conditions of initial input of S content



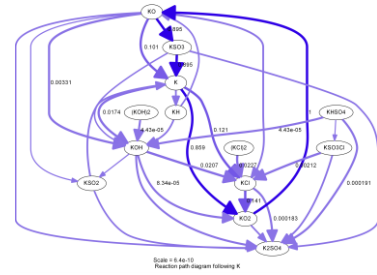
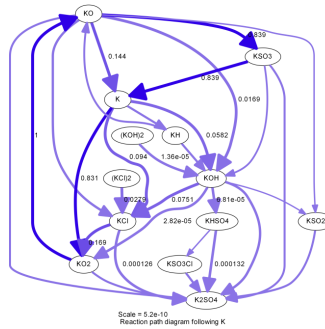
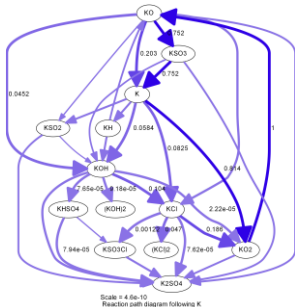
727°C



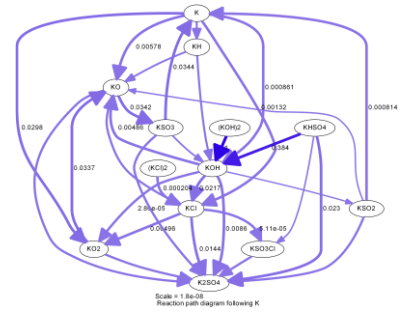
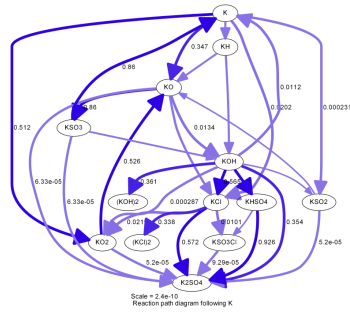
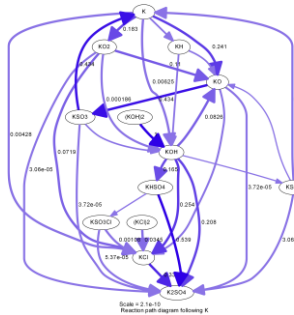
827°C



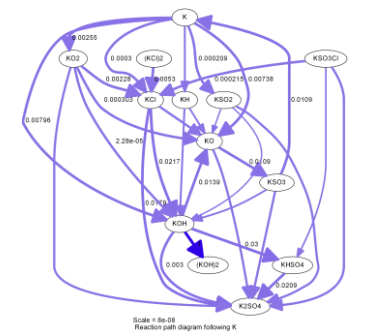
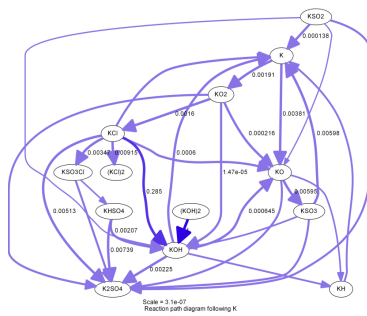
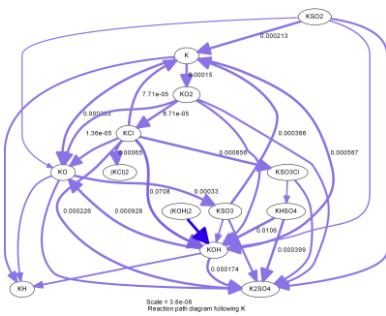
927°C



1027°C

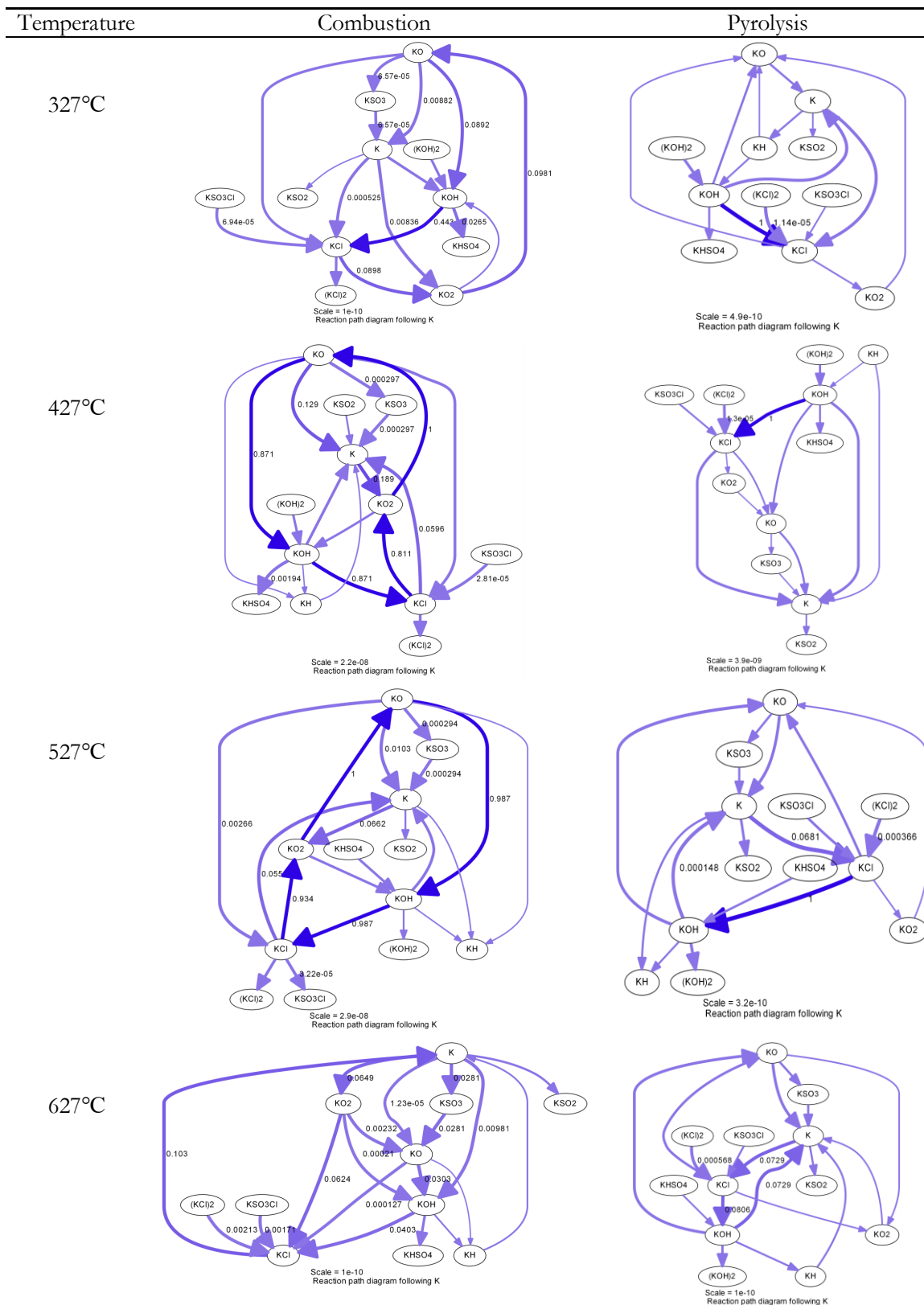


1127°C

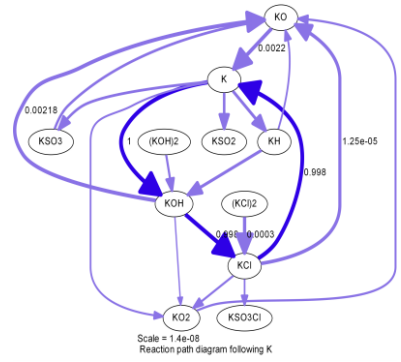
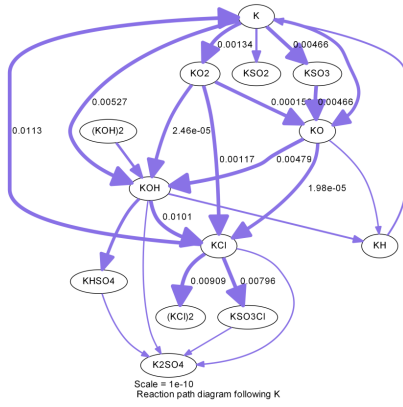


## Appendix V

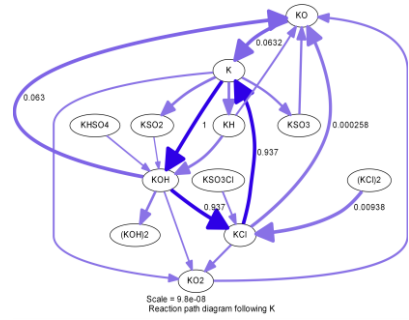
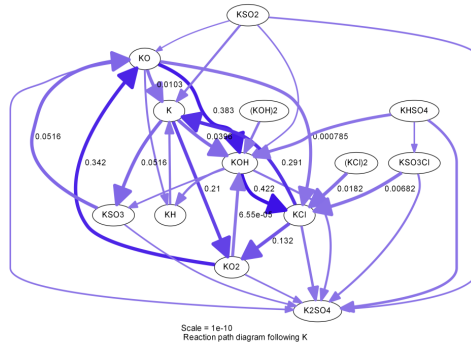
Table V Detailed reaction paths of K species under different conditions of combustion and pyrolysis



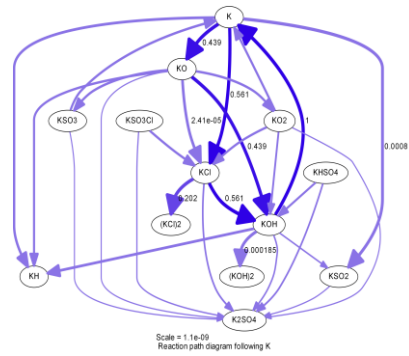
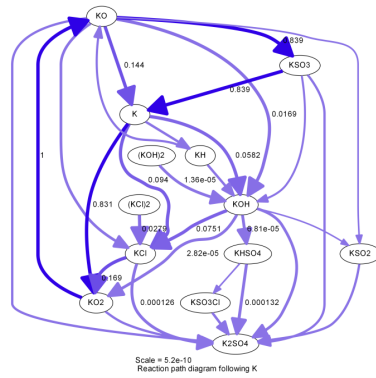
727°C



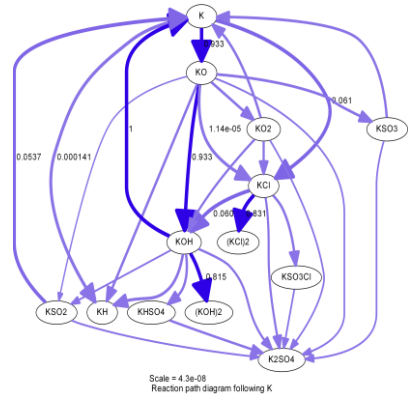
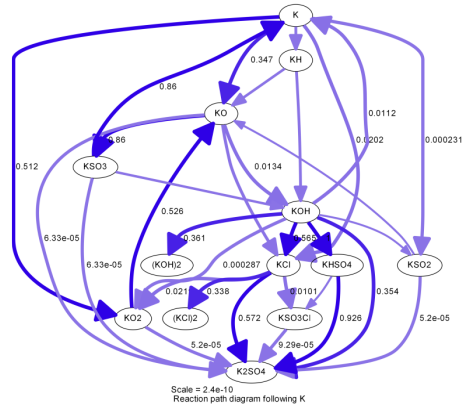
827°C



927°C



1027°C



1127°C

